ANDREWS, LESLEY

OXIDATION BEHAVIOR OF ARSENOPYRITE DURING ACID FERRIC SULPHATE AND BACTERIAL LEACHING

MSc UP 1998

Oxidation behaviour of arsenopyrite during acid ferric sulphate and bacterial leaching.

by

Lesley Andrews

Thesis submitted in partial fulfilment of the requirements
for the degree MAGISTER SCIENTIAE,
in the Faculty of Science,
University of Pretoria.

Promoter: Professor R.K.W. Merkle

December 1998

SYNOPSIS

The acid ferric sulphate and bacterial leach behaviour of gold-bearing arsenopyrite concentrates from four different ore deposits in Southern Africa was compared. The arsenopyrite crystals, which were compositionally distinct, were isolated and their major and trace element contents were determined on the electron microprobe. The four arsenopyrite types all proved to be sulphur-rich overall, as is most naturally occurring arsenopyrite, but they possess widely differing patterns of zonation into arsenic-rich and sulphur-rich compositional zones. These zone patterns range from weak to strong and from coarsely to finely interspaced depending on the source of the arsenopyrite. Trace elements such as gold were found to be associated with arsenic-rich zones, antimony with sulphur-rich zones, and nickel and cobalt apparently substituted for iron irrespective of zone composition.

The four crystal types were then subjected to ferric sulphate leaching, and to leaching in a mixed bacterial culture. The changes during leaching were monitored microscopically, and post-leach samples were characterised by electron microprobe analysis and Auger Electron Spectroscopy. A link between the reflectivity and colour and the depth of oxidation of the arsenopyrite crystals was observed, as has been suggested by previous authors.

Particles of pyrite, pyrrhotite, gersdorffite, chalcopyrite, sphalerite, galena, tetrahedrite and gold were also analysed on the electron microprobe and observed during leaching. This provided information on the leach rate of these minerals relative to arsenopyrite, and on the effect of galvanic interaction between sulphide minerals in contact.

Results showed the oxidation rate of arsenopyrite to be determined by its composition, both of major and trace elements. Arsenopyrite types that showed strong compositional zonation leached rapidly, under both ferric sulphate and bacterial leach conditions. Arsenopyrite with finely interspaced zones leached more quickly than that with a coarse zone distribution. The presence of trace elements can also accelerate leach behaviour, and in this study a cobalt content of up to two mass per cent has been shown to increase the arsenopyrite oxidation rate. Arsenopyrite in contact with pyrite showed accelerated leach rates due to galvanic interaction, where the more passive pyrite is protected by the arsenopyrite.

During both bacterial and acid ferric sulphate oxidation, arsenic appeared to be removed first from the surface of the arsenopyrite crystals, followed by iron, and eventually a non-

passivating sulphur layer built up which remained until the crystals were completely leached away. The leach rate accelerated when bacteria were present, but the *relative* leach rate of the four arsenopyrite types did not change between bacterial and sterile ferric sulphate leaching. Apart from the accelerated leach rate, the major differences observed between bacterial and non-bacterial leaching were the stronger dependence on crystal orientation during ferric sulphate leaching, and the stronger galvanic effects present during bacterial leaching. Since the orientation effect would be minimal during fine powder leaching, it is clear that cheaper and more controllable ferric sulphate leach amenability tests could safely be used to predict the relative leach rate of an ore under bacterial conditions. It has also been established that a prior mineralogical examination of the ore could provide a great deal of information on its subsequent leach behaviour.

UITTREKSEL

Die logingsgedrag van vier Suid Afrikaanse gouddraende arseenpiriet afsettings is vergelyk onder 'n ystersulfaatsuur- en bakteriese loging. Die arseenpirietkristalle, wat samestellingsgewys verskil, is geïsoleer en hulle hoof- en spoorelement inhoude is met behulp van die elektronmikrosonde bepaal. Al vier arseenpiriet tipes, soos die meeste natuurlik voorkomende arseenpiriete, is swaelryk gevind, maar het verskil in terme van hulle arseen- en swaelryke soneringspatrone. Die soneringspatrone wissel van swak tot sterk en van fyn tot grof gespasiëer, afhangende van die oorsprong van die arseenpiriet. Spoorelemente soos goud is gevind om met die arseenryke sones te assosieer, antimoon met die swaelryke sones, terwyl nikkel en kobalt klaarblyklik die yster vervang en dus nie beperk is tot 'n spesifieke sonesamestelling nie.

Die vier kristaltipes is onderwerp aan ystersulfaat loging sowel as aan 'n gemengde bakteriese kultuur. Die veranderinge wat gedurende die logingsproses plaasvind is mikroskopies gemonitor terwyl die residue met die elektronmikrosonde en Auger elektron spektroskoop bestudeer is. Soos wat deur vorige navorsers voorgestel is, is daar 'n verwantskap tussen die reflektiwiteit en kleur van die arseenpiriet en die mate van oksidasie vasgestel. Piriet-, pirrotiet-, gersdorffiet-, chalkopiriet-, sfaleriet-, galena-, tetrahedriet- en goudkorrels is ook met behulp van die elektronmikrosonde geanaliseer en gemonitor gedurende die logingsproses. Dit het inligting oor die logingstempo van die minerale relatief tot dié van arseenpiriet gelewer, en ook data verskaf oor die galvaniese interaksie effek tussen aangrensende sulfiedminerale.

Die resultate wat verkry is dui aan dat die oksidasietempo van arseenpiriet afhang van die samestelling, en dat beide die hoof en spoorelemente belangrik is. Arseenpiriettipes met sterk samestellingsonering loog vinnig onder beide ystersulfaat en bakteriese logingstoestande. Arseenpiriet met nou-gespasieerde sones loog vinniger as die met grof-gespasieerde soneringspatrone. Die teenwoordigheid van spoorelemente kan ook die logingstempo verhoog, en hierdie studie het getoon dat 'n kobaltinhoud van tot 2 massa persent vergroot die arseenpiriet oksidasie tempo. Arseenpiriet in kontak met piriet het 'n toename in logingstempo getoon as gevolg van die galvaniese interaksie tussen die verskillende fases, wat veroorsaak dat die meer passiewe piriet beskerm word deur die arseenpiriet.

Gedurende beide bakteriese en ystersulfaatsuur oksidasie wil dit voorkom asof arseen eerste van die oppervlak van die arseenpiriet verwyder word. Dit word gevolg deur die verwydering van yster en die opbou van 'n passiverende swael lagie. Die swael lagie is teenwoordig totdat die arseenpirietkristal volledig geloog is. Die logingstempo verhoog in die aanwesigheid van bakterië, maar die *relatiewe* logingstempo tussen die verrskillende arseenpiriettipes is dieselfde as dit wat vasgestel is vir die ystersulfaat loging.

Behalwe die verhoogde logingstempo is die grootste verskil tussen die bakteriese en nie-bakteriese loging die sterker invloed van kristaloriëntasie gedurende die ystersulfaat loging en die teenwoordigheid van 'n sterker galvaniese effek gedurende bakteriese loging. Omrede die oriëntasie effek minimaal sal wees gedurende fyn poeierloging is dit duidelik dat die meer koste effektiewe en beheerbare ystersulfaatloging gebruik kan word om die relatiewe logingstempo van 'n erts onder bakteriese toestande te voorspel. Dit is ook aangetoon dat 'n voorafgaande mineralogiese ondersoek van 'n erts voldoende data oor die logingsgedrag van die erts kan verskaf.

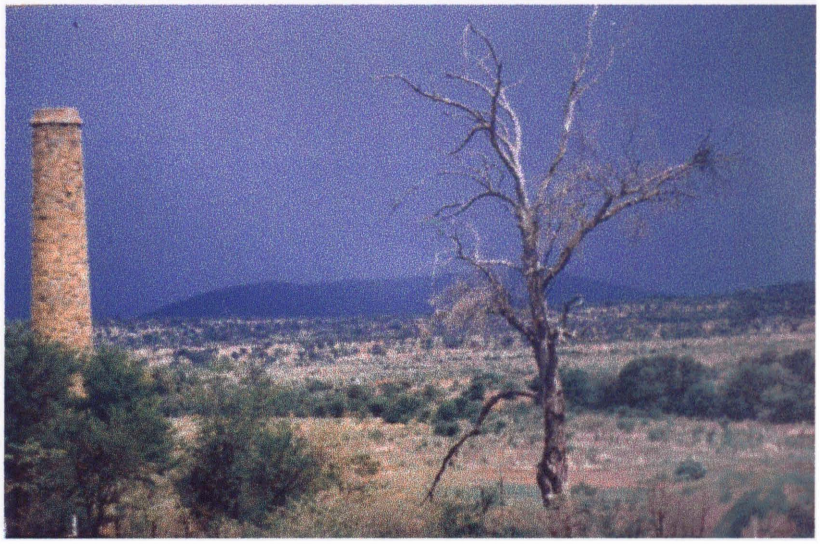

The old chimney at Eersteling, built from Aberdeen granite imported from Scotland, and transported by ox-wagon. Gold was mined at Eersteling from 1871, making it the oldest gold mine in South Africa. The view looks over the Marabastad Gold Field and Zandrivier Prospect.

Much have I travelled in the realms of gold…

John Keats 1795–1821

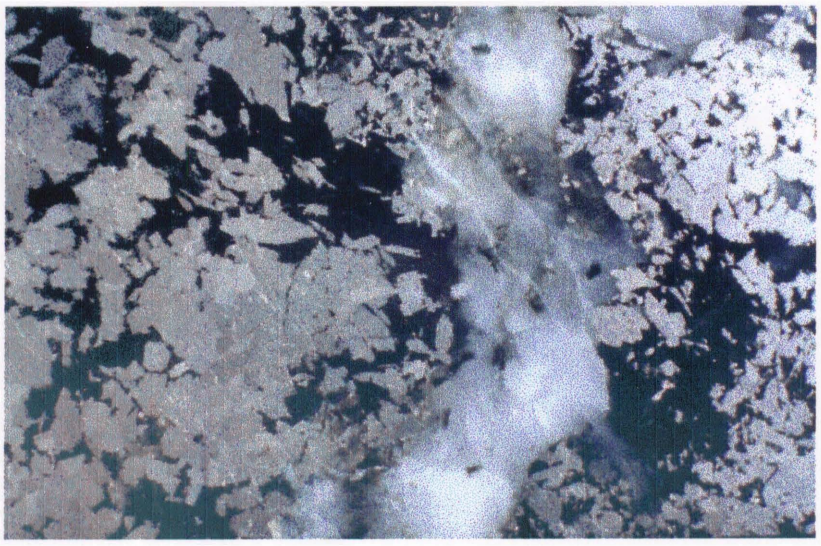

Polished Zandrivier rock showing arsenopyrite (metallic lustre), tourmaline (black) and a quartz vein (white).

CONTENTS

1 INTRODUCTION..... 1
2 AIM OF THIS STUDY..... 2
3 PREVIOUS WORK..... 3
3.1 Arsenopyrite composition..... 4
3.2 Inorganic arsenopyrite oxidation..... 6
3.3 Bacterial oxidation of arsenopyrite..... 9
4 SOURCE AND GEOLOGICAL SETTING..... 16
5 EXPERIMENTAL TECHNIQUES..... 18
5.1 Analytical and mineralogical techniques..... 18
5.1.1 X-ray powder diffraction..... 19
5.1.2 Section preparation..... 19
5.1.3 Isolation of the arsenopyrite..... 19
5.1.4 Image analysis..... 20
5.1.5 Reflectance..... 21
5.1.6 Electron microprobe analysis..... 21
5.1.7 Auger electron spectroscopy..... 26
5.1.8 Chemical analysis..... 28
5.2 Acid ferric sulphate leaching..... 28
5.3 Bacterial leaching..... 32
6 MINERALOGY OF THE UNLEACHED SAMPLES..... 33
6.1 Mineralogy of the Klipwal sample..... 33
6.2 Mineralogy of the Sheba rock sample..... 35
6.3 Mineralogy of the Zandrivier rock sample..... 38
6.4 Mineralogy of the West African rock sample..... 39
6.5 Modal sulphide analysis..... 40
6.6 Gold deportment and composition..... 41
7 COMPOSITION OF THE MAJOR SULPHIDE MINERALS..... 46
7.1 ICP-MS analysis results..... 46
7.2 Quantitative electron microprobe analysis of sulphide minerals..... 48
7.2.1 Arsenopyrite analysis..... 48
7.2.1.1 Major element analysis..... 49
7.2.1.2 Minor to trace element analysis..... 51

7.2.1.3 Results of arsenopyrite analysis..... 53
7.2.1.4 Discussion of arsenopyrite composition..... 60
7.2.2 Analysis of other sulphide minerals..... 61
7.2.3 Formation temperatures of the sulphide minerals..... 67
8 INTRODUCTION TO THE LEACH PROGRAM..... 74
8.1 The leach program..... 74
8.2 Stages of bacterial oxidation and ore microscopy..... 75
8.3 Sulphide oxidation colours..... 76
9 CRYSTAL AND MILLED SECTION LEACH TESTS..... 78
9.1 Ferric sulphate leach 1..... 78
9.2 Ferric sulphate leach 2..... 81
9.3 Ferric sulphate leach tests 3 and 4..... 83
9.4 Ferric sulphate leach 5..... 84
9.5 Bacterial leach 1..... 88
9.6 Discussion of results of the first six sterile and bacterial leach tests..... 91
10 LEACH TESTS FOR MODAL ANALYSIS..... 92
10.1 Ferric sulphate leach 6..... 92
10.2 Modal analysis results..... 93
10.3 Bacterial leach 2..... 100
11 ROCK SECTION LEACH TESTS..... 101
11.1 Ferric sulphate leach 7..... 101
11.2 Bacterial leach 3..... 101
11.3 Results of rock section leach tests..... 102
11.3.1 Arsenopyrite leach behaviour..... 102
11.3.1.1 Klipwal arsenopyrite..... 103
11.3.1.2 Zandrivier arsenopyrite..... 105
11.3.1.3 Sheba arsenopyrite..... 110
11.3.1.4 West African arsenopyrite..... 114
11.3.2 Sulphides other than arsenopyrite..... 122
11.3.2.1 Pyrite..... 122
11.3.2.2 Gersdorffite..... 126
11.3.2.3 Pyrrhotite..... 128
11.3.2.4 Chalcopyrite..... 128
11.3.2.5 Tennantite-tetrahedrite..... 129

11.3.2.6 Galena..... 130
11.3.2.7 Sphalerite..... 131
11.3.2.8 Complex sulphide intergrowths..... 131
11.3.3 Influence of surrounding rock..... 134
11.3.4 Gold..... 134
11.4 Features of leaching sulphide surfaces..... 135
11.5 Discussion of results of rock section leach tests..... 140
12 MINERALOGY OF LEACHED SULPHIDES..... 141
12.1 Electron microprobe analysis results..... 141
12.1.1 Silver contamination..... 144
12.2 Reflectance of leached arsenopyrite..... 145
12.2.1 Ferric sulphate leach 8..... 145
12.2.2 Reflectance measurement results..... 145
12.3 Auger Electron Spectroscopy..... 147
12.3.1 Ferric sulphate leach tests 9 and 10..... 147
12.3.2 AES analysis..... 147
12.4 Discussion of leached arsenopyrite mineralogy..... 151
13 POWDER LEACHING AND ARSENIC SPECIES IN SOLUTION..... 151
13.1 Ferric sulphate powder leach tests 11 and 12..... 151
13.2 Results of liquor analysis..... 153
13.3 Discussion of liquor analysis results..... 155
14 DISCUSSION..... 157
15 CONCLUSIONS..... 165
16 RECOMMENDATIONS..... 166
17 ACKNOWLEDGEMENTS..... 167
REFERENCES..... 169
APPENDIX..... 179

LIST OF FIGURES

Figure 1	Schematic diagram of indirect and direct bacterial leaching of arsenopyrite	12
Figure 2	The locations of Zandrivier Prospect, and Sheba and Klipwal Gold Mines	17
Figure 3	Diagram showing the dimensions of a composite polished section	19
Figure 4	Proza curves plotted for arsenopyrite	23
Figure 5	The depth of Auger electron excitation compared to that produced by an electron beam	27
Figure 6	Diagram of the apparatus used for ferric sulphate leach tests	29
Figure 7	The PVC reactor	30
Figure 8	The ferric sulphate leach reactor running in the laboratory	30
Figure 9	Diagram showing the bacterial leach test apparatus	33
Figure 10	Twinning in arsenopyrite	34
Figure 11	Zonation patterns in arsenopyrite	36
Figure 12	BSE-image of Sheba gersdorffite showing atoll texture	37
Figure 13	The size distribution of gold inclusions	43
Figure 14	Mineral association of gold	44
Figure 15	Variation of arsenic and sulphur in the Mintek As-2 standard	50
Figure 16	Variation of arsenic and sulphur in ASP-1	50
Figure 17	Wavescans over Se-Lα and Se-Lβ peak positions on arsenopyrite	52
Figure 18	Arsenopyrite compositions in atomic per cent plotted on a ternary diagram	54
Figure 19	Variation of arsenic and sulphur in Klipwal arsenopyrite	55
Figure 20	Variation of arsenic and sulphur in Zandrivier arsenopyrite	55
Figure 21	Variation of arsenic and sulphur in Sheba arsenopyrite	56
Figure 22	Variation of arsenic and sulphur in West African arsenopyrite	56

Figure 23 Arsenopyrite zone compositions in atomic per cent plotted on a ternary diagram..... 59

Figure 24 Relationship between gold and arsenic in the Sheba arsenopyrite used in this study..... 63

Figure 25 Relationship between gold and arsenic in more typical Sheba MRC arsenopyrite..... 63

Figure 26 Relationship between antimony and arsenic in Sheba arsenopyrite..... 64

Figure 27 Relationship between (Co + Ni) and iron in West African arsenopyrite... 64

Figure 28 Variation of nickel and iron in Sheba gersdorffite..... 65

Figure 29 Variation of arsenic and sulphur in Sheba gersdorffite..... 66

Figure 30 Variation of antimony and iron in Sheba gersdorffite..... 66

Figure 31 Variation of antimony and nickel in Sheba gersdorffite..... 67

Figure 32 Pyrite compositions in atomic per cent plotted on a ternary diagram..... 68

Figure 33 Formation temperatures of Sheba arsenopyrite..... 71

Figure 34 Formation temperatures of Klipwal arsenopyrite..... 72

Figure 35 Formation temperatures of Zandrivier arsenopyrite..... 73

Figure 36 Formation temperatures of West African arsenopyrite..... 74

Figure 37 Klipwal arsenopyrite crystals leached for one week in ferric sulphate leach 1..... 80

Figure 38 Zandrivier arsenopyrite particles leached for one week in ferric sulphate leach 1..... 80

Figure 39 West African arsenopyrite crystals leached for one week in ferric sulphate leach 1..... 80

Figure 40 Sheba arsenopyrite crystals leached for one week in ferric sulphate leach 1..... 80

Figure 41 Pyrite in Klipwal arsenopyrite after one week in ferric sulphate leach 1... 81

Figure 42 Klipwal arsenopyrite crystals after five days in ferric sulphate leach 5.... 85

Figure 43 Zandrivier arsenopyrite particles after five days in ferric sulphate leach 5 85

Figure 44 West African arsenopyrite crystals after five days in ferric sulphate leach 5..... 86

Figure 45 Sheba arsenopyrite crystals after five days in ferric sulphate leach 5..... 86

Figure 46 Zoned Sheba arsenopyrite crystal after four days in ferric sulphate leach 5..... 86

Figure 47 The same crystal after eight days in ferric sulphate leach 5..... 86

Figure 48 Mimetic twinning in Sheba arsenopyrite..... 87

Figure 49 Mimetic twinning in West African arsenopyrite..... 87

Figure 50 Faster-leaching rims around West African arsenopyrite crystals after four days in ferric sulphate leach 5..... 87

Figure 51 Faster-leaching rims around West African arsenopyrite crystals after one week in ferric sulphate leach 5..... 87

Figure 52 Klipwal arsenopyrite crystals after one week in bacterial leach 1..... 89

Figure 53 Zandrivier arsenopyrite particles after one week in bacterial leach 1..... 89

Figure 54 West African arsenopyrite crystals after one week in bacterial leach 1.... 90

Figure 55 Sheba arsenopyrite crystals after one week in bacterial leach 1..... 90

Figure 56 Accelerated leaching of West African arsenopyrite in contact with pyrite 90

Figure 57 Modal analysis results from point counting the four arsenopyrite types after twelve hours in ferric sulphate leach 6..... 96

Figure 58 Modal analysis results from point counting the four arsenopyrite types after one day in ferric sulphate leach 6..... 97

Figure 59 Modal analysis results from point counting the four arsenopyrite types after two days in ferric sulphate leach 6..... 98

Figure 60 Modal analysis results from point counting the four arsenopyrite types after four days in ferric sulphate leach 6..... 99

Figure 61 An example of an unusually strongly-zoned Klipwal arsenopyrite..... 105

Figure 62 The Klipwal arsenopyrite crystal after twelve days in ferric sulphate leach 7..... 105

Figure 63 BSE-image of Zandrivier arsenopyrite A28..... 106

Figure 64 Unleached Zandrivier arsenopyrite A28..... 107

Figure 65 Zandrivier arsenopyrite A28 after one day in ferric sulphate leach 7..... 107

Figure 66 Zandrivier arsenopyrite A28 after two days in ferric sulphate leach 7..... 107

Figure 67 Zandrivier arsenopyrite A28 after ten day in ferric sulphate leach 7..... 107

Figure 68 BSE-image of Zandrivier arsenopyrite A30..... 108

Figure 69 Zandrivier arsenopyrite A30 after six days in ferric sulphate leach 7..... 108

Figure 70 Zandrivier arsenopyrite A30 after eight days in ferric sulphate leach 7..... 109

Figure 71 BSE-image of Zandrivier arsenopyrite A47..... 109

Figure 72 Zandrivier arsenopyrite A47 after six days in bacterial leach 3..... 110

Figure 73 Zandrivier arsenopyrite A47 after two weeks in bacterial leach 3..... 110

Figure 74 BSE-image of Sheba arsenopyrite crystals A8 and A9..... 111

Figure 75 SE-image of the crystals after two weeks in ferric sulphate leach 7..... 111

Figure 76 Sheba arsenopyrite crystals A8 and A9 before leaching..... 112

Figure 77 Sheba arsenopyrite crystals A8 and A9 after two days in ferric sulphate leach 7..... 112

Figure 78 Sheba arsenopyrite crystals A8 and A9 after eight days in ferric sulphate leach 7..... 112

Figure 79 Sheba arsenopyrite crystals A8 and A9 after two weeks in ferric sulphate leach 7..... 112

Figure 80 BSE-image of Sheba arsenopyrite A11 showing the S-rich core and As-rich rim..... 113

Figure 81 SE-image of arsenopyrite A11 after two weeks in ferric sulphate leach 7. 113

Figure 82 Arsenopyrite A11 after four days in ferric sulphate leach 7..... 114

Figure 83 Arsenopyrite A11 after six days in ferric sulphate leach 7..... 114

Figure 84 West African twinned arsenopyrite G46 after one day in ferric sulphate leach 7..... 115

Figure 85 West African twinned arsenopyrite G46 after eight days in ferric sulphate leach 7..... 115

Figure 86 West African twinned arsenopyrite G46 after ten days in ferric sulphate leach 7..... 116

Figure 87 BSE-image of West African arsenopyrite crystals G47A and G47B showing pyrrhotite attached to the arsenopyrite..... 117

Figure 88 High-contrast BSE-image of the same field showing the two Co-rich arsenopyrite phases..... 117

Figure 88A Enlargement of the area shown in Figure 88..... 117

Figure 89 West African arsenopyrite G47A after three hours in ferric sulphate leach 7..... 118

Figure 90 West African arsenopyrite G47A after two days in ferric sulphate leach 7..... 118

Figure 91 West African arsenopyrite G47A after eight days in ferric sulphate leach 7..... 118

Figure 92 West African arsenopyrite G47A after two weeks in ferric sulphate leach 7..... 118

Figure 93 An enlarged post-leach SE-image of West African arsenopyrite G47A... 119

Figure 94 Schematic topographic scan across the line A–B shown in Figure 93..... 119

Figure 95 G48 West African arsenopyrite crystal..... 120

Figure 96 G48 West African arsenopyrite after three days in ferric sulphate leach 7 120

Figure 97 BSE-image of West African arsenopyrite G51 showing pyrrhotite attached to the arsenopyrite..... 121

Figure 98 High-contrast BSE-image of arsenopyrite G51 showing the Co-rich areas..... 121

Figure 99 West African arsenopyrite G51 after six days in bacterial leach 3..... 122

Figure 100 West African arsenopyrite G51 after two weeks in bacterial leach 3..... 122

Figure 101 BSE-image of a large, zoned Sheba pyrite..... 123

Figure 102 The appearance of the zoned pyrite after eight days bacterial leaching.... 123

Figure 103 The zoned Sheba pyrite after nine days in the bacterial leach..... 124

Figure 104 The zoned Sheba pyrite after ten days in the bacterial leach..... 124

Figure 105 BSE-image of G10 Sheba pyrite-arsenopyrite galvanic couple..... 125

Figure 106 G10 pyrite after five days in ferric sulphate leach 7..... 125

Figure 107 Zandrivier G37 pyrite-arsenopyrite galvanic couple after three days in bacterial leach 3..... 125

Figure 108 G37 pyrite-arsenopyrite after one week in bacterial leach 3..... 125

Figure 109 Topographic SE-image of an area of Zandrivier arsenopyrite in contact with pyrite..... 126

Figure 110 BSE-image of Sheba G3 gersdorffite in contact with pyrite..... 127

Figure 111 Photomicrograph of G3 Sheba gersdorffite before leaching..... 127

Figure 112 G3 gersdorffite after only three hours in bacterial leach 3..... 127

Figure 113 An area of West African pyrrhotite after twelve hours in ferric sulphate leach 7..... 128

Figure 114 Photomicrograph of Zandrivier chalcopyrite G25 in arsenopyrite before leaching..... 129

Figure 115 G25 after ten days in ferric sulphate leach 7..... 129

Figure 116 BSE-image of G1 Sheba tetrahedrite in contact with arsenopyrite..... 130

Figure 117 G1 tetrahedrite after two weeks in ferric sulphate leach 7..... 130

Figure 118 Photomicrograph of West African G45 sphalerite, chalcopyrite and pyrrhotite in contact before leaching..... 131

Figure 119 G45 after one hour in ferric sulphate leach 7..... 131

Figure 120 West African G46 pyrite, arsenopyrite, sphalerite and pyrrhotite intergrowth..... 132

Figure 121 West African G46 sulphide intergrowth before leaching..... 133

Figure 122 G46 after three hours in ferric sulphate leach 7..... 133

Figure 123 G46 after two days in ferric sulphate leach 7..... 133

Figure 124 G46 after twelve days in ferric sulphate leach 7..... 133

Figure 125 Unleached Zandrivier arsenopyrite in a quartz vein..... 134

Figure 126 Unleached Sheba arsenopyrite in quartz..... 134

Figure 127 BSE-image of Zandrivier G30 gold in arsenopyrite..... 135

Figure 128 G30 gold after ten days in ferric sulphate leach 7..... 135

Figure 129 SE-image showing the influence of particle size on the leach rate of Sheba arsenopyrite crystals during ferric sulphate leach 7..... 136

Figure 130 SE-image showing the influence of particle size on the leach rate of Sheba arsenopyrite crystals during bacterial leach 3..... 136

Figure 131 Leach channel development in Zandrivier arsenopyrite after six days in ferric sulphate leach 7..... 137

Figure 132 Leach channel development in Zandrivier arsenopyrite after six days in ferric sulphate leach 7 (2)..... 137

Figure 133 Leach channel formation in Klipwal arsenopyrite after two weeks in ferric sulphate leach 7..... 137

Figure 134 Leach channel formation in Zandrivier arsenopyrite after two weeks in ferric sulphate leach 7..... 137

Figure 135 Leach channel formation in West African arsenopyrite after two weeks in ferric sulphate leach 7..... 138

Figure 136 Leach channel formation in Sheba arsenopyrite after two weeks in ferric sulphate leach 7..... 138

Figure 137 Pores and channels in a strongly-zoned Sheba pyrite after two weeks bacterial leaching..... 139

Figure 138 Pores which formed in a weakly-zoned Sheba pyrite after two weeks in ferric sulphate leach 7..... 139

Figure 139 BSE-image of G46 West African pyrite and pyrrhotite after two weeks in ferric sulphate leach 7..... 139

Figure 140 Plot of averaged Δ(As/S) against the leach colour attained after four days in sterile leach 6..... 140

Figure 141 BSE-image of a typical Sheba arsenopyrite crystal before leaching..... 142

Figure 142 BSE-image of the same crystal after bacterial leaching for three weeks... 142

Figure 143 BSE-image of a residual Sheba arsenopyrite after two weeks bacterial leaching..... 143

Figure 144 X-ray map of elemental distribution in the partially-leached arsenopyrite 143

Figure 145 Balls of elemental sulphur which formed over Zandrivier arsenopyrite after two weeks in bacterial leach 3..... 144

Figure 146 Change in arsenopyrite reflectance at 589 mm as leach colours advance.. 146

Figure 147 Change in arsenopyrite reflectance at 546 mm as leach colours advance.. 146

Figure 148 Depth profile produced by sputtering into unleached arsenopyrite..... 148

Figure 149 Depth profile produced by sputtering into arsenopyrite leached for three days in As-saturated ferric sulphate solution..... 149

Figure 150 Depth profile produced by sputtering into arsenopyrite leached in ferric sulphate solution for three days..... 149

Figure 151 Depth profile produced by sputtering into arsenopyrite leached in ferric sulphate solution for one week..... 150

Figure 152 Corrected total arsenic in solution for the ferric sulphate leach tests on powdered Sheba and Zandrivier arsenopyrite..... 155

LIST OF TABLES

Table 1	Electron microprobe analysis conditions for arsenopyrite and gersdorffite	22
Table 2	Electron microprobe analysis conditions for pyrite	22
Table 3	Electron microprobe analysis conditions for pyrrhotite	24
Table 4	Detection limits in arsenopyrite	24
Table 5	Detection limits in pyrite, pyrrhotite and gersdorffite	24
Table 6	Reproducibility of microprobe analysis of arsenopyrite	25
Table 7	Zone analysis of arsenopyrite	26
Table 8	Sulphide minerals other than arsenopyrite analysed on the electron microprobe	26
Table 9	Ferric sulphate leach conditions	31
Table 10	Liquor sampling and analysis schedule for loose powder ferric sulphate leaches	32
Table 11	Bioleaching program	32
Table 12	Modal analysis of rock sections	40
Table 13	Modal sulphide analysis	41
Table 14	Gold inclusion distribution as determined on the image analyser	42
Table 15	Semi-quantitative gold analysis results	45
Table 16	Chemical analysis of the arsenopyrite HF concentrates	46
Table 17	ICP-MS analysis of arsenopyrite HF concentrates	47
Table 18	Possible source of ICP-MS elements	48
Table 19	Average trace element concentrations in arsenopyrite	58
Table 20	Distribution of the trace elements in the zoned arsenopyrite types	60
Table 21	Semi-quantitative microprobe analysis results for Sheba tennantite-tetrahedrite	61
Table 22	Average trace element concentrations in pyrite	62
Table 23	Average trace element concentrations in gersdorffite	62

Table 24 Average trace element concentrations in West African pyrrhotite..... 62

Table 25 Range of As atomic % and temperature of formation of arsenopyrite..... 70

Table 26 Range of pyrrhotite composition and temperature of formation..... 73

Table 27 Bacterial oxidation stages identified microscopically..... 76

Table 28 Definition of leach colours described for arsenopyrite..... 77

Table 29 Definition of leach colours described for pyrite and pyrrhotite..... 78

Table 30 pH and ORP variation during ferric sulphate leach 1..... 79

Table 31 pH and ORP variation during ferric sulphate leach 2..... 81

Table 32 pH and ORP variation during ferric sulphate leaches 3 and 4..... 84

Table 33 pH and ORP variation during ferric sulphate leach 5..... 84

Table 34 pH and ORP variation during bacterial leach 1..... 88

Table 35 pH and ORP variation during ferric sulphate leach tests 6a and 6b..... 93

Table 36 Modal analysis results from point counting from leach 6a..... 94

Table 37 Modal analysis from point counting results from leach 6b..... 95

Table 38 pH and ORP variation during bacterial leach tests 2 and 3..... 100

Table 39 pH and ORP variation during ferric sulphate leach tests 7 and 8..... 102

Table 40 Δ(As/S) factors for contacting compositional zones in Sheba, Zandrivier and West African arsenopyrite types..... 104

Table 41 pH and ORP variation during ferric sulphate loose crystal leaches 9 and 10..... 147

Table 42 pH and ORP variation during ferric sulphate leach 11..... 152

Table 43 pH and ORP variation during ferric sulphate leach 12..... 152

Table 44 Chemical analysis of Zandrivier and Sheba powder samples before and after ferric sulphate leaching..... 153

Table 45 Semi-quantitative XRF analysis of trace elements in Zandrivier and Sheba powder samples before and after ferric sulphate leaching..... 153

Table 46 Results of leach liquor chemical analysis during ferric sulphate leach 11. 154

Table 47 Results of leach liquor chemical analysis during ferric sulphate leach 12. 154

Table 48 Total arsenic in solution corrected for liquor removal during ferric sulphate leaches 11 and 12..... 154

Table 49 Variables affecting leach rate..... 158

APPENDIX TABLES

Table A1 Abbreviations used in the text..... 179

Table A2 Formulae of sulphide minerals..... 179

Table A3 Formulae of non-sulphide minerals..... 180

Table A4 Formulae of the more common leach products produced during the bacterial oxidation of arsenopyritic gold concentrates..... 180

Table A5 Arsenopyrite reflectance readings..... 181

Table A6 Homogeneity tests on As-2..... 186

Table A7 Homogeneity tests on ASP-1..... 188

Table A8 Random microprobe analysis of Klipwal arsenopyrite..... 190

Table A9 Random microprobe analysis of Zandrivier arsenopyrite..... 194

Table A10 Random microprobe analysis of Sheba arsenopyrite..... 198

Table A11 Random microprobe analysis of West African arsenopyrite..... 202

Table A12 Zone analysis of Klipwal arsenopyrite..... 206

Table A13 Zone analysis of Zandrivier arsenopyrite..... 207

Table A14 Zone analysis of Sheba arsenopyrite..... 211

Table A15 Zone analysis of West African arsenopyrite..... 216

Table A16 Quantitative analysis of Klipwal pyrite..... 221

Table A17 Quantitative analysis of Zandrivier pyrite..... 222

Table A18 Quantitative analysis of West African pyrite..... 224

Table A19 Quantitative analysis of Sheba pyrite..... 226

Table A20 Quantitative analysis of pyrrhotite..... 228

Table A21 Quantitative analysis of Sheba gersdorffite..... 230

Table A22 Klipwal arsenopyrite colour variation with time in leach..... 231

Table A23 Zandrivier arsenopyrite colour variation with time in leach..... 232

Table A24 West African arsenopyrite colour variation with time in leach..... 233

Table A25 Sheba arsenopyrite colour variation with time in leach..... 234

Table A26 Progress of pre-analysed sulphide minerals during ferric sulphate leach 7 and bacterial leach 3..... 235

1. INTRODUCTION

Over 490 tonnes of gold were produced from South African gold mines during 1997, and of this over ninety-five per cent was mined from free-milling Witwatersrand type ores. The balance was produced from refractory gold deposits (gold ores not directly amenable to cyanide leaching). As distinct from the situation in South Africa, refractory gold deposits are now the main source of gold production in many countries (GENKIN *et al.*, 1998). The distribution of refractory gold ores in Southern Africa is related to that of the Archaean host rocks, particularly greenstone belts, the highest tonnage being mined from the greenstones of the Barberton area, where it is produced from the Sheba, Fairview and New Consort Gold Mines.

An ore is classified as refractory if gold extraction is less than eighty per cent after fine grinding, as such a low yield is usually not economically viable (IGLESIAS & CARRANZA, 1993). Several factors may be responsible for refractory behaviour (ANHAEUSSER, 1976; SWASH, 1986): a) the ore deposit may contain cyanicides, such as certain sulphides, b) it may be carbonaceous, c) the size of the gold particles may be so small that they can not be liberated by fine milling, or d) gold can be present in a submicroscopic form in sulphide minerals.

A number of treatments have been developed to address the problem of small inclusions and submicroscopic gold in sulphide minerals, the most popular treatments being roasting, pressure leaching, and bacterial oxidation (WEIR & BEREZOWSKY, 1986, SWASH, 1988, AFENYA, 1991, IGLESIAS & CARRANZA, 1993). Each process has its advantages, but bacterial oxidation is becoming increasingly popular because of environmental considerations. In South African ores the most common sulphides to contain submicroscopic gold are arsenopyrite and arsenical pyrite. Both of these minerals contain arsenic, and process feeds commonly contain ten mass per cent, or more. Arsenic is a substance that is highly toxic to life in certain forms, especially as soluble oxides, hydrated oxides and arsine gas (AsH_3). As distinct from roasting, bacterial oxidation gives rise to negligible atmospheric pollution, and it consumes less energy than pressure leaching. Provided that strict process control is adhered to, arsenic may be removed as a stable solid waste product such as basic iron- or iron-calcium arsenates. The main limitations of bacterial oxidation are that it is a relatively slow

process, it is exothermic, requiring cooling water, and there is also an oxygen requirement. Research is underway to alleviate these problems.

The bacterial oxidation process involves the treatment of a sulphide flotation concentrate under acid conditions, where the reaction is catalysed by a mixed culture of bacteria, normally *Thiobacillus ferrooxidans, Thiobacillus thiooxidans* and *Leptospirillum ferrooxidans.* Ideally, the products of the reaction are sulphuric acid, ferric sulphate, stable ferric arsenate, and a solid arsenic-free concentrate, which, after neutralisation, can proceed to the cyanide leach.

The bacterial oxidation rate of a concentrate, and hence the rate of gold recovery, is frequently unpredictable, so laboratory scale amenability tests are an essential part of process planning. A mineralogical examination of the concentrate before oxidation trials begin is often helpful, but oxidation behaviour can differ between arsenopyrite deposits depending on the source of the ore. The research carried out in this study was initiated to address this problem, which, it should be noted, is not confined solely to the bacterial oxidation of gold ores, but to bacterial oxidation of sulphide-bearing ores in general.

2. AIM OF THIS STUDY

During 1991, bacterial oxidation amenability tests were performed at Mintek on sulphide concentrates from a number of refractory gold deposits. The relative leaching rate of the major gold-bearing sulphides was already established as arsenopyrite > arsenical pyrite > pyrite (NESTEROVICH, 1988, ATTIA & EL-ZEKY, 1990). There was also evidence that the presence of gold in arsenic-rich zones of compositionally zoned arsenopyrite accelerated the bacterial oxidation rate (CLAASSEN, 1991, MARION *et al.*, 1991). The oxidation behaviour within a sulphide mineral type, however, was still largely unpredictable, and remains so at the present time.

One arsenopyrite concentrate, from Zandrivier Prospect, near Eersteling, leached extremely slowly, and produced large amounts of arsenate precipitate, which effectively brought oxidation to a standstill. This precipitate was environmentally unacceptable, as it was not stable to dissolution over time such as would be required of arsenic in a mine effluent. The

arsenopyrite was claimed to produce a higher As^{3+}/As^{5+} ratio in solution than was normal, and this was said to inhibit bacterial activity. Subsequent investigation (ANDREWS & NEALE, 1994) identified the precipitate as zykaite ($Fe_4^{3+}(AsO_4)_3(SO_4)OH{\cdot}15H_2O$) and established that its formation was almost certainly due to the high arsenic content of the feed and hence in the leach liquor (the flotation concentrate contained 87% arsenopyrite).

The problem of the slow leaching rate for this, and many other arsenopyrite concentrates still remained, however, unsolved.

Under the bacterial oxidation conditions of the normal amenability test, too many variables are involved to allow assessment of the effect of sulphide composition. In this investigation an attempt has been made to remove as many variables as possible, firstly by the isolation of sulphide minerals from the other minerals present in the concentrates, and secondly, by removing the bacteria and running (sterile) acid ferric sulphate leach tests in a reactor, where physical and chemical conditions could be controlled and measured.

The use of sterile (inorganic) amenability tests to predict behaviour during bacterial oxidation of sulphide concentrates is now generally accepted for the bacterial oxidation of copper concentrates (NEALE *et al.*, 1996). The method is not usually employed, however, for gold-bearing ores.

The aim of this study, therefore, was to compare the acid ferric sulphate leaching behaviour of arsenopyrite from a number of different source areas, to establish if this is affected by the sulphide composition, and to evaluate whether the method gives a true reflection of oxidation behaviour in the presence of bacteria.

3. PREVIOUS WORK

Previous work which has been documented in the fields of arsenopyrite composition and oxidation is described below. A glossary of the abbreviations used in this work is presented in Table A1 (page 179). Similarly, the formulae of sulphide and non-sulphide minerals described in the text are listed in Tables A2 to A4 (pages 179–180).

3.1 Arsenopyrite composition

The major element composition of arsenopyrite varies in nature from $FeAs_{1.15}S_{0.8}$ to $FeAs_{0.9}S_{1.1}$ (KRETSHMAR & SCOTT, 1976). The compositional variation of naturally-occurring arsenopyrite was compiled from the existing literature (KLEMM, 1965), and it was deduced that most (but not all) analyses fell within a compositional field with boundaries of: 32–35 atm.% iron, 30–36 atm.% arsenic and 30–37 atm.% sulphur. A part of this variation, however, is likely to be due to analytical uncertainties.

Compositional zonation has been observed in both arsenopyrite and glaucodot ((Co,Fe)AsS) (PETRUK *et al.*, 1971), but optically zoned arsenopyrite is not necessarily compositionally zoned. Crystals of compositionally zoned S-rich arsenopyrite usually have S-rich centres and As-rich rims, whereas in As-rich types zonation is rarer, but reversed. Lack of compositional zonation in arsenopyrite may be due to very slow cooling rates during formation, or the existence of equilibrium growth conditions (LOWELL & GASPARRINI, 1982). The growth of sector zones has been shown to be related to resistance to growth in certain crystallographic directions, rather than to supersaturation of the ore forming solution (VESSELINOV & KERESTEDJIAN, 1995). Strong compositional zonation has also been described from synthetically-prepared arsenopyrite (FLEET & MUMIN, 1997).

Arsenopyrite frequently contains trace to minor amounts of cobalt, and there is no clear miscibility gap in the CoAsS – FeAsS solid solution. High-cobalt arsenopyrite is termed glaucodot, but authors vary in their definition of this mineral. Arsenopyrite containing more than 9 mass % of cobalt was defined as glaucodot (GAMMON, 1966) but other authors maintain that glaucodot should contain 19-24 mass % cobalt (IXER *et al.*, 1979).

Arsenopyrite equilibrated above 500° C is always As-rich (SHUEY, 1975). Arsenopyrite found with pyrite is always As-poor, with löllingite, As-rich. As-poor arsenopyrite should be a n-type semiconductor, even close to stoichiometric composition, but when As-rich, arsenopyrite should be p-type (KRETSCHMAR & SCOTT, 1976). Both p- and n-types can be present in one deposit, and even in one crystal. Cobalt and nickel substitution in arsenopyrite leads to arsenopyrite becoming n-type, whereas antimony has no obvious effect.

Trace elements first described in arsenopyrite were Ni, Bi, Sb, Au, Ag, Cu and Pb (DANA, 1944). Other trace elements occasionally found in arsenopyrite are Mn and Zn (MORIMOTO & CLARK, 1961). Kiryskoye arsenopyrite contains up to 0.02 mass % of both selenium and tellurium (SINDEEVA, 1964). The presence of selenium has also been confirmed, in levels of up to 35 ppm, in a variety of sulphide minerals from Australia and Canada (HAWLEY & NICOL, 1959, EDWARDS & CARLOS, 1954, both quoted by STANTON, 1973).

There is a fair amount of literature on the nature of trace gold in arsenopyrite, and its submicroscopic character. The range of gold content of arsenopyrite world-wide has been compiled (HENLEY, 1993) and the maximum amount of gold that can occur submicroscopically in natural arsenopyrite is defined as 1.5 mass % (DUNN & CHAMBERLAIN, 1997). The major parameters influencing the mode of occurrence of gold in auriferous sulphides are temperature of formation, rate of cooling, nature of post-depositional metamorphism, sulphide chemistry and solution chemistry. Gold can be incorporated into the lattice of pyrite or arsenopyrite at elevated temperatures, and later thermal events may cause migration of the gold to fractures or grain boundaries (SWASH, 1986, 1988). Temperature is not an essential factor in determining the form of gold in arsenopyrite, but rapid crystal growth under non-equilibrium conditions is the major factor producing gold-bearing arsenopyrite with a needle-shaped form (WU *et al.*, 1990).

Gold-bearing arsenopyrite, including material from Sheba, was investigated using techniques such as secondary ion mass spectrometry (SIMS), and high-resolution transmission electron microscopy (HRTEM) (CABRI *et al.*, 1989). Particulate gold was not detected even down to 'almost the atomic level', and was suspected to occur in clusters of atoms or in solid solution.

The ready acceptance of 'invisible' gold into arsenopyrite is related to its crystal chemistry (COOK & CHRYSSOULIS, 1990). Gold replaces excess arsenic, which occupies iron sites in arsenic-rich arsenopyrite.

Mössbauer spectroscopy was employed to investigate the nature of submicroscopic gold in Fairview arsenopyrite (FRIEDL *et al.*, 1994). Gold was found to be present in two forms – chemically bound in the lattice, and as a metallic gold-silver alloy. The chemically-bound gold was presumed to be trivalent.

In both naturally-occurring and synthetic gold-bearing arsenopyrite, gold is chemisorbed onto arsenopyrite from ore solutions at As-rich and Fe-deficient sites to form a metastable solid solution (FLEET & MUMIN, 1997). These authors, however, contend that the oxidation state of invisible gold in arsenopyrite is uncertain, and that gold is more likely to be present as Au^{0} or Au^{1+} than as Au^{3+}.

Of the four arsenopyrite types described in this study, two have been studied by previous workers. Klipwal arsenopyrite was described as being sulphur-rich and not compositionally zoned (RUSSELL, 1985). No significant difference was found between the composition of the gold-bearing and non-gold-bearing arsenopyrite.

The composition of Sheba arsenopyrite has been well documented. (SCHOUWSTRA & DE VILLIERS, 1988, CABRI *et al.*, 1989, SCHOUWSTRA, 1990, CLAASSEN, 1991). Sheba arsenopyrite is, on average, sulphur-rich and contains submicroscopic gold to levels of up to 0.5 atm. % (SCHOUWSTRA & DE VILLIERS, 1988). The majority of the arsenopyrite crystals are compositionally zoned, with a variation of arsenic content of up to 6 atm. %. Gold is associated with As-rich, S-poor zones, and antimony with S-rich, As-poor zones (CLAASSEN, 1991).

3.2 Inorganic arsenopyrite oxidation

Previous work on the inorganic (non-bacterial) oxidation of arsenopyrite has been documented in the fields of sterile leaching (*e.g.* sulphate (BREED *et al.*, 1997) chloride (FERNANDEZ *et al.*, 1996, LINGE & WELHAM, 1997) and nitrate (BJORLING & KOLTA, 1965) oxidation, electrochemical leaching (LINGE & WELHAM, 1997), pressure leaching (WEIR & BEREZOWSKY, 1986, KOSLIDES *et al.*, 1992), and weathering (NESBITT *et al.*, 1995).

A number of techniques have been used to investigate sulphide surface oxidation, including reflectance, staining, pore density, X-ray photoelectron spectroscopy (XPS), and Auger electron spectroscopy (AES). Many authors rely on the measurement of species concentration in leach solutions. All this work is described in more detail below.

The reflectance of the surface of an oxidised arsenopyrite will be affected by the character of the oxidised phases covering it, and the final reflectance is consistently proportional to the oxidation depth as determined by AES (RICHARDSON & VAUGHAN, 1989).

When pyrite and arsenopyrite are treated with a stain solution of $KMnO_4$ in 1:1 H_2SO_4 it is possible to distinguish crystal orientation, zonation and twinning by colour (FLEET *et al.*, 1993). It can be shown, by XPS, that the surface layer causing the interference colours is elemental sulphur. The resulting colours are analogous to the first-order colours of optical interference, requiring a sulphur film thickness of only around 0.2μm, but these will eventually alter or fade upon exposure to air.

Arsenopyrite is stable in air and water at room temperature (RICHARDSON & VAUGHAN, 1989). This assumption was challenged by later authors (see below). Arsenopyrite was exposed to air, steam, ammonium hydroxide, hydrogen peroxide, sulphuric acid, and electrochemical leaching. Results showed that of these, the sulphuric acid was the only agent to produce As^{5+} as well as As^{3+} species on the surface. This may be due to the low pH, since the stability field of As_2O_5 is limited to low Eh and high pH (RICHARDSON & VAUGHAN, 1989).

An investigation of arsenopyrite weathering provided XPS data on surface speciation after oxidation in air and in distilled water (NESBITT *et al.*, 1995). After 8 hours in distilled water, the dominant Fe surface species was a ferric oxyhydroxide, and arsenic was present as As^{5+}, As^{3+}, As^{1+} and As^{1-}. Sulphate was also detected. The authors claim that, in air, arsenic is the most readily oxidised species, and sulphur the slowest. In water arsenic and iron are fastest, sulphur still slowest. AES shows As to diffuse from the interior of the mineral to the surface during oxidation. Large amounts of As^{3+} and As^{5+} are produced in the near-surface zone and are leached selectively as arsenites and arsenates.

N-type sulphides behave as reducing agents, and p-type sulphides as oxidising agents (NESTEROVICH, 1988). During the electrochemical oxidation of arsenopyrite in dilute hydrochloric acid, however, no obvious difference in leaching rate for stoichiometric (ideal formula), non-stoichiometric S-rich/n-type or non-stoichiometric As-rich/p-type arsenopyrite was detected (FERNANDEZ *et al.*, 1996). The ratio of Fe:As:S species produced in solution was also independent of arsenopyrite composition. These authors describe the surface

conversion to an oxidised metal-deficient sulphide phase in air or solution – As and Fe were removed first, and there was an increase in oxidation rate with time. The high experimental activation energy, the influence of electrode potential, and pH, all suggested that the oxidation rate was controlled by a surface reaction, not diffusion. Factors increasing the rate were increasing temperature, electrode potential, and lower pH.

There are a number of papers in the literature which refer to the influence of sulphide mineral electronic structure upon leaching behaviour (see below), but no reference to arsenopyrite has been found. This may be due to the uncertainty of the arsenopyrite electron structure (FERNANDEZ *et al.*, 1996).

Models were developed for pyrite, chalcopyrite, covellite, chalcocite, sphalerite and galena using molecular orbital and band theory to predict leach behaviour (VAUGHAN, 1984). The results were then tested practically using spectroscopic methods, including XPS, and the predictions were found to be satisfactory.

The influence of electronic structure on the anodic dissolution and leaching behaviour of semiconducting sulphides has been elucidated using energy level models and semiconductor electrochemistry (CRUNDWELL, 1988). Again the work was mainly carried out on base metal sulphides, but since arsenopyrite is a semiconductor, its electronic configuration will certainly influence leaching behaviour to some degree.

Very little mention has been made of ferric sulphate leaching in the literature, except as the part it plays in the bacterial leaching process (see section 3.3)

The equation describing the ferric leaching of arsenopyrite can be written as:

$$FeAsS + 5Fe^{3+} \rightarrow S^0 + As^{3+} + 6Fe^{2+}$$

(BREED *et al.*, 1997).

Arsenopyrite and pyrite from the Sheba and New Consort Mines were leached in ferric sulphate solutions of various concentrations, and compared with bacterial oxidation experiments. Post-leach SEM examination showed minimal attack, mainly at crystal edges, and as small 'etch pits' along cracks. No selective chemical attack on different compositional

zones in Sheba arsenopyrite was observed, and the author concluded that this must be a feature solely of bacterial oxidation (CLAASSEN, 1991).

The reaction rate of pyrite oxidised with ferric iron is dependent on the square root of the ferric iron concentration in solution (MCKIBBEN & BARNES, 1986). The reaction rate of arsenopyrite leached in ferric sulphate solution is proportional to the solids content (the mass % of solid material in the leach liquor) (BARRETT *et al.*, 1990). Only 1% of the dissolved arsenic is present as As^{5+}.

The leaching rate of arsenopyrite in ferric sulphate solution is more likely to be a function of the redox potential than of the absolute ferric ion concentration. (BREED *et al.*, 1997). No leaching of arsenopyrite takes place in the absence of Fe^{3+}. An excess of ferric ions, however, may cause passivation of the mineral surface due to ferric arsenate precipitate formation. At certain pH levels, arsenopyrite oxidation, As^{3+} oxidation to As^{5+}, and arsenate precipitation all become competing reactions in the system. The pH was not controlled (or measured, apparently) but the precipitation of ferric arsenate suggests that $pH \geq 2.0$.

Previous work on the aspects which ferric sulphate and other forms of inorganic leaching have in common with bacterial oxidation will be discussed in the following section.

3.3 Bacterial oxidation of arsenopyrite

The addition of bacteria to a sterile arsenopyrite oxidation system catalyses oxidation to a varying degree, depending on initial chemical conditions and also the species, abundance, and motility of the bacteria. At 1–2% solids and pH 1.0, a six-fold increase in oxidation rate relative to identical conditions without bacteria, has been estimated (BARRETT *et al.*, 1990).

The bacteria involved are said to be chemolithotropic ('rock-eating') – they obtain energy from the oxidation of metals and ores – and autotrophic, which means that they synthesise cell tissue from carbon dioxide. The best known of these bacteria is *Thiobacillus ferrooxidans*, a species which thrives in warm, acidic environments and is able to oxidise ferrous iron and sulphur. Another species, *Thiobacillus thiooxidans*, can oxidise sulphur (BRIERLEY, 1982). The third bacterial species normally present in commercial bacterial oxidation systems is *Leptospirillium ferrooxidans*, which oxidises only iron. The relative populations of the three

populations of the three bacterial species varies naturally from batch tests to continuous pilot plant runs, and depends on sulphur concentration (LAWSON, 1997).

Outside the natural situation, nutrient salts, oxygen, and carbon dioxide must be added to bacterial oxidation liquors so that the bacteria can thrive, reproduce, and oxidise sulphide minerals effectively.

Bacteria oxidise sulphide minerals by direct attachment to the surface, and also by indirect oxidation by free bacteria in solution (see below). The ease, or preference, of attachment has recently been shown to be pyrite > pyrrhotite > chalcopyrite > arsenopyrite (OHMURA & BLAKE, 1997). Bacteria attach themselves to the surface of sulphide minerals using excreted exopolymers. The organic film is gradually thickened until it forms a biofilm with an enclosed mini-environment with controlled pH, dissolved oxygen, and chemical species content (GEESEY, 1997, LITTLE *et al.*, 1997).

The effect of the bacteria is invariably catalytic. Almost twice as much arsenic was dissolved from arsenopyrite in an aqueous system when bacteria were added, but iron dissolution was virtually unaffected (EHRLICH, 1964). During the electrochemical oxidation of arsenopyrite in ferric sulphate solution with and without bacteria, the bacteria accelerate arsenopyrite dissolution by preferential attachment to the sulphide surface, which decreases the charge transfer resistance (ZHANG *et al.*, 1996).

The overall reaction for the bacterial oxidation of arsenopyrite can be represented as :

$$2FeAsS + 7O_2 + 2H_2O \rightarrow 2FeAsO_4 + 2H_2SO_4$$

(ANDREWS & NEALE, 1995).

The various sub-reactions which take place are thought to be either direct or indirect (PINCHES, 1975, TAXIARCHOU *et al.*, 1994, MONROY FERNANDEZ *et al.*, 1995, BREED *et al.*, 1997, HACKL & JONES, 1997). Direct oxidation involves attachment of the bacteria to the sulphide surface, and may be a reaction between the cell envelope and the mineral surface. The iron is oxidised from ferrous (Fe^{2+}) to ferric (Fe^{3+}), which, with sulphate, diffuses away from the surface. Indirect oxidation takes place close to, but not on, the mineral surface, and involves the oxidation of the sulphide by ferric ions, and the oxidation of sulphur within a bacterial microenvironment. This microenvironment forms just above the leaching sulphide

surface. It may vary from a protein monolayer to hundreds of microns in depth, and is often referred to as a *biofilm* (GEESEY, 1997, LITTLE *et al.*, 1997).

Authors differ as to the relative importance of the direct and indirect mechanisms. Some workers claim that, specifically in the case of arsenopyrite oxidation, the indirect mechanism predominates (see below).

The major reactions which take place in solution during the bacterial oxidation of arsenopyrite are:

Direct mechanism

$$4FeAsS + 13O_2 + 6H_2O \rightarrow 4Fe^{2+} + 4SO_4^{2-} + 4H_3AsO_4 \quad \textit{(bacterial)}$$

$$4Fe^{2+} + O_2 + 4H^+ \rightarrow 4Fe^{3+} + 2H_2O \quad \textit{(bacterial)}$$

Indirect mechanism

$$2FeAsS + 6O_2 + 4H_2O + 2Fe^{3+} \rightarrow 4Fe^{2+} + 2SO_4^{2-} + 2H_3AsO_4 + 2H^+ \quad \textit{(non-bacterial)}$$

(TAXIARCHOU *et al.*, 1994)

In practice, elemental sulphur is also produced by the chemical reaction of arsenopyrite with ferric iron, but it is not stable in a bacterial medium (KARAVAIKO *et al.*, 1986). While ferrous sulphate is being oxidised to ferric sulphate by *T. ferrooxidans,* elemental sulphur is oxidised by *T. thiooxidans:*

$$2S^0 + 3O_2 + 2H_2O \rightarrow 2SO_4^{2-} + 4H^+$$

Depending on the solution composition and acidity, arsenates, ferric sulphates, iron hydroxides and jarosite may precipitate during bacterial oxidation. The formulae of the more common leach products are given in Table A4 in the Appendix (page 180).

The reactions which take place during bacterial oxidation of arsenopyrite are shown schematically in Figure 1 below.

Certain authors further distinguished between the oxidation reactions of p- and n-type arsenopyrite –

p-type arsenopyrite

$$16FeAsS + 51O_2 + 26H_2O \rightarrow$$
$$12Fe^{3+} + 4Fe^{2+} + 8H_3As^{V}O_4 + 8H_2As^{V}O_4^- + 4H_2SO_4 + 12SO_4^{2-} + 4H^+ + 16e^-$$

n-type arsenopyrite

$$4FeAsS + 9O_2 + 10H_2O \rightarrow 4Fe^{2+} + 2SO_4^{2-} + 2HAs^{III}O_2 + 2H_3As^{V}O_4 + 2HSO_4^{-} + 10H^{+} + 12e^{-}$$

(KARAVAIKO *et al.*, 1986).

These authors also suggest that bacterial oxidation of p-type arsenopyrite should give rise only to pentavalent arsenic products, whereas n-type arsenopyrite would produce a mixture of trivalent and pentavalent arsenic.

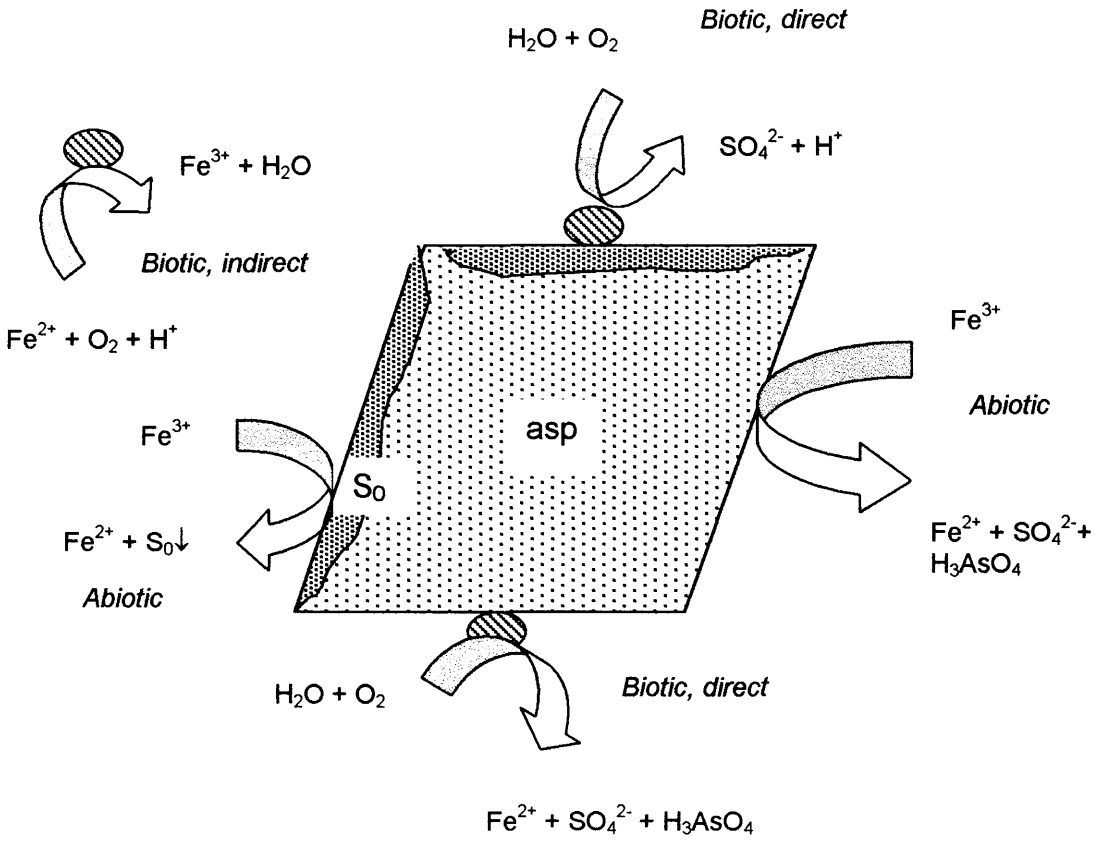

Figure 1. Schematic diagram of indirect and direct bacterial leaching of arsenopyrite, as well as bacterial sulphur oxidation, adapted from FREE *et al.* (1993). The ovals represent bacteria. The involvement of CO_2, nutrients, and bacterial reproduction has not been included for the sake of simplicity. All ions in solution will be aqueous.

Three stages can be distinguished in the bacterial oxidation of arsenopyrite (FERNANDEZ *et al.*, 1996) :

1. The growth and adhesion of bacteria on to the mineral surface enhancing direct bacterial oxidation and solubilisation of Fe^{2+}, As^{3+} and S^{6+}, and the formation of superficial

elemental sulphur. The high concentration of ferrous iron in solution subsequently encourages the growth of non-attached bacteria.

2. The large number and high activity of non-attached bacteria allow oxidation of Fe^{2+} to Fe^{3+} and As^{3+} to As^{5+}. The ferric ions so produced can oxidise both As^{3+} and sulphides. This causes the high reaction rate stage where direct oxidation is accelerated by adhering bacteria, and indirect chemical oxidation is accelerated by the ferric ions generated by the non-attached bacteria.
3. During the third stage the increasing concentration of As^{5+} and Fe^{3+} in solution leads to precipitation of ferric arsenate on the arsenopyrite surface which passivates the surface and reduces indirect chemical oxidation.

It is felt that the indirect chemical oxidation may in fact predominate during the second and third stages of the reaction (FERNANDEZ *et al.*, 1996).

A 'lag phase' is commonly experienced at the beginning of a bacterial oxidation operation; this is due to the establishment of bacterial activity and growth after inoculation. The lag phase in arsenopyrite oxidation is due to a delay in the attachment of bacteria to the mineral surface which is now thought to be caused by the formation of a thin layer of As_2S_2 (similar to realgar) on the surface of arsenopyrite (LAZARO *et al.*, 1997).

Too much arsenic in solution can be toxic to the oxidising bacteria, which then become less active. The relative toxicity of As^{3+} to As^{5+} was once considered always to be in the region of 3:1, but this has recently been queried. The toxicity is now thought to also be dependent on the availability of an energy source, such as oxygen (BREED *et al.*, 1996).

The release of gold during bacterial oxidation is due not only to the release of tiny inclusions after sulphide dissolution, but to the reduction of trivalent chemically-bound gold to the metallic state (FRIEDL *et al.*, 1994).

A number of authors have described pit and pore formation in arsenopyrite and pyrite during both bacterial and ferric sulphate leaching (HILTUNEN *et al.*, 1981, KELLER & MURR, 1982, LAZER *et al.*, 1986, MARION *et al.*, 1991, CLAASSEN, 1991, FERNANDEZ *et al.*, 1995). Although oxidation of pyrite frequently leads to pore formation parallel to the crystallographic axes of the mineral, the picture is not so clear with arsenopyrite. Ferric sulphate leaching of arsenopyrite produces no pores (FERNANDEZ *et al.*, 1996), but small

etch pits along cracks (CLAASSEN, 1991). Bacterial leaching gives rise to ovoid pits related to crystal orientation (FERNANDEZ *et al.*, 1996), to channels along crystallographic axes (CLAASSEN, 1991), and along screw dislocations in the arsenopyrite crystal (MARION *et al.*, 1991). However some authors claim that there is no conclusive crystallographic control on pores produced in bacterially-leached arsenopyrite (LAZER *et al.*, 1986). In fact it is difficult to distinguish the action of bacterial or non-bacterial forces during pore formation, and other structurally-related attack during bacterial leaching (GEESEY, 1997).

The sites of pore formation may be structurally or compositionally-controlled. Prime sites of oxidative attack are crystal defects such as dislocations, stacking faults, grain boundaries, lattice vacancies, and related areas of crystal strain (BANFIELD & HAMERS, 1997). Crystal strain may also be caused by substitution of foreign atoms in the lattice (CLAASSEN, 1991, CLAASSEN *et al.*, 1993, GEESEY, 1997).

Pitting tends to be concentrated in the As-rich areas of compositionally-zoned arsenopyrite (MARION *et al.*, 1991, CLAASSEN, 1991). As bacterial oxidation of arsenopyrite proceeds, the arsenic-rich zones are selectively leached in preference to the sulphur-rich zones (MARION *et al.*, 1991, MONROY *et al.*, 1993, ANDREWS & NEALE, 1994).

The processes involved in the dissolution of sulphide minerals are physical, chemical and electrochemical, with the electrochemical path now being considered the most important (BALLESTER *et al.*, 1990). Electrochemical oxidation of arsenopyrite in ferric sulphate solution, with and without bacteria, has been compared (ZHANG *et al.*, 1996). Even though the dissolution rate was diffusion-controlled, the rate-determining step was electrochemical, involving the first electron transfer during the reduction of surface-absorbed oxygen. This is also the controlling step in pressure leaching of arsenopyrite.

The order in which co-existing sulphide minerals will be oxidised is determined by the electrode potential in solution. It is possible to predict, therefore, which sulphide in a mixed system will be oxidised first. The existence of n- and p-types of certain sulphides such as pyrite and arsenopyrite can complicate the issue, and separate electrode potentials should be considered (NESTEROVICH, 1988). In addition, although pyrite is usually less reactive than arsenopyrite, pyrite which occurs in coal reverses the trend, apparently because of its morphology and lattice imperfections (LINGE & WELHAM, 1997).

When two or more sulphide minerals are in contact during oxidation, a phenomenon known as galvanic interaction may occur. The minerals form a galvanic couple where the sulphide with the higher and more negative rest potential will be leached preferentially, frequently at a faster rate than if it had been isolated in solution, transferring electrons to the more noble sulphide (BALLESTER *et al.*, 1992, HOLMES & CRUNDWELL, 1995). During bacterial oxidation, the same eletrochemical sequence and galvanic effects are observed, but the rates are enhanced (MEHTA & MURR, 1983, KWONG *et al.*, 1995, quoted by NORDSTROM & SOUTHAM, 1997).

Passivation of the surface of arsenopyrite by precipitation can occur during ferric sulphate or bacterial oxidation, frequently due to lack of control of solids content of the leach liquor and pH. The most common precipitates are elemental sulphur, jarosite, and various iron arsenates and sulpharsenates. Researchers differ as to the degree of passivation caused by precipitates. A thick layer of α-sulphur was produced on the arsenopyrite surface, as well as an 'arsenate' precipitate, but neither of these reduced the reaction rate (ZHANG *et al.*, 1996). Ferric arsenate precipitates *did* passivate arsenopyrite, by limiting chemical oxidation (FERNANDEZ *et al.*, 1995, BREED *et al.*, 1997). As mentioned earlier, hydrated iron sulpharsenate precipitates consisting mainly of zýkaite were found to passivate Zandrivier arsenopyrite during bacterial leaching (ANDREWS & NEALE, 1994). Jarosite has been found to passivate pyrite and other sulphides during bacterial oxidation (BOON & HEIJNEN, 1993).

A number of workers have described the effect of sulphur layer formation on the leaching rate of chalcopyrite. It seems that in this case layers of differing porosity can form, the less porous reducing reaction rate drastically, but the more porous having virtually no effect (MILLER & PORTILLO, 1979, BOON & HEIJNEN, 1993). The same is likely to hold true for arsenopyrite.

Various agents catalyse both ferric sulphate and bacterial oxidation of sulphide minerals. These include light, galvanic interactions and the addition of certain foreign ions to the leach solution. Light and UV radiation have a catalytic effect on sphalerite and galena oxidation (VAUGHAN, 1984). The radiation enhances conductivity among semiconducting sulphide minerals. Illumination also enhances galvanic interaction effects (HOLMES & CRUNDWELL, 1995). Certain metal ions have a catalytic effect on the rate of leaching sphalerite and chalcopyrite, during sterile and bacterial leaching (BALLESTER *et al.*, 1990, 1992,

ESCUDERO *et al.*, 1993). The leaching rate can be increased by the addition to solution of catalytic ions such as Ag^{+}, Hg^{2+}, Bi^{3+} and Co^{2+}. These ions substitute for surface layer metal ions and increase the conductivity, which boosts dissolution. Impurities in solid solution, as well as ions in solution, catalyse leaching. They influence the kinetics by modifying the electron transfer speed.

Silver, in particular, is a strongly catalytic ion. This may be because it prevents the formation of passivating jarosite (BOON & HEIJNEN, 1993), because it increases the porosity of the jarosite layer (SUKLA *et al.*, 1990), or because it forms a conducting medium (of Ag_2S) in elemental sulphur layers (MILLER & PORTILLO, 1979, GOMEZ *et al.*, 1997). The fact that silver ions also catalyse bacterial sulphide oxidation is curious, as very small amounts of silver in solution have been shown to be toxic to *T. ferrooxidans* (NORRIS & KELLY, 1978, DE *et al.*, 1997). The surfaces of sulphide minerals, however, have a strong affinity for dissolved metals (AL *et al.*, 1997), and the catalytic ion concentration is very low. The silver in solution disappears very quickly, by attaching itself to the solid surface as silver sulphide. This effectively removes any toxic bacterial reaction from the system (ESCOBAR *et al.*, 1997).

4. SOURCE AND GEOLOGICAL SETTING

The source locations of the three South African arsenopyrite types are shown in Figure 2.

Klipwal Gold Mine is situated 80 km south-east of Piet Retief, and overlooks the Pongola River. The mine has been worked intermittently since 1898. The gold occurs in Archaean rocks of the Pongola Sequence, in a sedimentary suite of phyllites, schists and quartzites, with gold mineralisation being closely associated with the Klipwal Fault or shear zone (RUSSELL, 1985).

Sheba Gold Mine is located 12 km north-east of Barberton, and has been in operation since 1886, two years after Edwin Bray, a Yorkshire coal miner, discovered gold in the Sheba hills (WAGENER & WIEGAND, 1986). Arsenopyrite, pyrite, and associated gold occur in meta-greywackes and in green quartz-carbonate-sericite schists (SCHOUWSTRA & DE VILLIERS,

1988). The arsenopyrite-rich rock investigated in this research was sampled from a meta-greywacke in the Main Reef Complex (MRC), at the 24th level of Sheba Mine.

Figure 2. The locations of Zandrivier Prospect, and Sheba and Klipwal Gold Mines in the north and east of South Africa.

The Zandrivier Prospect is situated in the Pietersburg greenstone belt, in the Mont Mare area, forming part of what was once known as the Marabastad Gold Field (WILLEMSE, 1938, HAMMERBECK, 1976, HAMER, 1991). The prospect was worked sporadically in the first half of the century. Sampling shafts were sunk in the area in 1990, from which the material for this research was collected. More recently, an adit has been blasted into the *koppie* and the deposit is being mined under license by Eersteling Gold Mine – South Africa's oldest operating gold mine, founded in 1872, and located 30 km south-west of Zandrivier. The material currently being mined does not bear a strong resemblance to the sampling shaft material, so any correlation of the mineralogy or arsenopyrite type with presently mined ore should be made with caution. The arsenopyrite at Zandrivier occurs in pods associated with quartz veins, fine-

grained quartz-tourmaline intergrowths, and chert bands. A zone of sulphide mineralisation runs in an east-west direction and is locally more rich in pyrrhotite than in arsenopyrite.

The West African arsenopyrite sample was taken during a prospecting drive. No information on the geology of the source area can be disclosed, but the deposit is not currently being mined.

5. EXPERIMENTAL TECHNIQUES

The samples were received as three rock samples and one crystal sample, presumably a HF concentrate. The Sheba rock sample weighed 340 g, but was unusually rich in arsenopyrite. The sample of West African weighed 45 g, and the sample of Zandrivier rock weighed approximately 20 kg. The crystals from Klipwal Mine weighed approximately 20 g.

To summarise the analytical procedures: after a mineralogical examination of the rock samples, the arsenopyrite crystals were extracted, and subjected to further mineralogical and chemical analyses. The quantitative analyses of major and trace elements in a number of particles were determined on the electron microprobe (EMP). The arsenopyrite particles were then leached in acid ferric sulphate solution to compare the relative oxidation rates of the four types, and bacterially leached to compare sterile and bacterial leaching methods. The arsenopyrite crystals were monitored under an ore microscope during leaching, and post-leach residues were examined using the electron microprobe and Auger Electron Spectroscopy (AES). Loose powder samples of Zandrivier and Sheba arsenopyrite HF concentrates were leached in ferric sulphate solution, and the liquor was analysed to determine the arsenic dissolution and the ratio of As^{3+} to As^{5+} in solution.

These techniques are described in more detail below.

5.1 Analytical and mineralogical techniques

A number of different mineralogical, chemical and surface science techniques were employed.

5.1.1 X-ray powder diffraction (XRD)

Samples of the Sheba, Zandrivier and West African ore were ground in the Siebtechnik vibratory mill followed by the McCrone micronising mill to reduce particle size to 75% passing 10 μm, the size required for good XRD resolution. The powders were then X-rayed on the Phillips PW1140 X-ray Diffractometer. XRD was used mainly as a complementary technique. No significant differences in the symmetry of the four arsenopyrite types was detected in powdered concentrates, and single crystal work is outside the scope of this study.

5.1.2 Section preparation

Polished sections were prepared of rock sections, and composite polished sections were prepared for leaching, where all four types of arsenopyrite were incorporated into one section (Figure 3). Later, similar composite sections were made up of crystals milled and screened to 38–150 μm, when it became evident that crystal size was affecting the leach rate.

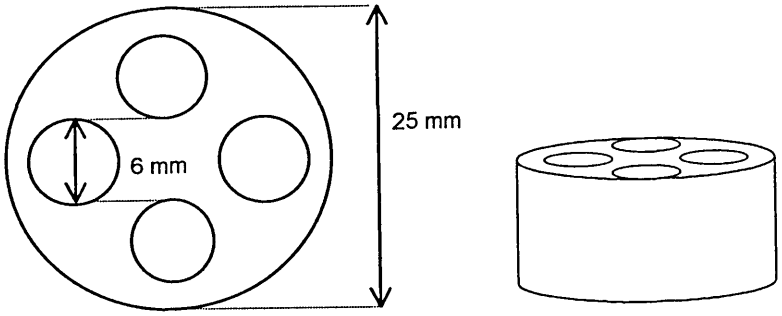

Figure 3. Diagram showing the dimensions of a composite polished section. A blank section is made from epoxy resin, and four holes drilled out. The powdered samples are mixed with resin, poured into the holes, and allowed to set. Finally, the section is ground and polished in the normal manner.

5.1.3 Isolation of the arsenopyrite

The rock samples were not milled, to avoid breaking up the crystals, but they were cut into one-inch cubes with a diamond saw so that leaching would not be excessively time-consuming. Arsenopyrite crystals were leached out of the host rock using the Neuerburg method (NEUERBURG, 1975). This involved digestion of the rock cubes in 52% technical grade hydrofluoric acid, with acid replacement every week, for four to six weeks (the

presence of carbonate extends the leaching time). Solid residues were then digested in 2M dibasic ammonium citrate for six hours, soaked in hydrofluoric acid overnight, and in 1M aluminium chloride solution for another six hours. The last two steps were repeated several times to remove all the fluorides which had formed.

This method preserves arsenopyrite, pyrite, sphalerite, chalcopyrite and gold, but pyrrhotite and galena are dissolved.

5.1.4 Image analysis

Modal analysis of sulphide minerals and gold deportment was performed using the Cambridge Morpho-chemical Analysis System. This incorporates a Quantimet 570 image analyser integrated with a Stereoscan 360 scanning electron microscope (SEM) and a LINK AN100000 energy dispersive X-ray spectroscopy (EDS) analyser at Mintek. Using this system, gold particles are initially located due to their high back-scattered electron intensity, then the composition is checked by EDS analysis to discriminate minerals such as galena. The coordinates and dimensions of the gold particles are stored, so that the operator can go back and check association and shape if required. Modal sulphide analysis uses back-scattered electron intensity to separate sulphide and gangue minerals, and then runs grid analyses similar to point counting to determine the relative proportion of the sulphides. The theory and applications of image analysis are dealt with in the literature (*e.g.* OOSTHUYZEN, 1983, 1987).

Four rock sections each from the Zandrivier, West African and Sheba ores were submitted for sulphide modal analysis and gold search. The sections were not of concentrates and insufficient sections were scanned to produce statistically representative results according to the grade of the material, but the gold search results serve to give some idea of the gold deportment in the ores. The Sheba and West African rock samples were relatively fine-grained, and of even texture, so the modal sulphide analyses should be reasonably accurate. The Zandrivier rock, however, was coarse-grained and varied in content from massive sulphide to large quartz-tourmaline veins. The modal analysis results are therefore not likely to be very meaningful, and for this reason a modal analysis of a run-of-mine (ROM) Zandrivier sample was also included. Obviously, the Klipwal material was not submitted for image analysis as no rock sections or concentrates were available.

Point counting on leached composite sections of ground arsenopyrite crystals was the method chosen for modal analysis of leach colours. The reason for point counting was that the image analyser was only able to distinguish between three colours, but the human eye could distinguish seven. Eight hundred points per arsenopyrite type were counted, *i.e.*, 3200 points per composite section, and five composite sections were measured per leach (see below).

5.1.5 Reflectance

The reflectance of arsenopyrite before, during and after leaching was determined using the Leitz MPV microscope photometer with a WTiC standard, and 546 mm (Hg) and 589 mm (Na) filters. Standard methods of reflectance determination are described in the literature (CAMERON, 1961, PILLER, 1977, JONES, 1987).

5.1.6 Electron microprobe analysis

Electron microprobe (EMP) instrumentation and applications have been described by various authors (RUCKLIDGE, 1976, VILJOEN & JOHNSON, 1983, GOLDSTEIN *et al.*, 1981, REED, 1996).

All the quantitative wavelength-dispersive X-ray spectroscopy (WDS) analysis, most of the energy-dispersive X-ray spectroscopy (EDS) analysis, and the back-scattered electron imaging of pre- and post-leach samples in this research were performed at Mintek on a JEOL 733 Superprobe with four WDS spectrometers, a light element EDS detector for simultaneous determination of all elements heavier than boron, and an integrated NORAN Voyager 3 WDS/EDS software system.

The analysis conditions and standards that were chosen for the quantitative major and trace element WDS analysis of arsenopyrite, gersdorffite, pyrite and pyrrhotite are shown in Tables 1 to 3, and the detection limits of the trace elements are shown in Tables 4 and 5.

Wherever possible, the accelerating voltage was set at 15 kV. It is common to use higher voltages for trace element measurement, but although this reduces the detection limit, it also excites X-rays from a larger volume of sample (as shown in the Proza curves in Figure 4). In

some arsenopyrite, notably from Sheba, compositional zonation was known to be extremely fine, so a low accelerating voltage of 15 kV was selected. Beam current was usually set at 30 nA, except during homogeneity tests on standards where 50 nA was selected.

TABLE 1

ELECTRON MICROPROBE ANALYSIS CONDITIONS FOR ARSENOPYRITE AND GERSDORFFITE

Element	X-ray line	Accelerating Voltage (kV)	Crystal	Peak Measurement Time (sec)	Standard formula
S	Kα	15	PET	100	FeAsS
Mn	Kα	15	LIF	150	Mn
Fe	Kα	15	LIF	100	FeAsS
Co	Kα	15	LIF	150	Co_9S_8
Ni	Kα	15	LIF	150	NiS
Cu	Lα	15	TAP	200	$CuFeS_2$
Zn	Lα	15	TAP	200	ZnS
Ge	Lα	15	TAP	200	Ge
As	Lα	15	TAP	100	FeAsS
Se	Lβ	15	TAP	200	CuSe
Ag	Lα	15	PET	200	Au-Ag alloy
Cd	Lα	15	PET	200	CdS
Sn	Lα	20	PET	200	Sn-Pd-Pt alloy
Sb	Lα	15	PET	200	Sb_2S_3
Te	Lα	15	PET	200	$FeTe_2$
Au	Mα	15	PET	200	Au-Ag alloy
Hg	Lα	20	PET	200	HgS
Pb	Mα	15	PET	200	PbS
Bi	Mβ	15	PET	200	$AgBiS_2$

TABLE 2

ELECTRON MICROPROBE ANALYSIS CONDITIONS FOR PYRITE

Element	X-ray line	Accelerating Voltage (kV)	Crystal	Peak Measurement time (sec)	Standard formula
S	Kα	15	PET	30	FeS_2
Fe	Kα	15	LIF	30	FeS_2
Co	Kα	15	LIF	50	Co_9S_8
Ni	Kα	15	LIF	50	NiS
Cu	Lα	15	TAP	80	$CuFeS_2$
As	Lα	15	TAP	50	FeAsS
Ag	Lα	15	PET	50	Au-Ag alloy
Sb	Lα	15	PET	80	Sb_2S_3
Au	Mα	15	PET	80	Au-Ag alloy

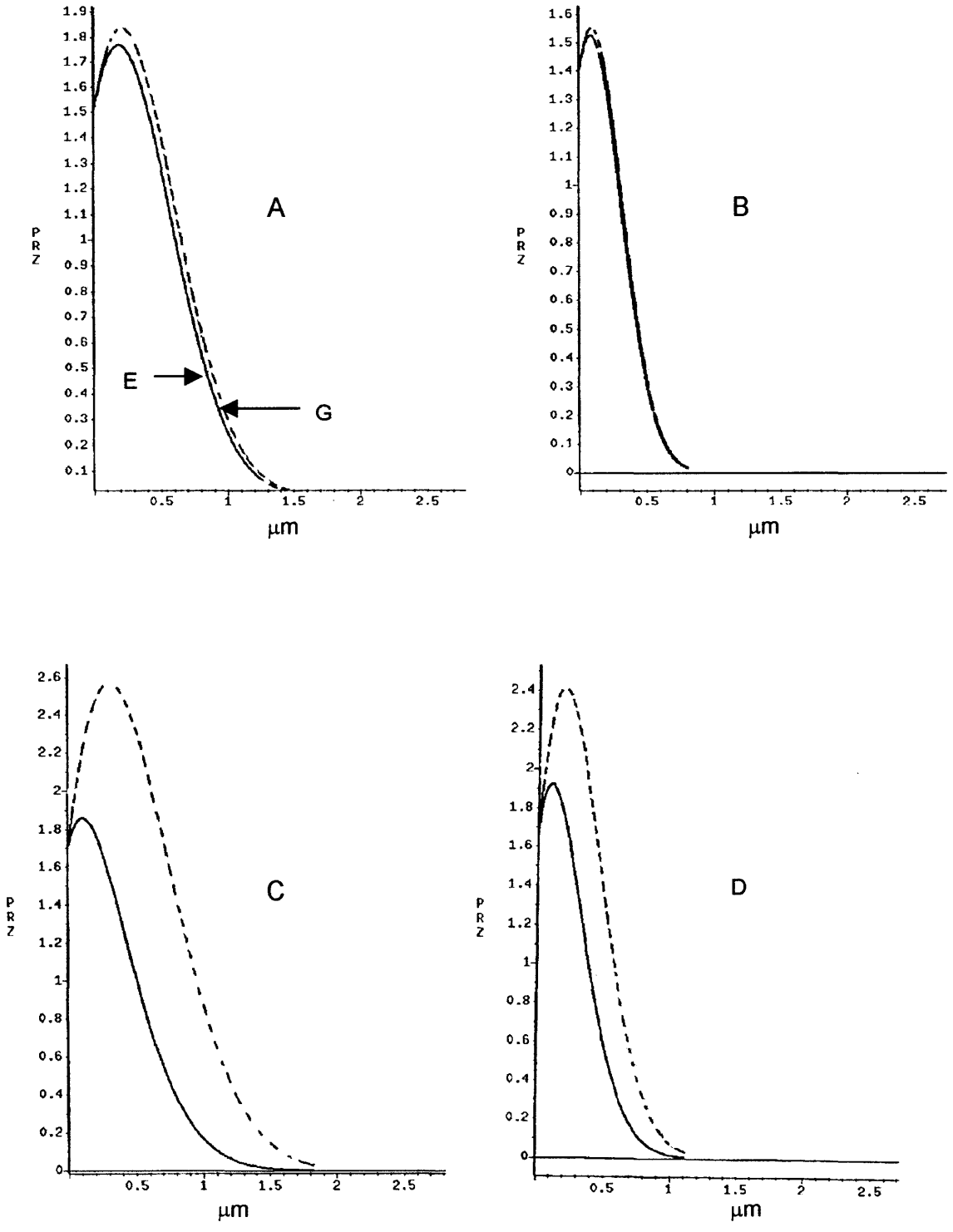

Figure 4. Proza curves plotted for arsenopyrite. Dotted lines (G) represent generated, and solid lines (E) emitted, radiation. The curves show the relative depth of radiation emitted from the sample for 0.6 mass % Ni in arsenopyrite at excitation voltages of 20kV and 15kV (Curves A and B), and for the same level of gold in arsenopyrite at 20kV and 15kV (curves C and D). The curves were plotted using the Voyager 3 software.

TABLE 3

ELECTRON MICROPROBE ANALYSIS CONDITIONS FOR PYRRHOTITE

Element	X-ray line	Accelerating Voltage (kV)	Crystal	Peak Measurement time (sec)	Standard formula
S	K-α	15	PET	30	FeS
Fe	K-α	15	LIF	30	FeS
Co	K-α	15	LIF	50	Co_9S_8
Ni	K-α	15	LIF	50	NiS
Cu	L-α	15	TAP	80	$CuFeS_2$
As	L-α	15	TAP	50	FeAsS
Ag	L-α	15	PET	50	Au-Ag alloy
Sb	L-α	15	PET	80	Sb_2S_3
Au	M-α	15	PET	80	Au-Ag alloy

TABLE 4

DETECTION LIMITS IN ARSENOPYRITE

(Detection limits in ppm at 3σ – 99% confidence level)

Mn	Co	Ni	Cu	Zn	Ge	Se	Ag
270	210	240	290	120	120	250	175
Cd	Sn	Sb	Te	Au	Hg	Pb	Bi
345	160	210	125	350	630	355	365

TABLE 5

DETECTION LIMITS IN PYRITE, PYRRHOTITE AND GERSDORFFITE

(Detection limits in ppm at 3σ – 99% confidence level)

	As	Cu	Sb	Co	Ni	Au	Ag
Pyrite	200	570	300	415	405	505	240
Pyrrhotite	230	705	305	410	425	505	275
Gersdorffite	Major element	320	200	230	Major Element	345	n.d.*

*n.d. = not determined.

Peak selection and background positions for trace element analysis were checked by running slow WDS wavescans from 6 mm below, to 6 mm above, theoretical peak position. Curved backgrounds were eliminated as far as possible by drawing background positions in towards peak position. PHA windows were invariably set, not only to cut out high order peaks, but also to reduce the detection limit. Examples of problem overlaps are given in section 7.2.1.2.

Quantitative WDS analysis results with total mass percent outside 98.5 to 101.0 were not accepted for the random arsenopyrite analyses, so that accurate atomic ratios could be calculated, as is recommended (KRETSCHMAR & SCOTT, 1976). The reproducibility of the results as measured by double point analyses (KAISER & SPECKER, 1956) is shown in Table 6.

TABLE 6

REPRODUCIBILITY OF MICROPROBE ANALYSIS OF ARSENOPYRITE

(Reproducibility at 1σ; N = 30)

Element	Reproducibility
As	0.293
Fe	0.259
S	0.130
Cu	0.004
Ni	0.008
Co	0.013
Au	0.018
Sb	0.016

Initially, forty arsenopyrite particles from each type were analysed for trace amounts of Co, Ni, Cu, Zn, Ge, Cd, Bi, Pb, Se, Sn Ag, Au, Sb and Hg, to establish which of these trace elements were present. Mn, Zn, Ge, Se, Cd, Sn, Te, Hg, Pb and Bi were found to be absent, or present only very rarely, possibly as submicroscopic inclusions, in the four arsenopyrite types.

The remaining trace elements were incorporated into the major element analysis and two programs were run - initially one hundred preprogrammed random points on each arsenopyrite type were analysed, and subsequently analyses were run manually on zones in arsenopyrite as visible on the back-scattered electron image.

Finally, a quantitative program for As, Fe, S, Co, Ni, Cu, Au, Ag, and Sb was used to analyse one hundred random positions per arsenopyrite type, on composite milled crystal sections, and manual trace analyses were performed according to compositional zones within the four arsenopyrite types (see Table 7 below). These analyses included all the random analysis elements apart from silver, and were accompanied by back-scattered electron images to allow leach monitoring. The analysis and imaging time per zone (two positions) was approximately 20 minutes, and so the number of such analyses had to be limited due to machine and operator time. Zone analyses were run on rock sections only – the Klipwal arsenopyrite crystals were embedded in resin which prevents the acquiring of high contrast back-scattered electron images (the resin burns off and contaminates the column of the microprobe) and only one crystal with obvious zonation was analysed.

TABLE 7

ZONE ANALYSIS OF ARSENOPYRITE
*Intensity refers to back-scattered electron intensity

Type (source)	Number of dark* zones	Number of medium* zones	Number of bright* zones	Number of very bright* zones
Klipwal	1	0	1	0
Zandrivier	15	10	15	0
Sheba	23	0	23	0
West African	15	9	15	11

In some areas of the Zandrivier arsenopyrite, zonation was not discernable on the BSE-image. Three of these areas were analysed in addition to the points shown in the table above.

Sulphide minerals other than arsenopyrite which were analysed quantitatively (WDS: two points per particle) are shown in Table 8 below.

TABLE 8

SULPHIDE MINERALS OTHER THAN ARSENOPYRITE ANALYSED QUANTITATIVELY ON THE ELECTRON MICROPROBE

Type (source)	Sulphide		
	Pyrite	Pyrrhotite	Gersdorffite
Klipwal	10	0	0
Zandrivier	15	4	0
Sheba	22	0	13
West African	17	21	0

In addition, semi-quantitative EDS analyses of gold inclusions were performed on thirteen Klipwal inclusions, and thirty each of Sheba, Zandrivier and West African inclusions.

5.1.7 Auger Electron Spectroscopy

Auger electrons are produced when incident radiation is of sufficient energy to remove an inner shell electron from an atom. The resulting unstable atom emits an X-ray or an Auger electron, the kinetic energy of which is characteristic of the atomic energy configuration of the mother atom. The Auger Electron Spectroscope consists of an electron gun for surface analysis, a sputter gun for depth analysis, and an electron multiplier to analyse the energy of the electrons produced. Auger electrons can only escape from near-surface locations, typically at depths of 0.5 to 3.0 nm, and the technique is therefore more applicable to surface layers than is electron microprobe analysis (see Figure 5).

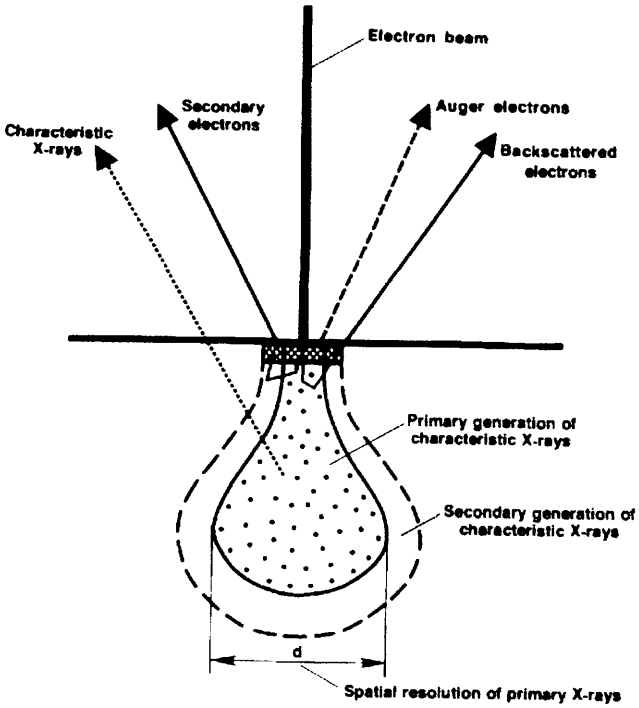

Figure 5. The depth of Auger electron excitation volume compared to that produced by an electron beam (VILJOEN & JOHNSON, 1983).

Pure surface analysis, as well as depth profiles can be produced by ion-sputtering down into the sample and repeated analysis at intervals. Although the technique is very sensitive, especially for the lighter elements, results are only semi-quantitative at best, and great care must be taken to prevent organic contamination of the surface to be analysed. Spatial

resolution of the older instruments is also quite limited. The theory and application of Auger Electron Spectroscopy is described in the literature (JOSHI, 1986).

The AES instrumentation housed at the Physics Department of the University of Pretoria consists of a PHI 545 System with a 137 PC interface and PHI surface analysis software. The instrument operates at vacuums down to $5x10^{-5}$ torr, the E_p used was 5 KeV, current 25 mA, with argon sputtering for depth profiles. Only the Klipwal arsenopyrite crystals were large enough to examine, and both ferric sulphate-leached and unleached crystals were analysed. No attempt was made to examine bacterially-leached crystals as organic surface contamination would have masked the other elements present.

5.1.8 Chemical analysis

The four arsenopyrite crystal concentrates were submitted for chemical analysis in the Analytical Services Division at Mintek. Chemical analyses were also run on the loose powder ferric sulphate leach solutions. Major and minor elements were determined using Atomic Absorption Spectroscopy (AA) and X-ray Fluorescence (XRF). Trace elements down to a detection limit of 1 ppm (by mass) were determined on the crystal concentrates using Inductively Coupled Plasma Mass Spectrometry (ICP-MS). The amounts of As_T, Fe_T and silver in the ferric sulphate leach solutions were determined by AA.

Wet chemical techniques – titration and gravimetric analysis – were used to determine As^{3+}, Fe^{2+}, and SO_4^{2-} in ferric sulphate leach solution. As^{3+} and As^{5+} are separated by ion exclusion chromatography, and As^{5+} is calculated by difference, as is Fe^{3+}. S, S^{2-} and S^0 were determined using the Leco wet chemical method, and SiO_2 by gravimetric or colourimetric techniques.

5.2 Acid ferric sulphate leaching

Thirteen acid ferric sulphate leach tests were run on the arsenopyrite samples (see Table 9). The first five were run on composite and milled crystal sections, varying physical conditions such as temperature, pH, and ferric iron concentration. Subsequent leaches were run with fixed physical conditions, the only variable being time in leach. Two of these (leach 6a and 6b) were on composite milled sections (five per leach) which were point counted, two on crystals for AES study (leach nos. 9 and 10), and two loose powder leaches (leach nos. 12 and

13) for liquor analysis. The loose powders were 38–150 μm sieve fractions of the Sheba and Zandrivier HF concentrates.

The leaching apparatus is shown diagrammatically in Figure 6. After leach no. 5, the glass beaker was replaced by a specially-made PVC reactor designed to exclude light and reduce evaporation from the system (Figure 7). Up to six composite or rock sections can be mounted in the inner sample holder, and these can be rotated at set time intervals. The speed of the stirrer was maintained at 1000 rpm, and temperature was controlled at 35±1°C by immersion of the reactor in a water bath. A photograph of the leach setup is shown in Figure 8.

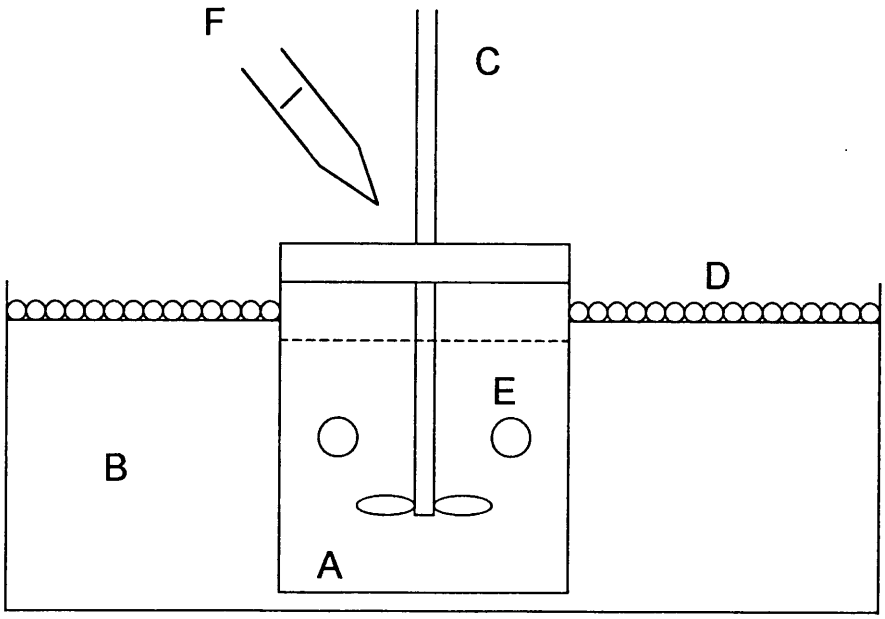

Figure 6. Diagram of the apparatus used for ferric sulphate leach tests. The beaker or reactor (A) is filled with 5 litres of acid ferric sulphate solution, placed in a water bath (B), and stirred with an overhead stirrer (C). Evaporation is controlled by using a tightly-fitting lid on the reactor, and by spreading a polystyrene layer (D) over the water. The composite polished sections (E) are suspended in the solution. The pH is controlled by addition of acid or alkali *via* a burette (F), and the pH and ORP (Oxygen Reduction Potential) are measured by inserting electrodes through stoppered ports in the reactor lid.

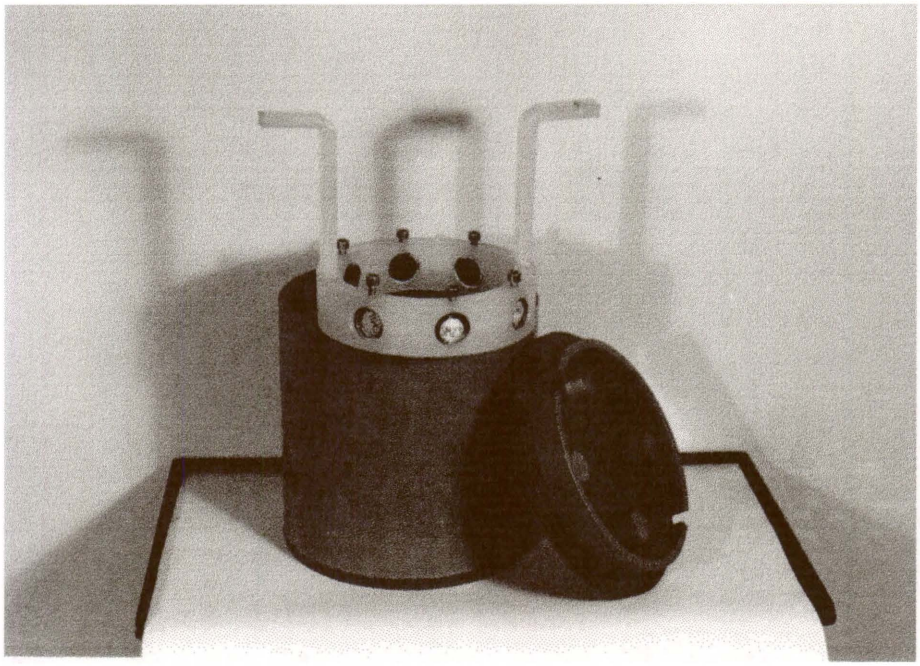

Figure 7. The PVC reactor. Polished sections fit into the light grey ring, and are lowered into the solution. The ring may be raised easily to allow removal of sections for microscopic monitoring.

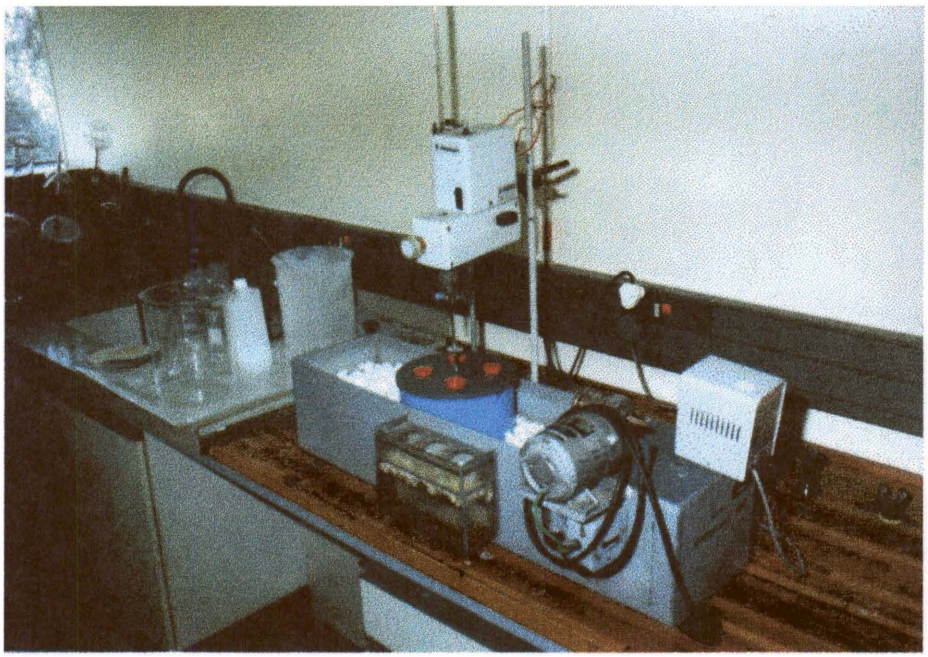

Figure 8. The ferric sulphate leach reactor running in the laboratory.

The leach liquors were prepared by adding ferric sulphate powder to a solution acidified by 30% sulphuric acid, and then slowly bringing up to temperature. The pH and ORP (Oxygen Reduction Potential, or redox) were monitored using an Eh/pH meter with a Ag/AgCl pH electrode and a Ag/AgCl combined platinum electrode. The pH was calibrated with phosphate buffers at pH 1 and 7, and the ORP was buffered at 495 mV. The ratio of Fe^{3+} to Fe^{2+} was kept as near to constant as possible by keeping the solids content of the leach very low – in theory this should result in constant ORP.

The loose powder leaches were run on 6g each of Sheba and Zandrivier HF residues, in the 38–150 µm size range. Both of these leaches were run for one week, with liquor samples being removed at intervals. The analytical schedule is shown in Table 10.

TABLE 9

FERRIC SULPHATE LEACH CONDITIONS

Leach no.	Sample in leach	Ferric iron conc. (g/l)	pH	ORP* (mV)	Temp. (°C)
1	1 composite crystal section	20	0.6	600-610	Ambient
2	1 composite crystal section and 1 composite milled section.	20	1.0	620-640	35
3	1 composite crystal section and 1 composite milled section.	20	0.8	620-640	35
4	1 composite crystal section and 1 composite milled section.	20	0.5	620-640	35
5	1 composite crystal section and 1 composite milled section.	40	0.5	650-700	35
6a + 6b	5 composite milled sections per leach	10	0.5	670-705	35
7	3 rock sections and 1 crystal section.	10	0.5-0.7	650-730	35
8	1 composite crystal section	10	0.5	650-680	35
9	2 loose crystals	10	0.5	610-620	35
10	2 loose crystals	10 + 4g/l As	0.5	±500	35
11	HF residue Powder	10	0.5	555-720	35
12	HF residue Powder	10	0.5	550-700	35

*ORP = Oxygen Reduction Potential.

TABLE 10

LIQUOR SAMPLING AND ANALYSIS SCHEDULE FOR LOOSE POWDER FERRIC SULPHATE LEACHES

Sampling time	Species analysed in liquor *
0 (initial)	As_T, Fe^{3+}, Fe^{2+}, Fe_T, SO_4^{2-}
1 hour	As_T, Fe_T, SO_4^{2-}
3 hours	As_T, Fe_T, SO_4^{2-}
8 hours	As^{3+}, As^{5+}, As_T, Fe^{2+}, Fe^{3+}, Fe_T, SO_4^{2-}
1 day	As^{3+}, As^{5+}, As_T, Fe^{2+}, Fe^{3+}, Fe_T, SO_4^{2-}
2 days	As_T, Fe_T, SO_4^{2-}
3 days	As^{3+}, As^{5+}, As_T, Fe^{2+}, Fe^{3+}, Fe_T, SO_4^{2-}
4 days	As_T, Fe_T, SO_4^{2-}
5 days	As_T, Fe_T, SO_4^{2-}
1 week	As^{3+}, As^{5+}, As_T, Fe^{2+}, Fe^{3+}, Fe_T, SO_4^{2-}

*As_T = Total Arsenic (As^{3+} + As^{5+}), and Fe_T = Total Iron (Fe^{2+} + Fe^{3+}).

5.3 Bacterial leaching

Two different vessels were used for the bacterial leaching tests. The composite crystal section was placed in a 10 litre pachuca, which was run on a continuous basis, and the rock and composite ground sections were placed in a smaller 1.5 litre pachuca. Both pachucas had been inoculated with a mixed culture of *Thiobacillus ferrooxidans, Thiobacillus thiooxidans* and *Leptospirillium ferrooxidans.* The loose powder present was a Sheba pyrite/arsenopyrite flotation concentrate at low solids percent. Nutrient salts were also added to nourish the bacteria, and oxygen was bubbled from the pachuca base to aerate and agitate the leach. Table 11 shows the conditions prevalent during the bacterial leaches, and Figure 9 shows a diagrammatic sketch of the apparatus.

TABLE 11

BIOLEACHING PROGRAM

Leach no.	Sections in leach	Ferric iron conc. (g/l)	pH	ORP* (mV)	Temp (°C)
1	1 composite crystal section	20	1.1–1.2	525-670	32
2	5 composite milled sections	10	0.8–1.0	550-600	35
3	3 rock sections and 1 crystal section	10	0.8–1.0	550-670	35

*ORP = Oxygen Reduction Potential.

The bacterial leach test work was mainly intended to provide an indication of the similarities or differences between the ferric sulphate and bacterial oxidation processes, and did not form a major part of the experimental program.

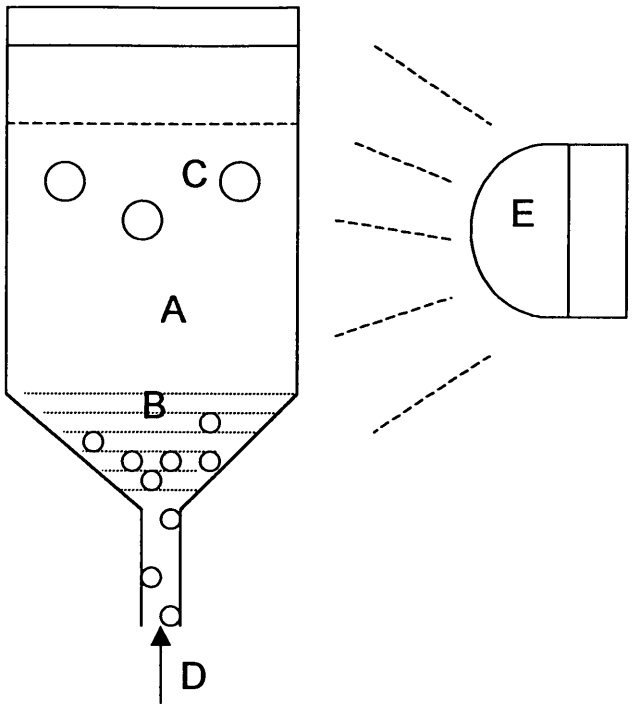

Figure 9. Diagram showing the bacterial leach test apparatus. The Perspex pachuca (reactor) (A) contains liquor, bacteria, nutrients, suspended solids (B) and polished sections (C). Air is bubbled in through the base of the pachuca (D), and the temperature is maintained by means of an infra-red light to one side of the pachuca (E).

6. MINERALOGY OF THE UNLEACHED SAMPLES

6.1 Mineralogy of the Klipwal sample

Because the Klipwal arsenopyrite crystals had already been isolated, no rock sample could be examined. The arsenopyrite was previously described, however, as being associated with pyrite, gold and chlorite (RUSSELL, 1985). Pyrite inclusions are seen in approximately 20% of the Klipwal arsenopyrite crystals, and rutile inclusions are common. Other inclusions are gold, galena, chalcopyrite, sphalerite and silicates. Compositional zonation is rarely observed

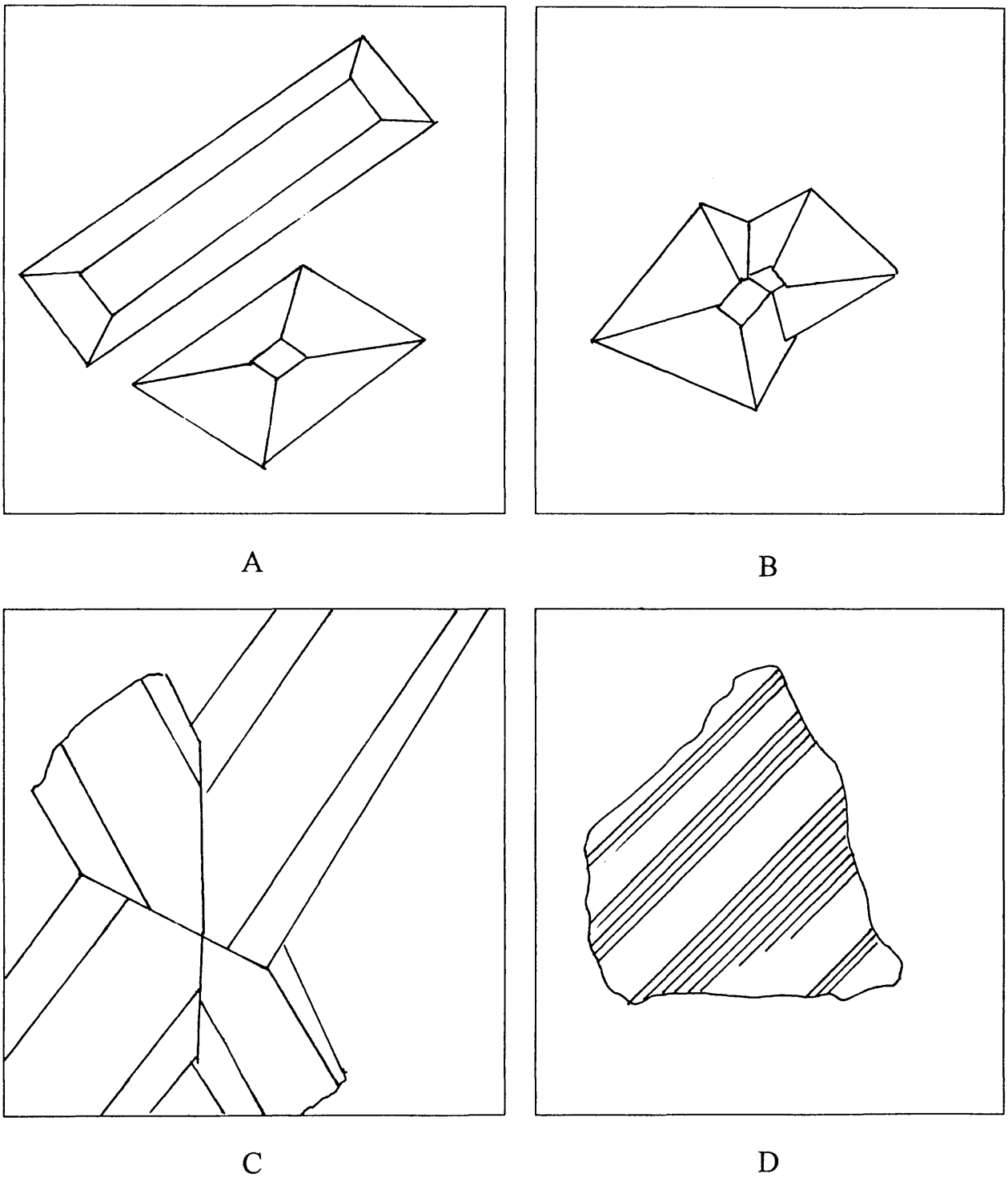

Figure 10. Twinning in arsenopyrite. A – mimetic twinning in Sheba arsenopyrite crystals, B – penetration and mimetic twinning in Sheba arsenopyrite, C – orientation effects in West African arsenopyrite penetration twins, D – polysynthetic twinning in Zandrivier arsenopyrite.

in the Klipwal crystals; if present it is relatively weak, and found as finely spaced zones towards the edge of the crystals. Several different types of twinning were observed in arsenopyrite during this study (Figure 10). No penetration twinning was found in the Klipwal crystals as received, but ubiquitous mimetic twinning became obvious upon leaching. The Klipwal arsenopyrite crystals are relatively large (up to 8mm in length). They were therefore the most suitable of the four arsenopyrite types for reflectance measurement and AES study. The reflectance of three unleached, as well as a number of leached crystals is listed in Table A5 (pages 181–185).

6.2 Mineralogy of the Sheba rock sample

The rock sample contains mainly quartz, mica, carbonate minerals and arsenopyrite.

Silicate minerals apart from quartz are sericite, biotite, chlorite and trace amounts of zircon. The carbonate minerals are represented mainly by ankerite and siderite, and other non-sulphide minerals present in small amounts are rutile, monazite, chromite and apatite. Gold is also present, and this is described in detail later.

By far the predominant sulphide mineral in the rock is arsenopyrite. In this way it differs from Sheba samples previously worked upon, where pyrite was found to be more common (SCHOUWSTRA, 1990). Pyrite is also present, as well as minor to trace amounts of gersdorffite, chalcopyrite, pyrrhotite, galena, tennantite-tetrahedrite, sphalerite, stibnite, and pentlandite. The sulphide minerals are dealt with in more detail below.
Arsenopyrite occurs as needle-like crystals, which may be up to 400 µm in size, but are usually less than 50 µm across. Arsenopyrite may be in contact with pyrite, gersdorffite, sphalerite, monazite, silicates or carbonates. Inclusions found within the arsenopyrite are rutile, gold, galena, pyrrhotite, stibnite, chalcopyrite, tetrahedrite, and silicate minerals. Sheba arsenopyrite crystals display variable compositional zonation, which can be strong and finely-interspaced (Figure 11). Zones may be as small as 2 µm across. Rhombs frequently display As-rich rims and S-rich cores. Back-scattered electron (BSE) images from the electron microprobe reveal that the cores are often cracked and the cracks do not extend into the As-rich rims. This could indicate an overgrowth by a later-stage, As-rich generation of arsenopyrite. Two types of twinning were observed in Sheba arsenopyrite – penetration and

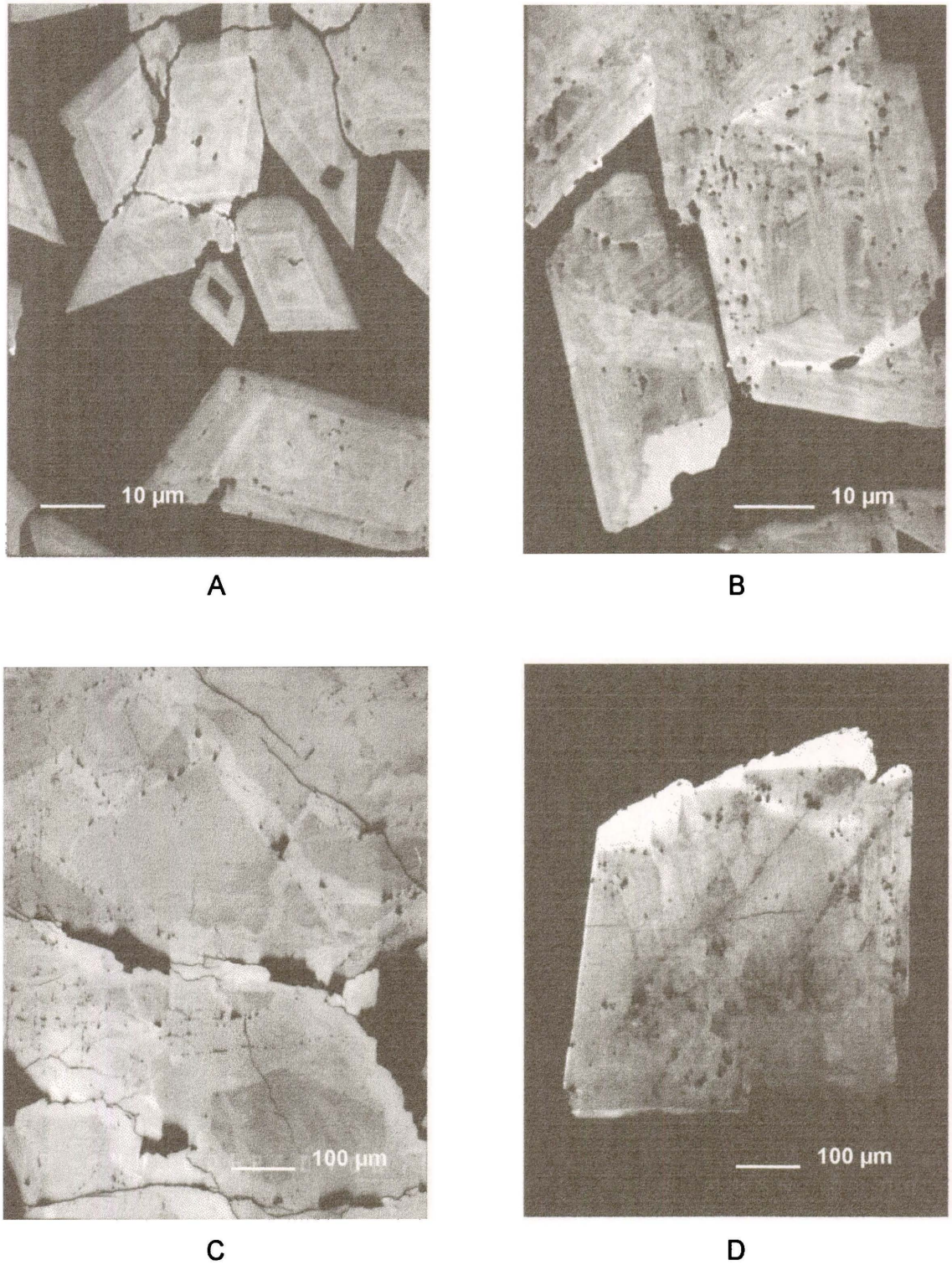

Figure 11. Zonation patterns in arsenopyrite. Sheba arsenopyrite (A and B) is strongly zoned on a fine scale. Zandrivier arsenopyrite (C) is weakly zoned on a coarse scale, with high As/S values associated with veins (bright). West African arsenopyrite crystals (D) show late-stage rims (bright) which are high in arsenic and/or cobalt.

mimetic twinning. The reflectance of the Sheba arsenopyrite was not measured because the crystals were too small in cross-section.

Pyrite is found in two forms - as rare, very large crystals (to over 1 mm) which may engulf many tiny arsenopyrite crystals, and as smaller (<50 μm) crystals usually not attached to arsenopyrite. Both types frequently show compositional zonation caused by the presence of a small amount of arsenic in the structure.

Gersdorffite, another member of the arsenopyrite-gersdorffite-cobaltite family, is occasionally found intergrown with pyrite and arsenopyrite. It is anhedral, and appears to be more common in carbonate-rich areas. The gersdorffite frequently displays atoll structure – previously described by Schouwstra (1990) – which is thought to have been inherited from pyrite (Figure 12). Atoll textures in Co-Ni-Fe sulpharsenides have also been described from northern Norway (VOKES & STRAND, 1982). Analysis of the Sheba gersdorffite shows that it always contains 10–15 mass % iron.

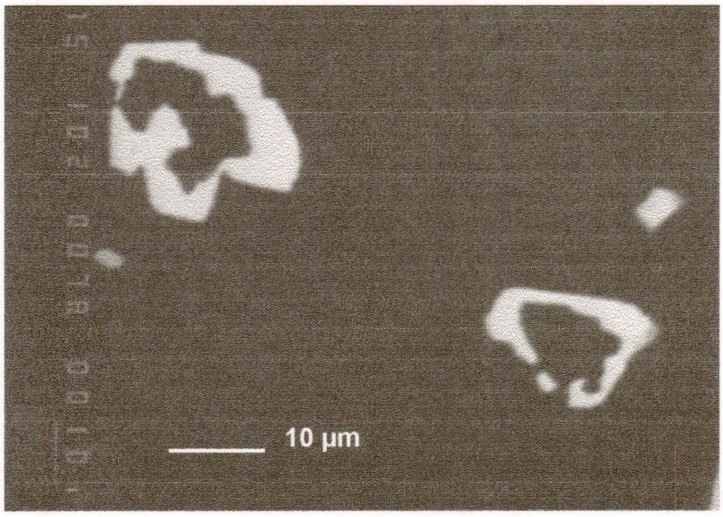

Figure 12. BSE-image of Sheba gersdorffite showing atoll texture.

Small amounts of chalcopyrite are found associated with carbonate-rich areas in the rock, and more rarely as inclusions in arsenopyrite. Trace amounts of sphalerite are present as intergrowths with arsenopyrite, and less commonly, with chalcopyrite. Galena and pyrrhotite are usually found as tiny inclusions in arsenopyrite; galena is occasionally present as veinlets within quartz and arsenopyrite. Tetrahedrite, the Sb end-member of the tennantite-tetrahedrite

series, is normally found as small inclusions in arsenopyrite, sometimes associated with gold. Some tennantite is present, however, and sometimes both types are found together. Trace amounts of stibnite occur as inclusions in arsenopyrite, and Fe-Ni sulphide is very occasionally found as small inclusions in pyrite.

6.3 Mineralogy of the Zandrivier rock sample

This sample consists almost entirely of massive arsenopyrite, with quartz veins and black tourmaline-rich areas in places.

Silicate minerals present, apart from the quartz and tourmaline, are chlorite, sericite, and orthoclase feldspar. The tourmaline has a green-brown colour in thin section and displays compositional zonation, with distinct variation in titanium content. There are some carbonate minerals present, the most common being siderite. Dolomite and ankerite are found in smaller amounts. Rutile is the predominant oxide mineral in the sample, although smaller amounts of ilmenite and goethite are present. Trace minerals, apart from gold, are monazite and xenotime.

Arsenopyrite is the major sulphide mineral present, but there is also pyrite, and trace amounts of pyrrhotite, sphalerite, galena and chalcopyrite. As mentioned earlier, most of the arsenopyrite is massive. A number of small crystals with rhombic or hexagonal profiles, however, were noted within a quartz vein, although these probably formed later than the main phase arsenopyrite. Various minerals are present as inclusions in the arsenopyrite, specifically all the sulphides mentioned above, gold, monazite, iron oxides, rutile, and tourmaline. Some of the Zandrivier arsenopyrite particles are compositionally unzoned, but in others zonation is weak to medium in strength. Arsenic-rich zones are found as veins within the main phase sulphide, and also close to the contact with quartz veins. In all cases the scale of the zonation is much coarser than in Sheba arsenopyrite (Figure 11). Penetration and mimetic twinning was not observed in the Zandrivier arsenopyrite, but this may merely be due to its massive nature. Polysynthetic twinning is sometimes seen, and becomes more marked as leaching progresses. The reflectance of four relatively inclusion-free Zandrivier arsenopyrite particles was measured, and the values are presented in Table A5 (pages 181–185).

Pyrite occurs as inclusions in the arsenopyrite, but larger pyrite grains form at the contact of quartz with arsenopyrite, and these may be up to 1 mm in size. The pyrite does not exhibit

compositional zonation. Pyrrhotite is not as common as pyrite, but it is present as inclusions of up to 100 µm within the arsenopyrite and pyrite. Only trace amounts of chalcopyrite are present as inclusions in the arsenopyrite. Sometimes the inclusions also contain gold. Galena is found as tiny inclusions in the arsenopyrite.

6.4 Mineralogy of the West African rock sample

This rock sample consists mainly of quartz, and ankerite, with minor mica, arsenopyrite, pyrrhotite and rutile.

The silicate minerals are predominantly quartz, with lesser amounts of sericite, orthoclase, albite, chlorite, and clay minerals. The carbonates are frequently compositionally zoned, with variation of calcium, magnesium and iron. Most of the carbonate appears to be ankerite. Rutile and iron oxides are present, and there are trace amounts of gold, fluor-apatite, barite, monazite, ilmenite, and xenotime.

The sulphide minerals are mainly arsenopyrite and pyrrhotite, with the predominance between the two varying from place to place in the ore body. Smaller amounts of pyrite, sphalerite and chalcopyrite are associated with the major sulphides.

Arsenopyrite is found as euhedral crystals to over 1 mm in size, which are nearly always in contact with pyrrhotite. Arsenopyrite is sometimes attached to pyrite, and surrounded by rutile, silicate or carbonate minerals. Minerals occurring as inclusions in the arsenopyrite are rutile, ilmenite, pyrrhotite, gold, monazite, silicates, and carbonates. The arsenopyrite displays compositional zonation, but this is usually only strongly developed towards the outer rim of crystals, often close to the contact with pyrrhotite (Figure 11). Both penetration and mimetic twinning, frequently occurring simultaneously, are present in this arsenopyrite. The reflectance of two West African arsenopyrite particles are reported in Table A5 (pages 181–185).

In places, pyrrhotite is more abundant than arsenopyrite. It forms large irregular masses up to several millimetres in size and may be isolated, or in contact with other sulphides, especially arsenopyrite and pyrite.

There may be two generations of pyrite in the sample. These comprise of larger, irregular particles to 200 µm, and smaller euhedral particles of 10 to 100 µm in size which are usually associated with pyrrhotite/arsenopyrite contact zones.

Small particles of chalcopyrite are occasionally found intergrown with pyrrhotite, and as tiny inclusions in sphalerite. Small amounts of sphalerite are associated with pyrite and pyrrhotite. Sometimes tiny inclusions of chalcopyrite in this sulphide form the texture known as 'chalcopyrite disease'.

6.5 Modal sulphide analysis

The results of modal sulphide analysis performed on three polished sections each of the Sheba, Zandrivier and West African ores using the Cambridge Morpho-chemical Analyser are presented in Tables 12 and 13. A modal analysis of the Zandrivier ROM (run of mine) ore is also given, because of the heterogeneity shown by the rock sections. Modal analysis was not run on the Klipwal sample because no rock sample was available and because any pyrrhotite present would have been dissolved by HF leaching.

TABLE 12

MODAL ANALYSIS OF ROCK SECTIONS

Source		Sulphide (vol %)	Gangue (vol %)	Sulphide (mass %)	Gangue (mass %)
Sheba	1	6.1	93.9	12.7	87.3
	2	6.3	93.7	13.1	86.9
	3	8.2	91.8	16.7	83.3
	4	3.9	96.1	8.4	91.6
	Average	6.1	93.9	12.7	87.3
Zandrivier	1	71.3	28.7	84.9	15.1
	2	80.5	19.5	90.3	9.7
	3	62.9	37.1	79.3	20.7
	4	31.4	69.6	67.1	32.9
	Average	61.5	38.7	80.4	19.6
	ROM*	23.1	76.9	39.4	60.6
W.African	1	5.8	94.2	9.9	90.1
	2	3.6	96.4	7.3	92.7
	3	6.7	93.3	11.3	88.7
	4	7.2	92.8	14.2	85.8
	average	5.8	94.2	10.7	89.3

*ROM = Zandrivier Run of Mine sample as referred to below.

TABLE 13

MODAL SULPHIDE ANALYSIS (in volume %)

Source		Arsenopyrite	Pyrite	Pyrrhotite	Other*
Sheba	1	96.7	2.3	0.0	1.0
	2	96.0	2.7	0.0	1.3
	3	94.8	2.1	1.3	1.8
	4	94.9	2.4	1.1	1.6
	Average	95.6	2.4	0.6	1.4
	$\sigma^{\#}$	0.9	0.3	0.7	0.4
Zandrivier	1	99.0	0.0	0.0	1.0
	2	99.0	0.0	0.0	1.0
	3	98.6	0.6	0.0	0.8
	4	98.9	0.0	0.0	1.1
	Average	98.9	0.2	0.0	1.0
	σ	0.2	0.3	0.0	0.1
W. African	1	19.0	0.5	79.4	1.1
	2	74.9	2.3	21.2	1.6
	3	16.5	1.6	80.5	1.4
	4	78.1	2.1	18.1	1.7
	Average	47.1	1.6	49.8	1.4
	σ	34.0	0.1	34.8	0.3

*Other – phases not identifiable because the analysis fell on the boundary of two or more particles.
$^{\#}\sigma$ = standard deviation.

6.6 Gold deportment and composition

Gold can occur as *discrete inclusions,* called 'free gold', detectable on the microscope, SEM or EMP (generally over 0.5 μm in diameter), and as *submicroscopic* gold in the form of very small inclusions not detectable on the SEM or EMP, or chemically bound in the sulphides as in a solid solution. This section deals with the occurrence of free gold, whereas submicroscopic gold will be dealt with under the trace element composition of arsenopyrite in Section 7.2.1.2.

The size distribution and association of the gold are shown in Table 14, and graphically presented in Figures 13 and 14. As mentioned earlier, the results should not be taken as a statistical investigation. A number of observations can be made, however. Firstly, there is a higher mass per cent of gold in the Zandrivier arsenopyrite sections than in the others. The Zandrivier inclusions are also coarser, and associated almost exclusively with arsenopyrite. Sheba gold particles are also usually associated with arsenopyrite, but the situation in the West African samples is different, where only 58 vol.% of the gold is associated with arsenopyrite. This factor would be important for the optimum gold recovery during ore processing.

The results of semi-quantitative EDS analysis of a number of gold inclusions from all four arsenopyrite types are presented in Table 15. The presence of copper was not detected (the EDS detection limit is approximately 2 mass %), and any iron detected was assumed to be due to contamination from the surrounding sulphide minerals, especially in the Sheba and West African samples, where the gold inclusions are too small to permit interference-free analyses.

TABLE 14

GOLD INCLUSION DISTRIBUTION AS DETERMINED ON THE IMAGE ANALYSER

(e.g. 89.4 mass % of the gold inclusions in the Sheba samples were situated in arsenopyrite particles. 18 inclusions were detected, with a size range of 1.3 –5.0 μm. The total area of gold inclusions in the Sheba sections was 112.4 μm^2).

Source and total area	Au mass %	Association	Number of particles	Size range (μm diam.)
Sheba	89.4	Arsenopyrite	18	1.3 – 5.0
(112.4μm^2)	9.5	Silicate	2	2.5 – 2.7
	1.1	Pyrite	1	1.3
Zandrivier	98.9	Arsenopyrite	51	1.8 – 50.2
	0.8	*Asp/pyrite	2	3.1 – 6.1
(4833.5μm^2)	0.3	Pyrite	2	1.8 – 4.0
	<0.1	Silicate	1	1.8
W. African	58.4	Arsenopyrite	8	2.4 – 5.3
	10.1	Pyrite	2	2.0 – 3.6
(130.4μm^2)	9.1	Carbonate	2	2.7 – 2.8
	8.1	Pyrrhotite	1	3.7
	7.6	#Asp/silicate	1	3.6
	6.7	Silicate	1	3.3

*Asp/pyrite = at the contact of arsenopyrite with pyrite
#Asp/silicate = at the contact of arsenopyrite with a silicate mineral

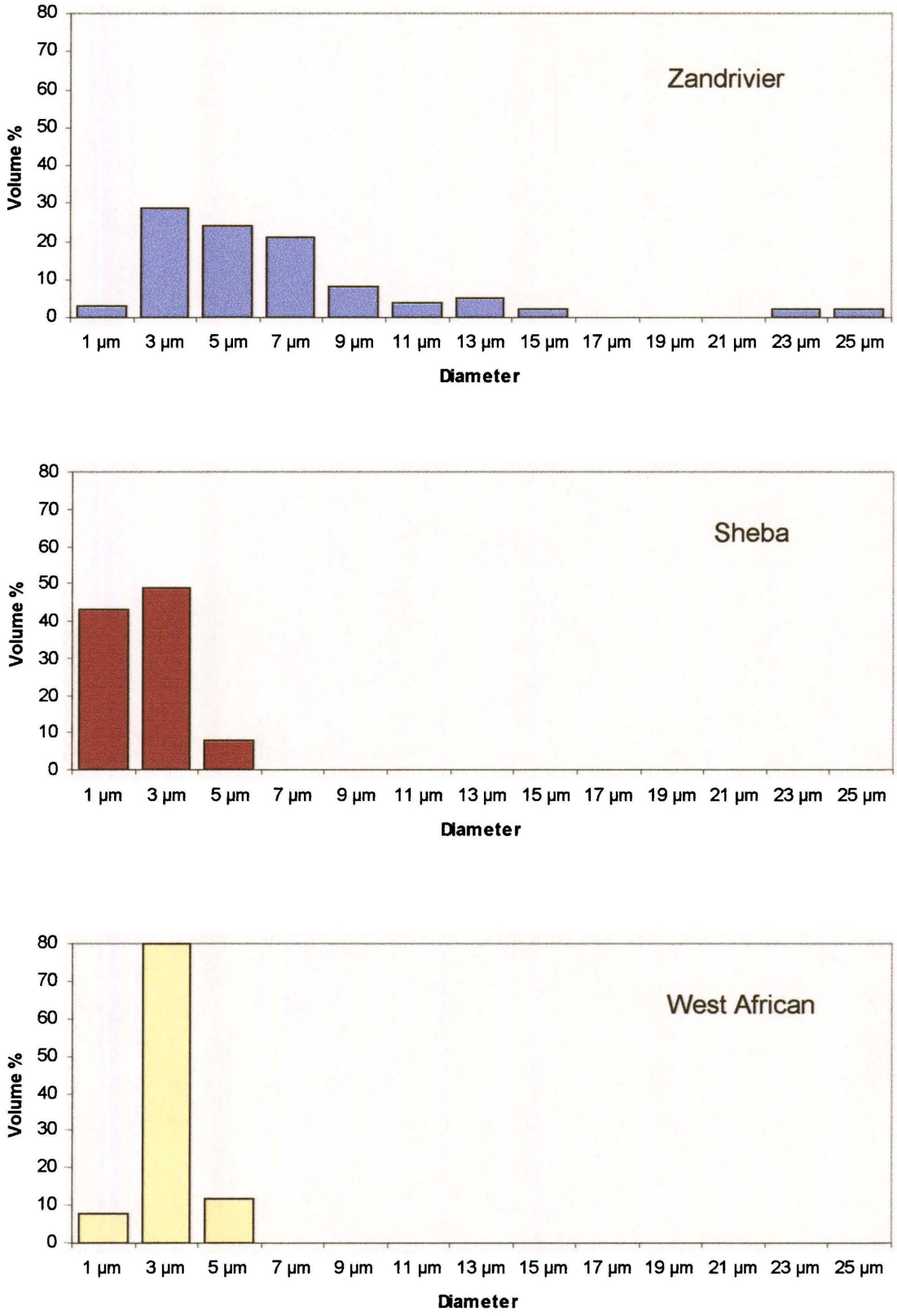

Figure 13. The size distribution of the gold inclusions.

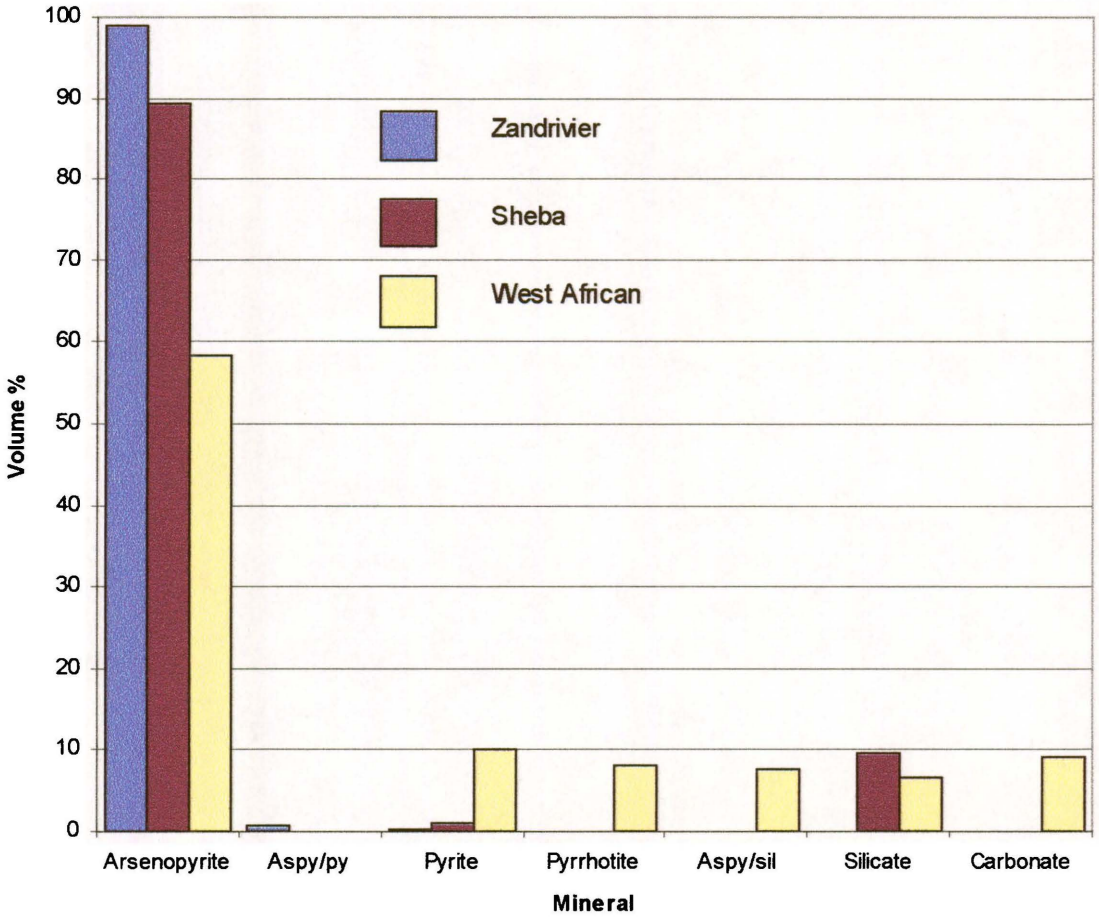

Figure 14. Mineral association of gold. Aspy/py = at contact of arsenopyrite and pyrite. Aspy/sil = at contact of arsenopyrite and silicate minerals.

The fineness, or Au/(Au+Ag), of the South African gold is higher than that of the West African gold. The average fineness of the Zandrivier gold is 947, of the Sheba gold 942, of the Klipwal gold 856, and of the West African gold 762.

TABLE 15

SEMI-QUANTITATIVE GOLD ANALYSIS RESULTS

	Klipwal		Zandrivier		Sheba		West African	
	Au mass %	Ag mass %	Au mass %	Ag mass %	Au mass %	Ag mass %	Au mass %	Ag mass %
	79.3	20.7	93.6	6.4	94.3	5.7	74.4	25.6
	85.3	14.7	95.2	4.8	93.2	6.8	77.4	22.6
	84.8	15.2	95.2	4.8	93.1	6.9	78.2	21.8
	86.4	13.6	95.4	4.6	97.7	2.3	73.1	26.9
	86.5	13.5	94.6	5.4	93.6	6.4	75.1	24.9
	87.7	12.3	94.3	5.7	92.6	7.4	80.5	19.5
	78.2	21.8	93.2	6.8	97.4	2.6	68.6	31.4
	87.3	12.7	94.3	5.7	93.1	6.9	74.7	25.3
	87.3	12.7	94.6	5.4	92.1	7.9	78.3	21.7
	84.9	15.1	95.0	5.0	93.6	6.4	74.3	25.7
	87.9	12.1	94.5	5.5	92.2	7.8	74.5	25.5
	89.0	11.0	95.2	4.8	93.9	6.1	75.7	24.3
	88.0	12.0	93.6	6.4	93.2	6.8	74.1	25.9
			94.7	5.3	92.6	7.4	74.9	25.1
			95.0	5.0	97.7	2.3	71.3	28.7
			93.3	6.7	93.7	6.3	77.0	23.0
			95.0	5.0	92.7	7.3	78.8	21.2
			95.1	4.9	94.0	6.0	76.1	23.9
			95.4	4.6	93.2	6.8	78.0	22.0
			95.2	4.8	93.3	6.7	76.5	23.5
			94.4	5.6	100.0	0.0	75.3	24.7
			95.4	4.6	92.8	7.2	76.0	24.0
			94.1	6.0	93.5	6.5	75.5	24.5
			94.2	5.8	95.2	4.8	76.2	23.8
			94.2	5.8	95.2	4.8	76.0	24.0
			95.6	4.4	90.7	9.3	75.3	24.7
			95.9	4.1	92.6	7.4	81.1	18.9
			94.8	5.2	96.4	3.6	77.7	22.3
			93.8	6.3	98.4	1.6	76.4	23.6
			95.1	4.9	93.7	6.3	86.1	13.9
ave	85.6	14.4	94.7	5.3	94.2	5.8	76.2	23.8
s.d.	3.3	3.3	0.7	0.7	2.1	2.1	3.1	3.1

7. COMPOSITION OF THE MAJOR SULPHIDE MINERALS

The major element composition of the four arsenopyrite HF concentrates as determined by chemical analysis is shown in Table 16. The low totals may be due to carbonate content, although later mineralogical analyses suggest that the arsenic results here may be low. As mentioned in Section 3 (Previous Work), the elements described in the literature as having been found in arsenopyrite include As, Fe, S, Co, Ni, Bi, Sb, Se, Au, Ag, Cu, Pb, Mn and Zn. There is, however, especially in the earlier references, some doubt as to whether the elements in question were chemically-bound, or present as inclusions of other minerals within the arsenopyrite.

TABLE 16

CHEMICAL ANALYSIS OF THE ARSENOPYRITE HF CONCENTRATES
(in mass %)

	Klipwal	Zandrivier	West African	Sheba
As	35.8	36.5	30.1	36.4
Fe	33.8	35.1	34.0	35.4
S	21.8	21.0	22.5	22.5
Si	0.6	0.2	0.0	0.1
Total	92.0	92.8	86.6	94.4

Trace amounts of various platinum group elements (PGE's), notably Rh, Ru, Os and Ir have been detected in cobaltite and gersdorffite from Sudbury (Canada) and Pechenga (Russia) (CABRI, 1994). These sulparsenides form two corners of a compositional triangle with arsenopyrite, and PGE's could also occur in traces in arsenopyrite. The base metal association of Sudbury and Pechenga, however, is not that of the arsenopyrite currently under investigation, so, in the view of this and ICP-MS results (see Section 7.1 below), the PGE have not been analysed.

7.1 ICP–MS analysis results

The results of these analyses, which were run on the arsenopyrite HF residues, are shown in Table 17. At first the results seem rather confusing, but many of the elements detected here must have come from inclusions of other minerals which were trapped within the arsenopyrite crystals, and were not leached out during the HF leaching process. The results show that certain elements are definitely not present, and the presence of other elements could possibly be accounted for as suggested in Table 18 below.

TABLE 17

ICP-MS ANALYSIS OF ARSENOPYRITE HF CONCENTRATES

(Results in ppm by mass unless otherwise stated).

	B	Na	Mg	Al	Ca	Ti	Cr	Mn	Co	Ni	Cu	Zn
Sheba	70	600	50	300	270	150	2	70	320	0.26%	35	80
West African	130	450	0.37%	570	1.20%	190	1	300	0.11%	680	300	70
Zandrivier	25	380	150	170	850	110	2	0	220	420	0	10
Klipwal	15	300	720	500	0.23%	150	3	150	280	750	150	20

	Se	Zr	Sb	Ce	Ta	W	Au	Hg	Pb	Cd	Ge
Sheba	10	20	200	3	3	3	120	2	110	0	0
West African	30	16	70	3	4	1	80	2	80	2	0
Zandrivier	25	10	70	0	7	2	0	0	30	0	16
Klipwal	5	30	60	8	6	5	3	15	115	0	20

These results are semi-quantitative only.
All elements detected in amounts > 1ppm by mass are reported in the table. Major elements As, Fe and S were not determined.
The following elements are not measured using this technique : C, N, O, P, Si, P, S, K and Cl. Na values tend to be inaccurate.

Based on the ICP-MS results, and also on the literature, it was decided to analyse for the following elements in arsenopyrite :

As, Fe, S, Co, Ni, Sb, Cu, Au, Ag, Mn, Zn, Ge, Se, Cd, Sn, Te, Hg, Pb and Bi.

7.2 Quantitative electron microprobe analysis of sulphide minerals

All the elements listed above were analysed for in arsenopyrite on the electron microprobe, using quantitative WDS analytical techniques. The analytical conditions have already been described in Section 5.1.6.

TABLE 18

POSSIBLE SOURCE OF ICP-MS ELEMENTS

Element	Possible source
B	Tourmaline
Na	Tourmaline, albite
Mg	Residual carbonates, chlorite
Al	Mica, chlorite
Ca	Residual carbonates, apatite, fluorite
Ti	Rutile, ilmenite
Mn	Residual carbonates
Co	Sulphides or arsenides
Ni	Sulphides esp. gersdorffite
Cu	Chalcopyrite, tetrahedrite-tennantite
Zn	Sphalerite
Ge	Not known
Se	Selenides or substituted sulphides
Zr	Zircon
Cd	Chemically bound in sphalerite
Sb	Sulphides or arsenides, such as tetrahedrite-tennantite
Ce	Monazite
Ta	*Tantalite**
W	Scheelite
Au	Metal or alloy
Hg	Gold
Pb	Galena

*Mineral has not been detected in any of the samples, but could be present.

7.2.1 Arsenopyrite analysis

Arsenopyrite was quantitatively analysed for major and trace elements, taking detection limits down to as low a level as was practical. The results are discussed below.

7.2.1.1 Major element analysis

Firstly, a suitable standard, or standards, had to be chosen for As, S and Fe calibration.

Natural arsenopyrite almost always shows some slight variation in composition, most commonly in the As/S ratio. The arsenopyrite standard in use at Mintek is As-2, usually known as ASP-200, which originates in Canada and has been described as a 'natural homogeneous S-rich arsenopyrite without detectable cobalt or nickel (in this case less than 0.05 mass %)' (KRETSCHMAR & SCOTT, 1976). Other workers have since, however, described higher concentrations of cobalt and nickel in ASP-200 as well as areas of inhomogeneity. Other standards available were a synthetic ferric arsenide ($FeAs_2$), synthetic orpiment (As_2S_3), synthetic pyrite (FeS_2), arsenic metal, and another natural arsenopyrite (ASP-1) made available by Professor Merkle. Calibration on arsenic metal is reported to produce errors in arsenic determination in arsenopyrite of up to 2% (IXER *et al.*, 1979), and arsenic sulphide is insufficiently stable. Tests were run on the electron microprobe to see the results of using ferric arsenide and pyrite as standards but this produced low arsenic values (by 1–2%) and high iron and sulphur values. Comprehensive tests showed the best standard to use for arsenopyrite analysis to be arsenopyrite itself.

Homogeneity tests were run on the As-2 and ASP-1 standards. This involved analysis over the surface of the standard using a high beam current (50 nA) and long counting times to reduce counting statistics. Counting times of 135–140 seconds were found to reduce counting statistics on arsenic to 0.1 mass %, and on iron and sulphur to 0.2 mass %. Fifty points on each standard were analysed and the results are presented in Tables A6 and A7 in the Appendix (pages 186–189).

Although the results show iron to be reasonably homogeneous in both standards, there is some As/S variation (see Figures 15 and 16). Neither standard is totally homogeneous, but As-2 is more so than ASP-1, and well within the degree of homogeneity cited in the literature (KRETSCHMAR & SCOTT, 1976). Some areas of the Mintek As-2 standard did, however, show higher cobalt and nickel values than those normally found in ASP-200.

Eventually it was decided to use As-2 as the arsenopyrite standard, but with multiple calibration points, away from areas of pyrite inclusions, and high trace element areas.

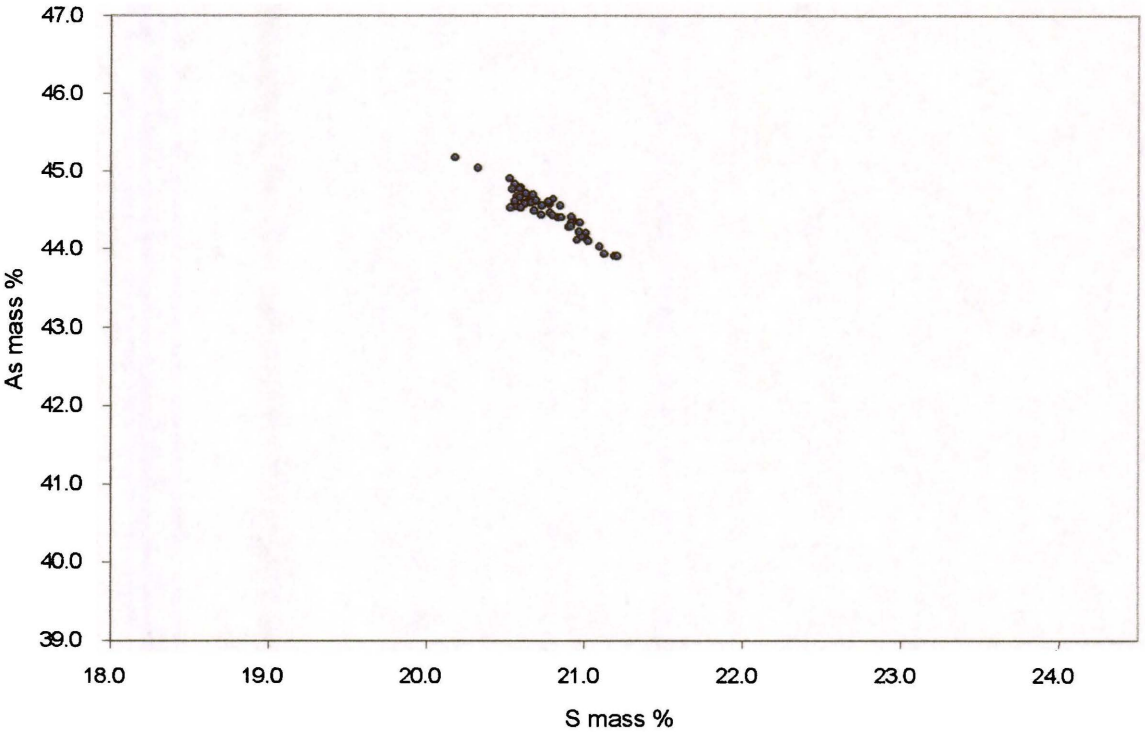

Figure 15. Variation of arsenic and sulphur in the Mintek As-2 standard. Values are normalised.

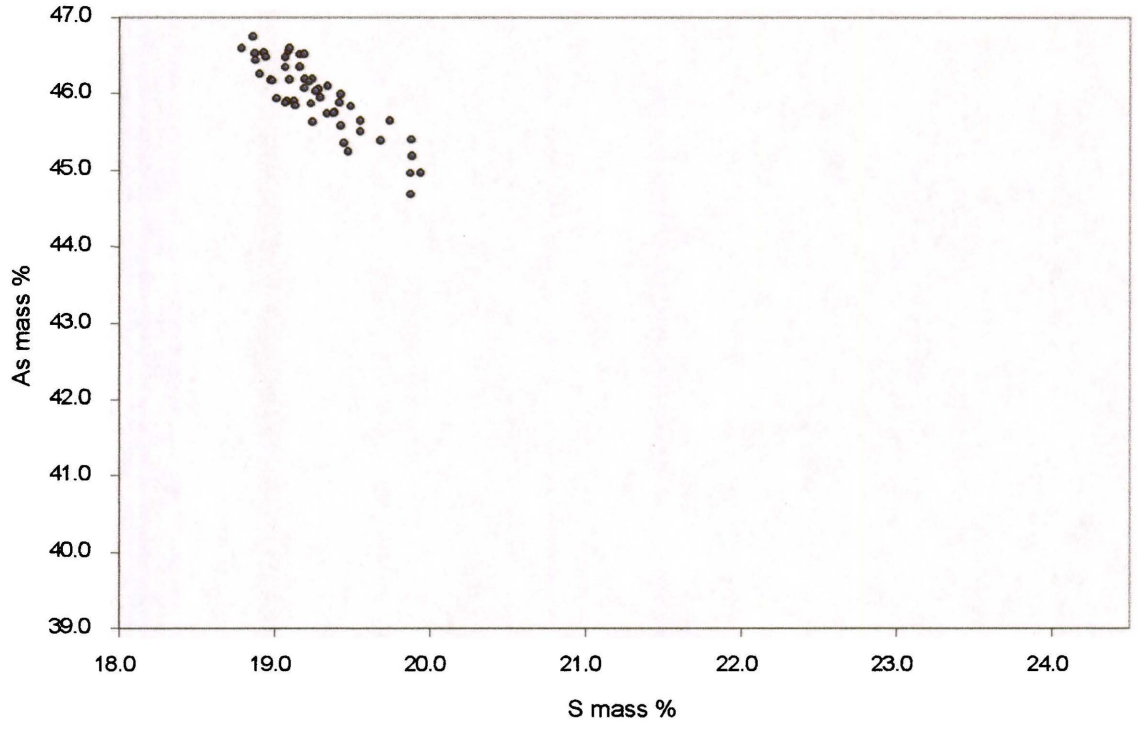

Figure 16. Variation of arsenic and sulphur in ASP-1. Values are normalised.

7.2.1.2 Minor to trace element analysis

Trace elements were analysed using long counting times, and four separate programs were used because of the long counting times involved.

Problems were experienced with the following elements –

Cobalt

Co analyses with spectrometer background positions set at ±5 mm produced values of 300-500 ppm in all the arsenopyrite types. The background positions had to be set much closer to the Co-Kα peak position (±1 mm) to avoid picking up counts from the Fe-Kβ peak.

Selenium

Counts were picked up at the Se-Lα peak position due to the presence of a broad As-Lβ peak (see the wavelength scans in Figure 17). This produced artificial levels of 300-600 ppm throughout, in contradiction with ICP-MS results. Reanalysis of Se-Lβ gave a slightly negative background, but this was the only option, as Se-K peaks would require an accelerating voltage of 30 kV, and column arcing starts at 25 kV, due to residual oil contamination.

Mercury

The Hg-Mα line experiences interference from gold, and the Hg-Mβ line from sulphur. The Hg-Lα line had to be used, which requires an accelerating voltage of 20 kV, and gives a high detection limit due to the low spectrometer position.

Bismuth

Analysis at the Bi-Mα peak position picks up counts from Au-Lα, and the Bi-Lα peak is overlapped by As-Kα. The Bi-Mβ peak was used with background positions set carefully to avoid S-Kβ. The resulting detection limit is rather high.

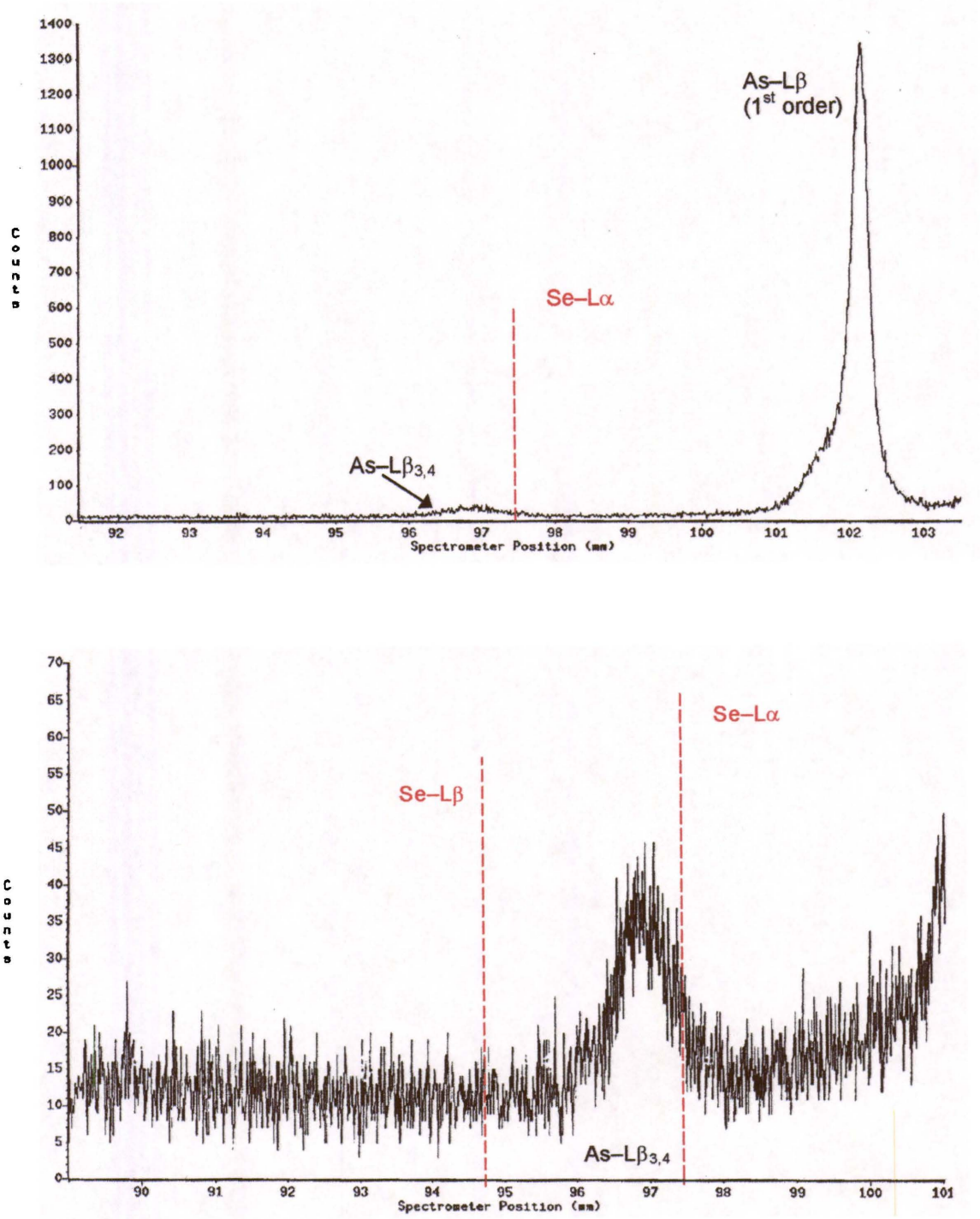

Figure 17. Wavescans over Se-Lα and Se-Lβ peak positions on arsenopyrite. Se-Lα sits on the shoulder of a first order As-Lβ peak, and cannot be used. Se-Lβ is interference-free, but background positions are problematical. The wavescans were generated using the Voyager 3 software.

7.2.1.3 Results of arsenopyrite analyses

Mn, Zn, Ge, Se, Cd, Sn, Te, Hg, Pb and Bi were found to be absent, or present only very rarely, possibly as submicroscopic inclusions, in the four arsenopyrite types. The results of the random and zone analyses for the remaining elements are shown in Tables A8 to A15 in the Appendix (pages 190–220). It should be noted here that silver was not detected in any of these analyses, and therefore has not been included in the tables. The original silver values may have been picked up from small gold inclusions.

Random analyses

The major element compositions of the arsenopyrite types are plotted on ternary diagrams in Figure 18. All four types are sulphur-rich overall, and display the S/As variation characteristic of arsenopyrite. The plots show that the major element distribution of the four types is very similar, although the Klipwal arsenopyrite shows less S/As compositional spread (Figures 19 to 22). The arsenopyrite compositions, apart from two outlying results from the West African arsenopyrite, fall within the compositional boundaries for natural arsenopyrite (KLEMM, 1965).

The compositional distribution on the ternary diagrams cannot be directly related to zone composition, because the positions analysed were random, and equal areas of S- and As-rich zones are not present.

Zone analyses

The distribution of compositional zonation within the arsenopyrite types is quite variable. Most of the Klipwal crystals display very weak zonation – where it is present it is as finely-spaced zones towards the edge of the crystal. The Zandrivier arsenopyrite is also commonly unzoned, but in some areas relatively coarse bright, medium and dark zones are apparent when investigated by BSE imagery. Later-stage arsenopyrite veins, and areas close to quartz veins, are frequently As-rich. The Sheba crystals are commonly strongly, but finely, zoned, and medium intensity zones are rare in BSE imagery. The cores of the crystals are frequently S-rich and the rims are As-rich. The extent of cracking from core to rim suggests that, in some cases at least, the outer zone may be a later-stage overgrowth. The West African arsenopyrite

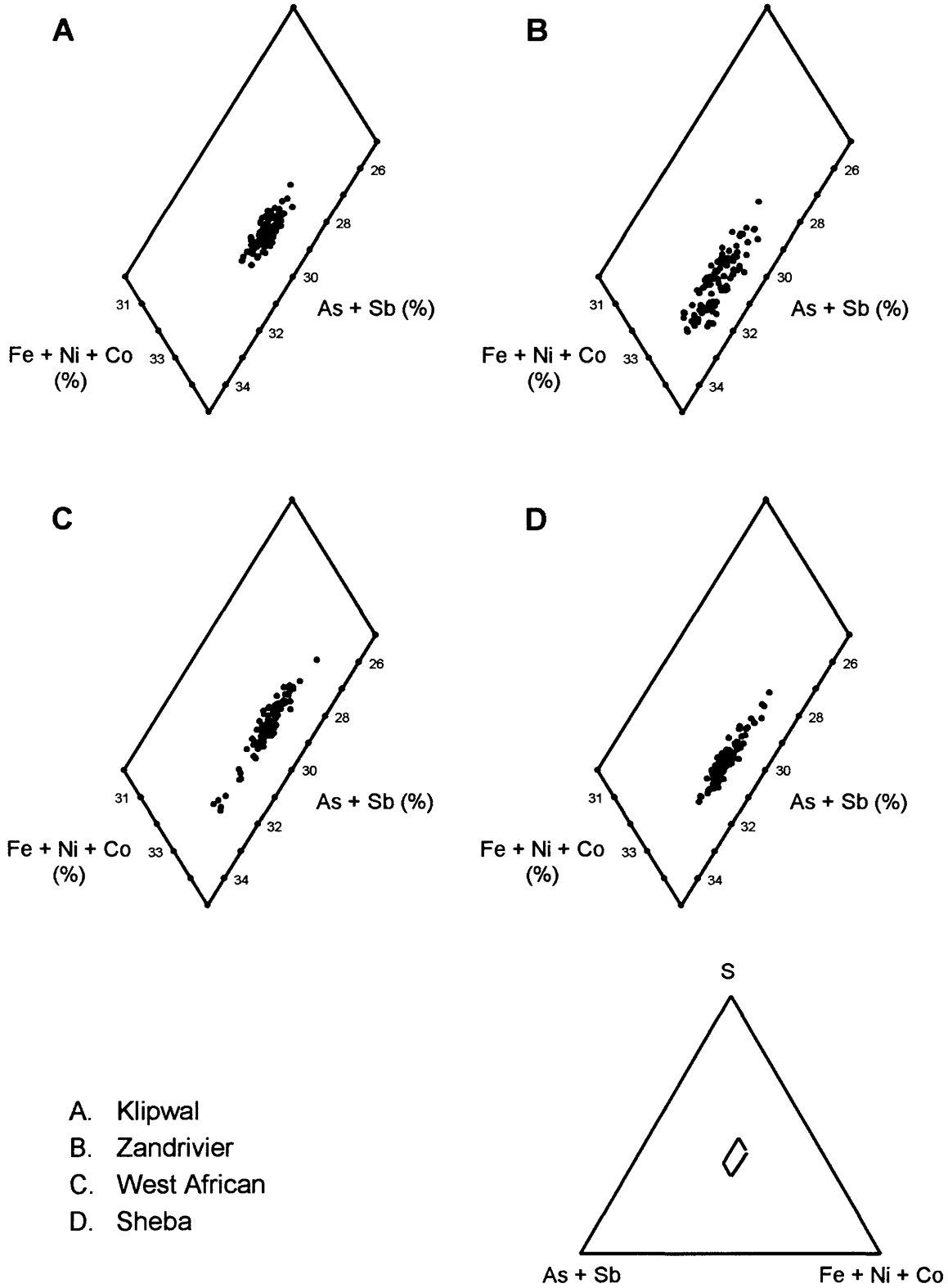

Figure 18. Arsenopyrite compositions in atomic per cent plotted on a ternary diagram. Each point represents one analysis.

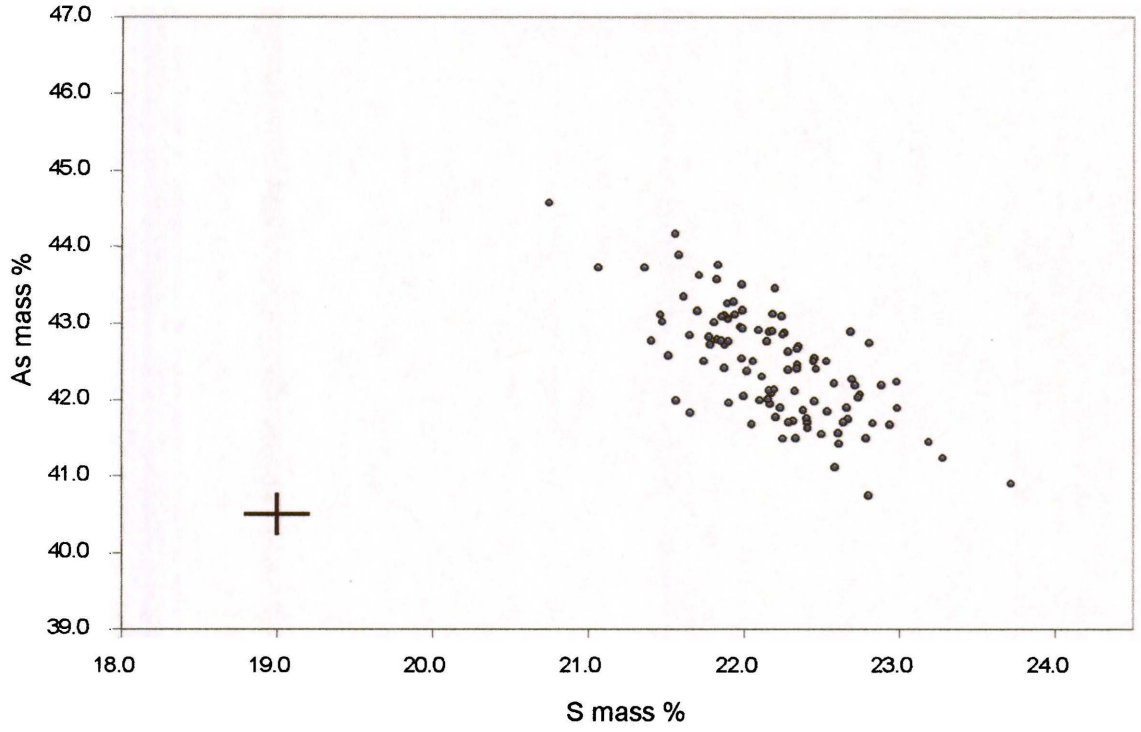

Figure 19. Variation of arsenic and sulphur for Klipwal arsenopyrite. The cross represents ±σ in As and S as determined on the As-2 standard.

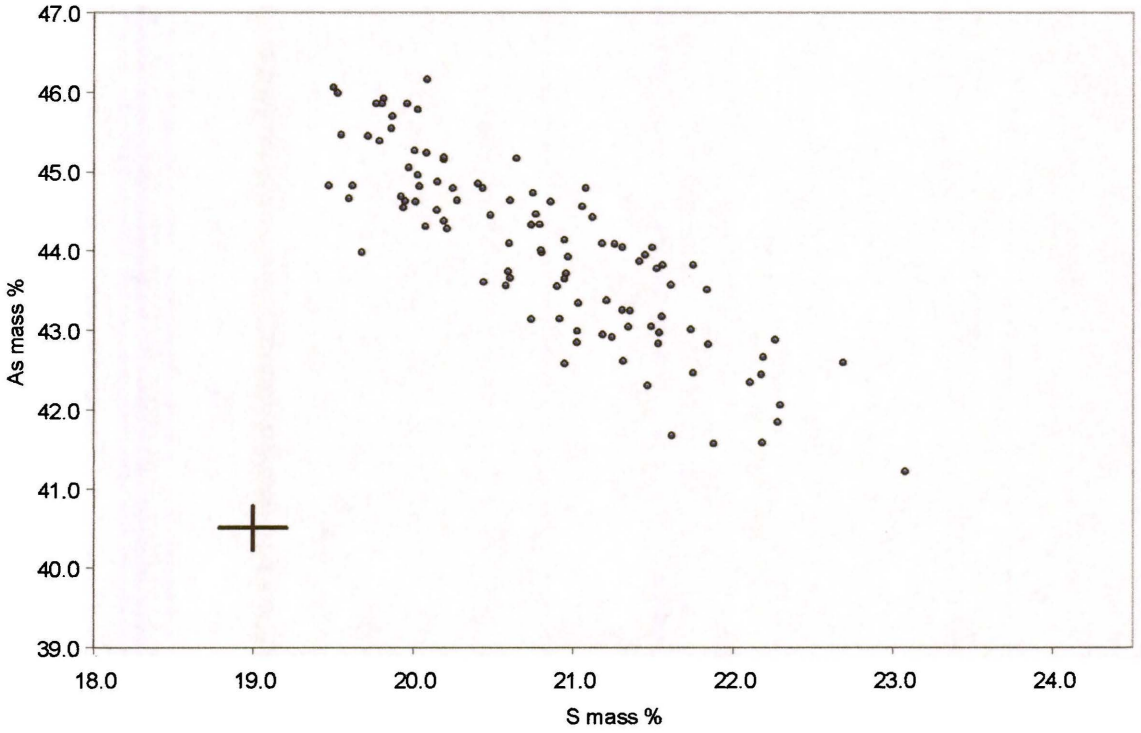

Figure 20. Variation of arsenic and sulphur in Zandrivier arsenopyrite. The cross represents ±σ in As and S as determined on the As-2 standard.

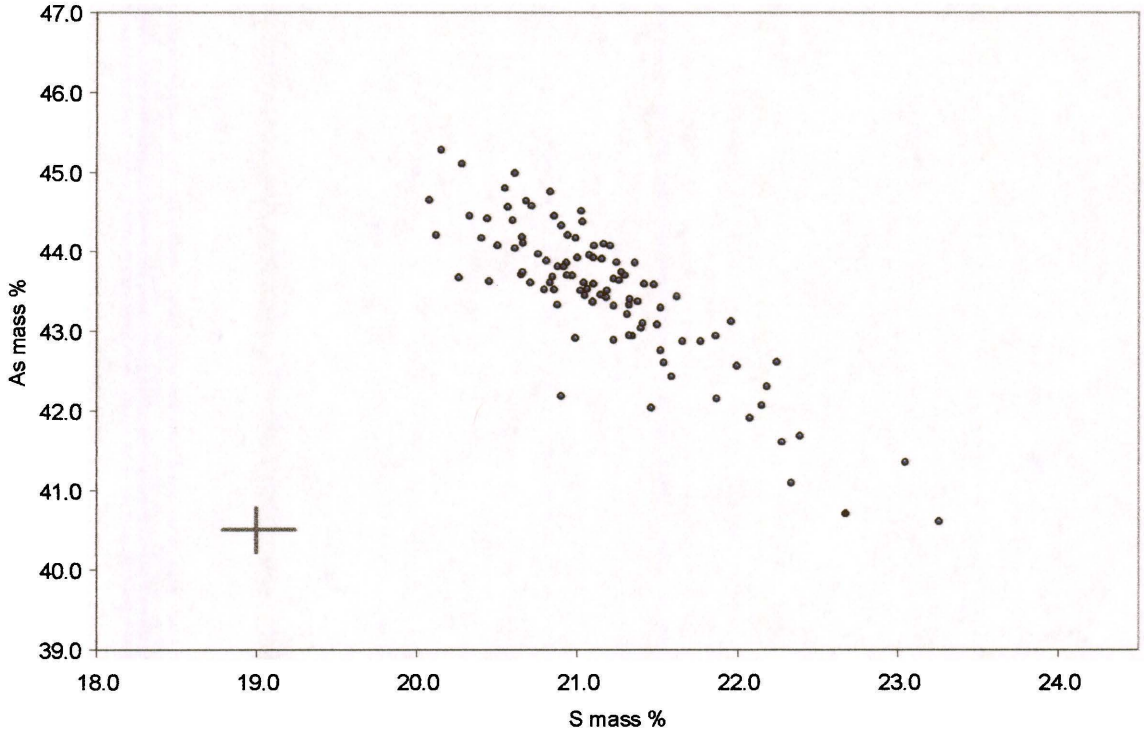

Figure 21. Variation of arsenic and sulphur in Sheba arsenopyrite. The cross represents ±σ in As and S as determined on the As-2 standard.

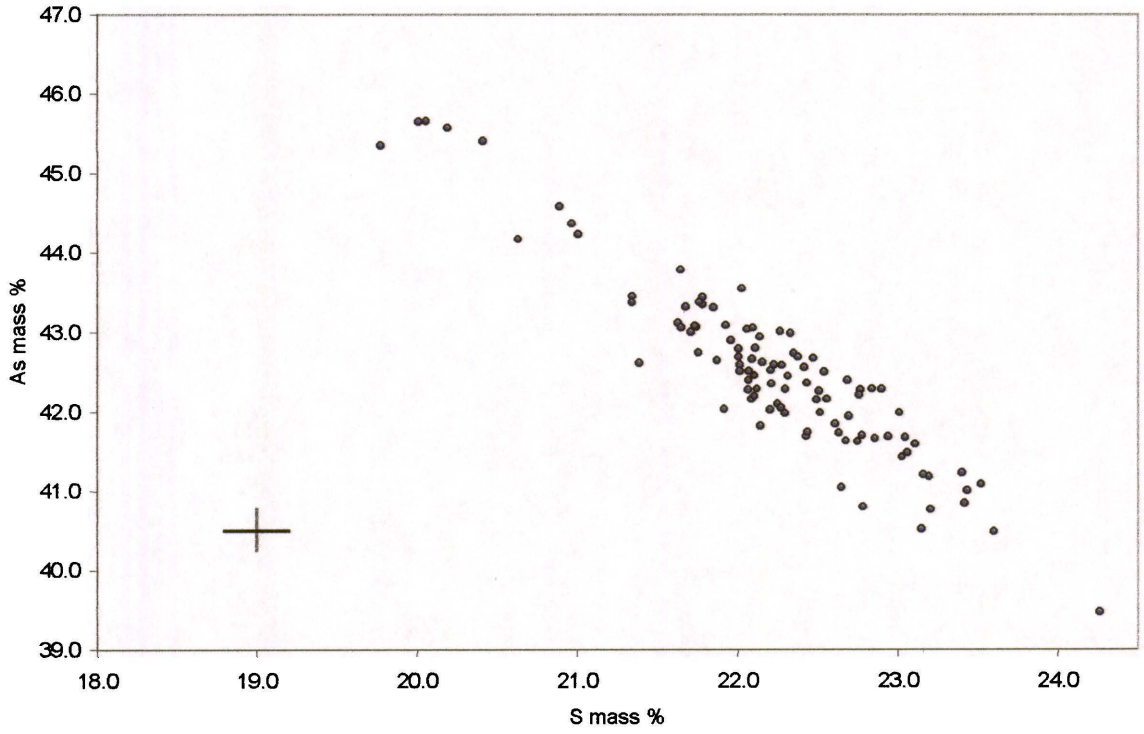

Figure 22. Variation of arsenic and sulphur in West African arsenopyrite. The cross represents ±σ in As and S as determined on the As-2 standard.

initially appear to be strongly zoned, but closer examination reveals that two arsenopyrite types are present. The main type is quite weakly zoned, and these crystals are often overgrown by a thin rim which consists of a slightly more As-rich, late stage arsenopyrite, itself differentiated into two zones. The late-stage arsenopyrite contains relatively high amounts of nickel and cobalt. Typical zonation patterns were discussed in Section 6, and are shown in Figure 11.

A trace element detected in this type of investigation can be present as an inclusion or chemically bound (in solid solution). Microscopic inclusions would have been noticed by their BSE intensity during manual analyses, but in order to establish the absence of submicroscopic inclusions, two positions per zone were analysed. The value of a trace element should be similar in both if that element is chemically bound.

The results of zone analyses are plotted in Figure 23. More spread is evident, especially in the Sheba and West African arsenopyrite, than on the random analysis plots. This is because finely-spaced zones could be pre-selected and analysed, and because minor zones are over-represented. Six points from the West African arsenopyrite analyses fell on, or outside, the maximum Fe+Ni+Co value of 35 atm.%. Two of these were not confirmed by the paired zone result, and therefore most likely represent submicroscopic pyrite or pyrrhotite inclusions. The other four results, however, in which iron ranges from 45.0 to 35.7 atm.%, are paired results all from one particle (arsenopyrite G50), so these appear to be true values. Arsenopyrite with iron values of up to 38 atm.%, has been described (KLEMM, 1965) although these results were gleaned from sources over 100 years old, and so should be treated with circumspection.

As can be seen from Table 19, certain trace elements are associated with S-rich (dark BSE intensity) or As-rich (bright BSE intensity) zones. For example, in Sheba arsenopyrite, Au is usually associated with the As-rich zones, and Sb with the S-rich zones (Figures 24–26). The gold levels in the Sheba arsenopyrite leached in this study are uncharacteristically low. Sheba MRC arsenopyrite analysed earlier in the investigation showed much higher gold values (Figure 25). There is a negative correlation (due to substitution) between Co + Ni and Fe in the West African arsenopyrite (Figure 27).

It can be inferred from the results that copper is probably not chemically bound in any of the arsenopyrite types, but may be present as submicroscopic chalcopyrite inclusions. Nickel is

TABLE 19

AVERAGE TRACE ELEMENT CONCENTRATIONS IN ARSENOPYRITE (in ppm)

Arsenopyrite Source	Zone[#]	Cu		Ni		Co		Au		Sb	
		%[+]	ave[o]	%	ave	%	ave	%	ave	%	ave
Klipwal	Random*	4	370	44	1340	39	595	2	435	22	505
Zandrivier	Random	12	350	21	470	26	545	3	435	19	315
	Bright	13	375	7	950	27	275	0	0	13	370
	Medium	10	505	20	395	35	340	0	0	30	335
	Dark	0	0	29	435	32	495	0	0	21	345
West African	Random	8	340	30	445	57	570	31	775	16	580
	Very bright	4	340	59	1520	100	3670	4	365	95	545
	Bright	7	345	47	465	70	8225	10	690	60	565
	Medium	6	665	22	1010	44	390	22	550	22	360
	Dark	7	310	33	435	53	505	10	420	37	805
Sheba	Random	3	400	73	805	16	330	27	640	60	935
	Bright	9	480	54	1265	22	1255	46	695	37	490
	Medium	40	410	50	625	10	215	50	695	50	490
	Dark	0	0	9	665	15	410	4	4860	100	2855

[#] Zone refers to the backscattered electron intensity on the microprobe.
* Random arsenopyrite analyses.
[+] Percentage of grains that contain a significant amount of the element.
[o] Average of those analyses above detection limit.
Detection limits are: Cu – 290ppm, Ni – 240ppm, Co – 210ppm, Au – 350ppm and Sb – 210ppm.

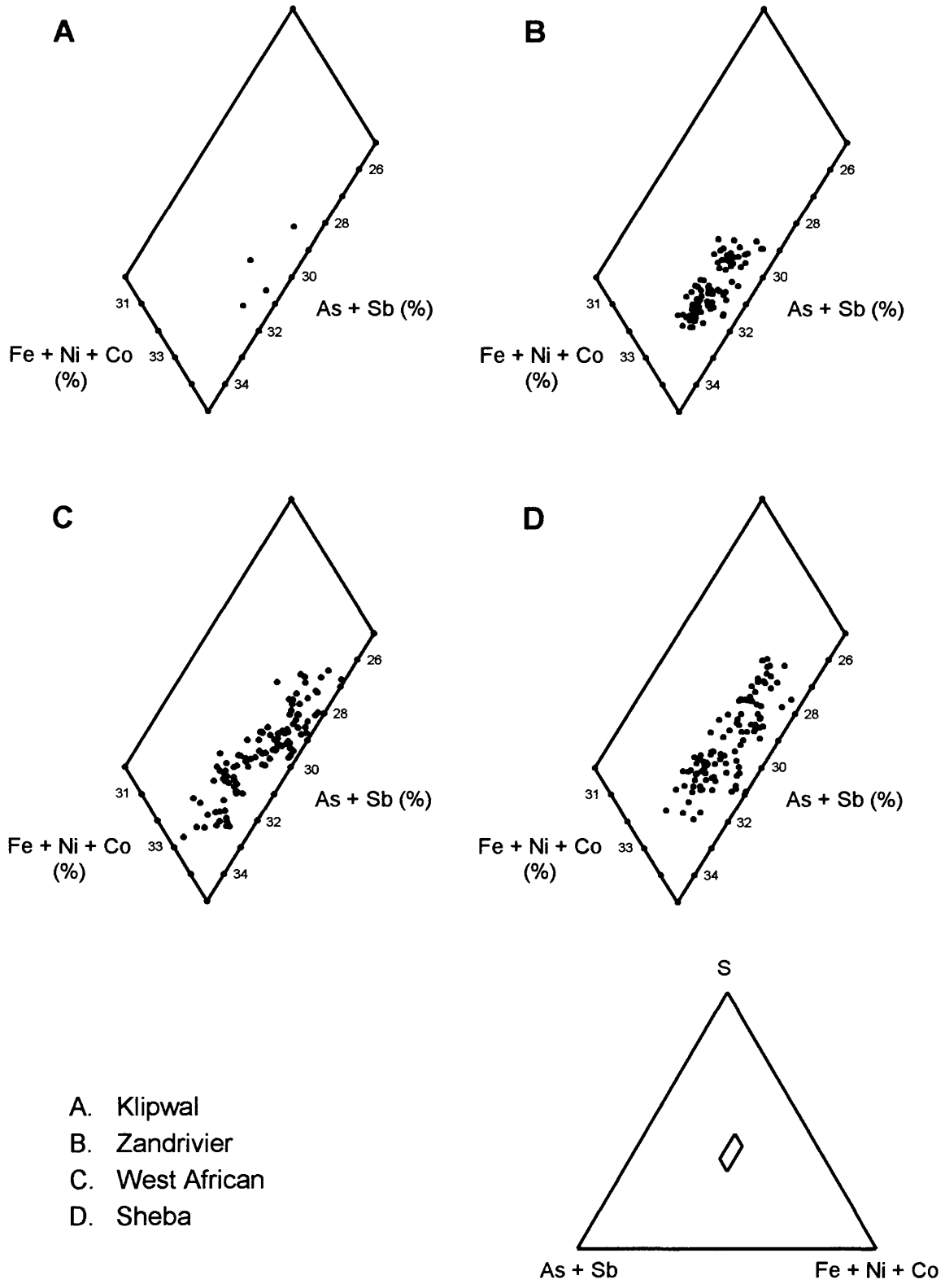

Figure 23. Arsenopyrite zone compositions in atomic per cent plotted on a ternary diagram. Each point represents one analysis.

likely to be chemically bound in some of the Sheba and West African arsenopyrite, but rarely in the Zandrivier arsenopyrite. Cobalt is frequently chemically bound in the West African, but rarely in the Sheba and Zandrivier arsenopyrite. Antimony appears to be chemically bound in the S-rich Sheba arsenopyrite zones, and gold in the As-rich zones.

This information is summarised in Table 20 below.

TABLE 20

DISTRIBUTION OF THE TRACE ELEMENTS IN THE ZONED ARSENOPYRITE TYPES

Source	Zone*	Cu	Ni	Co	Au	Sb
Zandrivier	Bright	i	I	i	–	i
	Medium	i	I	(c), i	–	i
	Dark	–	(c), I	(c), i	–	i
Sheba	Bright	i	(c), I	(c), i	(c), i	(c), i
	Dark	–	I	i	i	c
West Africa	Very bright	i	(c), I	c	i	c
	Bright	i	(c), I	(c), i	i	(c)
	Medium	i	(c), I	(c), i	(c)	i
	Dark	i	(c), I	(c), i	i	(c), i

*Zone – BSE image intensity
Chemically bound = c
Sometimes chemically bound = (c)
Present as inclusions = i

7.2.1.4 Discussion of arsenopyrite composition

In summary, the compositional similarity and differences between the four arsenopyrite types imply –

- All types are S-rich overall, with similar As-S distribution plots.

- Klipwal arsenopyrite is weakly, and finely, zoned, with a low trace element content. It does not contain submicroscopic gold, but Ni, Co, and Sb are occasionally chemically bound

- The Zandrivier arsenopyrite shows variable zonation – in some areas it is absent, but in others it is relatively well developed, and three zones are usually present, on a coarser

scale than those observed in Klipwal arsenopyrite. The Zandrivier arsenopyrite contains very low amounts of trace elements; Co and Ni are rarely chemically bound, and submicroscopic gold is absent.

- The Sheba arsenopyrite is frequently strongly zoned on a fine scale, and contains higher amounts of trace elements. Au, Sb, Co and Ni are commonly chemically bound.

- The West African arsenopyrite is of two types. The main phase arsenopyrite is weakly zoned with a similar trace element content to that of Sheba arsenopyrite. Au, Sb, Ni and Co are often chemically bound. The later-stage arsenopyrite rims are also weakly zoned (but As-rich compared to the main phase) with a relatively high trace element content. Co, Ni and Sb are more often chemically bound than not.

7.2.2 Analysis of other sulphide minerals

Quantitative WDS analyses on the electron microprobe were run on pyrite from all four samples, on West African and Zandrivier pyrrhotite, and on Sheba gersdorffite. The results are tabulated in Tables A16 to A21in the Appendix (pages 221–230). The results of semi-quantitative WDS analysis of three Sheba tennantite and tetrahedrite particles are presented in Table 21. Trace element results are presented in Tables 22–24.

TABLE 21

SEMI-QUANTITATIVE MICROPROBE ANALYSIS RESULTS FOR SHEBA TENNANTITE-TETRAHEDRITE

	As mass %	Sb mass %	Cu Mass %	S mass %	Fe mass %	Ag mass %	Zn mass %	Total mass %
G1 tetrahedrite	0.2	28.7	38.7	23.9	2.5	0.1	5.9	100.0
	1.3	27.3	38.5	24.0	2.3	0.1	6.5	100.0
G1 tennantite	13.1	11.8	42.3	25.7	6.1	0.1	0.9	100.0
	12.4	11.9	41.6	25.4	4.6	0.1	4.0	100.0
G2 tetrahedrite	0.3	29.4	39.9	24.3	5.1	n.d.*	1.0	100.0

*n.d. = not determined

TABLE 22

AVERAGE TRACE ELEMENT CONCENTRATIONS IN PYRITE (in ppm)

Pyrite source*	Cu		Ni		Co		Au		Sb		Ag	
	%+	ave0	%	ave	%	ave	%	ave	%	ave	%	ave
KW	0	0	40	1260	0	0	0	0	10	410	0	0
ZR	7	910	10	2300	7	675	0	0	7	1535	7	300
WA	6	665	85	2655	82	7960	0	0	9	565	3	355
SH	17	1080	40	4830	8	3480	8	865	10	420	0	0

* Pyrite source – KW is Klipwal, ZR is Zandrivier, WA is West African, and SH is Sheba.
+ Percentage of grains that contain a significant amount of the element.
0 Average of those analyses above detection limit.
Detection limits are: Cu – 570 ppm, Ni – 405 ppm, Co – 415 ppm, Au – 505 ppm and Ag – 240 ppm.

TABLE 23

AVERAGE TRACE ELEMENT CONCENTRATIONS IN GERSDORFFITE (in ppm)

Cu		Co		Au	
%+	average0	%	average	%	average
50	700	92	2555	4	595

+ Percentage of grains that contain a significant amount of the element.
0 Average of those analyses above detection limit (in ppm).
Detection limits are: Cu – 320 ppm, Co – 230 ppm, Au – 345 ppm.

TABLE 24

AVERAGE TRACE ELEMENT CONCENTRATIONS IN WEST AFRICAN PYRRHOTITE (in ppm)

As		Cu		Ni		Co		Au		Sb	
%+	ave0	%	ave	%	ave	%	ave	%	ave	%	ave
19	350	2	1450	93	885	38	720	2	520	2	310

+ Percentage of grains that contain a significant amount of the element.
0 Average of those analyses above detection limit (in ppm).
Detection limits are: As – 230 ppm, Cu – 705 ppm, Ni – 425 ppm, Co – 410 ppm, Au – 505 ppm, Sb – 275 ppm.

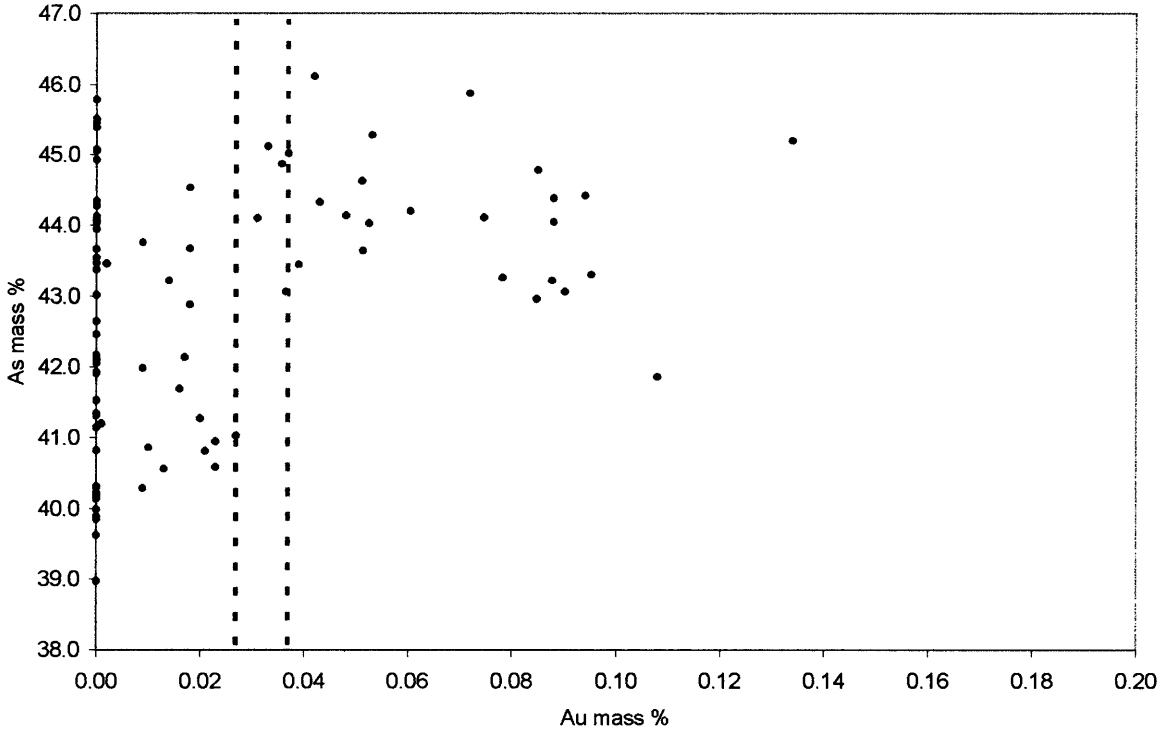

Figure 24. Relationship between gold and arsenic in the Sheba arsenopyrite used in this study. Red dashed lines show detection limits at 95% and green dashed lines at 98% confidence.

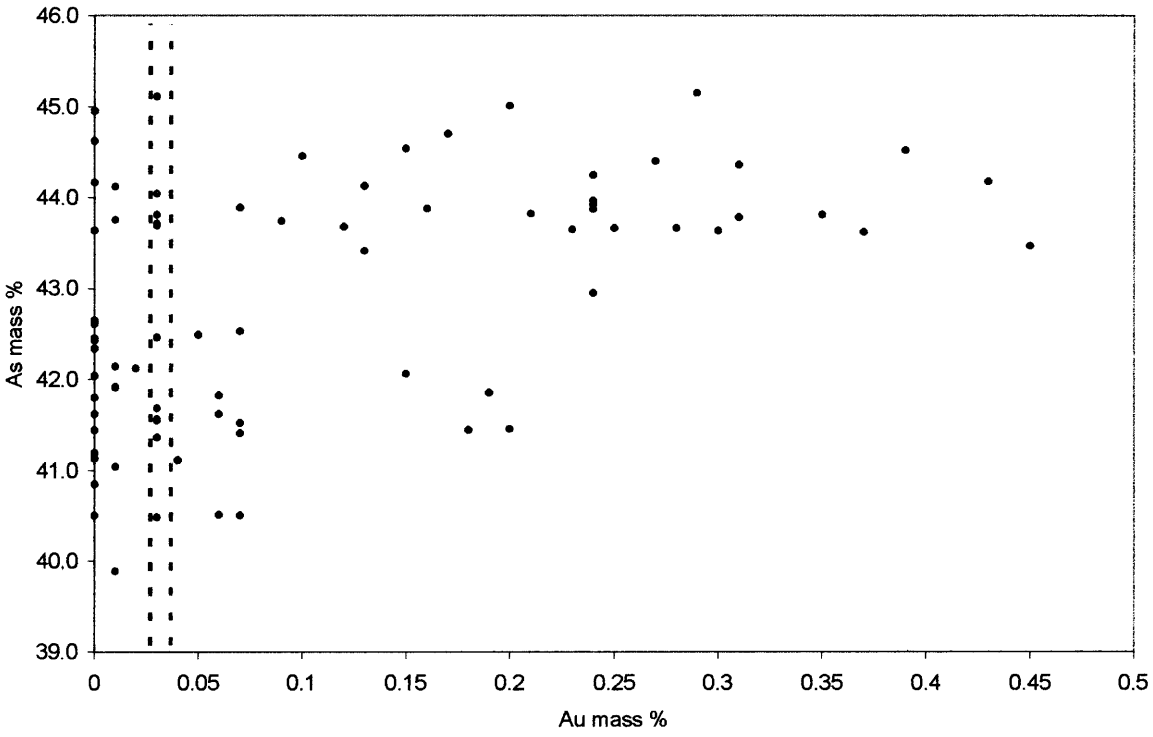

Figure 25. Relationship between gold and arsenic in more typical Sheba MRC arsenopyrite examined earlier in the investigation (see text). Note the difference in scale on the X-axis as compared to Figure 24 above.

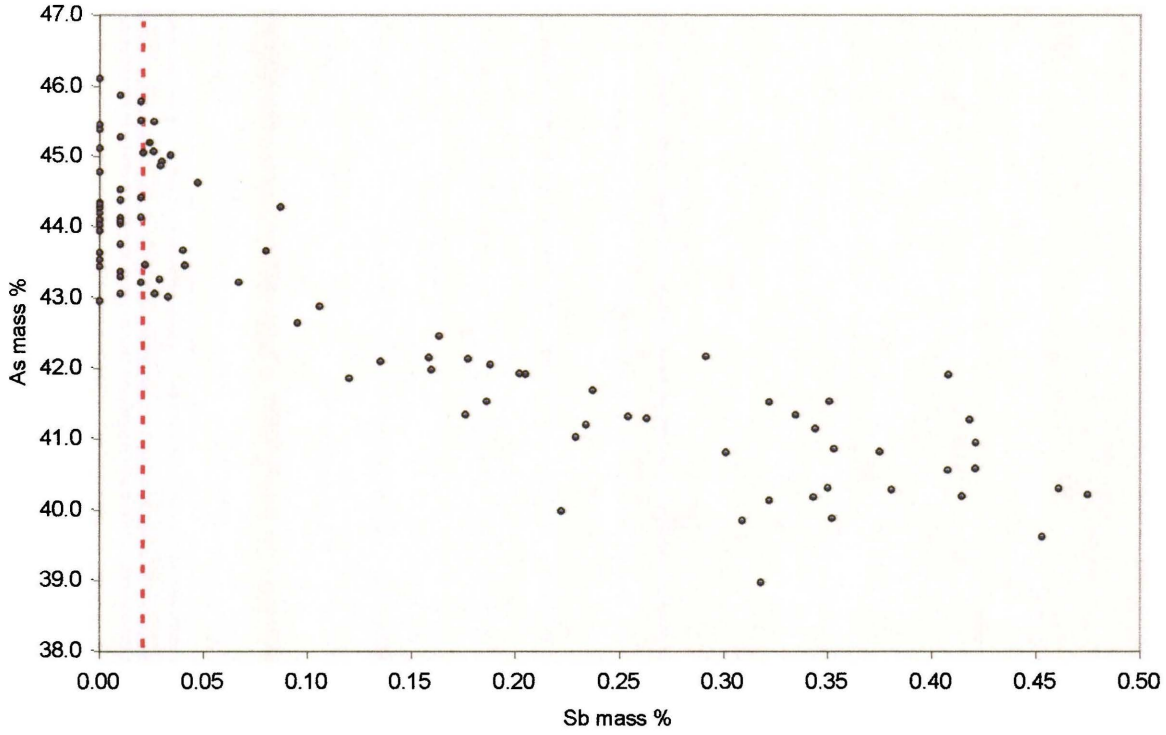

Figure 26. Relationship between antimony and arsenic in Sheba arsenopyrite. The red dashed line represents the detection limit at the 98% confidence level.

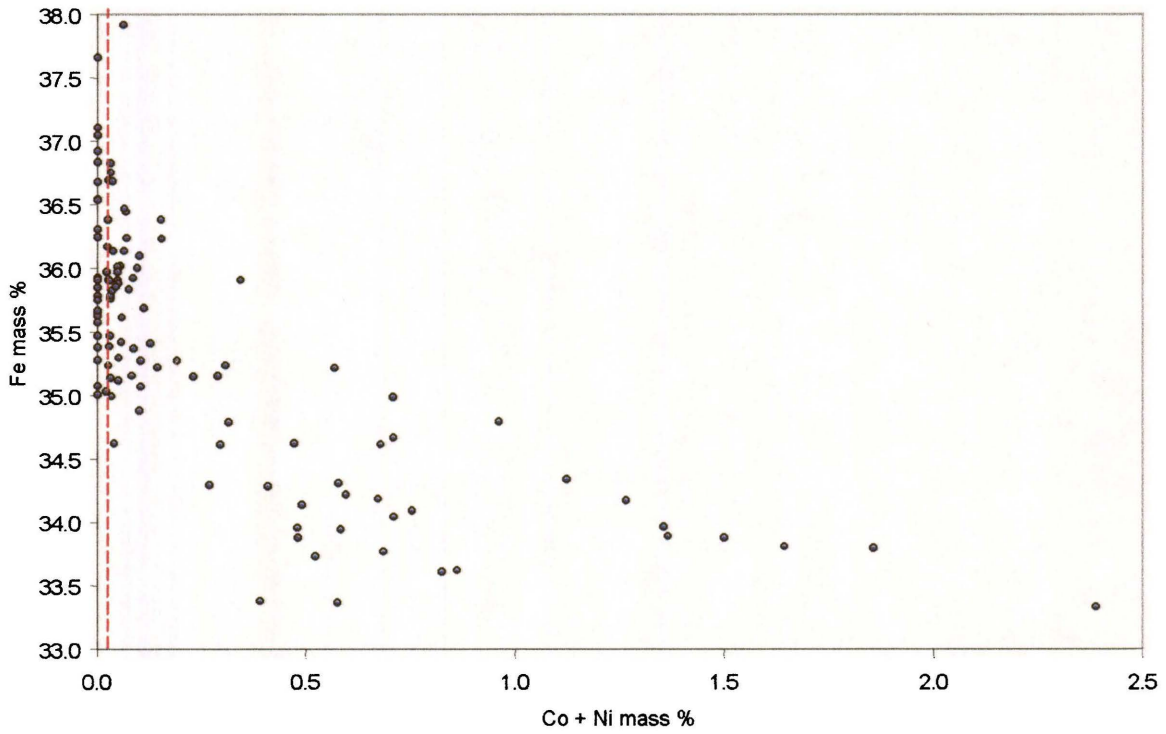

Figure 27. Relationship between (Co + Ni) and iron in West African arsenopyrite. The dashed red line represents the detection limit at the 98% confidence level.

The Sheba gersdorffite is not of end-member NiAsS composition, and contains 6–14 mass % iron. The iron appears to substitute for the nickel, as can be seen in Figure 28. The As/S variation seen in the arsenopyrite is not evident in the gersdorffite (Figure 29). The antimony contents appear to be proportional to nickel and are therefore inversely proportional to iron content rather than to sulphur content (Figures 30 and 31).

The pyrite analysis results are plotted in Figure 32. Examination of the plots shows that whereas Zandrivier pyrite is close to pure FeS_2, Klipwal and West African pyrite contains a little As, and the Sheba pyrites up to 6 atomic % As. Zonation of Sheba, and certain of the West African, pyrite crystals can be seen on the BSE-image of the electron microprobe.

The relatively high Ni and Co content of the later stage West African arsenopyrite is also evident in the pyrite and pyrrhotite of this sample. These sulphides are commonly in contact with the late stage arsenopyrite as they also tend to rim the main arsenopyrite phase.

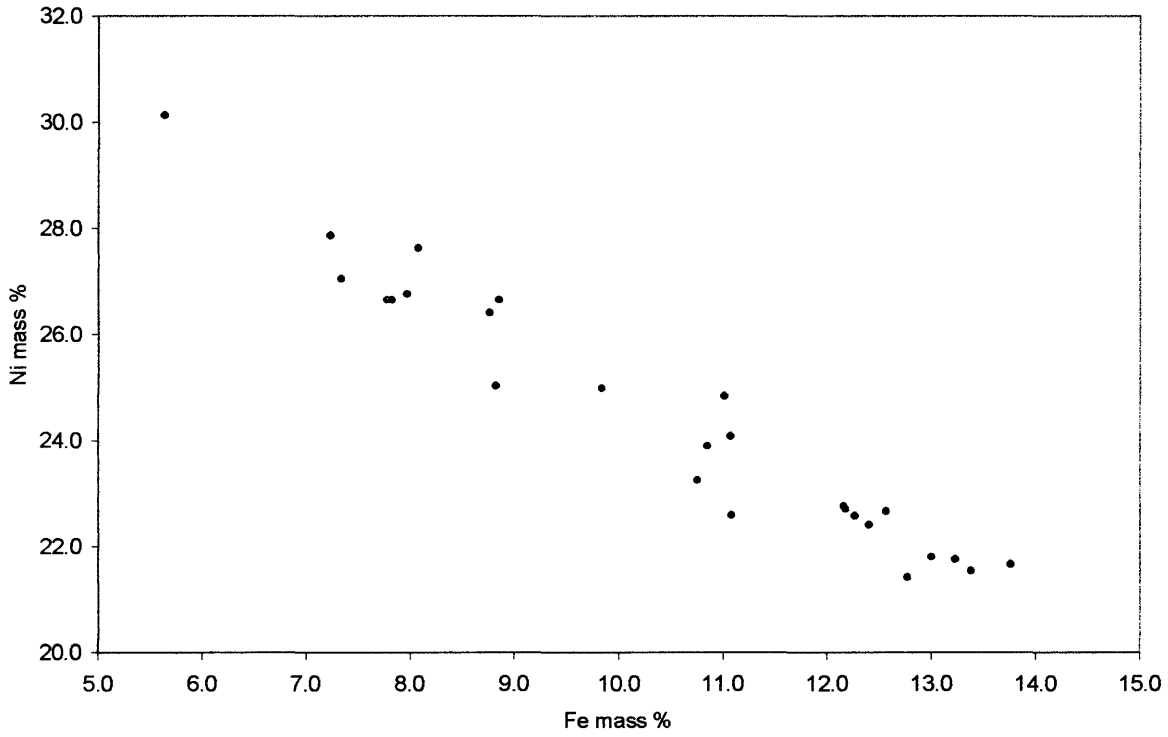

Figure 28. Variation of nickel and iron in Sheba gersdorffite.

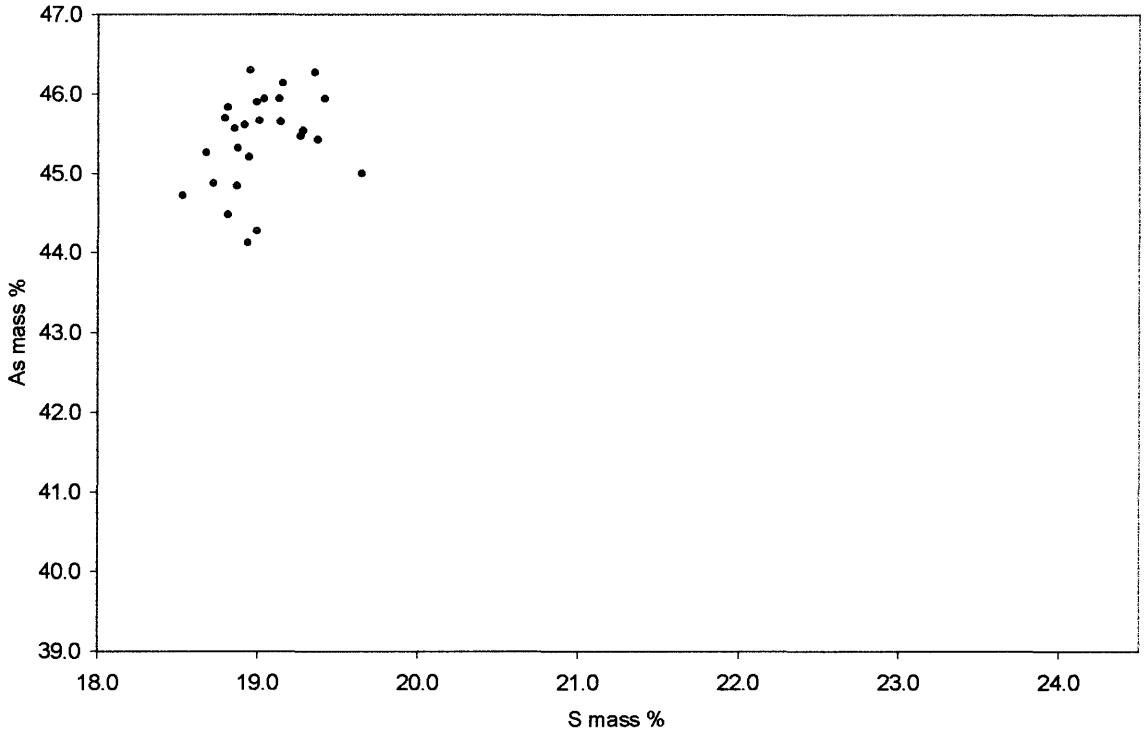

Figure 29. Variation of arsenic and sulphur in Sheba gersdorffite, plotted to the same scale as the arsenopyrite.

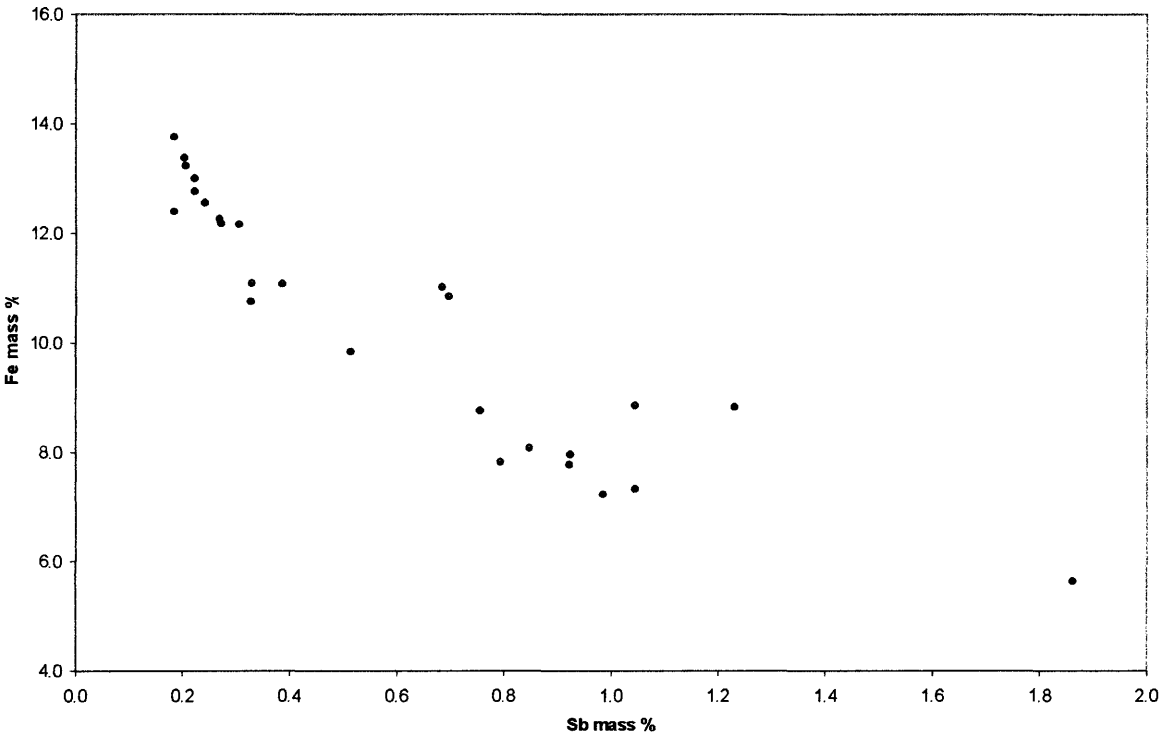

Figure 30. Variation of antimony and iron in Sheba gersdorffite.

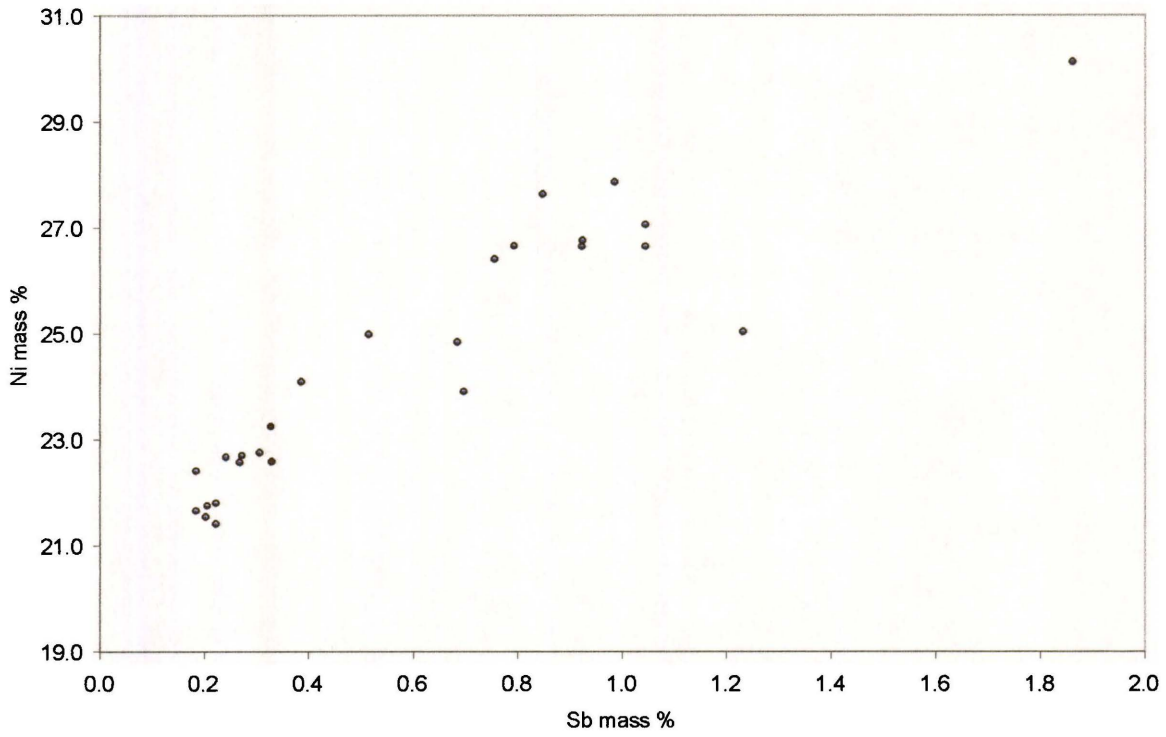

Figure 31. Variation of antimony and nickel in Sheba gersdorffite.

The Zandrivier pyrrhotite invariably contains some arsenic, but no other trace elements were detected. The pyrite, like its arsenopyrite counterpart, is also low in trace elements compared to pyrite from the other samples.

Both the tennantite and the tetrahedrite contain zinc. Zincian tetrahedrite has been described from low- to medium-temperature hydrothermal vein deposits (PETERSEN *et al.*, 1990).

7.2.3 Formation temperatures of the sulphide minerals

When arsenopyrite forms under conditions of buffered sulphur activity ($a(S_2)$), the As/S ratio is mainly a function of temperature (KRETSCHMAR & SCOTT, 1976, KOH *et al.*, 1992). Several provisos apply to this statement :

The effect of pressure on such a system has been claimed to be negligible (KRETSCHMAR & SCOTT, 1976) contradicting previous work (CLARK, 1960), so any pressure effect is therefore not compensated for using the formation temperature calculations. The amount of arsenopyrite present in the system should be sufficient to produce statistically good

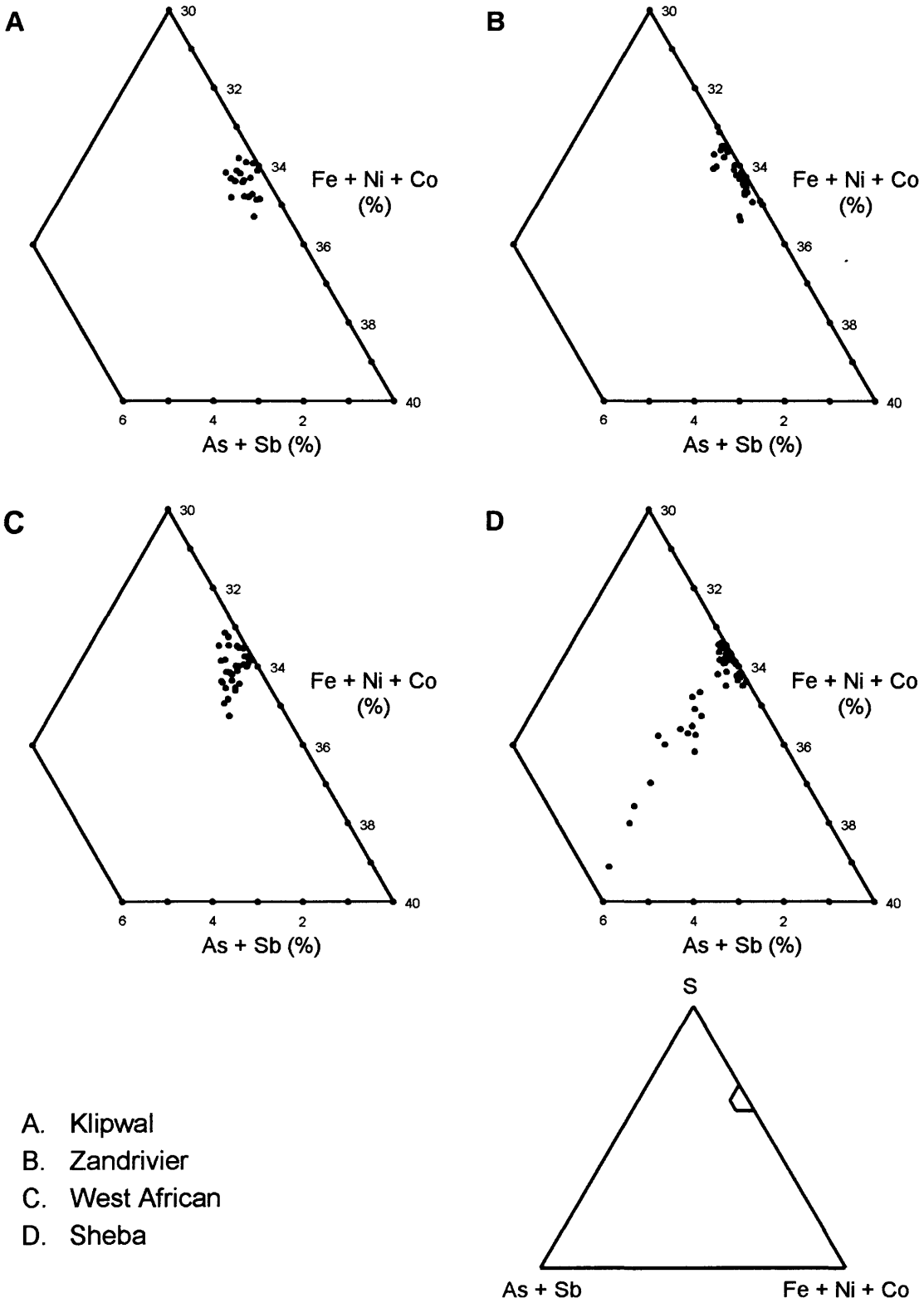

Figure 32. Pyrite compositions in atomic per cent plotted on a ternary diagram. Each point represents one analysis.

compositional analyses, but should 'not be so high as to act as a buffer itself' (KRETSCHMAR & SCOTT, 1976).

The system must be in equilibrium – and this is notoriously difficult to prove. Arsenopyrite is refractory and unlikely to change its composition rapidly with later changes in its environment. This means that initially-formed arsenopyrite, and co-forming minerals, in a vein would be in equilibrium with the depositing fluid. Later alteration, however, could alter co-existing minerals, and not the arsenopyrite, although younger arsenopyrite overgrowths may form around the original crystals (KRETSCHMAR & SCOTT, 1976). Strongly compositionally zoned arsenopyrite may represent non-equilibrium systems, and could reflect a variation in formation temperature values of over 200°C within one crystal (CATHELINEAU *et al.*, 1988).

The temperature range becomes uncertain at low arsenic atomic per cent, because the investigation of the system does not deal with arsenic contents of less than 28 atm. %. Many arsenopyrite crystals, especially when gold-bearing, 'form at temperatures below 200°C' (CATHELINEAU *et al.*, 1988), and again this is outside the field of the investigation by Kretschmar and Scott.

To estimate the temperature of formation, the presence of a sulphur activity buffer should be established by analysing arsenopyrite *only* when it forms a triple junction with pyrrhotite and pyrite (KRETSCHMAR & SCOTT, 1976). This is an infrequent occurrence, however, and some workers have been content to measure the arsenopyrite composition when all three minerals are present in one polished section (SUNDBLAD *et al.*, 1984).

Yet another problem is the presence of trace elements. The trace element content in arsenopyrite must be below 1 mass % in order to use the composition for formation temperature calculations (KRETSCHMAR & SCOTT, 1976). Other authors put this figure at 0.2 mass %, and have proved that antimony, in particular, can produce low temperature estimates when present above this level. Nickel and cobalt also affect temperature estimates (SUNDBLAD *et al.*, 1984).

In fact, the arsenopyrite geothermometer should only be used in conjunction with a knowledge of the background geology of the deposit, the silicate petrology, and, if possible, with fluid inclusion studies.

In the light of these restrictions, it is unlikely that any of the four arsenopyrite types in this study will provide a reliable formation temperature. The only type in which triple junctions occur are in the later stage West African arsenopyrite, and these are frequently too high in trace elements. Very tiny (<5 μm) inclusions of pyrrhotite are found in Sheba arsenopyrite in the same section as pyrite, and pyrite and pyrrhotite occur in mutual, but not triple junction, contact in the Zandrivier samples. No pyrrhotite was observed associated with Klipwal arsenopyrite, probably due to its removal by HF, but it was described as being present in the original ore samples (RUSSELL, 1985).

The range in normalised As atomic per cent values for the zone analysis of the four arsenopyrite types from this study is shown in Table 25, as are the temperatures of formation estimated from the Kretschmar-Scott diagram. Minimum temperatures cannot be established.

TABLE 25

RANGE OF As ATOMIC % AND TEMPERATURE OF FORMATION OF ARSENOPYRITE

	As atomic %	Formation temperature (°C)
Klipwal	28.8–32.0	Up to 430
Zandrivier	29.4–33.3	Up to 510
Sheba	27.4–33.6	Up to 520
West African (early)	26.8–31.4	Up to 400
West African (late)	28.9–34.4	Up to 550

Based on the method used by KRETSCHMAR & SCOTT (1976).

The results for Sheba arsenopyrite can be compared to the results of previous workers (SCHOUWSTRA, 1990) which suggested formation temperatures of less than 300°C to 440°C (see Figure 33). The greater spread of results from this study could be due to the selected zone analysis, which leads to a larger range in As atomic %. There is also the possibility of later stage As-rich overgrowths on some arsenopyrite crystals, as mentioned earlier.

The results for Klipwal arsenopyrite can be compared (Figure 34) to temperatures of formation previously calculated from triple junction analysis at 350–400°C (RUSSELL, 1985). It should be noted that no evidence of compositional zonation was found, so again the results of this study will give a broader temperature range.

Higher-arsenic areas of Zandrivier arsenopyrite are found in veins cutting through the main arsenopyrite, and adjacent to quartz veins. These appear to have had a higher formation temperature, but it is difficult to establish whether both phases coexisted with pyrite and pyrrhotite. The temperature field of Zandrivier arsenopyrite is plotted in Figure 35.

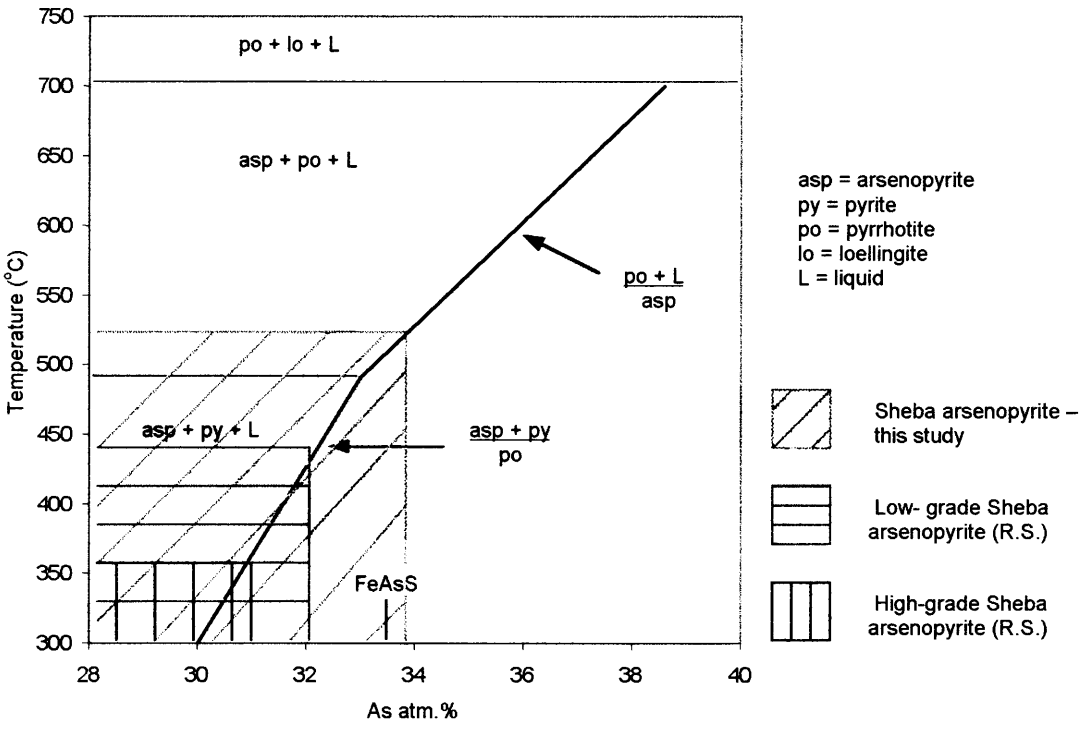

Figure 33. Formation temperatures of Sheba arsenopyrite. Data from this study, and from Schouwstra (1990) – R.S. in the key. The plot is after Kretschmar and Scott (1976).

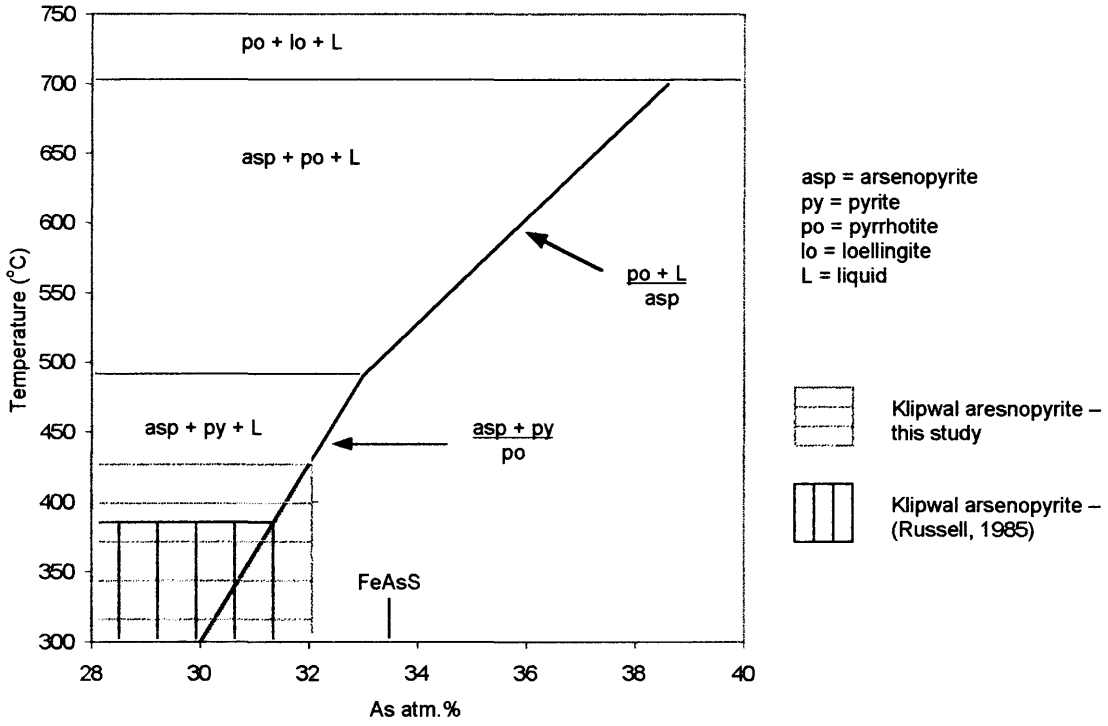

Figure 34. Formation temperatures of Klipwal arsenopyrite. Data from this study, and from Russell (1985). The plot is after Kretschmar and Scott (1976).

If the trace element content of the West African arsenopyrite can be disregarded, it seems likely that the later stage arsenopyrite rims formed at higher temperatures than the initial main phase arsenopyrite, indicating hydrothermal activity after deposition (Figure 36).

The temperature of formation of the West African and Zandrivier sulphides was also calculated from the composition of pyrrhotite in equilibrium with pyrite. The method used was taken from the literature (FROESE, 1976). The results of the calculation are pressure-dependent, and are presented in Table 26. The range of pyrrhotite compositions is produced only from the analysis of pyrrhotite in contact with pyrite in the West African samples, but the Zandrivier pyrrhotite compositions are produced from same-section analyses. Given that the pyrrhotite in the West African samples is associated exclusively with late-stage arsenopyrite formation, the results of the pyrrhotite/pyrite geothermometer calculations are reasonably consistent with those of the arsenopyrite geothermometer estimates. The Zandrivier pyrrhotite/pyrite results produce very wide-ranging results.

TABLE 26

RANGE OF PYRRHOTITE COMPOSITIONS AND TEMPERATURE OF FORMATION

	Mole fraction FeS (X)		1 atm.	2 kb	5 kb	10 kb
Zandrivier	X min	0.87	657°C	632°C	595°C	533°C
	X max	0.92	233°C	208°C	171°C	109°C
West African	X min	0.87	657°C	632°C	595°C	533°C
	X max	0.90	437°C	412°C	375°C	265°C

Based on the method used by FROESE (1976).

In the absence of supporting geological and petrological evidence, it can be concluded that all four arsenopyrite types probably formed at relatively low temperatures, as hydrothermal vein deposits, but that later stage alteration or deposition may have taken place at higher temperatures in the Sheba, Zandrivier and West African deposits.

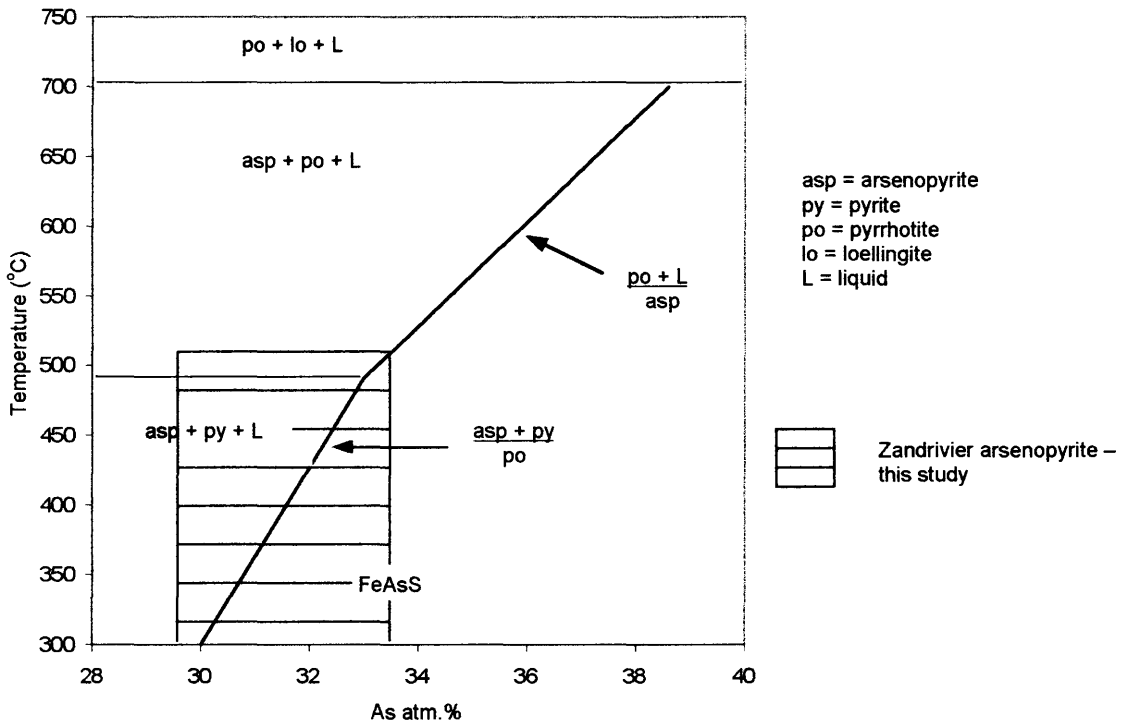

Figure 35. Formation temperatures of Zandrivier arsenopyrite (this study). Plot after Kretschmar and Scott (1976).

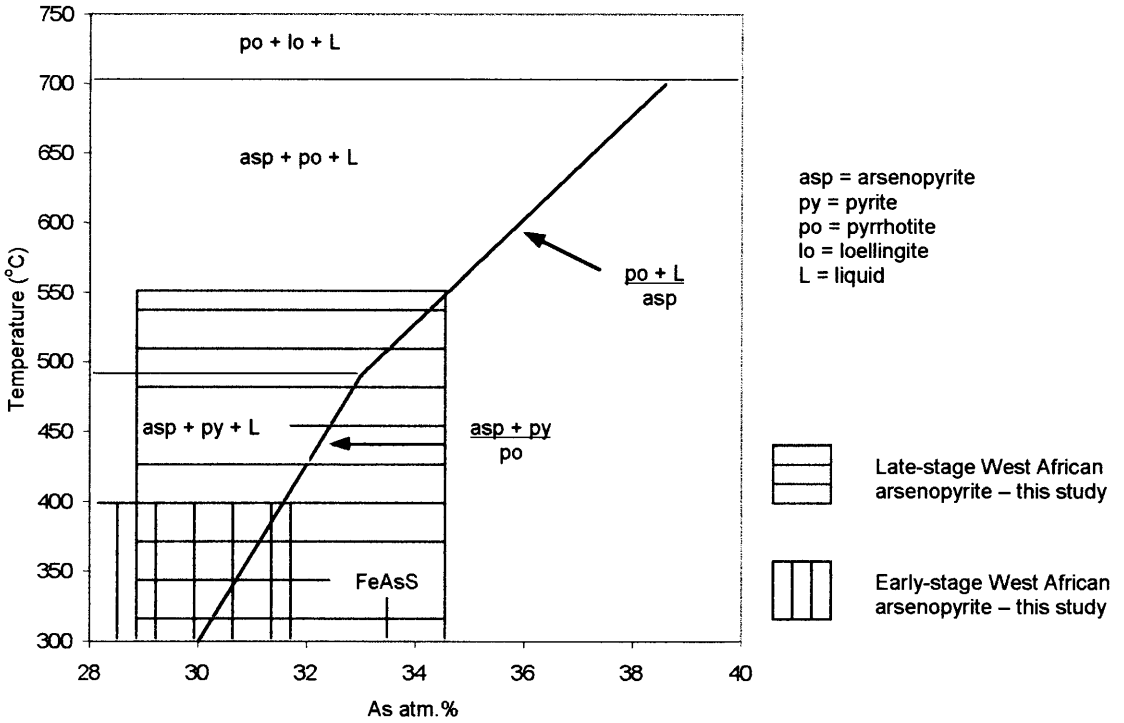

Figure 36. Formation temperature of West African arsenopyrite. The late stage arsenopyrite has a high trace element content, which may make this interpretation dubious (see text). Plot after Kretschmar and Scott (1976).

8. INTRODUCTION TO THE LEACH PROGRAM

The experimental setup used for ferric sulphate and bacterial leach tests was described in Section 5. The PVC reactor is an ideal sterile leaching vessel, as it excludes light, which is known to increase the reactivity of arsenopyrite, a semi-conductor (VAUGHAN, 1984, HOLMES & CRUNDWELL, 1995). The vessel also contains sufficient liquor to produce a high liquid to solids ratio, under which conditions it is easy to maintain constant pH and Oxygen Reduction Potential (ORP).

8.1 The leach program

The average physical conditions during the sixteen bacterial and sterile ferric sulphate leach tests are described in Section 5, and tabulated in Tables 9 and 11. Ferric sulphate leach tests 1 to 5 were performed to establish the effects of varying physical leach conditions such as temperature, concentration of ferric iron in solution, pH, and arsenopyrite particle size. The

object was to try and keep the conditions within the range of those commonly used during bacterial leaching (*i.e.* ferric iron concentrations of 10 to 40 g/l, pH 0.8 to 1.2, and temperatures of approximately 35° C). The results of bacterial leach test 1 gave a preliminary indication of the catalytic role played by the bacteria. Duplicate ferric sulphate leach tests 6a and 6b (results combined and presented as leach test 6) defined semi-quantitatively the relative leach rates of the four arsenopyrite types, and bacterial leach test 2 was an attempt to repeat this with bacteria. The rock section leach tests (ferric sulphate leach 7 and bacterial leach 3) produced more detailed information about the effect of compositional variation in arsenopyrite, and interaction between different sulphide minerals, on leach rate. Ferric sulphate leach 8, run simultaneously with leach 7, was used for reflectivity measurements. The surface oxidation of the loose crystals leached in ferric sulphate leach tests 9 and 10 was studied by Auger Electron Spectroscopy (AES). Finally, loose powder ferric sulphate leach tests 11 and 12 were intended to provide information on arsenic speciation in solution.

The variation of physical conditions during leaching is tabulated with the individual leach descriptions below. Composite sections, crystals, and powders were added after the ORP and pH of the solutions had stabilised. A slight fall-off in ORP (but no rise in pH) was observed in most of the sterile ferric sulphate leach tests between the initial readings and the first measurement after sample addition. This did, however, not affect the comparative leach rate studies, due to the use of composite sections.

8.2 Stages of bacterial oxidation and ore microscopy

Ten distinct stages of oxidative attack, based on the leach colours of sulphide minerals, can be distinguished under the ore microscope during the bacterial oxidation of arsenopyrite-pyrite concentrates in polished section. The stages are described in Table 27 below.

In the course of a successful bacterial leach, Stage 8 can be achieved within 10 days of bacterial inoculation, and Stage 10 within 15 days. There is always a lag in bacterial activity after inoculation, which leads to the Oxygen Reduction Potential (ORP) only reaching maximum after 10 to 15 days. This means that sections placed in the leach after the ORP has settled would reach Stage 10 far more quickly. Certain sulphides, such as chalcopyrite, remain untarnished even at Stage 10, but this is usually not a problem in refractory gold recovery processes, since most submicroscopic gold would be present in arsenopyrite and pyrite.

TABLE 27

BACTERIAL OXIDATION STAGES IDENTIFIED MICROSCOPICALLY

STAGE	OPTICAL CHARACTERISTICS
1	Pyrrhotite tarnishes to brown. Pyrrhotite inclusions in arsenopyrite are leached out.
2	All pyrrhotite has leached out. Arsenopyrite in contact with pyrite is slightly etched.
3	Faint etching is visible in all arsenopyrite.
4	Deeper etching evident in arsenopyrite, according to compositional zones. Appearance of channels along cracks in arsenopyrite. Arsenopyrite starts to colour cream to brown.
5	Most arsenopyrite is multicoloured. Strongly-zoned arsenopyrite is blue in As-rich zones.
6	As-rich zones grey, S-rich blue in arsenopyrite. Zoned pyrite starts to colour cream to brown. Unzoned pyrite still appears white.
7	Most arsenopyrite is now grey. Some zoned pyrite is blue.
8	Arsenopyrite appears grey. Channels and pits form in zoned pyrite. Unzoned pyrite now starts to colour.
9	Many internal reflections in surface coating over arsenopyrite. Channels and pits evident in all types of pyrite.
10	Arsenopyrite totally leached out leaving small residue or disappearing completely. Most pyrite extensively attacked.

8.3 Sulphide oxidation colours

The stages outlined above are observed under typical bacterial oxidation conditions *i.e.* in a 5 to 40 g/l ferric sulphate solution, at pH 0.8 to 1.5, at a temperature of 30 to 35°C, and populated with a mixed culture of bacteria, such as those described in Section 1. Although the HF concentrates used in this study contain far more arsenopyrite than the normal bioleaching concentrates, the same microscopic characteristics could be observed as leaching progressed. A fuller suite of surface colours could be distinguished during sterile ferric sulphate leaching conditions as compared to bacterial, due to the slower rate of oxidation and the absence of biological films and adhering solids from the pachuca or reaction vessel.

The leach colours given below can be described according to the system used by the Geological Society of America (GSA) (GODDARD *et al.*, 1963) and also, in the case of arsenopyrite, by reflectance in filtered light. The colours are shown in Tables 28 and 29.

TABLE 28

DEFINITION OF THE LEACH COLOURS DESCRIBED FOR ARSENOPYRITE

(Where the colour is variable, a range is given)

Colour (this study)	GSA standard colour	Colour code*	Reflectance (%) (Na 589)#	Reflectance (%) (Hg 546)@
White	Pale greenish yellow	10Y 8/2	51–54	51–54
Cream	Greyish yellow	5Y 8/4	36–48	38–45
Beige	Yellowish grey	5Y 7/2	20–35	20–35
Brown	Dark yellowish orange to light brown	10 YR 6/6 – 5YR 5/6	7–15	5–20
Dark multicoloured:			4–7	3–6
Maroon	Moderate red	5R 4/6		
Purple	Moderate dark red to very dusky purple	5R 3/6 – 5P 2/2		
Bright blue (Blue 2)	Light blue	5B 7/6	4–8	5–9
Cream 2	Moderate greyish yellow	5Y 7/4	8–10	9–12
Bright multicoloured:			n.d.	n.d.
Lime	Greenish yellow	5Y 7/6		
Turquoise	Light blue-green	5BG 6/6		

* Code as defined by the GSA. This consists of a hue, a value and a chroma component. The handbook gives more detail (GODDARD *et al.*, 1963).
# Reflectance in light passed through a sodium 589 filter.
@ Reflectance in light passed through a mercury 546 filter.
n.d. = not determined.

The colour changes visible on the polished surface of arsenopyrite are as follows: *white (unleached) → cream → beige → brown → dark multicoloured (mainly purple and maroon) → bright blue → cream 2 → bright multicoloured (lime and turquoise) → grey.* Cream 2 is darker than the initial cream colour, but this is not easy to distinguish late in the leach. Colour changes in pyrite during leaching are: *white → cream → yellow → brown → pink-mauve → purple → bright blue → cream-yellow 2 → lime-turquoise → grey.* Colour changes in pyrrhotite are: *cream → beige → brown → chocolate brown → petrol blue → dark blue-black → yellowish beige.* The final coating in each of these sequences has increasing internal reflections as leaching progresses. Insufficient amounts of other sulphide minerals were found

to give a full picture of their colour oxidation sequence. Gersdorffite, however, appears to behave very similarly to arsenopyrite.

TABLE 29

DEFINITION OF THE LEACH COLOURS DESCRIBED FOR PYRITE AND PYRRHOTITE WHICH ARE NOT OBSERVED IN ARSENOPYRITE

(Where the colour is variable, a range is given)

Colour (this study)	GSA standard colour	Colour code*
Yellow	Moderate yellow	5Y 7/6
Cream yellow 2	Yellowish orange	10YR 7/6
Yellow beige	Olive brown	5Y 4/6
Chocolate brown	Moderate brown	5YR 3/4
Pink mauve	Moderate orange pink to pale purple	10R 7/4 – 5P 6/2
Petrol blue	Moderate blue green to moderate blue	5BG 4/6 – 5B 4/6
Blue black	Dusky blue	5PB 3/2

* Code as defined by the GSA. This consists of a hue, a value and a chroma component. The handbook gives more detail (GODDARD *et al.*, 1963).

Colour changes in leaching arsenopyrite can not only be characterised by optical reflectance readings, but also directly related to depth of oxidation as demonstrated using Auger Electron Spectroscopy (AES) (see Section 12 below).

9. CRYSTAL AND GROUND SECTION LEACH TESTS

The leach colours which developed in arsenopyrite during ferric sulphate leach tests 1 to 5, and bacterial leach test 1, are shown in Tables A22 to A25 in the Appendix (pages 231 to 234).

9.1 Ferric sulphate leach 1

A composite crystal section was leached at room temperature in a liquor containing 20 g/l ferric iron (as ferric sulphate), and adjusted to pH 0.6–0.7 with dilute sulphuric acid. The

crystals were leached for one week, with regular microscopic monitoring of leach colour. The variation of pH and ORP is shown in Table 30 below.

TABLE 30

pH AND OXYGEN REDUCTION POTENTIAL (ORP) VARIATION DURING FERRIC SULPHATE LEACH 1
(20 g/l ferric iron concentration, ambient temperature)

Time	pH	ORP (mV)
0	0.68	625
6 hours	0.74 *	618
1 day	0.58	605
2 days	0.57	614
3 days	0.62	612
4 days	0.62	612
7 days	0.61	612

* Acid added.

Although some appeared to be more leached, most of the Klipwal and Zandrivier arsenopyrite particles were still cream to beige after one week in the leach. The West African and Sheba crystals displayed a wide range of leach colours, the majority being beige. A very striking effect of crystal orientation was observed, especially in the Sheba and West African sections, where crystals sectioned length-ways showed the most advanced leach colours. In contrast, some of the crystals sectioned basally were still white, and showed no evidence of any leach attack. General views of the four crystal types after one week in the leach are shown in Figures 37 to 40.

Pyrite particles were not visibly leached at all, and remained white in all four types (Figure 41). No pyrrhotite, galena or chalcopyrite was monitored during this leach. These sulphides are present only as tiny inclusions, although larger particles of pyrrhotite and galena may have once been present but were leached out by HF.

A post-leach examination of the section using the electron microprobe showed that the preferred leaching of arsenopyrite was almost entirely orientation-controlled, with no obvious zone-related leaching except in one or two very As-rich particles of West African arsenopyrite. Oxidation had not proceeded to the extent that oxygen could be detected by EDS analysis, or for any sulphur-enrichment to be found in the residues. No channels or pits were seen in any of the sulphide minerals.

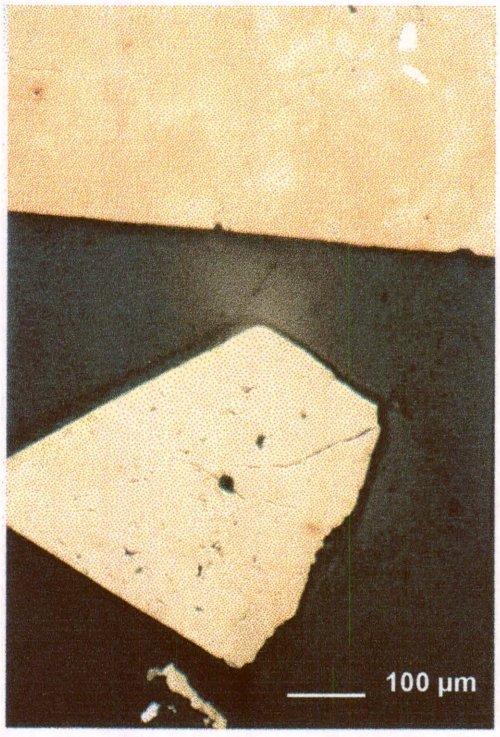

Figure 37. Klipwal arsenopyrite crystals leached for one week in ferric sulphate leach 1.

Figure 38. Zandrivier arsenopyrite particles after one week in ferric sulphate leach 1.

Figure 39. West African arsenopyrite crystals after one week in ferric sulphate leach 1.

Figure 40. Sheba arsenopyrite crystals after one week in ferric sulphate leach 1.

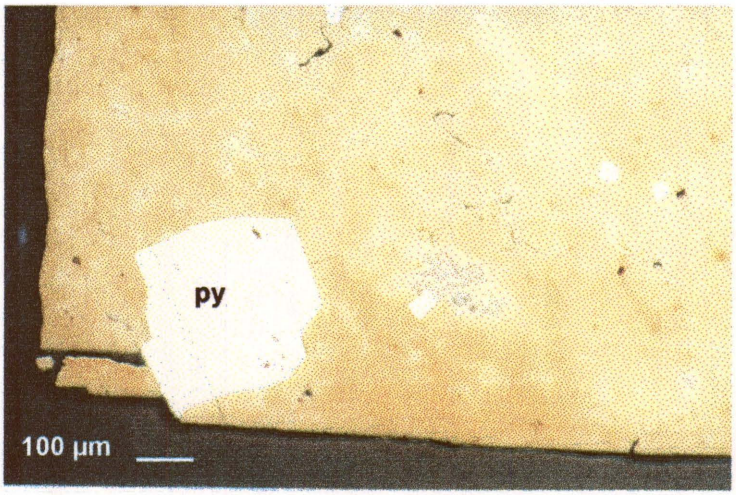

Figure 41. Pyrite (py) in Klipwal arsenopyrite after one week in ferric sulphate leach 1.

9.2 Ferric sulphate leach 2

One composite crystal section and one milled section were leached in liquor containing 20 g/l ferric iron (as ferric sulphate), and adjusted to pH 1.0 with dilute sulphuric acid. The sections were leached for one week, in a leach vessel held at 35°C by submersion in a water bath. The variation of pH and ORP is shown in Table 31 below.

TABLE 31

pH AND OXYGEN REDUCTION POTENTIAL (ORP) VARIATION DURING FERRIC SULPHATE LEACH 2
(20g/l ferric iron concentration, temperature 35±1 °C)

Time	pH	ORP (mV)
0	1.00	700
1 day	0.96	640
2 day	0.95	640
4 days	0.95	630
5 days	0.98	n.d.

n.d. = not determined.

After a week in the leach, the most common leach colours of Klipwal and Zandrivier crystals were beige and brown, West African crystals were mainly brown, and most of the Sheba crystals were dark multicoloured or blue. Again, the effect of crystal orientation was obvious. Also noticeable, especially in Sheba crystals, was the accelerated leaching of As-rich zones in arsenopyrite (this is referred to as zone-related leaching). The milled section showed similar behaviour, but the leaching colours were more advanced when compared to the crystal section. The presence of mimetic twinning in Klipwal, Sheba and West African arsenopyrite crystals was detected under crossed nicols under the microscope after one day in the leach, and became so marked by the second and third day that the twinning could be seen in plane polarized light. Towards the end of the leach the twins were masked by pitting and oxidation.

A black precipitate, probably jarosite, formed on some of the leaching surfaces of both crystal and milled sections. The leached sections were not examined using the electron microprobe at this point – the milled section was repolished and leached in ferric sulphate leach tests 3 and 4 below, after which precipitates were examined.

9.3 Ferric sulphate leach tests 3 and 4

One composite milled section was leached in liquor containing 20 g/l ferric iron (as ferric sulphate), with pH adjusted to pH 0.8 (leach test 3) and then 0.5 (leach test 4) with dilute sulphuric acid. The section was leached for one week per leach at 35° C. The objective of these tests was to prevent the formation of the jarosite precipitate which formed in ferric sulphate leach test 2. The variation of pH and ORP is shown in Table 32 below.

The development of leach colours, twin etching and zone-related leaching with time was very similar to those of ferric sulphate leach 2, but the lower pH in leach 4 definitely inhibited precipitate formation. The precipitate was examined using the electron microprobe, but the coating proved to be so thin that positive identification was impossible. The material was tentatively identified as hydronium jarosite ($(H_3O)Fe_3(SO_4)_2(OH)_6$) – no elemental sulphur or arsenate phases were detected.

TABLE 32

pH AND OXYGEN REDUCTION POTENTIAL (ORP) VARIATION DURING FERRIC SULPHATE LEACHES 3 AND 4
(20 g/l ferric iron concentration, temperature 35±1 °C)

3	Time	pH	ORP (mV)
	0	0.82	640
	1 day	0.82	n.d.
	4 days	0.77	n.d.
	5 days	0.82	630
	6 days	0.82	n.d.
	7 days	0.81	630

4	Time	pH	ORP (mV)
	0	0.50	635
	1 day	0.46	n.d.
	3 days	0.40 *	n.d.
	4 days	0.52	640
	6 days	0.53	n.d.
	7 days	0.45	640

* Added NaOH solution.
n.d. = not determined

9.4 Ferric sulphate leach 5

One crystal and one milled section were leached in liquor containing 40 g/l ferric iron (as ferric sulphate), with pH adjusted to 0.5 with dilute sulphuric acid. The sections were leached for one week per leach at 35° C. Unfortunately, the pH meter developed an electrical fault on the second day of the leach, and the stand-in proved later to be inaccurate. Final pH readings suggest that the liquor may have been as low as pH 0.4 towards the end of the leach. The variation of pH and ORP is shown in Table 33 below.

TABLE 33

pH AND OXYGEN REDUCTION POTENTIAL (ORP) VARIATION DURING FERRIC SULPHATE LEACH 5
(40 g/l ferric iron concentration, temperature 35±1 °C)

Time	pH	ORP (mV)
0	0.48	715
1 day	0.51	702
4 days	0.42 *	688
6 days	*	685
8 days	0.4?	670

* No functional pH meter available until after end of leach.

The entire suite of arsenopyrite leach colours appeared during this leach, with some Sheba and West African crystals achieving second order bright multicolours, and Zandrivier and Klipwal grains leaching as far as second order cream. General views of the four arsenopyrite types after five days in the leach are shown in Figures 42 to 45.

Orientation effects in arsenopyrite were obvious throughout, as was zone-related leaching, especially in Sheba crystals (Figures 46 and 47). Mimetic twinning was strongly developed in Sheba, West African and Klipwal arsenopyrite crystals, and visible after one day in the leach (Figures 48 and 49).

Many West African arsenopyrite crystals developed rims which were more extensively leached than the central area of the crystal. This effect was independent of crystal orientation,

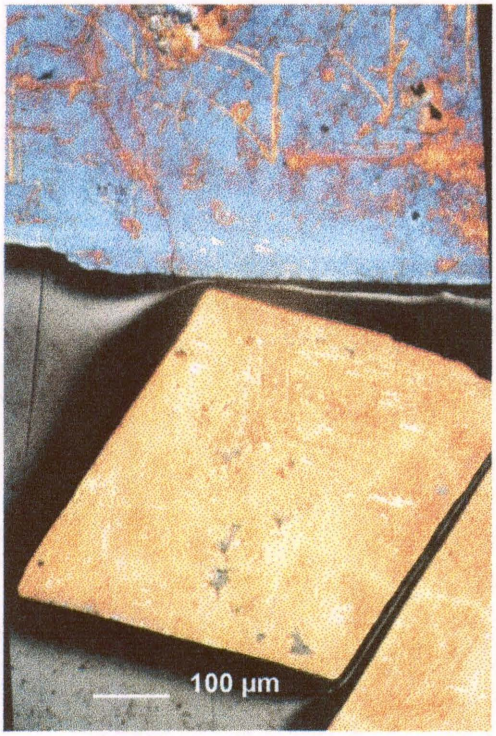

Figure 42. Klipwal arsenopyrite crystals after five days in ferric sulphate leach 5.

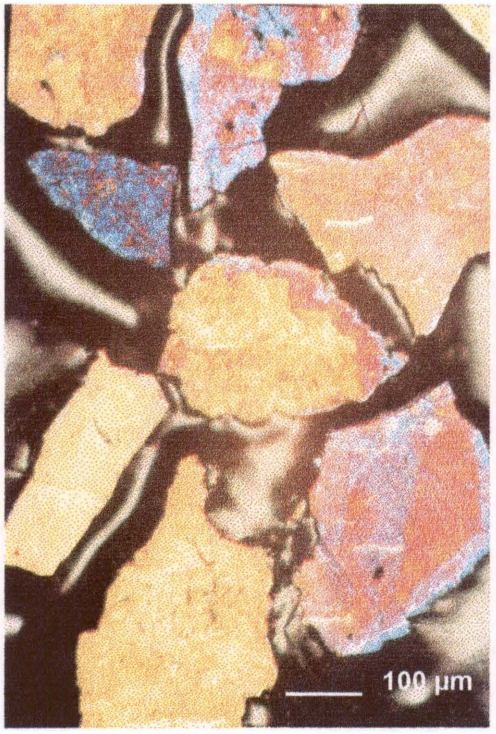

Figure 43. Zandrivier arsenopyrite particles after five days in ferric sulphate leach 5.

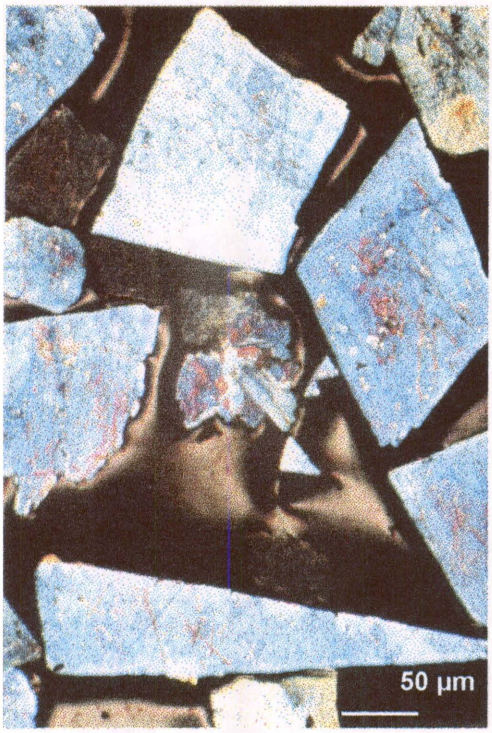

Figure 44. West African arsenopyrite crystals after five days in ferric sulphate leach 5.

Figure 45. Sheba arsenopyrite crystals after five days in ferric sulphate leach 5.

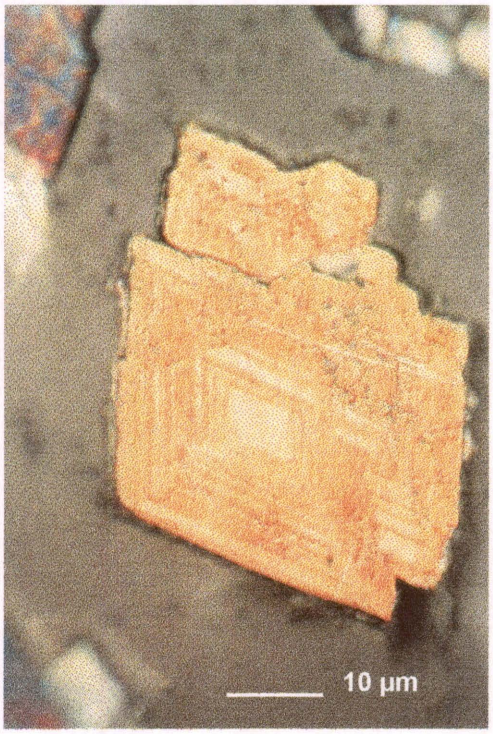

Figure 46. Zoned Sheba arsenopyrite crystal after four days in ferric sulphate leach 5.

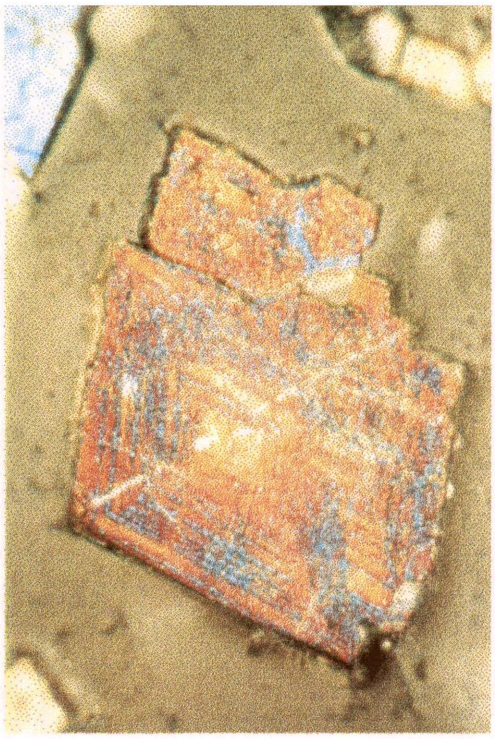

Figure 47. The same crystal after eight days in ferric sulphate leach 5.

Figure 48. Mimetic twinning apparent in plane light in a Sheba arsenopyrite crystal after six days in ferric sulphate leach 5.

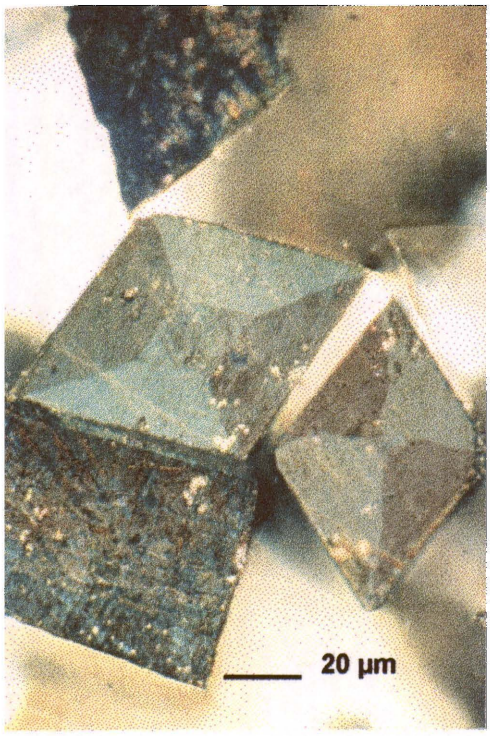

Figure 49. Mimetic twinning in West African arsenopyrite crystals, visible in 93° cross-polarised light, after four days in ferric sulphate leach 5.

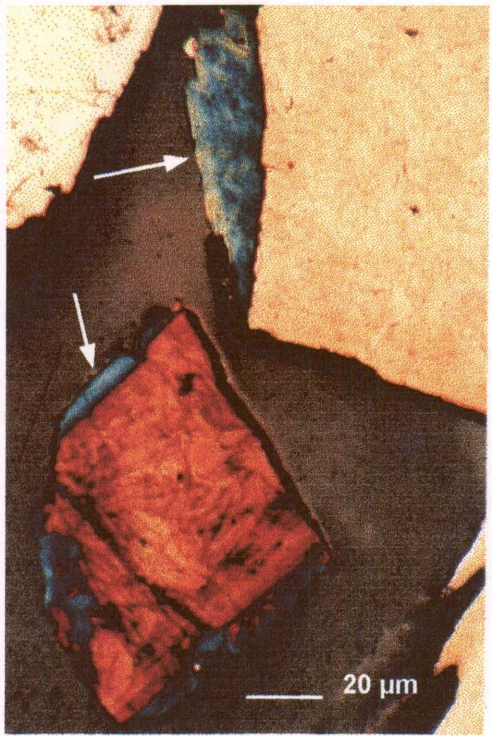

Figure 50. Faster-leaching rims around West African arsenopyrite crystals after four days in ferric sulphate leach 5.

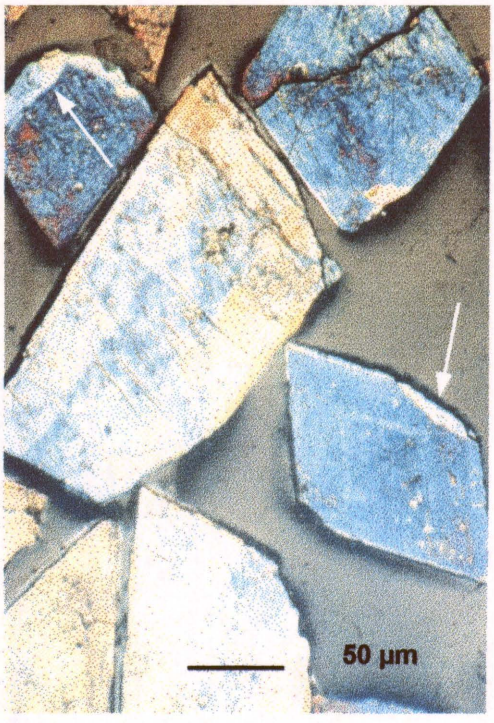

Figure 51. Faster-leaching rims around West African arsenopyrite crystals after one week in ferric sulphate leach 5.

and is due to a compositional difference towards the rim of the arsenopyrite particle (see Figures 50 and 51).

Pyrite leach colours were found to vary depending on their association. Pyrite in contact with arsenopyrite had usually attained only a beige colour by the end of the leach, but the colours of free pyrites were more advanced, especially in the Sheba and West African samples where some showed orange and purple shades.

Some pitting and channel formation, especially along cracks, was visible in pyrite and arsenopyrite. Electron microprobe examination of the leached sections confirmed that As-rich zones in arsenopyrite were preferentially leached, and examination of leached arsenopyrite surfaces with a defocused beam showed sulphur-enrichment. Occasionally a small amount of oxygen was detected in the more extensively-leached particles.

9.5 Bacterial leach 1

A composite crystal section was leached in liquor containing 20 g/l ferric iron, populated with a mixed culture of bacteria. The reactor was running on a continuous basis, and addition of the weekly solids feed (Sheba flotation concentrate) caused a temporary dip in ORP. The section was leached for one week, at temperatures of 29–32° C, which is slightly lower than the usual 34–36° C. The variation of pH and ORP is shown in Table 34 below.

TABLE 34

pH AND OXYGEN REDUCTION POTENTIAL (ORP) VARIATION DURING BACTERIAL LEACH 1
(20 g/l ferric iron concentration)

Time	pH	ORP (mV)	Temperature (°C)
0	1.19	613	31
1 day	1.29	525*	31
3 days	1.11	661	29
1 week	1.20	671	32

*Low ORP due to weekly solids addition.

The fact that the reactor had been running continuously for some time produced a problem with fine solids settling on the surface of the leaching sections, but these were usually quite easy to remove. The rate of arsenopyrite oxidation was much greater than that of the preceding ferric sulphate leaches, particularly as the section was added when bacterial activity

was already established, and the ORP was above 600 mV during most of the leach. Arsenopyrite leached as far as grey in all four types, but the Sheba crystals leached more quickly than the West African, and much more quickly than Zandrivier and Klipwal particles. General views of the four arsenopyrite types after one week in the leach are shown in Figures 52 to 55. Zone-related leaching was very strongly developed in arsenopyrite, especially in the Sheba crystals, but crystal orientation and mimetic twin etching effects were not observed.

Free pyrite particles showed colour changes after two days in the leach, and by one week most were multicoloured. Many pyrite particles attached to, or included in, arsenopyrite, however, still appeared virtually unleached (see Figure 56). The arsenopyrite crystals attached to such pyrite often appeared further leached than their pyrite-free counterparts – this is an example of galvanic interaction (BALLESTER *et al.*, 1992, HOLMES & CRUNDWELL, 1995).

Figure 52. Klipwal arsenopyrite crystals after one week in bacterial leach 1.

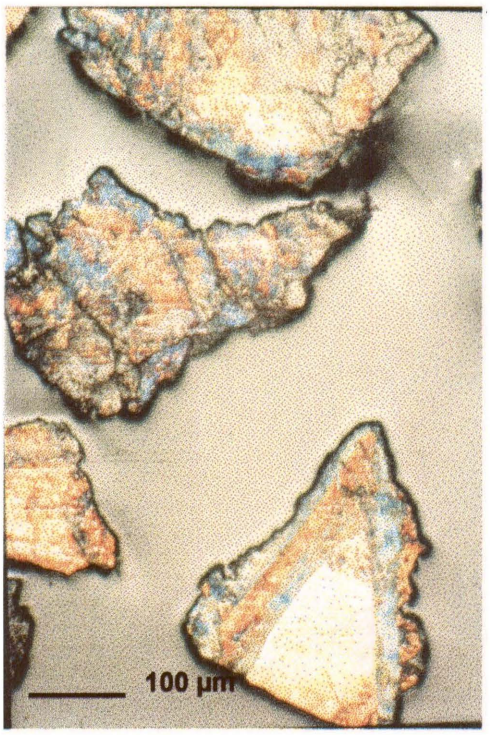

Figure 53. Zandrivier arsenopyrite particles after one week in bacterial leach 1.

Figure 54. West African arsenopyrite crystals after one week in bacterial leach 1.

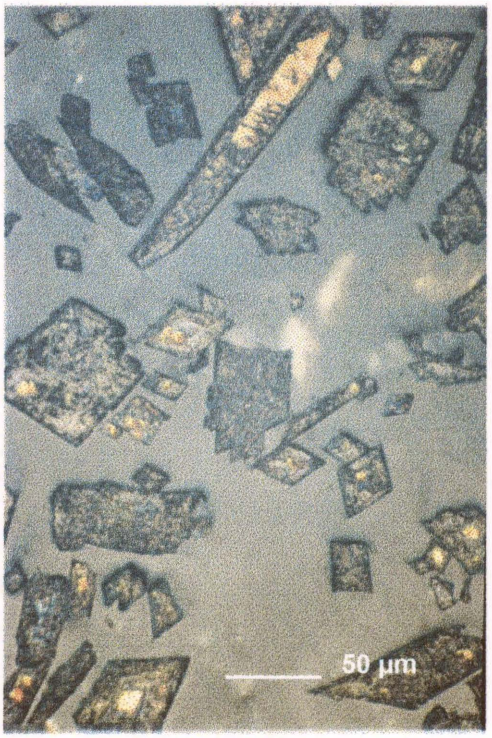

Figure 55. Sheba arsenopyrite crystals after one week in bacterial leach 1.

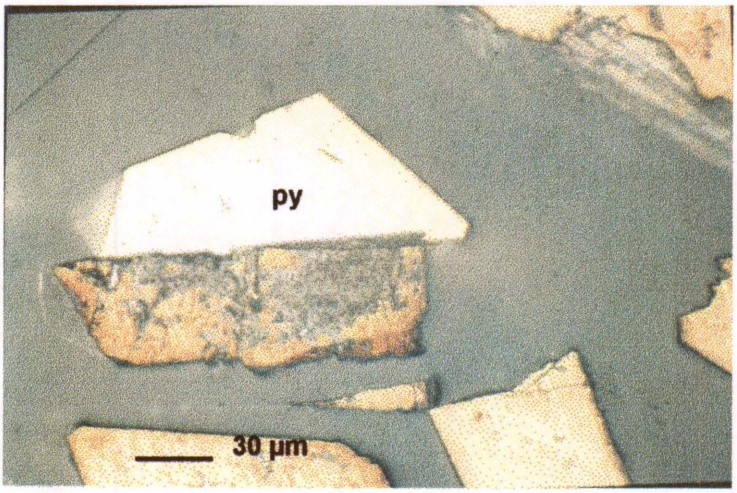

Figure 56. Accelerated leaching of West African arsenopyrite in contact with pyrite (py) after three days in bacterial leach 1.

Pits, channels and crack-enlargement were present in all arsenopyrite types after one week in the leach. Electron microprobe analyses of leached arsenopyrite surfaces showed sulphur-enrichment. The Sheba crystal surfaces were the most enriched, followed by West African crystals. The degree of sulphur enrichment of leached Zandrivier arsenopyrite particles was

variable, but generally higher than those measured on Klipwal crystal surfaces. Some jarosite had precipitated on arsenopyrite surfaces.

9.6 Discussion of results of the first six sterile and bacterial leach tests

The purpose of these leach tests was not so much to provide detailed laws of rate dependency on physical leach conditions (which is outside the scope of this study) but rather to give some indication of the factors most important in determining leach behaviour, and to investigate the relative rate of ferric sulphate leaches with their bacterial counterparts. The information was used to determine the most suitable leach conditions for the work on the relative leach rates of the four arsenopyrite types, for study of compositional effects within arsenopyrite particles, and for the powder leach tests.

The leach results described for the first six leaches, and the leach colours shown in Tables A22 to A25 (Appendix pages 231 – 234) can be interpreted as follows:

- The leach rate is increased by higher temperature, smaller particle size, and the presence of bacteria.
- The leach rate may also be *slightly* increased by lower pH and higher ferric iron concentration.
- Galvanic effects and zone-related leaching of arsenopyrite are increased at higher temperatures and by the presence of bacteria.
- Crystal orientation effects and twin etching in arsenopyrite are much more obvious in the absence of bacteria.
- Precipitation of jarosite on arsenopyrite surfaces is reduced at lower pH.
- Sheba arsenopyrite particles leach the fastest under all leach conditions, followed by West African arsenopyrite particles, then the slowly-leaching Zandrivier and Klipwal arsenopyrite particles.

(Other factors, such as ORP and arsenopyrite composition, also affect leach rate, but these are discussed later).

On the basis of the above results, the ferric sulphate leach conditions selected for the remaining tests were:

- A temperature of 35° C (similar to bacterial leaching),
- 10 g/l ferric iron (the lowest level commonly used in bacterial leaching) and
- A pH of 0.5 (generally lower than bacterial leach pH, although bacteria in Sheba continuous leach pachucas have been recorded to leach at this pH (NEALE *pers. com.*, 1997). The low pH and ferric iron concentrations were chosen to limit jarosite precipitation as much as possible.

10. LEACH TESTS FOR MODAL ANALYSIS

The purpose of ferric sulphate leach 6 and bacterial leach 2 was to provide leached milled sections for modal analysis by point counting. The object was to achieve at least a semi-quantitative assessment of the relative leach rate of the four arsenopyrite types during sterile and bacterial leaching.

10.1 Ferric sulphate leach 6

Leach tests 6a and 6b were run keeping physical conditions as similar as possible, and the point counting results were averaged. Ten composite milled sections were prepared from arsenopyrite HF concentrates screened to 38–150 µm and five sections per leach were oxidised in a liquor of 10 g/l ferric iron concentration, at pH 0.5, to minimise jarosite precipitation. The pH and ORP conditions are shown in Table 35 below.

The sections were leached for periods of 12 hours, 1 day, 2 days and 4 days, but no longer because of the difficulty in distinguishing first and second order leach colours after that time.

TABLE 35

pH AND OXYGEN REDUCTION POTENTIAL (ORP) VARIATION DURING FERRIC SULPHATE LEACHES 6a AND 6b
(10 g/l ferric iron concentration, temperature 35±1 °C)

6a	Time	pH	ORP (mV)
	0	0.52	710
	1 day	0.55	695
	4 days	0.56	686

6b	Time	pH	ORP (mV)
	0	0.53	705
	1 day	0.49	687
	2 days	0.53	685
	3 days	0.50	676
	4 days	0.50	672
	5 days	0.51	670

10.2 Modal analysis results

Eight hundred points on each arsenopyrite type per section were counted. The results in volume % are presented in Tables 36 and 37 below. The spread in results within each group, and the increase of the spread with time, is largely due to the effects of crystal orientation. There is some discrepancy in the leach rate of the two West African arsenopyrite samples between the two leaches, possibly because of the two arsenopyrite compositional types present (Section 7.2), but the overall picture confirms that Sheba arsenopyrite particles leach faster than the other three types, although there seems to be an initial lag phase. The averaged results of point counting are plotted in Figures 57 to 60.

TABLE 36
MODAL ANALYSIS RESULTS FROM POINT COUNTING FROM LEACH 6a
(error % is absolute)

*Colour of arsenopyrite after leaching.

12 hours	Zandrivier		Klipwal		West African		Sheba	
Asp. Colour*	vol.%	error %	vol.%	error %	vol.%	error %	vol.%	error %
White	8.2	1.8	8.5	1.8	4.0	1.4	13.8	2.4
Cream	64.0	3.5	67.8	3.4	73.4	3.1	35.3	3.4
Beige	24.9	3.3	21.2	2.8	19.5	2.8	33.4	3.4
Brown	2.3	1.0	2.5	1.0	2.7	1.0	13.3	2.4
M/coloured	0.3	<0.5	0.0	0.0	0.3	<0.5	4.0	1.4
Blue	0.3	<0.5	0.0	0.0	0.0	0.0	0.3	<0.5
Cream 2	0.0	0.0	0.0	0.0	0.0	0.0	0.0	0.0
Higher	0.0	0.0	0.0	0.0	0.0	0.0	0.0	0.0

24 hours	Zandrivier		Klipwal		West African		Sheba	
Asp. Colour	vol.%	error %	vol.%	error %	vol.%	error %	vol.%	error %
White	4.1	1.4	6.9	1.7	5.2	1.5	6.0	1.6
Cream	36.9	3.4	36.3	3.4	35.2	3.4	13.7	2.4
Beige	37.6	3.4	28.3	3.2	38.1	3.5	35.3	3.4
Brown	16.3	2.6	17.2	2.6	12.7	2.4	21.6	2.8
M/coloured	4.6	1.5	9.2	2.0	5.9	1.6	15.2	2.5
Blue	0.5	<0.5	2.1	1.0	1.8	0.8	6.0	1.6
Cream 2	0.0	0.0	0.0	0.0	1.1	0.5	1.2	0.5
Higher	0.0	0.0	0.0	0.0	0.0	0.0	1.0	0.5

48 hours	Zandrivier		Klipwal		West African		Sheba	
Asp. Colour	vol.%	error %	vol.%	error %	vol.%	error %	vol.%	error %
White	0.7	<0.5	2.8	1.2	1.0	0.5	2.2	1.0
Cream	30.9	3.3	32.4	3.3	30.5	3.3	14.1	2.5
Beige	50.3	3.6	39.9	3.5	46.2	3.5	52.2	3.6
Brown	13.1	2.4	13.6	2.4	12.6	2.4	23.9	3.0
M/coloured	3.7	1.4	6.1	1.6	7.0	1.7	5.4	1.5
Blue	1.1	0.5	3.4	1.3	2.5	1.1	1.7	0.8
Cream 2	0.2	<0.5	1.2	0.5	0.2	<0.5	0.4	<0.5
Higher	0.0	0.0	0.6	<0.5	0.0	0.0	0.0	0.0

96 hours	Zandrivier		Klipwal		West African		Sheba	
Asp. Colour	vol.%	error %	vol.%	error %	vol.%	error %	vol.%	error %
White	0.7	<0.5	1.2	0.5	1.0	0.5	0.0	0.0
Cream	18.1	2.7	18.2	2.7	9.1	2.0	1.8	0.8
Beige	43.8	3.5	38.6	3.5	28.4	3.2	7.1	1.7
Brown	27.0	3.1	29.4	3.3	28.9	3.2	20.5	2.8
M/coloured	6.5	1.7	8.7	2.0	17.5	2.9	26.2	3.0
Blue	3.0	1.2	2.7	1.1	11.3	2.2	35.6	3.4
Cream 2	0.7	<0.5	0.7	<0.5	2.6	1.1	8.3	1.9
Higher	0.2	<0.5	0.5	<0.5	1.2	0.5	0.5	<0.5

TABLE 37
MODAL ANALYSIS RESULTS FROM POINT COUNTING FROM LEACH 6b
(error % is absolute)

*Colour of arsenopyrite after leaching.

12 hours	Zandrivier		Klipwal		West African		Sheba	
Asp. Colour*	vol.%	error %	vol.%	error %	vol.%	error %	vol.%	error %
White	10.5	2.2	11.2	2.2	6.5	1.6	7.8	1.8
Cream	67.1	3.4	67.4	3.4	55.8	3.5	45.9	3.5
Beige	21.5	2.8	21.1	2.8	36.8	3.4	42.8	3.5
Brown	0.6	<0.5	0.5	<0.5	0.9	0.5	2.9	1.2
M/coloured	0.3	0.0	0.0	0.0	0.1	<0.5	0.6	<0.5
Blue	0.0	0.0	0.0	0.0	0.0	0.0	0.0	0.0
Cream 2	0.0	0.0	0.0	0.0	0.0	0.0	0.0	0.0
Higher	0.0	0.0	0.0	0.0	0.0	0.0	0.0	0.0

24 hours	Zandrivier		Klipwal		West African		Sheba	
Asp. Colour	vol.%	error %	vol.%	error %	vol.%	error %	vol.%	error %
White	1.9	1.0	2.8	1.2	1.8	0.9	2.4	1.0
Cream	40.3	3.5	45.9	3.5	39.8	3.5	23.0	2.9
Beige	44.6	3.5	39.7	3.5	49.9	3.6	42.0	3.5
Brown	8.5	1.9	8.3	1.9	6.2	1.6	15.1	2.5
M/coloured	3.0	1.2	2.4	1.0	1.5	0.8	11.3	2.3
Blue	1.3	0.7	0.6	<0.5	0.5	<0.5	4.3	1.4
Cream 2	0.3	<0.5	0.3	<0.5	0.3	<0.5	1.3	0.7
Higher	0.1	<0.5	0.0	0.0	0.0	0.0	0.6	<0.5

48 hours	Zandrivier		Klipwal		West African		Sheba	
Asp. Colour	vol.%	error %	vol.%	error %	vol.%	error %	vol.%	error %
White	2.5	1.1	2.4	1.0	2.8	1.2	2.5	1.1
Cream	33.0	3.4	44.5	3.5	27.6	2.9	15.2	2.5
Beige	41.9	3.5	43.0	3.5	41.4	3.5	41.7	3.5
Brown	14.8	2.5	7.2	1.7	16.8	2.6	24.3	3.0
M/coloured	5.4	1.5	2.3	1.0	6.8	1.7	11.0	2.2
Blue	2.0	1.0	0.4	<0.5	3.3	1.2	3.1	1.2
Cream 2	0.1	<0.5	0.1	<0.5	0.9	0.5	1.6	0.8
Higher	0.3	<0.5	0.3	<0.5	0.5	<0.5	0.5	<0.5

96 hours	Zandrivier		Klipwal		West African		Sheba	
Asp. Colour	vol.%	error %	vol.%	error %	vol.%	error %	vol.%	error %
White	1.0	0.5	0.8	0.5	1.1	0.5	1.1	0.5
Cream	7.9	1.8	11.7	2.3	11.7	2.3	4.9	1.5
Beige	32.8	3.4	36.0	3.4	39.6	3.5	9.5	2.2
Brown	31.2	3.3	27.6	3.2	23.9	3.0	20.7	2.8
M/coloured	14.8	2.5	13.1	2.4	11.3	2.2	30.4	3.4
Blue	7.0	1.7	6.2	1.6	6.5	1.6	22.8	2.9
Cream 2	3.0	1.2	2.8	1.2	3.6	1.4	7.2	1.7
Higher	2.4	1.0	1.9	1.0	2.3	1.0	3.4	1.3

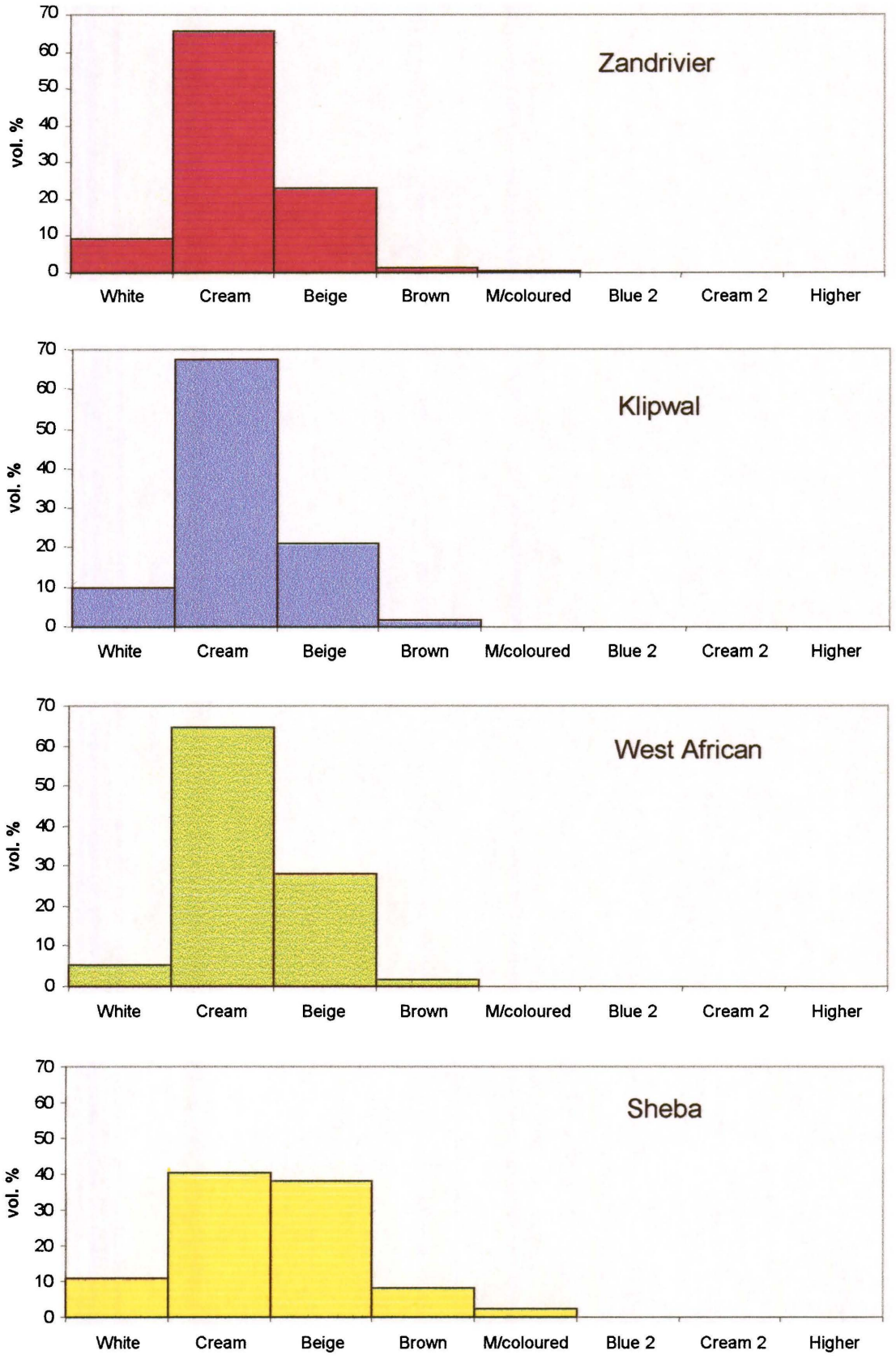

Figure 57. Modal analysis results from point counting the four arsenopyrite types after twelve hours in ferric sulphate leach 6.

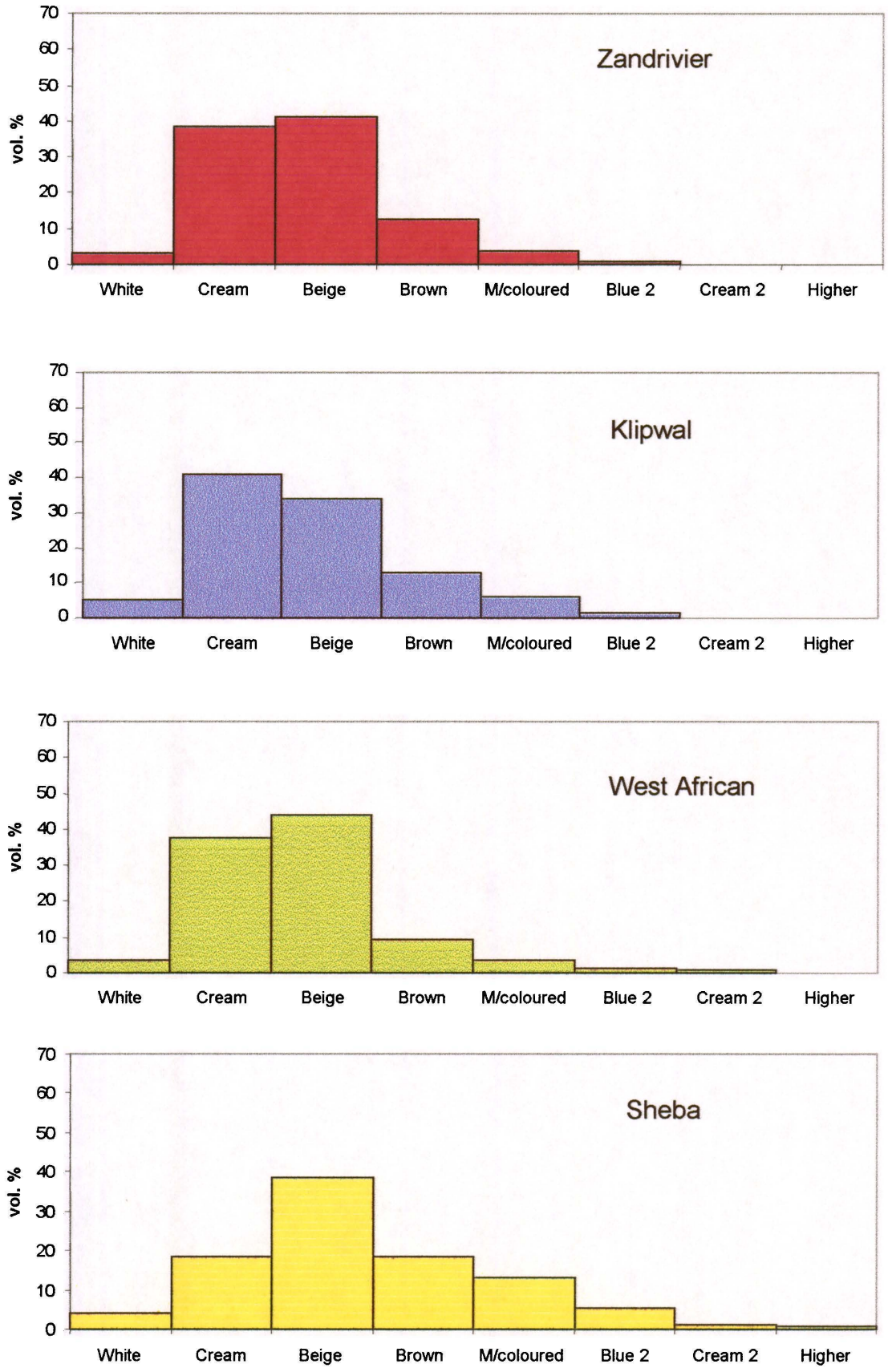

Figure 58. Modal analysis results from point counting the four arsenopyrite types after one day in ferric sulphate leach 6.

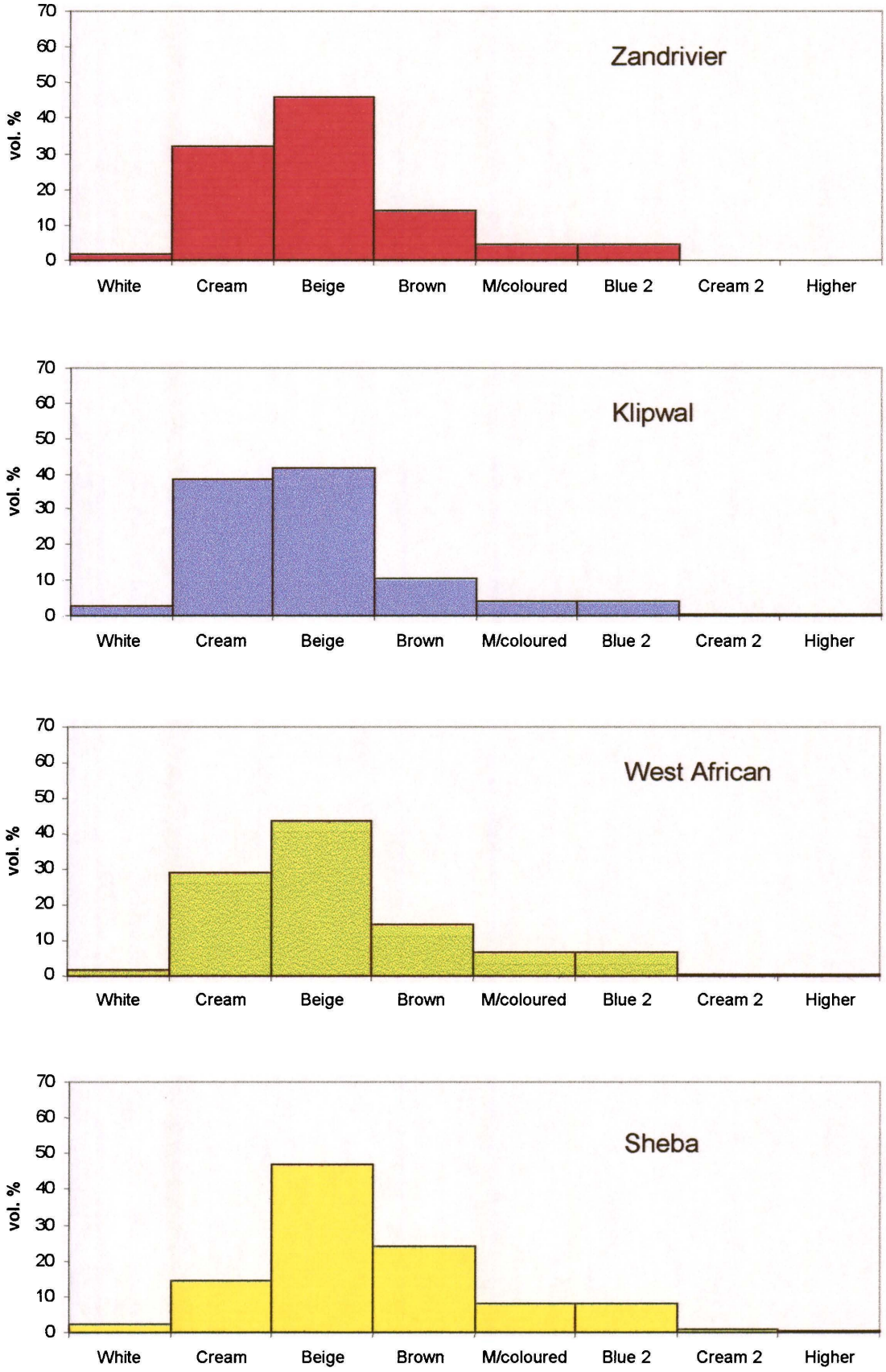

Figure 59. Modal analysis results from point counting the four arsenopyrite types after two days in ferric sulphate leach 6.

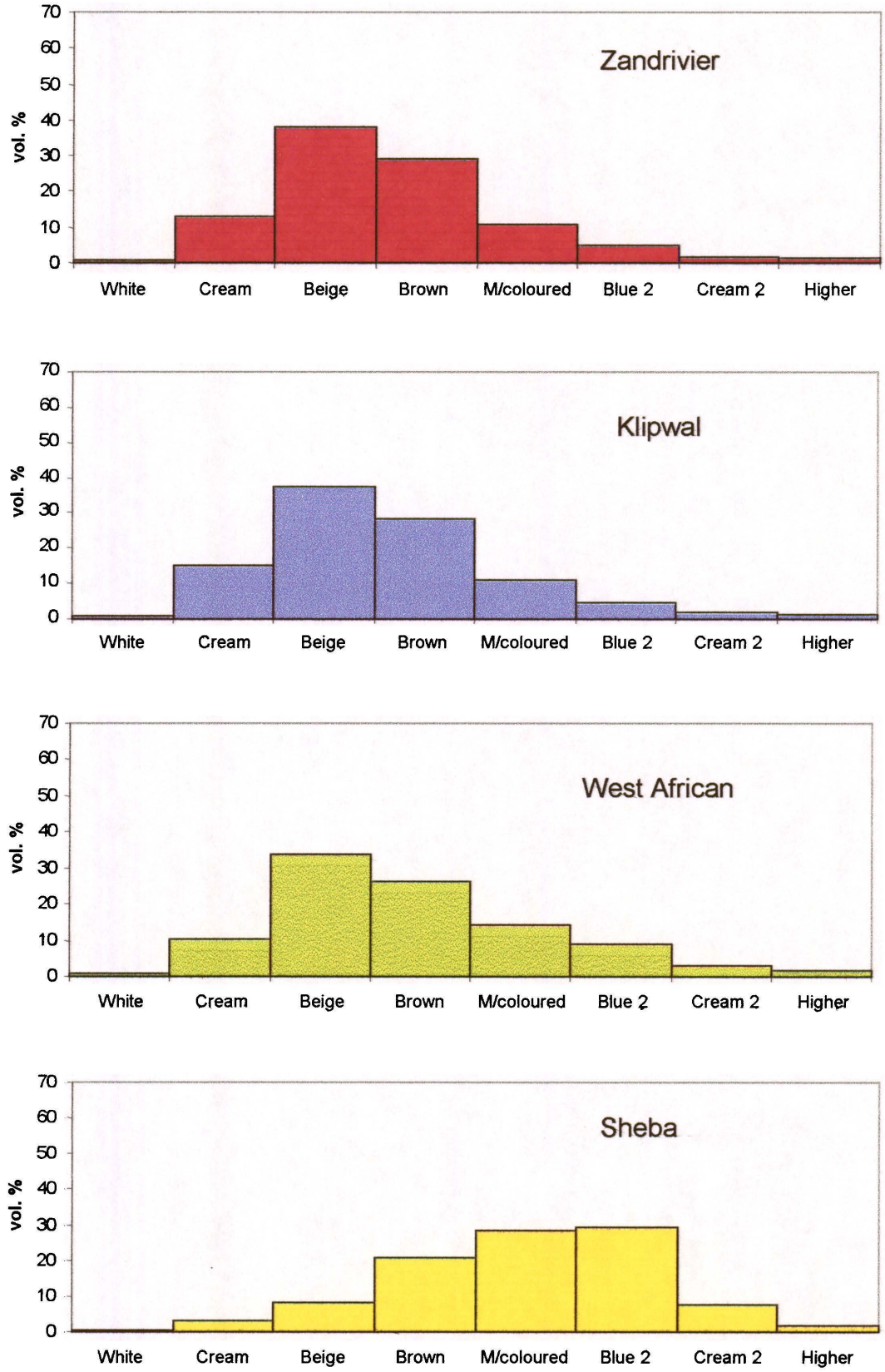

Figure 60. Modal analysis results from point counting the four arsenopyrite types after four days in ferric sulphate leach 6.

10.3 Bacterial leach 2

Five composite ground sections were leached in the laboratory pachuca in the presence of bacteria, the objective being to point count the resulting leached particles in the same way as in ferric sulphate leaches 6a and 6b. This would have provided a more quantitative comparison than that of bacterial leach 1. The attempt was not successful, however, due to the erratic manner of bacterial attachment.

At the end of one week in the bacterial leach, little could be concluded except that Sheba arsenopyrite was definitely the furthest leached over all. The pH and ORP conditions during this leach, and bacterial leach 3 which was run in parallel, are shown in Table 38 below.

TABLE 38

pH AND OXYGEN REDUCTION POTENTIAL (ORP) VARIATION DURING BACTERIAL LEACH TESTS 2 AND 3
(10 g/l ferric iron concentration)

	Time (days)	pH	ORP (mV)	Temperature (°C)
Rock sections added	0	1.33	541	34.1
(start of leach 3)	1	1.31	544	33.3
	2	1.31	549	34.2
Milled sections added	3	1.33	557	34.1
(start of leach 2)	4	1.23	572	33.8
	5	1.44	570	34.4
	6	1.29	573	34.6
	7	1.27	589	38.1
	8	1.30	605	37.8
	9	1.33	621	37.1
	10	1.18	635	35.8
Milled sections removed	11	1.16	643	36.4
(end of leach 2)	12	1.16	663	36.7
	13	1.20	668	36.5
	14	1.19	671	37.3
Rock sections removed	15	1.19	678	35.7
(end of leach 3)				

11. ROCK SECTION LEACH TESTS

Six rock sections, and one Klipwal crystal section, containing arsenopyrite and other sulphide particles which had already been imaged, quantitatively analysed on the electron microprobe, and relocated under the ore microscope, were leached under sterile and bacterial conditions, so that sulphide composition could be related to leach behaviour.

11.1 Ferric sulphate leach 7

Three of the rock sections, and one Klipwal crystal section, were leached in a 10 g/l ferric iron (as sulphate) solution, at 35° C, with a pH as close to 0.5 as possible in the presence of acid-consumers such as pyrrhotite and carbonate minerals. The entire leach solution had to be renewed twice in the course of the leach due to acid consumption and precipitate formation by dissolving minerals. The actual conditions of the leach are shown in Table 39 below.

The leach behaviour of arsenopyrite, and other sulphide minerals, will be discussed in Section 11.3, where the results are compared and contrasted with leach behaviour during bacterial leach 3.

11.2 Bacterial leach 3

The pH and ORP conditions during the leach have already been shown in Table 38 under bacterial leach 2. Initially the leach was run at pH 0.5 to allow a more direct comparison, but bacterial activity did not increase sufficiently in the time available. The pH was raised to over pH 1.0 and when bacterial activity was sufficiently high, the rock sections were leached for two weeks. The ORP did not rise to over 600 mV until the second week, which may explain the relatively slow sulphide leach rate of these samples as compared to the crystals leached in bacterial leach 1. The behaviour of sulphide minerals in bacterial leach 3 is discussed below.

TABLE 39

pH AND OXYGEN REDUCTION POTENTIAL (ORP) VARIATION DURING FERRIC SULPHATE LEACH TESTS 7 AND 8
(10 g/l ferric iron concentration, temperature 35±1 °C)

Time (days)	Remarks	pH	ORP (mV)
0		0.50	712
0.25		0.68 → 0.50 *	670
1	New leach solution[+]	0.40	730
2		0.50	710
3		0.49	687
4	Reflectance readings[0]	0.56 → 0.48	673
5		0.49	667
6		0.55 → 0.50	660
7		0.50	656
8	New leach solution	0.47	716
9		0.56 → 0.49	697
10	Reflectance readings	0.50	681
11		0.50	672
12	Reflectance readings	0.46	668
13		0.51	661
14	Reflectance readings	n.d.	n.d.
15		0.48	653
17		0.53	651

*Acid added
[+] Leach solution replaced with fresh solution.
[0] Sections were removed for reflectance readings to be taken.
n.d. = not determined.

11.3 Results of rock section leach tests

As many pre-analysed sulphide minerals as possible were monitored during leaching. As expected, a number of particles fell out during the leach, especially where these were surrounded by carbonate minerals. Certain sulphides from all leach types were selected and photographed during the leach, and some of these are presented below as case histories. The observed progress of the other sulphide minerals is tabulated in Table A26 in the Appendix (pages 235–243). The sulphide identities, *e.g.* A3 arsenopyrite or G24 pyrite, can be related to their composition as reported in Tables A13 to A15 (Appendix pages 207–220), and Tables A17 to A21 (Appendix pages 222–230).

11.3.1 Arsenopyrite leach behaviour

The behaviour of the sulphide minerals in the rock section leach tests was very similar to their behaviour in crystal section – zone-related leaching was marked in Sheba arsenopyrite, and orientation effects were marked in all four arsenopyrite types. One factor apparent in the rock

section leach was the effect of the surrounding minerals in the rock. Arsenopyrite particles surrounded by quartz leached more slowly than those surrounded by mica or feldspar. The rock sections were leached for over two weeks, and during that time pores and leach channels developed in all arsenopyrite types.

Arsenopyrite leach rate in bacterial leach 3 was also affected by the nature of the surrounding rock. The progress of the sulphide minerals in the leach was typical, in that zone-related and galvanic effects were strong, whereas orientation and twinning effects were negligible. Once again, leach pores and channels appeared in all arsenopyrite types.

The leaching progress of selected examples of the four arsenopyrite types is outlined below. The value of As/S, as calculated from the microprobe analysis results, for the various compositional zones is quoted. The difference in As/S at the contact of zones, Δ(As/S), is also given; these factors for all the zoned arsenopyrite particles, with the exception of Klipwal arsenopyrite, are shown in Table 40 below.

11.3.1.1 Klipwal arsenopyrite

Since no rock sample was available, five Klipwal arsenopyrite crystals were leached in the ferric sulphate leach. The leach colours developed are shown in Table A26 (Appendix pages 235 – 243). Arsenopyrite A53 showed the strongest compositional zonation of the five, and its leach progress is described below.

A53 arsenopyrite crystal (BSE-image shown in Figure 61)
Bright zone average As/S = 2.15
Dark zone average As/S = 1.93
Δ(As/S) = 0.22
Zone-related leaching was observed, with the bright (As-rich) zone leaching to blue and the dark (As-poor) zone to brown after twelve days in the leach (Figure 62). It should be emphasized that this crystal showed unusually strong compositional zonation as compared to most Klipwal crystals examined.

TABLE 40

Δ(As/S) FACTORS FOR CONTACTING COMPOSITIONAL ZONES IN SHEBA, ZANDRIVIER AND WEST AFRICAN ARSENOPYRITE TYPES

Sheba	Zone*	Δ(As/S)	Zandrivier	Zone*	Δ(As/S)	West African	Zone*	Δ(As/S)
A1	b-d	0.46	A26	b-d	0.08	A51	b-m	0.19
A2	b-d	0.28	A27	b-m	0.09		m-d	0.29
A3	b-d	0.38		m-d	0.11	G47A	vb-b	0.16
A4	b-m	0.11	A28	b-m	0.07		b-m	0.09
	m-d	0.29		m-d	0.16		m-d	0.34
A5	b-d	0.28	A29	b-m	0.35	G47B	vb-b	0.13
A6	b-d	0.38		m-d	0.01		b-m	0.23
A8	b-d	0.44	A30	b-d	0.20		m-d	0.09
A9	b-d	0.36	A31	b-m	0.19	G48	vb-b	0.33
A10	b-d	0.30		m-d	0.09		b-m	0.08
A11	b-m	0.17	A35	b-d	0.29		m-d	0.09
	m-d	0.27	A36	b-d	0.22	G49	vb-b	0.19
A12	b-d	0.22	A37	b-d	0.13		b-m	0.12
A13	b-d	0.36	A38	b-d	0.10		m-d	0.13
A15	b-d	0.43	A46	b-m	0.12	G50	b-m	0.25
A16	b-d	0.32		m-d	0.12		m-d	0.18
A17	b-d	0.28	A47	b-m	0.03	G51	vb-b	0.23
A18	b-m	0.13		m-d	0.18		b-m	0.21
	m-d	0.16	A48	b-m	0.09		m-d	0.20
A19	b-d	0.31		m-d	0.10	G53	vb-b	0.23
A21	b-d	0.38	A49	b-m	0.08		b-m	0.18
A22	b-m	0.07		m-d	0.05		m-d	0.08
	m-d	0.11	A50	b-m	0.10	G55	b-m	0.26
A23	b-d	0.22		m-d	0.17		m-d	0.09
G1	b-d	0.24				G57	b-d	0.11
						G58	vb-b	0.14
							b-m	0.17
							m-d	0.02
						G60	b-d	0.34
						G61	b-d	0.17
						G65	b-d	0.17
						G66	vb-b	0.20
							b-m	0.17
							m-d	0.15

*vb = very bright, b = bright, m = medium and d = dark BSE intensity.

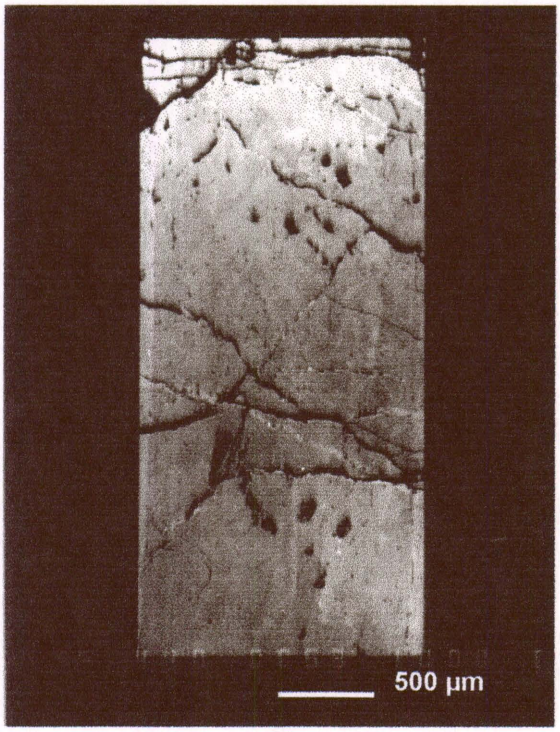

Figure 61. An example of an unusually strongly-zoned Klipwal arsenopyrite. BSE-image.

Figure 62. The Klipwal crystal after twelve days in ferric sulphate leach 7.

11.3.1.2 Zandrivier arsenopyrite

The behaviour of arsenopyrite in the Zandrivier rock sections was zone–related in both sterile (ferric sulphate) and bacterial leaches, but the effect of orientation was dominant in the sterile leach. In other words, differing leach rates *within* a particle of one orientation was zone-related, but the leach rate and colour of similarly-composed zones in another particle was not compatible because of the over-riding effect of crystal orientation (see arsenopyrite A28 below). In contrast to this, orientation effects were not really noticeable during bacterial leaching (see arsenopyrite A47). Certain areas of the massive arsenopyrite showed As-rich veins, and these leached preferentially under both sterile and bacterial leach conditions (see arsenopyrite A30).

As with the Klipwal A53 crystal, the areas of Zandrivier arsenopyrite selected for study here were among the most strongly zoned which could be found. Most of this arsenopyrite was unzoned or very weakly zoned. Areas such as those shown in arsenopyrite particles A28 and

A47 commonly showed three zones, with the Δ(As/S) at the contact of these being relatively low.

A28 area of massive arsenopyrite (BSE-image shown in Figure 63)

Bright zone average As/S = 2.22

Medium zone average =2.15

Dark zone average As/S = 1.98

$\Delta(As/S)_{(b-m)}$= 0.07 $\Delta(As/S)_{(m-d)}$= 0.17

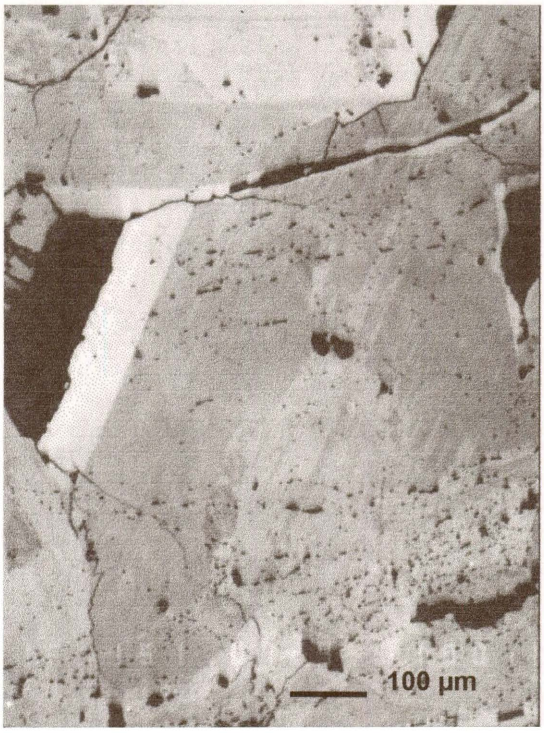

Figure 63. BSE-image of Zandrivier arsenopyrite A28.

The sequence of leach colours developed during ferric sulphate leaching of this area of arsenopyrite is shown in Figures 64 to 67. Careful examination shows that the field may be divided into two main areas, both of which show zone-related leaching, but the lighter-coloured area at the top is of a different orientation. Different orientations cannot be distinguished on the BSE-image in Figure 63 because it only shows compositional variation.

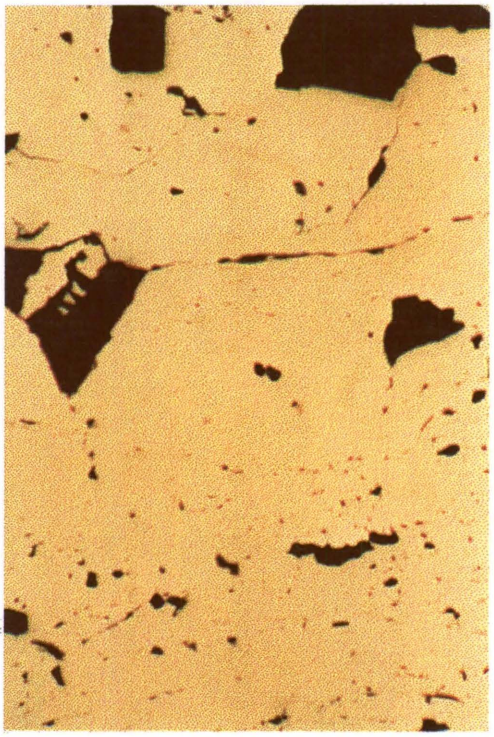

Figure 64. Unleached Zandrivier arsenopyrite A28.

Figure 65. Zandrivier arsenopyrite A28 after one day in ferric sulphate leach 7.

Figure 66. Zandrivier arsenopyrite A28 after two days in ferric sulphate leach 7.

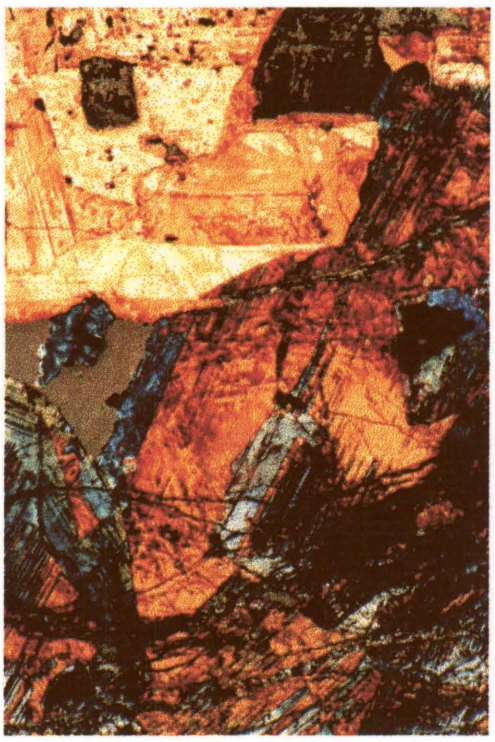

Figure 67. Zandrivier arsenopyrite A28 after ten days in ferric sulphate leach 7.

A30 massive arsenopyrite with As-rich veins (BSE-image shown in Figure 68).

Bright zone average As/S = 2.22 (veins)

Dark zone average As/S = 2.02 (main phase)

Δ(As/S) = 0.20

The colour sequence developed during ferric sulphate leaching of this veined area of arsenopyrite is shown in Figures 69 and 70. The As-rich veins leached preferentially to the main area.

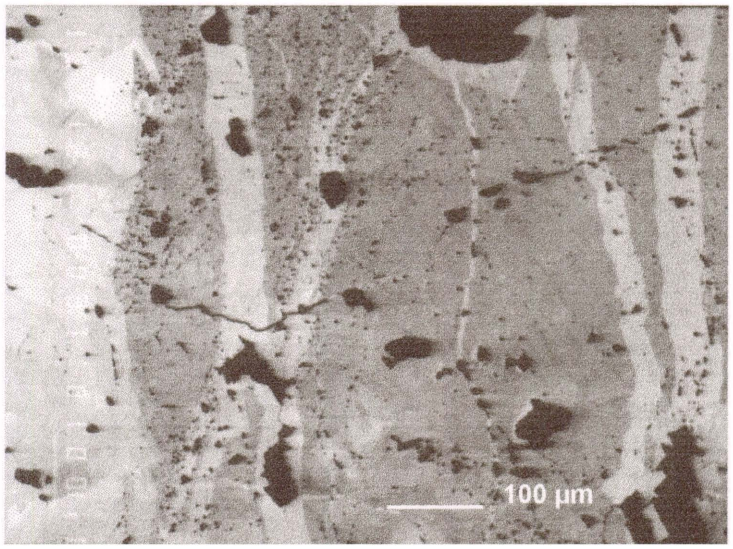

Figure 68. BSE-image of Zandrivier arsenopyrite A30. The brighter areas are late stage As-rich veins.

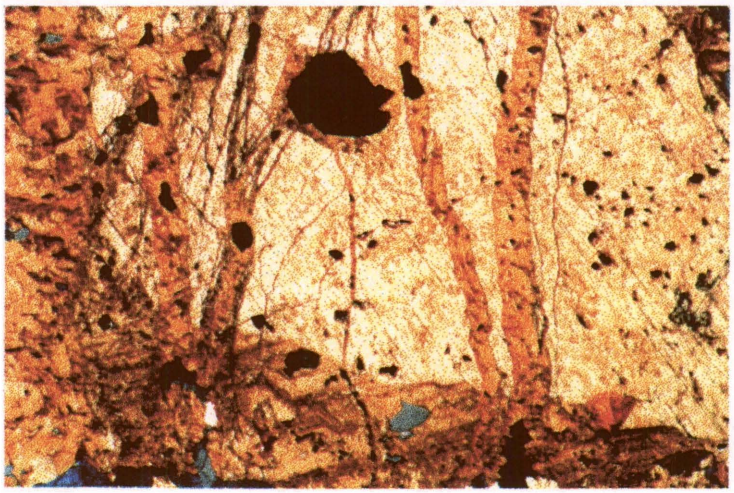

Figure 69. Zandrivier arsenopyrite A30 after six days in ferric sulphate leach 7.

Figure 70. Zandrivier arsenopyrite A30 after eight days in ferric sulphate leach 7.

A47 area of massive arsenopyrite (BSE-image shown in Figure 71).

Bright zone average As/S = 2.22

Medium zone average = 2.19

Dark zone average As/S = 2.01

$\Delta(As/S)_{(b-m)}$= 0.03 $\Delta(As/S)_{(m-d)}$= 0.18

There is very little compositional difference between the bright (As-rich) and medium zones here, so they could probably be considered as one zone. Bacterial leach progress is shown in Figures 72 and 73. The As-rich zones achieved brown to blue colouration after two weeks in

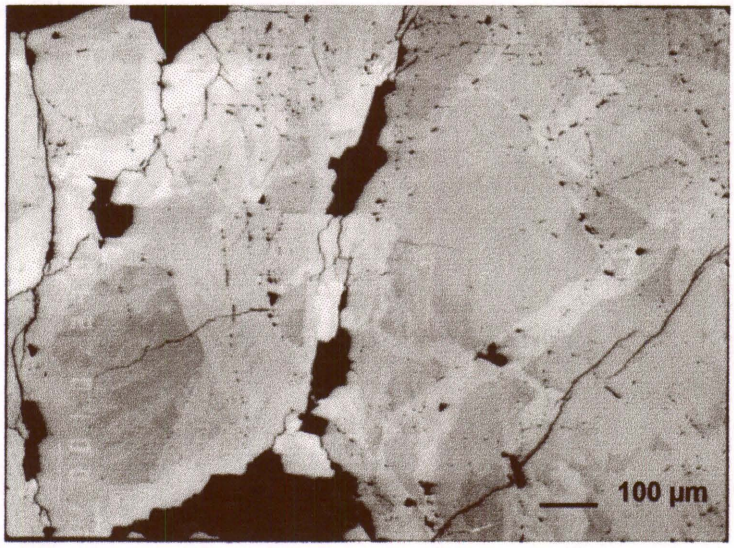

Figure 71. BSE-image of Zandrivier arsenopyrite A47.

the leach, while the As-poor zone was still cream-beige. There was no sign of orientation effects between the particles in this area, and this was typical of the whole section.

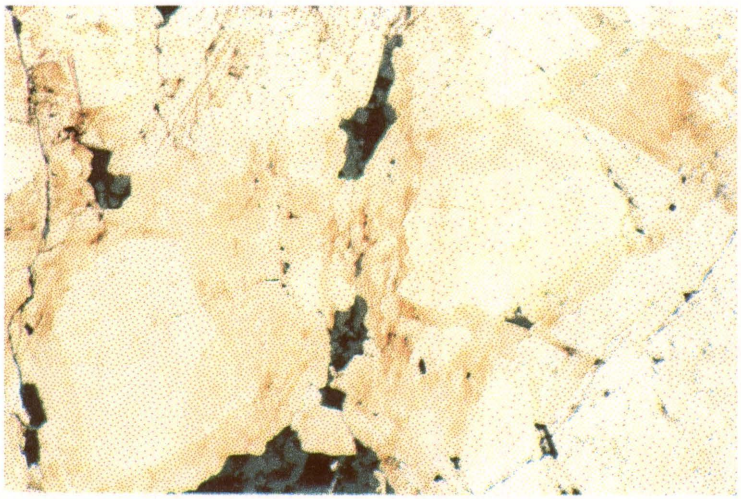

Figure 72. Zandrivier arsenopyrite A47 after six days in bacterial leach 3.

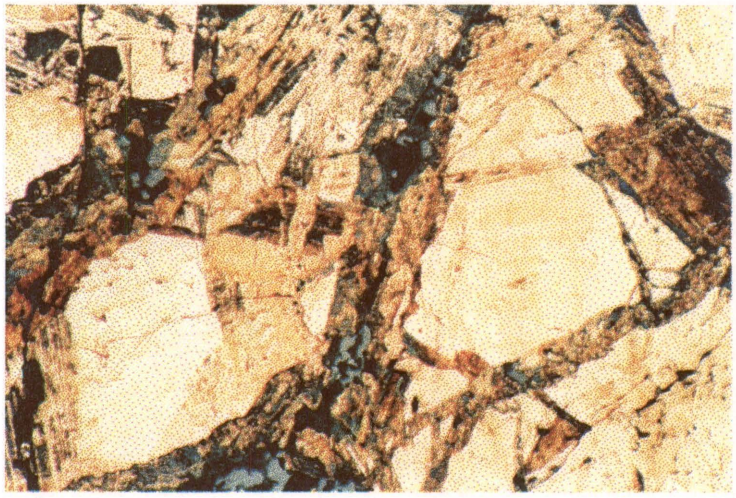

Figure 73. Zandrivier arsenopyrite A47 after two weeks in bacterial leach 3.

11.3.1.3 Sheba arsenopyrite

These arsenopyrite crystals show the strongest zone-related leach effects of all four types under both sterile and bacterial leaching conditions. Sheba crystals may show three zones per crystal, but normally only two are present with a relatively high Δ(As/S) at the contact. Examples of pre- and post-bacterial leached Sheba crystals are shown in Figures 141 and 142 in Section 12, and three examples from the sterile leach are shown below.

A8 arsenopyrite crystal (Small crystal in BSE-image in Figure 74).

Bright zone average As/S = 2.16

Dark zone average As/S = 1.72

Δ(As/S) = 0.44

A9 arsenopyrite crystal (large crystal in BSE-image in Figure 74).

Bright zone average As/S = 2.25

Dark zone average As/S = 1.89

Δ(As/S) = 0.36

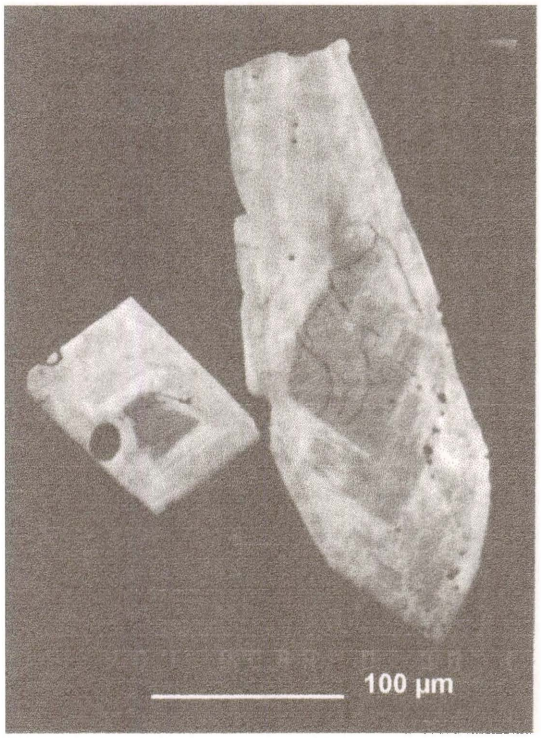

Figure 74. BSE-image of Sheba arsenopyrite crystals A8 and A9.

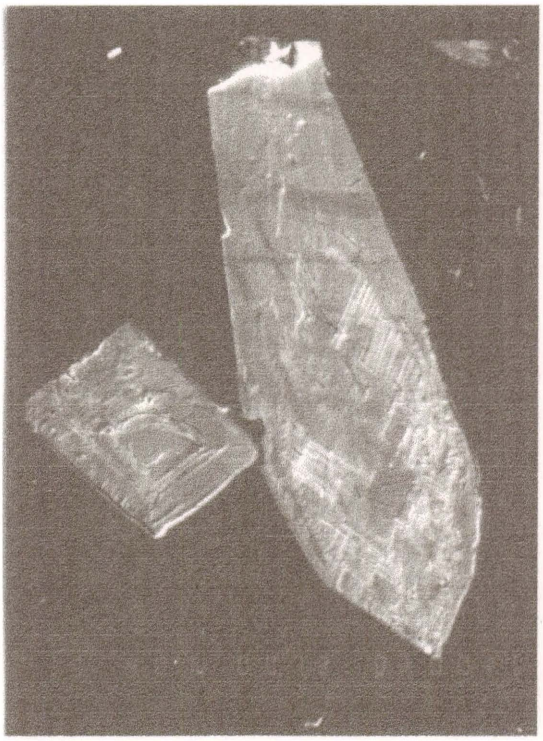

Figure 75. SE-image of the arsenopyrite crystals after two weeks in ferric sulphate leach 7.

Both crystals are in the same field of view. The smaller arsenopyrite A8 crystal exhibits typical Sheba form and zonation, while the larger arsenopyrite A9 exhibits an unusual shape, and shows complex, finely spaced zonation. The leach colours which were recorded during the leach are shown in Figures 76 to 79. Leaching is strongly zone-related, with high Δ(As/S) values between zones in contact. A scanning electron (SE) image of the two crystals after

leaching is shown in Figure 75, where the more advanced leach colours can be seen to be related to depth of etching.

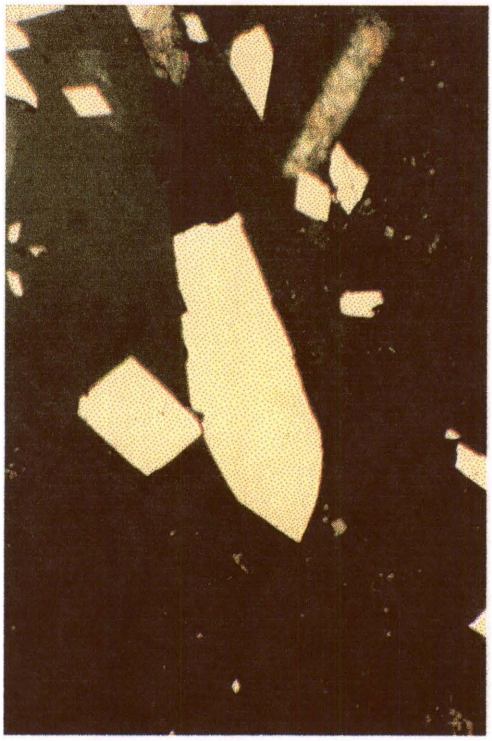

Figure 76. Sheba arsenopyrite crystals A8 and A9 before leaching.

Figure 77. Sheba arsenopyrite crystals A8 and A9 after two days in ferric sulphate leach 7.

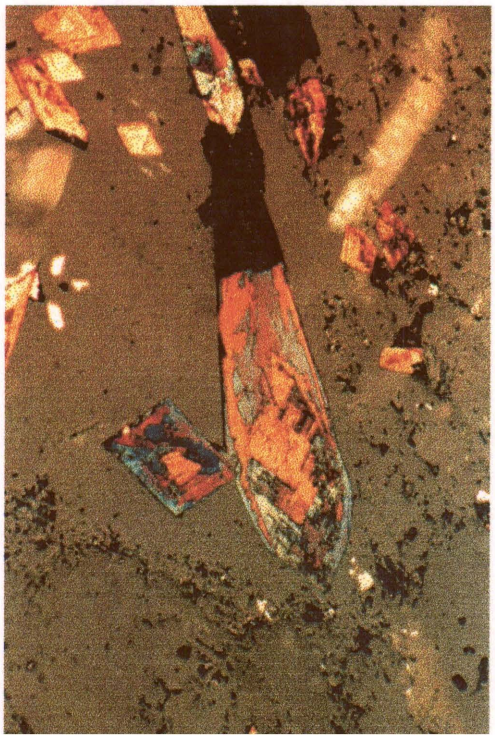

Figure 78. Sheba arsenopyrite crystals A8 and A9 after eight days in ferric sulphate leach 7.

Figure 79. Sheba arsenopyrite crystals A8 and A9 after two weeks in ferric sulphate leach 7.

A11 arsenopyrite crystal (BSE-image shown in Figure 80).

Bright zone average As/S = 2.32

Medium zone average As/S = 2.15

Dark zone average As/S = 1.87

$\Delta(As/S)_{(b-m)}$= 0.17 $\Delta(As/S)_{(m-d)}$= 0.28

A less usual Sheba arsenopyrite crystal showing three compositional zones, with the bright (As-rich) and medium zones both situated in the rim. The leach colours after four and six days in the leach are shown in Figure 82 and 83. After a week the small As-rich zones are blue to cream 2 in colour, and the dark (As-poor) zone is brown. The medium zone is dark multicoloured-blue. The post-leach scanning electron image (Figure 81) does not show etching very clearly, but it does show that leach attack has exploited and enlarged existing cracks in the crystal, and that pits are developing in the As-rich zone by the end of leach.

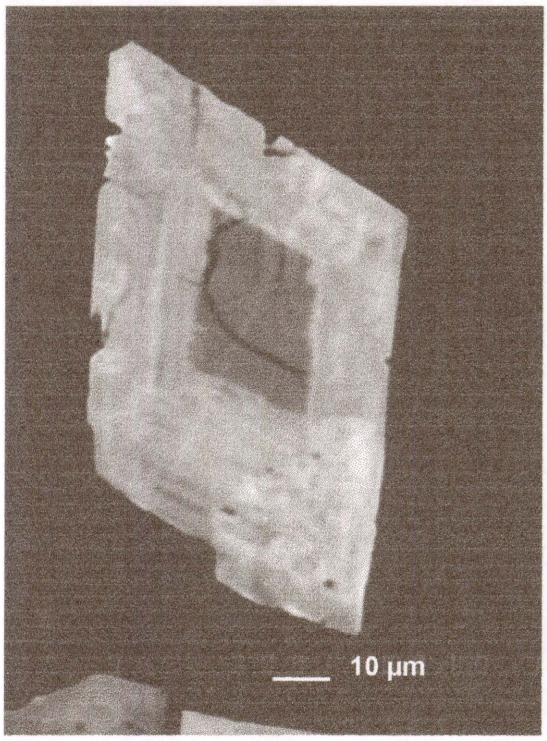

Figure 80. BSE-image of Sheba arsenopyrite A11, showing the S-rich core (dark) and the As-rich rim (bright).

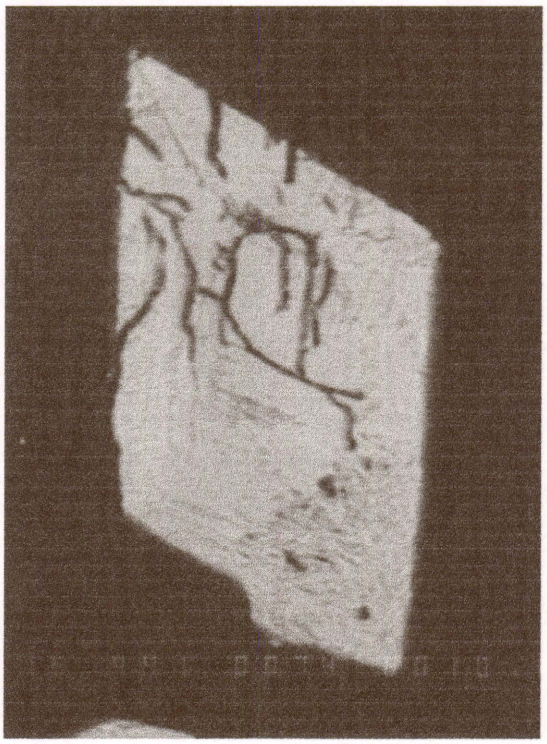

Figure 81. SE-image of arsenopyrite A11 after two weeks in ferric sulphate leach 7.

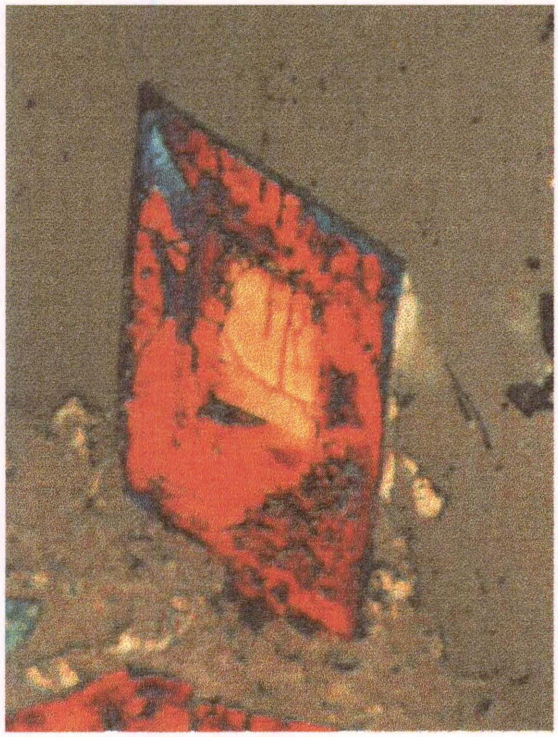

Figure 82. Arsenopyrite A11 after four days in ferric sulphate leach 7.

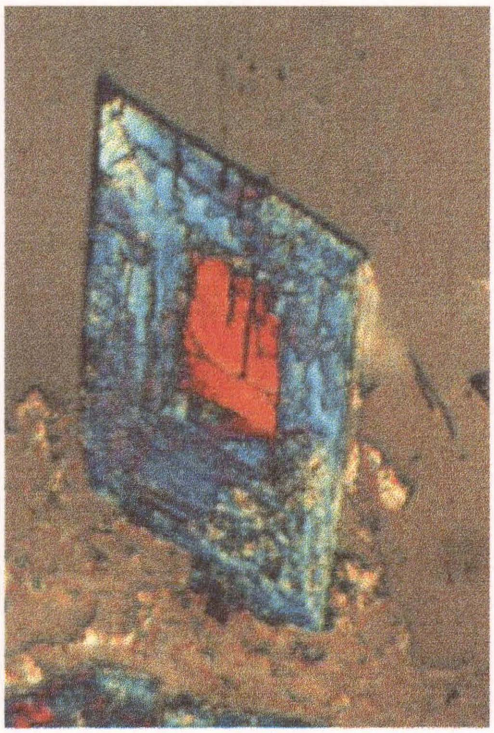

Figure 83. Arsenopyrite A11 after six days in ferric sulphate leach 7.

11.3.1.4 West African arsenopyrite

Nearly all the West African crystals were surrounded by pyrrhotite in rock section (in contrast to the crystal sections where the pyrrhotite had been dissolved by hydrofluoric acid). The relatively slow leach rate of these arsenopyrite crystals, especially in the bacterial leach of the rock section, may have been due to a galvanic interaction between the two sulphides where pyrrhotite was protecting the arsenopyrite. By the end of bacterial leach test 3, only the smaller arsenopyrite crystals had oxidised significantly, although etching could be distinguished microscopically. Three case studies are shown below as examples of orientation effects (G46), and of the effect of cobalt on sterile and bacterial leaching (G47A and G51).

<u>G46 twinned arsenopyrite crystal</u>

Very bright zone average As/S = 2.34 Co = 0.27 mass %

Bright zone average As/S = 2.20 Co = 0.46 mass %

Medium zone average As/S = 1.97 Co = <0.02 mass %

Dark zone average As/S = 1.88 Co = <0.02 mass %

$\Delta(As/S)_{(vb-b)} = 0.16$ $\Delta(As/S)_{(b-m)} = 0.23$ $\Delta(As/S)_{(m-d)} = 0.09$

The bright and very bright zones combined form only a thin deposit on the end of the twinned crystal in the photomicrographs below. Figures 84 to 86 show the part which twin orientation played in leach colour development.

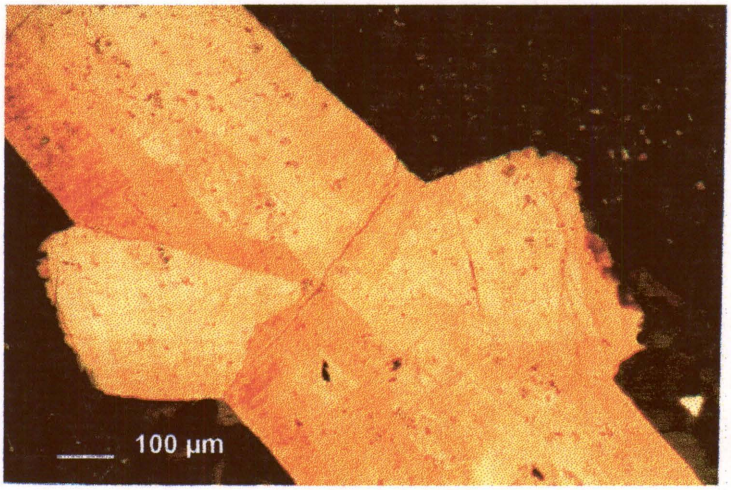

Figure 84. West African twinned arsenopyrite G46 after one day in ferric sulphate leach 7.

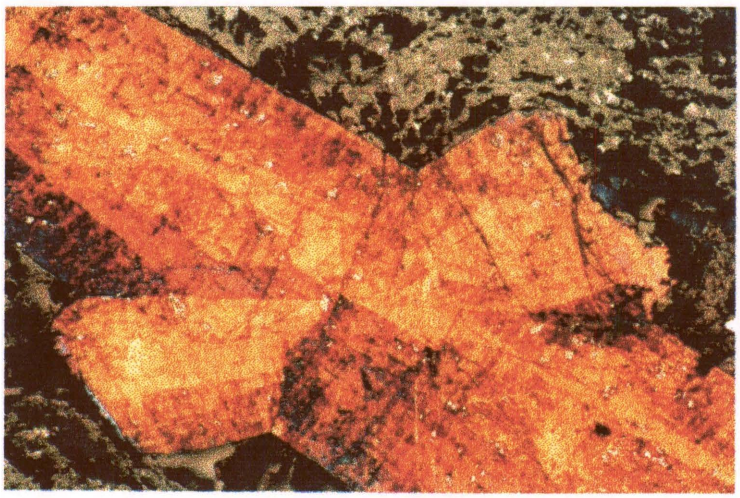

Figure 85. West African twinned arsenopyrite G46 after eight days in ferric sulphate leach 7.

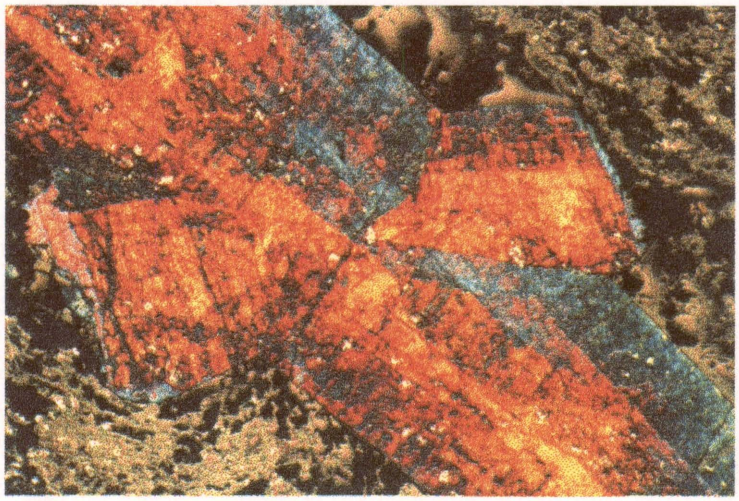

Figure 86. West African twinned arsenopyrite G46 after ten days in ferric sulphate leach 7.

G47A arsenopyrite crystal (BSE-images shown in Figures 87 and 88).

Very bright zone average As/S = 2.32 Co = 0.55 mass %

Bright zone average As/S = 2.16 Co = 0.48 mass %

Medium zone average As/S = 2.07 Co = <0.02 mass %

Dark zone average As/S = 1.73 Co = <0.03 mass %

$\Delta(As/S)_{(vb-b)} = 0.16$ $\Delta(As/S)_{(b-m)} = 0.09$ $\Delta(As/S)_{(m-d)} = 0.34$

The ferric sulphate leaching behaviour of this crystal showed a number of features (see Figures 89 to 92). Initially, the pyrrhotite crystals can be seen leaching, then the arsenopyrite, while the pyrite remained unleached. The later-stage Co-bearing zones of the arsenopyrite leach preferentially to a degree that seems unjustified by the Δ(As/S) between zones (that of the medium/dark contact is only 0.09, yet that is the point of the highest leach rate difference). It is likely that the presence of cobalt is accelerating the leach rate here, and in other crystals too, where the Co-bearing zones are invariably leached in preference. An enlarged area of the crystal edge is shown in the scanning electron image in Figure 93 and a schematic topographic linescan across this showing relative relief is shown in Figure 94.

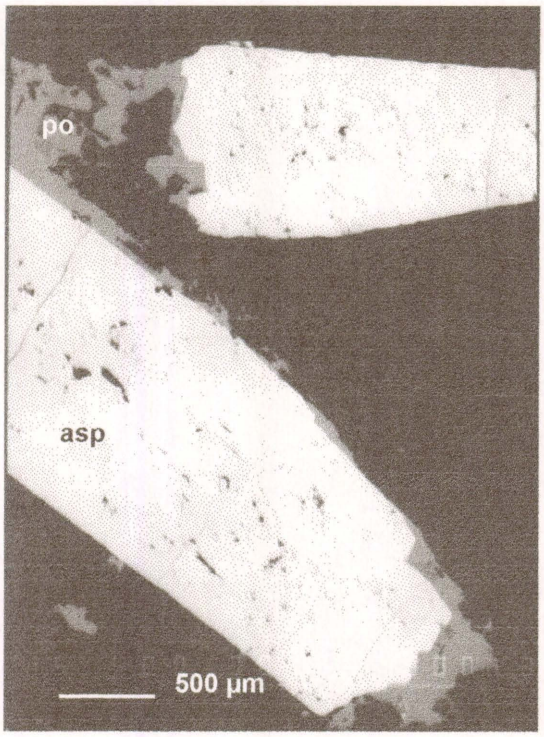

Figure 87. BSE-image of West African arsenopyrite grains G47A and G47B showing pyrrhotite (po) attached to the arsenopyrite (asp).

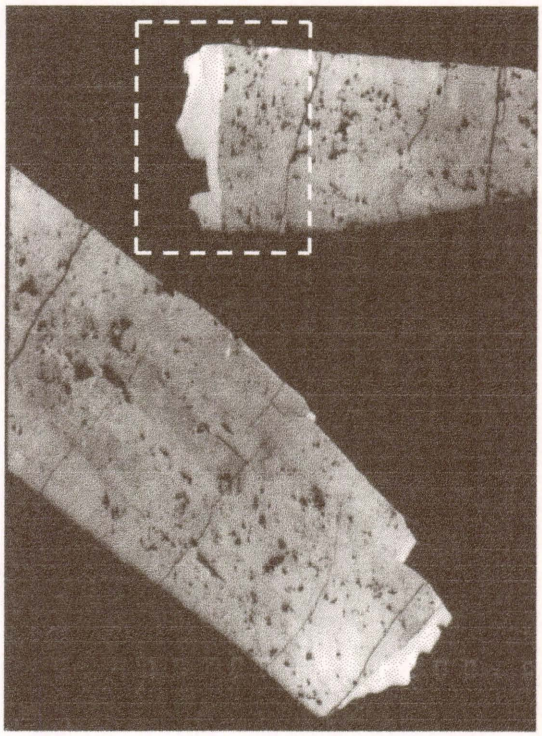

Figure 88. High-contrast BSE-image of the same field showing the two Co-rich arsenopyrite phases (bright and very bright).

Figure 88A. Enlargement of the area shown in Figure 88.

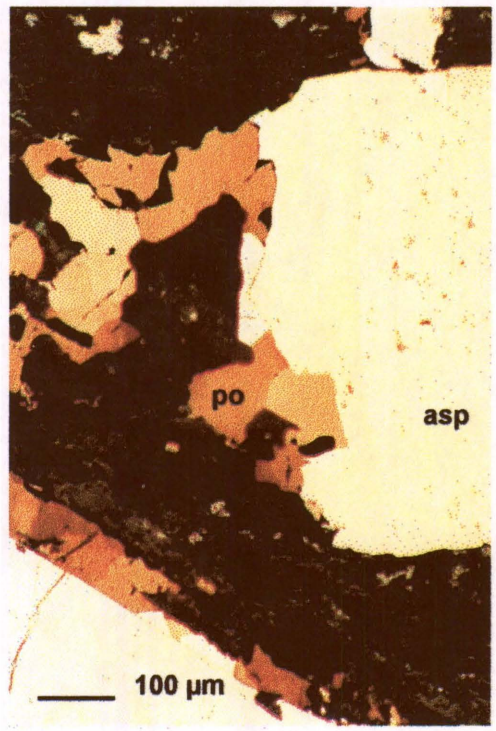

Figure 89. West African arsenopyrite G47A after three hours in ferric sulphate leach 7.

Figure 90. West African arsenopyrite G47A after two days in ferric sulphate leach 7.

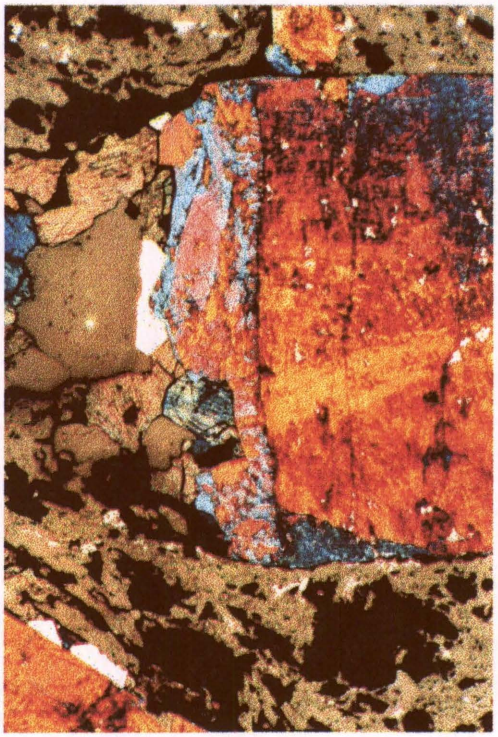

Figure 91. West African arsenopyrite G47A after eight days in ferric sulphate leach 7.

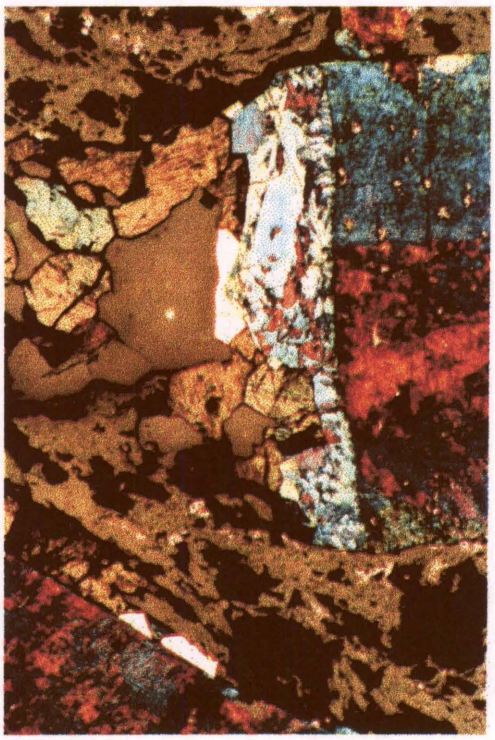

Figure 92. West African arsenopyrite G47A after two weeks in ferric sulphate leach 7.

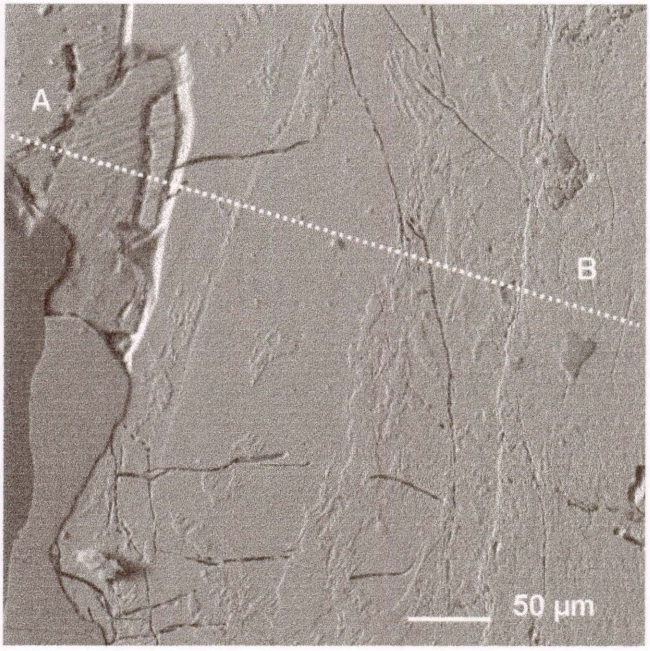

Figure 93. An enlarged post-leach SE-image of West African arsenopyrite G47A. The line A–B is shown in a topographical profile in Figure 97 below.

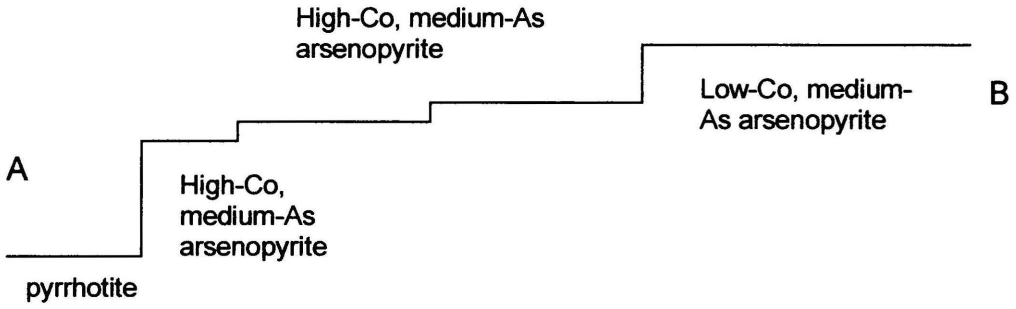

Figure 94. Schematic topographic scan across the line A–B shown in Figure 93 above. The line shows the relative leach depth of the various phases present.

G48 twinned arsenopyrite crystal (BSE-image shown in Figure 95).

Very bright zone average As/S = 2.46 Co = 0.42 mass %

Bright zone average As/S = 2.12 Co = 0.98 mass %

Medium zone average As/S = 2.05 Co = 0.04 mass %

Dark zone average As/S = 1.96 Co = 0.00 mass %

$\Delta(As/S)_{(vb-b)}$ = 0.33 $\Delta(As/S)_{(b-m)}$= 0.08 $\Delta(As/S)_{(m-d)}$= 0.09

This arsenopyrite crystal was sectioned longitudinally and displayed a mimetic twinning effect when leached in ferric sulphate solution. There are also penetration twins, one of which is sectioned near-basally. Examination of the BSE-image and the photomicrograph of the leaching crystal (Figure 96) shows once again that sterile leaching effects are controlled by both composition and crystal orientation. Within a given crystal orientation, Co-rich areas have leached in preference.

Figure 95. G48 West African arsenopyrite crystal. BSE-image.

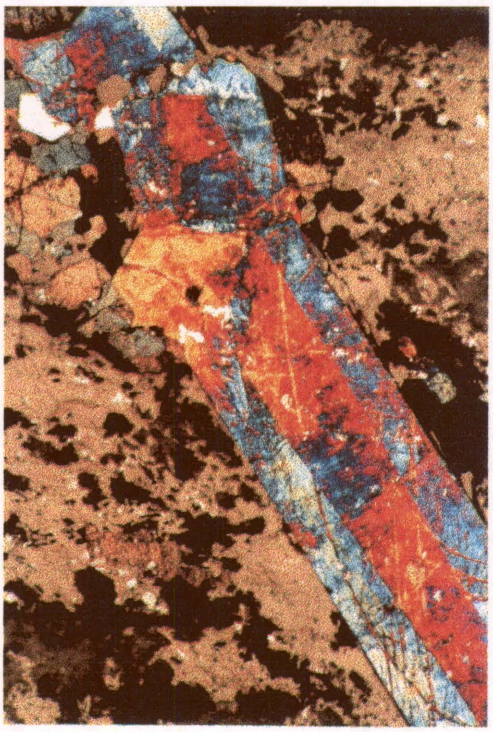

Figure 96. G48 West African arsenopyrite after three days in ferric sulphate leach 7.

G51 arsenopyrite crystal (BSE-images shown in Figures 97 and 98).

Very bright zone average As/S = 2.38 Co = 0.51 mass %

Bright zone average As/S = 2.15 Co = 1.28 mass %

Medium zone average As/S = 1.95 Co = 0.00 mass %

Dark zone average As/S = 1.74 Co = 0.07 mass %

$\Delta(As/S)_{(vb-b)} = 0.23$ $\Delta(As/S)_{(b-m)} = 0.20$ $\Delta(As/S)_{(m-d)} = 0.21$

The progress of this crystal during bacterial leaching was very similar to that of G47A, and is shown in Figures 99 and 100. Again the Co-bearing zones leached preferentially to a greater extent than could be explained by Δ(As/S) at contact.

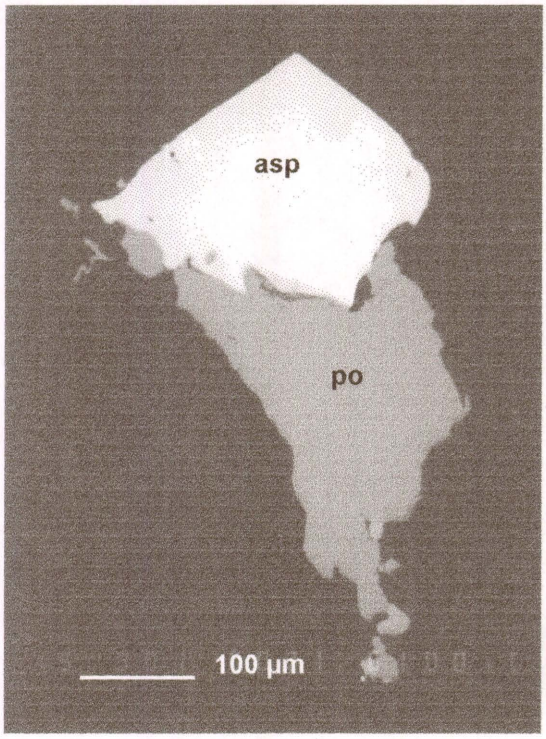

Figure 97. BSE-image of West African arsenopyrite G51, showing pyrrhotite (po) attached to the arsenopyrite (asp).

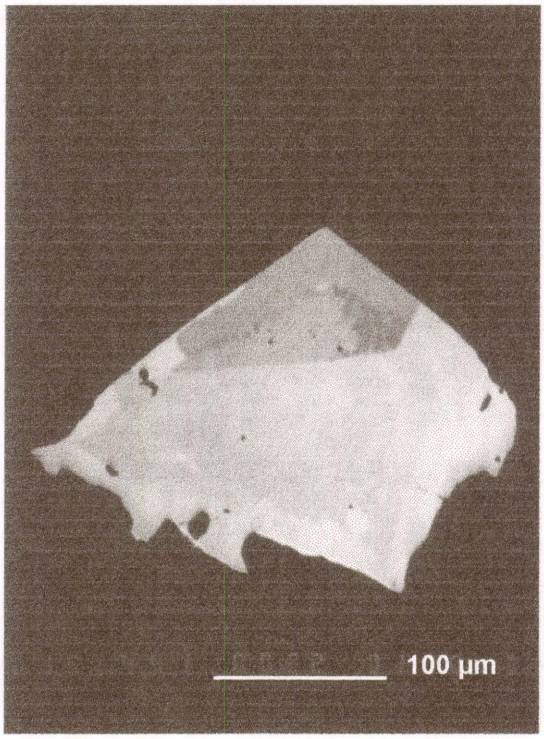

Figure 98. High-contrast BSE-image of arsenopyrite G51 showing the Co-rich (bright) areas.

Figure 99. West African arsenopyrite G51 after six days in bacterial leach 3.

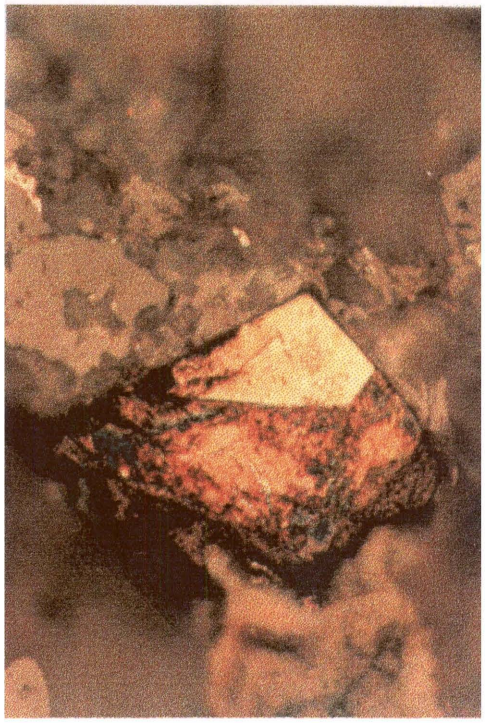

Figure 100. West African arsenopyrite G51 after two weeks in bacterial leach 3.

11.3.2 Sulphides other than arsenopyrite

11.3.2.1 Pyrite

Pyrite particles showed variable leach rate, with no obvious difference between ferric sulphate and bacterial leaching. Sheba and West African pyrite which was compositionally zoned always leached faster than unzoned pyrite. Unzoned pyrite particles in Klipwal, Zandrivier and West African samples were leached only to very pale cream by end of leach with only one or two exceptions (see, for example, G46 complex sulphide intergrowth below). Most Sheba pyrites, however, were reasonably well-leached by the end of the leach, possibly due to their much smaller particle size, and to the fact that they were usually not galvanically protected by arsenopyrite. Pyrite attached to arsenopyrite leached slowly compared to free pyrite of similar size and composition. The small, zoned Sheba pyrite particles were too small for the production of well-focussed photographs (due to depth-of-field difficulties), but their colour sequence has been described in Section 8.3, and their progress is recorded in Table A26 (Appendix pages 235 – 243). A large, zoned Sheba pyrite from an earlier bacterial leach run by the author is used below to illustrate leach behaviour.

Large Sheba zoned pyrite (BSE-image shown in Figure 101).

This was not one of the pre-analysed particles. Post-leach analysis of the repolished particle showed that arsenic was present in the brighter BSE areas in amounts of up to 3.5 mass %. The progress of this particle during bacterial leaching is shown in Figures 102 to 104. The As-rich zones are second order cream in colour after nine days, and extensively pitted after ten days (leach time here is in days after inoculation).

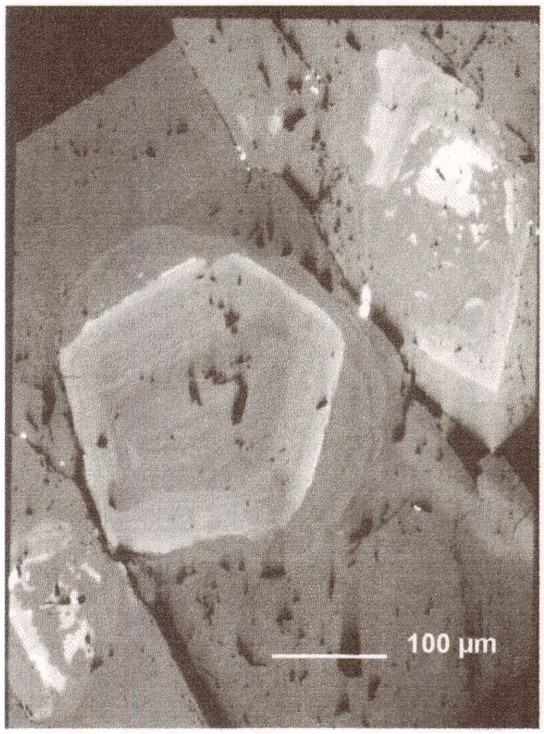

Figure 101. BSE-image of a large Sheba zoned pyrite, bright areas being As-rich. The very bright area at the top right of the image is pyrrhotite.

Figure 102. The appearance of the zoned pyrite after eight days bacterial leaching. Note that the pyrrhotite has leached out.

Figure 103. The zoned Sheba pyrite after 9 days in the bacterial leach.

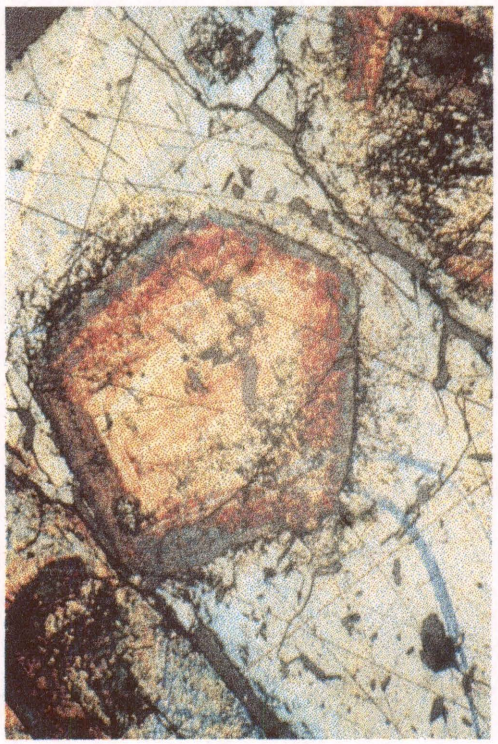

Figure 104. The zoned Sheba pyrite after 10 days in the bacterial leach. Note pore formation in As-rich areas.

G10 Sheba pyrite in contact with arsenopyrite

The smaller arsenopyrite particle in this galvanic couple had leached out completely after five days in the ferric sulphate leach, but the pyrite remained unleached (see Figures 105 and 106).

G37 Zandrivier pyrite in contact with arsenopyrite

After three days bacterial leaching, the coating over the arsenopyrite showed strong zone-related leach effects, and by one week it was dark grey with internal reflections. The attached pyrite was unaffected (see Figures 107 and 108). Since nearly all the pyrite in the Zandrivier rock sections was in contact with massive arsenopyrite, this is a widespread effect during both sterile and bacterial leaching. A topographical scanning electron image of a pyrite-arsenopyrite contact in the ferric sulphate-leached Zandrivier rock section is shown in Figure 109.

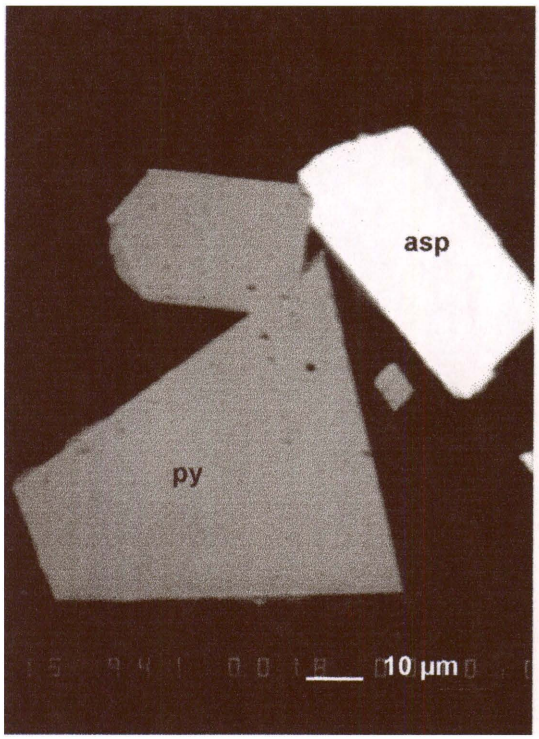

Figure 105. BSE-image of G10 Sheba pyrite (py) – arsenopyrite (asp) galvanic couple.

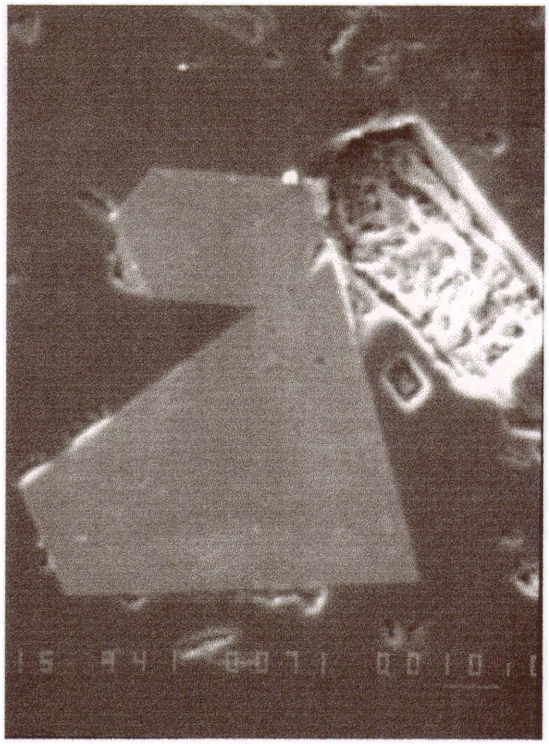

Figure 106. G10 pyrite after five days in ferric sulphate leach 7. Arsenopyrite has leached out completely.

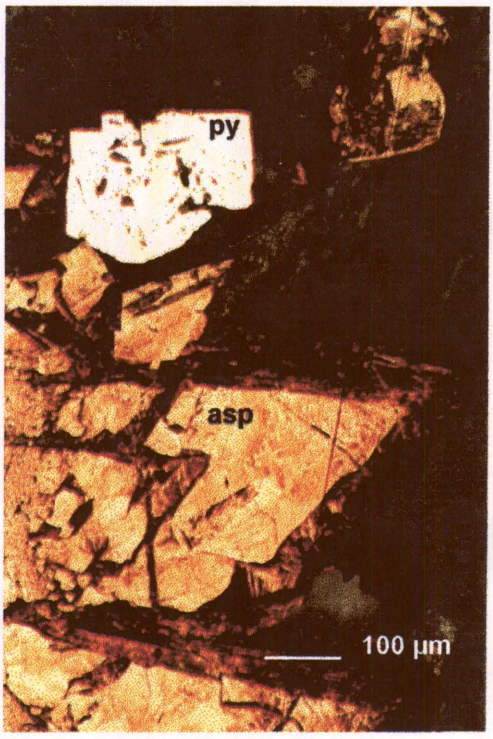

Figure 107. Zandrivier G37 pyrite (py) – arsenopyrite (asp) galvanic couple after three days in bacterial leach 3. Arsenopyrite leach rate is zone-related.

Figure 108. G37 pyrite/arsenopyrite after a week in bacterial leach 3. The arsenopyrite is well-leached, but the pyrite is still untarnished.

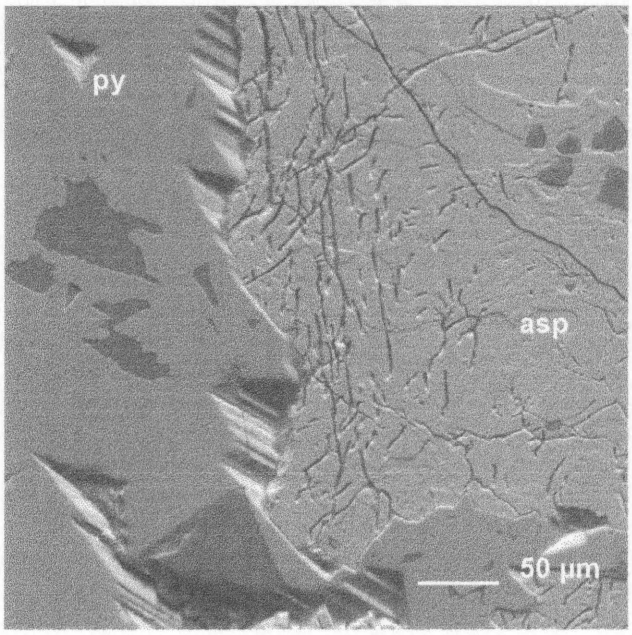

Figure 109. Topographic SE-image of an area of Zandrivier arsenopyrite (asp) in contact with pyrite (py). Note the relative depth of the sulphides after two weeks in ferric sulphate leach 7. Channels are also visible in the arsenopyrite. The darker area in the pyrite is tourmaline.

11.3.2.2 Gersdorffite

This sulphide mineral showed a wide range in leaching rate. Gersdorffite appeared to leach more quickly in the bacterial leach, where it was well-leached in one day or less, than in the ferric sulphate leach where well-leached particles took up to a week to develop. This could be a reflection of galvanic activity since most of the gersdorffite is found attached to pyrite or arsenopyrite, in which situation it leaches first. There was no obvious relationship between the variable Ni:Fe ratios in the Sheba gersdorffite grains and their leach rate, and gersdorffite locked in quartz leached far more slowly than in other silicates.

G3 Sheba gersdorffite in contact with pyrite (BSE-image shown in Figure 110).

Within three hours of the start of bacterial leaching, the gersdorffite had leached out completely (see Figures 111 and 112). The pyrite particles fell out before the end of the leach, probably because the surrounding rock was a carbonate-silicate intergrowth.

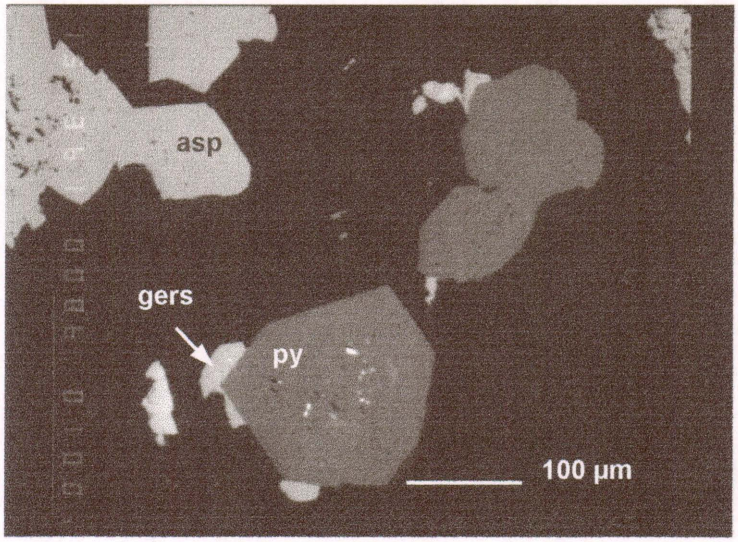

Figure 110. BSE-image of Sheba G3 gersdorffite (gers) in contact with pyrite (py).

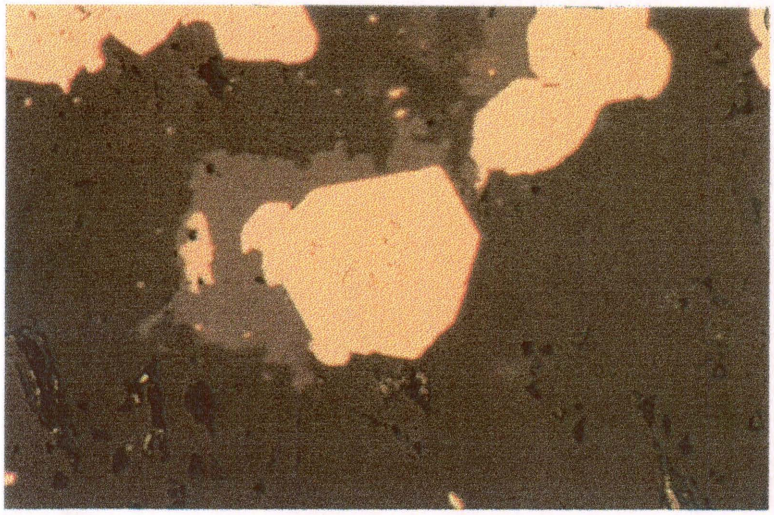

Figure 111. Photomicrograph of G3 Sheba gersdorffite before leaching.

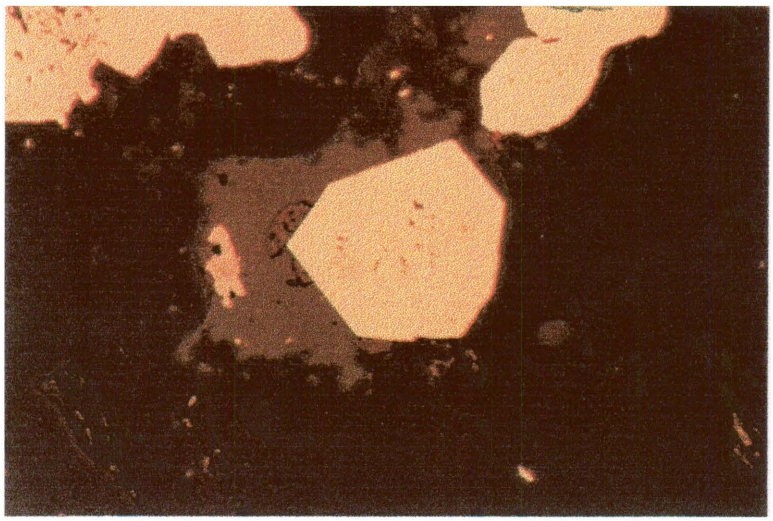

Figure 112. G3 gersdorffite after only three hours in bacterial leach 3.

11.3.2.3 Pyrrhotite

This sulphide mineral always leached quickly, under sterile and bacterial conditions. Small pyrrhotite inclusions in pyrite or arsenopyrite were leached out within hours. Large areas of pyrrhotite in the West African samples formed thick sulphur coatings which remained until the end of the leach. Orientation effects and cross-hatching appeared during the ferric sulphate leach (a good example of these is shown below). Examples of pyrrhotite in contact with arsenopyrite have already been discussed under G47A and G53 arsenopyrite above.

S33 massive West African pyrrhotite

The appearance of an area of this pyrrhotite after twelve hours in the ferric sulphate leach is shown in Figure 113. The leach rate is dependent on crystal orientation and the cross-hatching effect especially over the blue-coloured areas. By the end of the leach this area was black with some internal reflections.

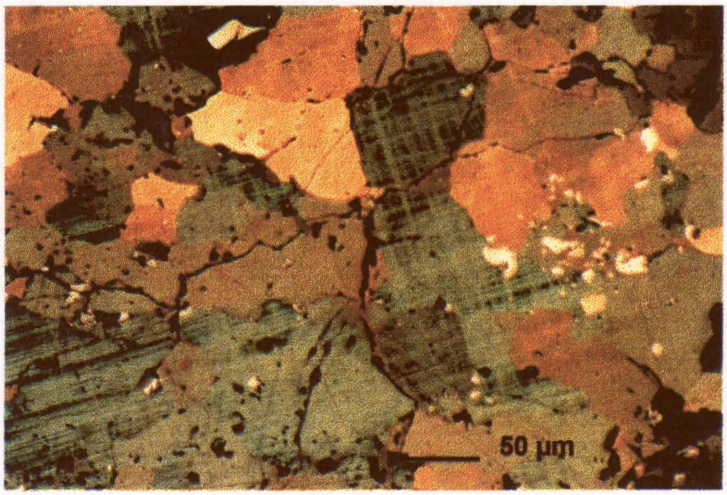

Figure 113. An area of West African pyrrhotite after 12 hours in ferric sulphate leach 7.

11.3.2.4 Chalcopyrite

Chalcopyrite always appeared unchanged by the end of the leach, whether sterile or bacterial. A typical example of a chalcopyrite inclusion in Zandrivier arsenopyrite is shown below. Two Zandrivier chalcopyrite particles in quartz (S30 and 31) were also monitored during bacterial leaching, and neither showed any sign of attack by the end of the leach.

G25 Zandrivier chalcopyrite in arsenopyrite

The chalcopyrite was unaltered and the arsenopyrite brown-multicoloured by ten days in the ferric sulphate leach (see Figures 114 and 115). The chalcopyrite was still unchanged by the end of the leach. This particle contained a gold inclusion 8µm in diameter, which would not have been released during leaching.

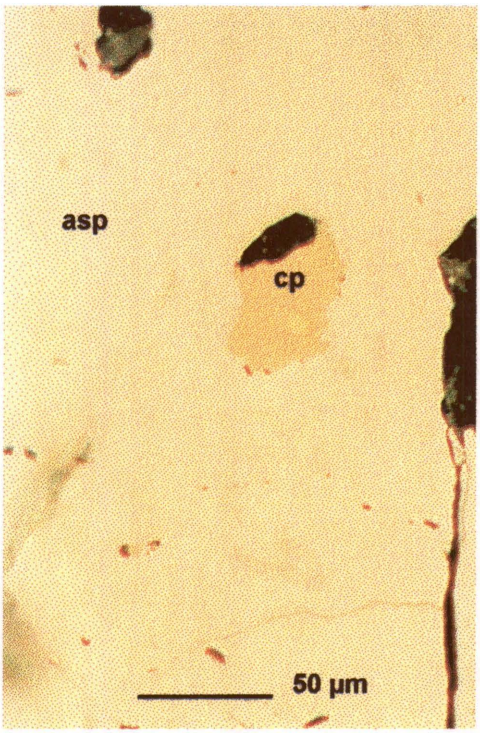

Figure 114. Photomicrograph of Zandrivier chalcopyrite G25 (cp) in arsenopyrite (asp) before leaching.

Figure 115. G25 after ten days in ferric sulphate leach test 7.

11.3.2.5 Tennantite-tetrahedrite

The sulphides of the tennantite-tetrahedrite series present in the Sheba sections were not affected noticeably by leaching, either under sterile or bacterial conditions.

G1 tennantite and tetrahedrite in contact with arsenopyrite (BSE-image shown in Figure 116). The appearance of these sulphides after two weeks in the ferric sulphate leach is shown in Figure 117. The arsenopyrite shows zone-related leaching, but the tennantite and tetrahedrite were unaltered.

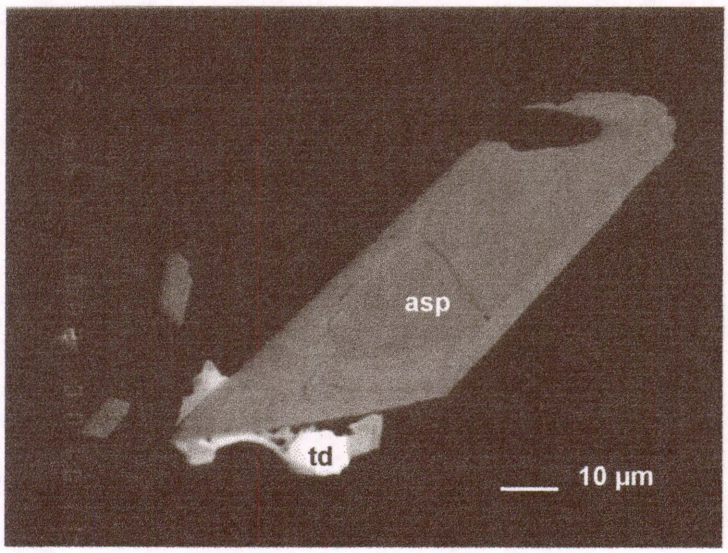

Figure 116. BSE-image of G1 Sheba tetrahedrite (td) in contact with arsenopyrite (asp).

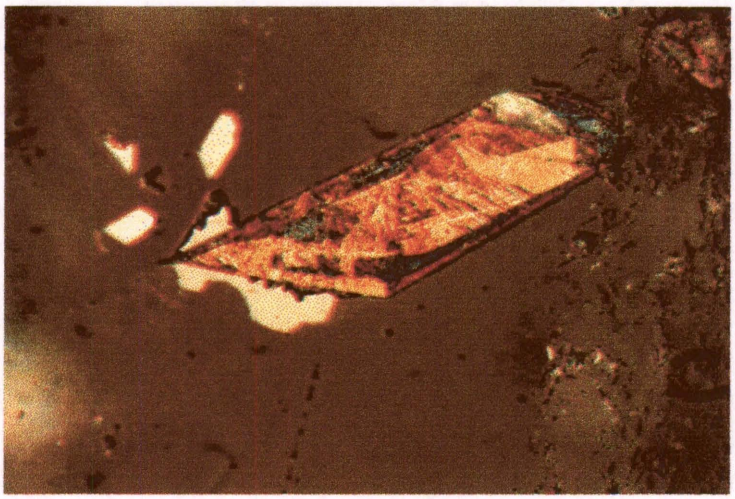

Figure 117. G1 tetrahedrite after two weeks in ferric sulphate leach 7.

11.3.2.6 Galena

Without exception, the galena inclusions in this study were too small to monitor properly microscopically. Post-leach examination showed all galena to be leached out by the end of the leach. Galena inclusions invariably leached in preference to surrounding arsenopyrite. It is likely that galena leaches as readily as pyrrhotite but this could not be confirmed.

11.3.2.7 Sphalerite

Five small sphalerite inclusions in pyrite, at the contact of pyrite and pyrrhotite, and sphalerite in contact with chalcopyrite and pyrrhotite (complex West African sulphide intergrowths G45 and G46) were the only examples of sphalerite to be monitored. The results are described under complex sulphides below. It appears that sphalerite leaches more slowly than pyrrhotite, but faster than arsenopyrite and pyrite.

11.3.2.8 Complex sulphide intergrowths

Two case histories where more than two sulphide minerals are in contact are described below. The contact of pyrite, pyrrhotite and arsenopyrite is relatively common in the West African rock sections, and one example was described earlier under G47A arsenopyrite.

G45 West African sphalerite-chalcopyrite-pyrrhotite intergrowth

Unfortunately this particle fell out after three hours in the ferric sulphate leach, because it was entirely surrounded by carbonates. As shown in Figures 118 and 119, however, pyrrhotite had already leached to brown within one hour, with the other sulphides not being altered.

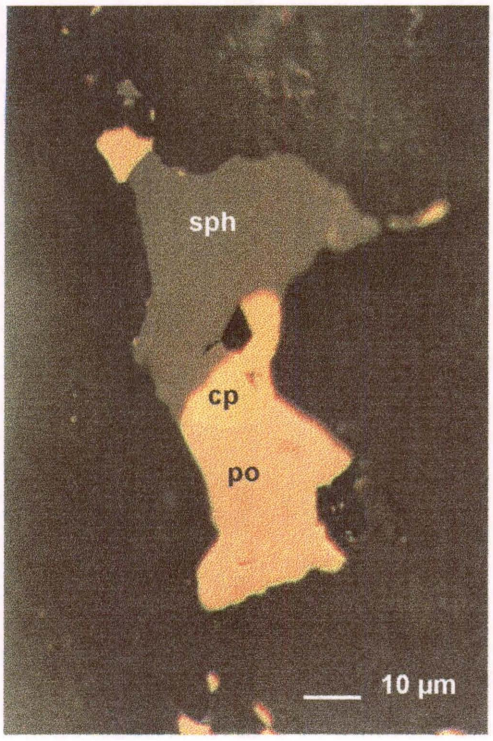

Figure 118. Photomicrograph of West African G45 sphalerite (sph), chalcopyrite (cp) and pyrrhotite (po) in contact, before leaching.

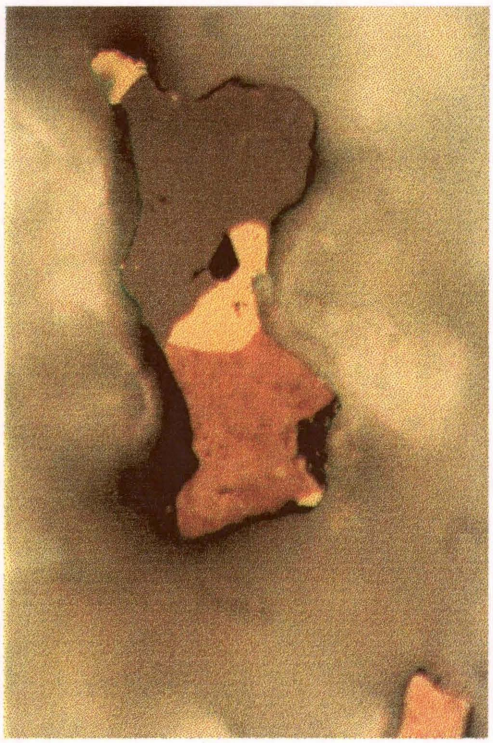

Figure 119. G45 after one hour in ferric sulphate leach 7. Pyrrhotite has already discoloured.

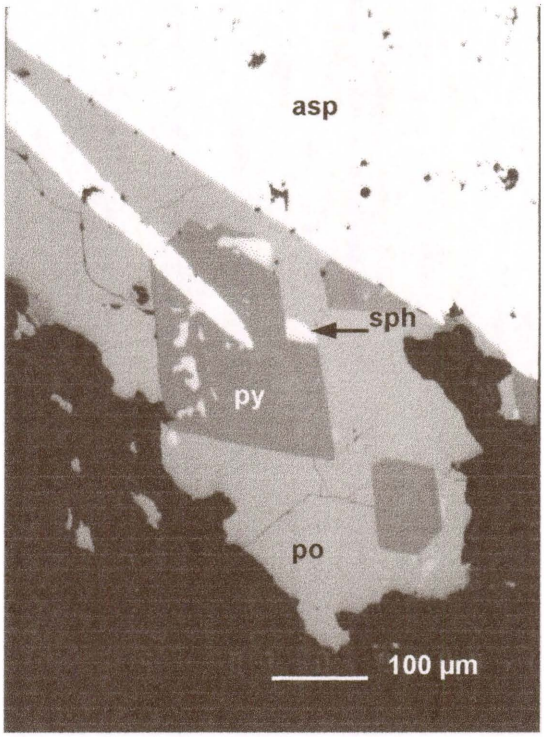

Figure 120. West African G46 pyrite (py), arsenopyrite (asp), sphalerite (sph) and pyrrhotite (po) intergrowth. BSE-image.

G46 West African sphalerite-pyrite-pyrrhotite-arsenopyrite intergrowth (BSE-image shown in Figure 120).

The progress of the various sulphides during ferric sulphate leaching is shown in Figures 121 to 124). It can be seen that pyrrhotite leaches most easily, followed by sphalerite, arsenopyrite, then pyrite. The pyrite in this area was leached to beige-brown by the end of the leach – as mentioned earlier, this is unusual for weakly zoned pyrite.

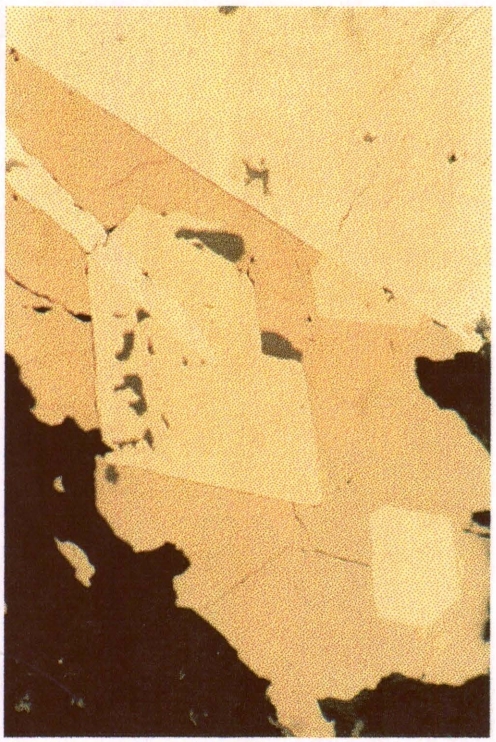

Figure 121. West African G46 sulphide intergrowth before leaching.

Figure 122. G46 after three hours in ferric sulphate leach 7.

Figure 123. G46 after two days in ferric sulphate leach 7.

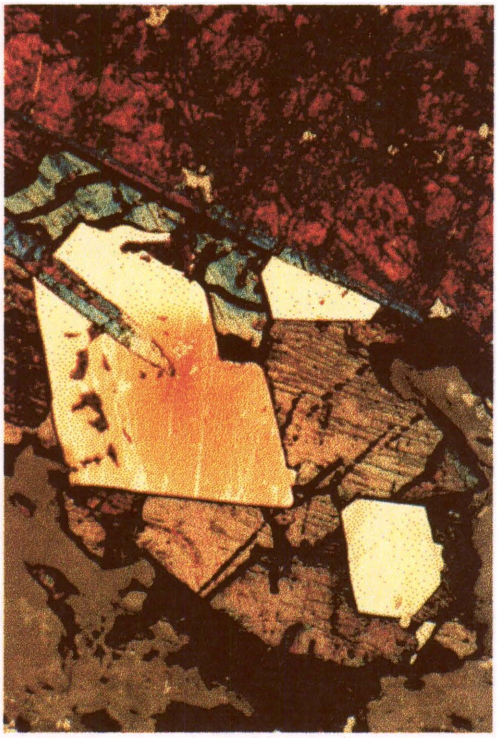

Figure 124. G46 after twelve days in ferric sulphate leach 7.

11.3.3 Influence of surrounding rock

The influence of the surrounding minerals on leaching sulphides is shown in Figures 125 and 126. Arsenopyrite surrounded by quartz leaches more slowly than that surrounded by feldspar or mica. This could be due to leach solution access, but it is more likely to be a galvanic effect.

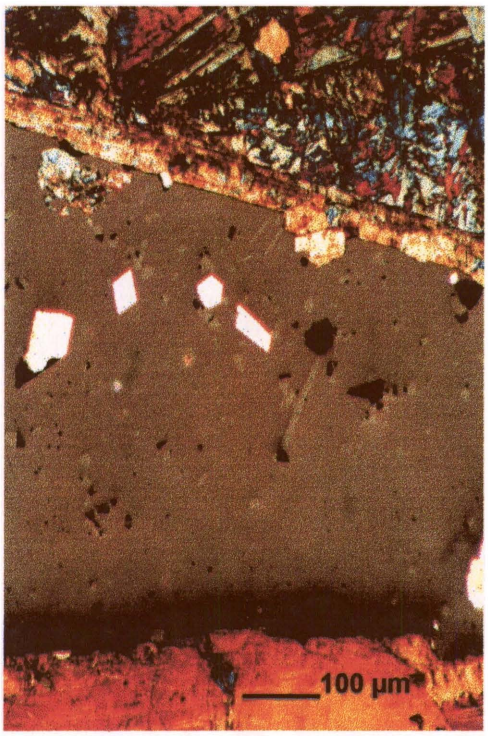

Figure 125. Unleached Zandrivier arsenopyrite crystals in a quartz vein. The surrounding massive arsenopyrite is quite well-leached.

Figure 126. Unleached Sheba arsenopyrite in quartz. Where sericite is in contact, arsenopyrite crystals are more extensively leached.

11.3.4 Gold

Gold inclusions large enough to be monitored microscopically were not altered by either sterile or bacterial leaching, irrespective of the enclosing mineral. A typical gold inclusion in arsenopyrite is shown below.

G30 gold in Zandrivier arsenopyrite (BSE-image shown in Figure 127).

The appearance of the gold after ten days in the ferric sulphate leach is shown in Figure 128. The gold was still unaltered at the end of the leach.

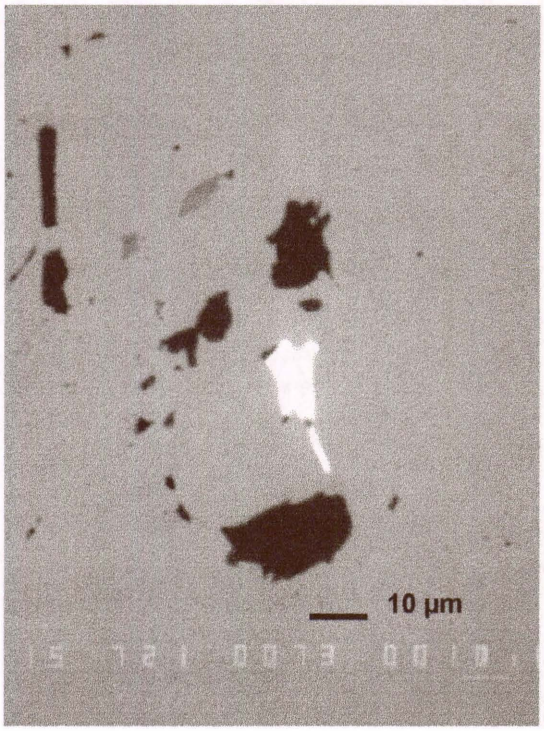

Figure 127. BSE-image of Zandrivier G30 gold (white) in arsenopyrite. The dark phase is siderite, and the medium intensity inclusions at the top of the field are chalcopyrite.

Figure 128. G30 gold after ten days in ferric sulphate leach 7. The gold is unaltered, as is the chalcopyrite, but the arsenopyrite has tarnished and the siderite has dissolved.

11.4 Features of leaching sulphide surfaces

The extent to which a sulphide mineral has leached is not only dependent on its orientation, and the surrounding rock type, but also on the particle size. Figures 129 and 130 show that smaller particles do leach faster during both sterile ferric sulphate and bacterial leaching. In this case the particles are surrounded by quartz, but this is also the case when the particles are surrounded by epoxy resin.

During leaching physical features such as pores (or pits), channels and enlarged cracks appeared on the surface of arsenopyrite, pyrite and pyrrhotite. This happened under sterile and bacterial conditions. Leach channels developed in all arsenopyrite types. These varied from 1 to 3 µm in diameter (sometimes wider in bacterially-leached samples) and were up to 200µm in length.

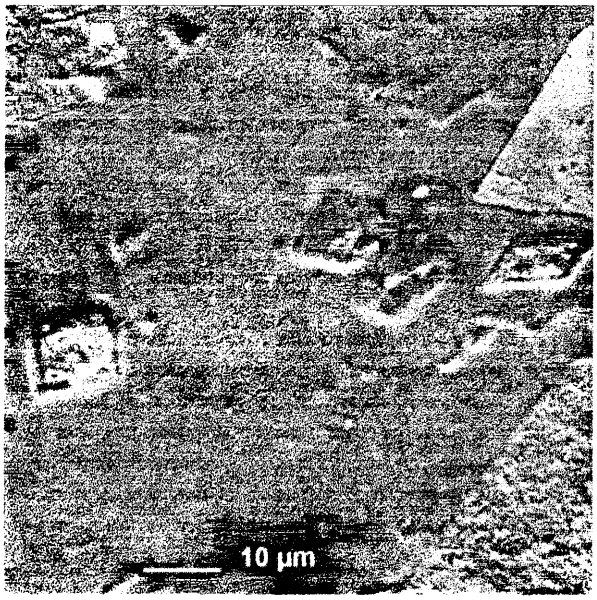

Figure 129. SE-image showing the influence of particle size on the leach rate of Sheba arsenopyrite crystals during ferric sulphate leach 7.

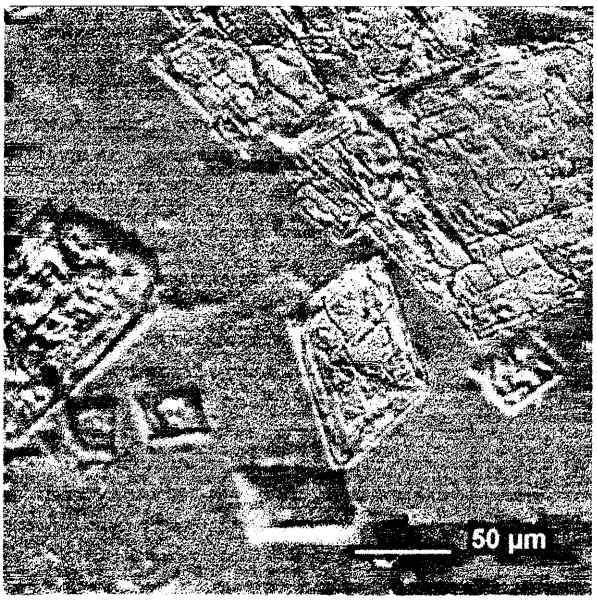

Figure 130. SE-image showing the influence of particle size on the leach rate of Sheba arsenopyrite crystals during bacterial leach 3.

Zandrivier arsenopyrite showed a strong tendency to develop swarms of small channels, many of which showed lineation (see Figures 131 and 132). Channels in Sheba arsenopyrite often followed pre-existing cracks or crystallographic directions, and lineation was evident in channels formed on the surface of Klipwal and West African crystals (see Figures 133 to 136). All pits and pores in arsenopyrite appeared rounded in cross-section, within the resolution of the scanning electron microscope (SEM) and did not show any shape that could be related to crystal symmetry.

Figure 131. Leach channel development in Zandrivier arsenopyrite after six days in ferric sulphate leach 7. The blue and red areas are also arsenopyrite, but of a different orientation.

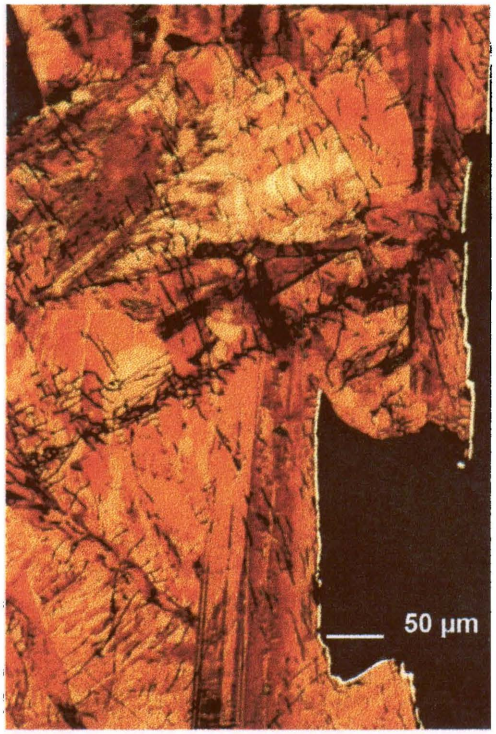

Figure 132. Leach channel development in Zandrivier arsenopyrite after six days in ferric sulphate leach 7. The thin white line is pyrite.

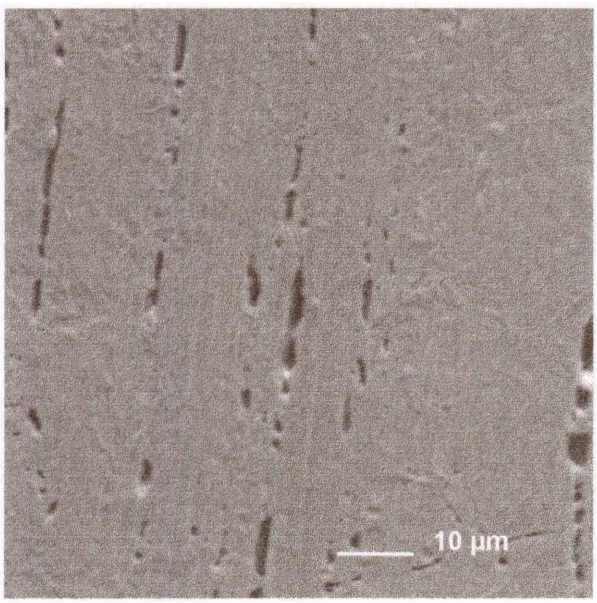

Figure 133. Leach channel formation in Klipwal arsenopyrite after two weeks in ferric sulphate leach 7.

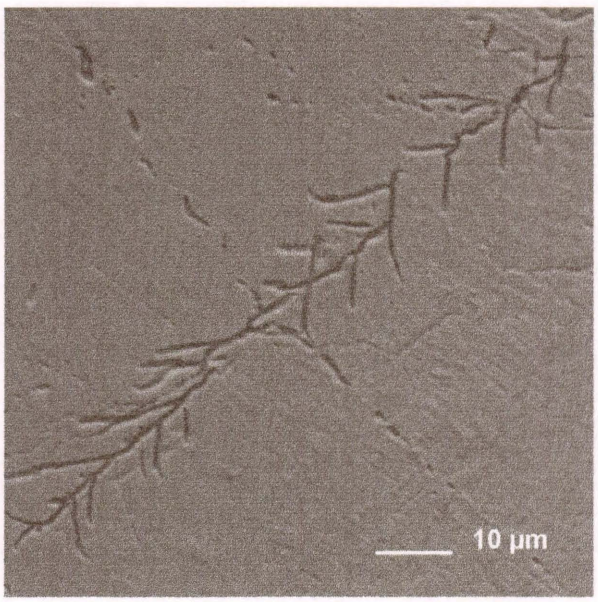

Figure 134. Leach channel formation in Zandrivier arsenopyrite after two weeks in ferric sulphate leach 7.

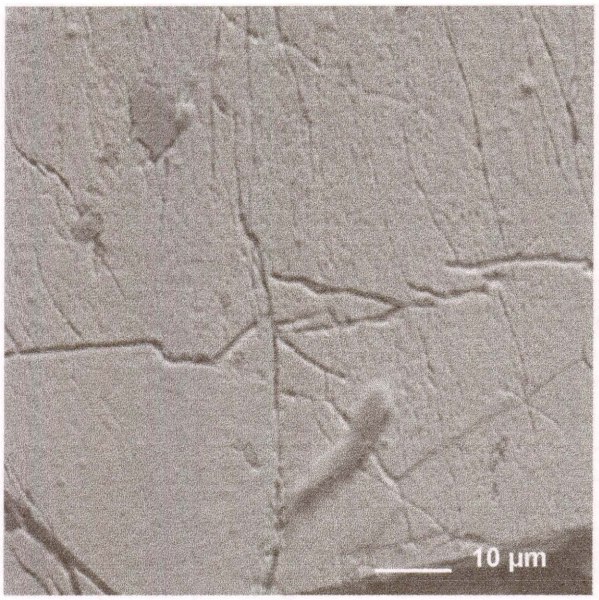

Figure 135. Leach channel formation in West African arsenopyrite after two weeks in ferric sulphate leach 7.

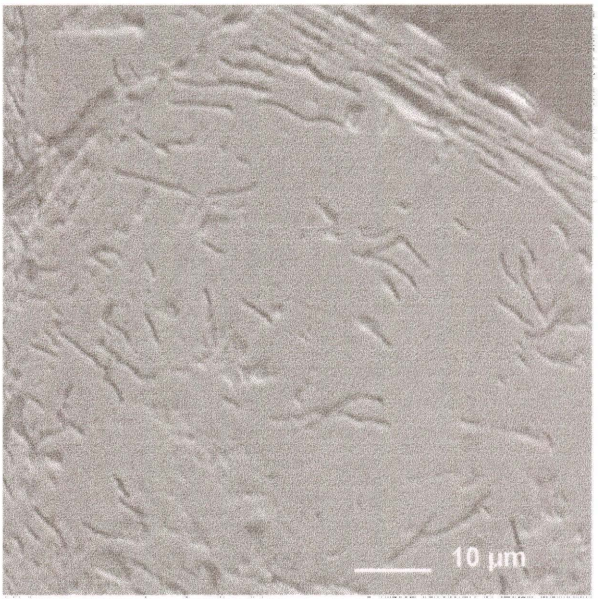

Figure 136. Leach channel formation in Sheba arsenopyrite after two weeks in bacterial leach 3.

Pores and channels which developed during bacterial leaching of a strongly-zoned pyrite crystal are shown in Figure 137, and pits in a weakly-zoned pyrite crystal during ferric sulphate leaching in Figure 138. Although pits and channels in pyrite form at zone boundaries, and are frequently parallel to crystal faces, this is not always the case. Pits and pores in pyrite also did not show cubic or rectangular profiles, but appeared rounded within the resolution of the SEM.

By the end of the leach, pyrrhotite particles were commonly completely eroded, but some were covered with a layer of elemental sulphur of unknown thickness. Pits and channels of up to 10 µm in diameter were seen in the sulphur layer, with channels often forming at grain boundaries (see Figure 139).

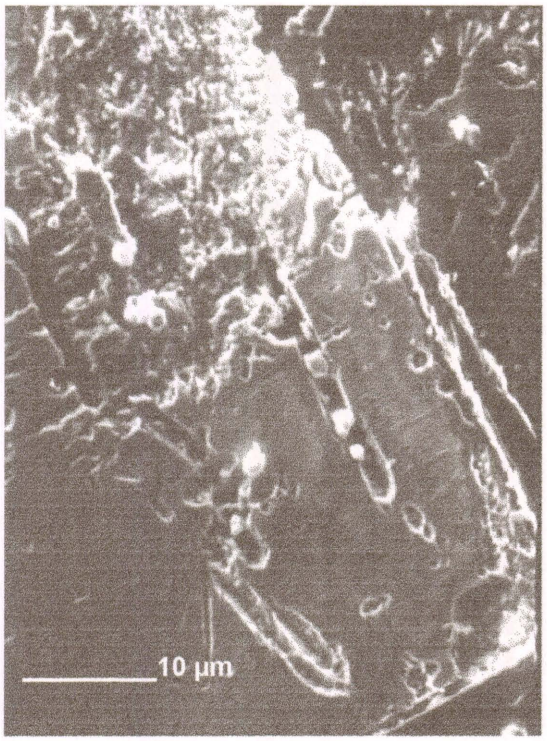

Figure 137. Pores and channels in a strongly-zoned Sheba pyrite after two weeks bacterial leaching. SE-image.

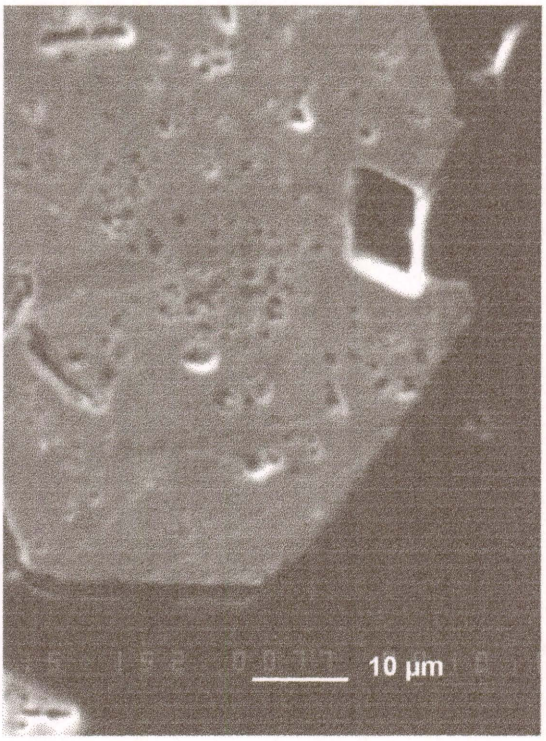

Figure 138. Pores which formed in a weakly-zoned Sheba pyrite after two weeks in ferric sulphate leach 7. The rhombic hole is the site of an arsenopyrite crystal which was leached out. BSE-image.

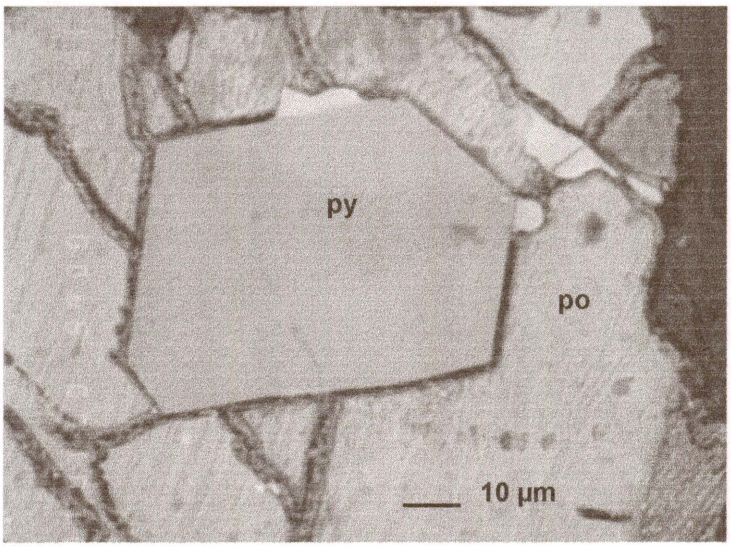

Figure 139. BSE-image of G46 West African pyrite (py) and pyrrhotite (po) after two weeks in ferric sulphate leach 7. The brighter area is chalcopyrite.

11.5 Discussion of results of the rock section leach tests

The rock section leach tests provided valuable information about the effect of compositional variation within a crystal on its leach rate, and on leaching behaviour of other sulphide minerals, particularly those removed by HF leaching, such as pyrrhotite and galena.

When there is a large Δ(As/S) at the contact of two zones in arsenopyrite, leaching is rapid. This effect is difficult to quantify with the limited amount of data available, but the averaged values in Table 40 suggest that on average the Δ(As/S) for Sheba arsenopyrite is considerably higher than that of the other arsenopyrite types, which leads to an enhanced leach rate. In Figure 140 the averaged values of Δ(As/S) are plotted against leach colour acquired by the fourth day of sterile leach 6. It should be noted that the leach behaviour of the West African arsenopyrite is also dependent on contained cobalt.

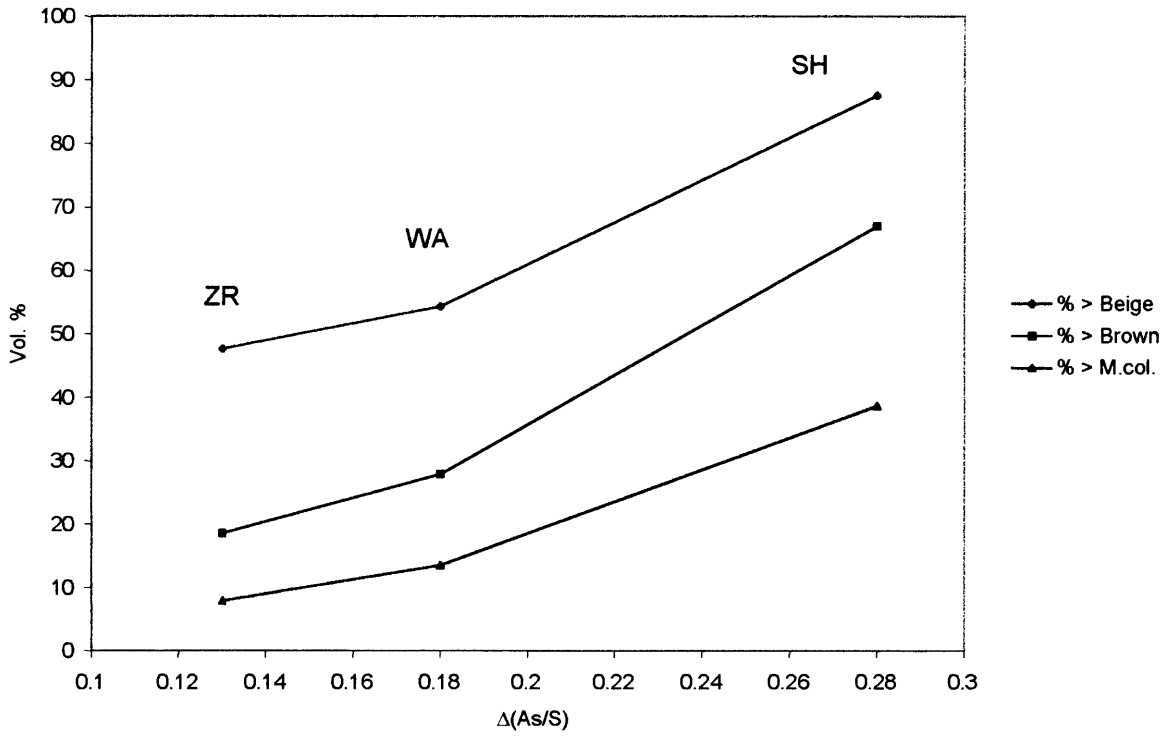

Figure 140. Plot of averaged Δ(As/S) against the leach colour attained after four days in sterile leach 6 for Zandrivier (ZR), West African (WA) and Sheba (SH) arsenopyrite. % > Beige – the volume per cent leached further than the beige leach colour. Similarly with brown and dark multicoloured.

The major findings in this section *in addition* to data from the early leach tests are as follows:

- The leach rate of a sulphide mineral in a rock depends on the surrounding minerals.
- Leach rates in both bacterial and sterile leaching are – pyrrhotite ≥ galena > sphalerite ≥ gersdorffite > arsenopyrite > pyrite > chalcopyrite, tennantite-tetrahedrite and gold.
- The rate and extent of zone-related leaching in arsenopyrite is dependent upon the difference in Δ(As/S) between zones in contact.
- The presence of cobalt in arsenopyrite leads to preferential oxidation during both sterile and bacterial leaching.
- Pits, pores and channels form in arsenopyrite, pyrite and pyrrhotite during sterile and bacterial leaching.
- Pores and channels in arsenopyrite occasionally follow crystal axial directions. They form at grain or zone boundaries or along cracks, and are rounded in cross-section.

12. MINERALOGY OF LEACHED SULPHIDES

The mineralogy of leaching and leached sulphide mineral surfaces was examined using the electron microprobe, on the microscope photometer, and by Auger Electron Spectroscopy (AES).

12.1 Electron microprobe analysis results

Qualitative EDS analyses of leached arsenopyrite surfaces from the crystal and rock sections showed progressive sulphur-enrichment throughout – the more leached the crystal, the more enriched was sulphur over arsenic and iron. (Most of the sulphur, as demonstrated by AES, is present as elemental sulphur, and not as a sulphate – see Section 12.3.2 below). Some well-leached particles, especially in the bacterial leach, showed the presence of a small amount of oxygen. Jarosite, probably hydronium jarosite, was seen in some of the bacterial leach residues, notably as a coating over a few Sheba arsenopyrite grains. No sulpharsenate minerals such as zykaite or arsenates such as scorodite were detected (the formulae of these leach products are given in Table A4 (Appendix page 180)).

The progress of bacterial oxidation of a typical Sheba arsenopyrite is shown in Figures 141 and 142, with the As-rich zone leaching first, and a core of S-rich arsenopyrite leaching more slowly. X-ray mapping of a partially-leached arsenopyrite crystal using the electron microprobe demonstrates that arsenic and iron dissolve preferentially during leaching, leaving a residual sulphur-rich layer (Figures 143 and 144). Eventually the entire crystal leaches out, leaving only a cavity in the surrounding rock. This behaviour was also observed in arsenopyrite during ferric sulphate leach tests in this study.

Elemental sulphur coatings which formed over bacterially-leached arsenopyrite grains appeared to be thicker than those formed over their ferric sulphate-leached counterparts (probably because they were better-leached) and curious sulphur balls that were first thought to be bacterial remains, but proved to be too large, were found in areas of the bacterially-leached Zandrivier rock section (see Figure 145). Similar balls of elemental sulphur have been described as forming on the surface of chalcopyrite during bacterial leaching with thermophilic bacteria (GÓMEZ *et al.,* 1996).

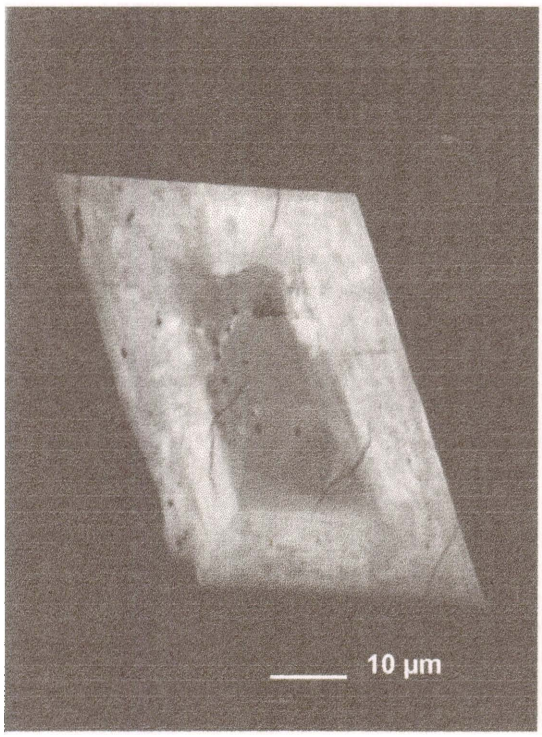

Figure 141. BSE-image of a typical Sheba arsenopyrite crystal before leaching. The bright rim is As-rich, and the darker core is S-rich.

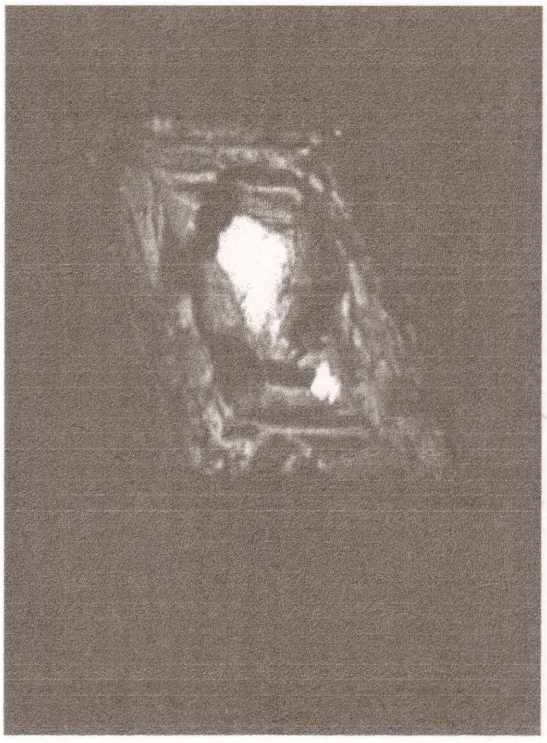

Figure 142. BSE-image of the same crystal after being bacterially leached for three weeks. The As-rich zone has leached preferentially, leaving the S-rich core.

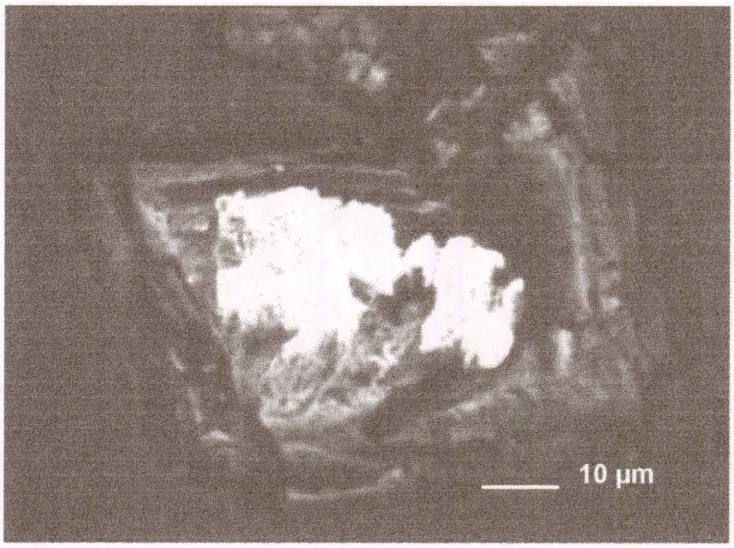

Figure 143. BSE-image of a residual Sheba arsenopyrite after two weeks bacterial leaching. The core remains, but the As-rich rim has gone.

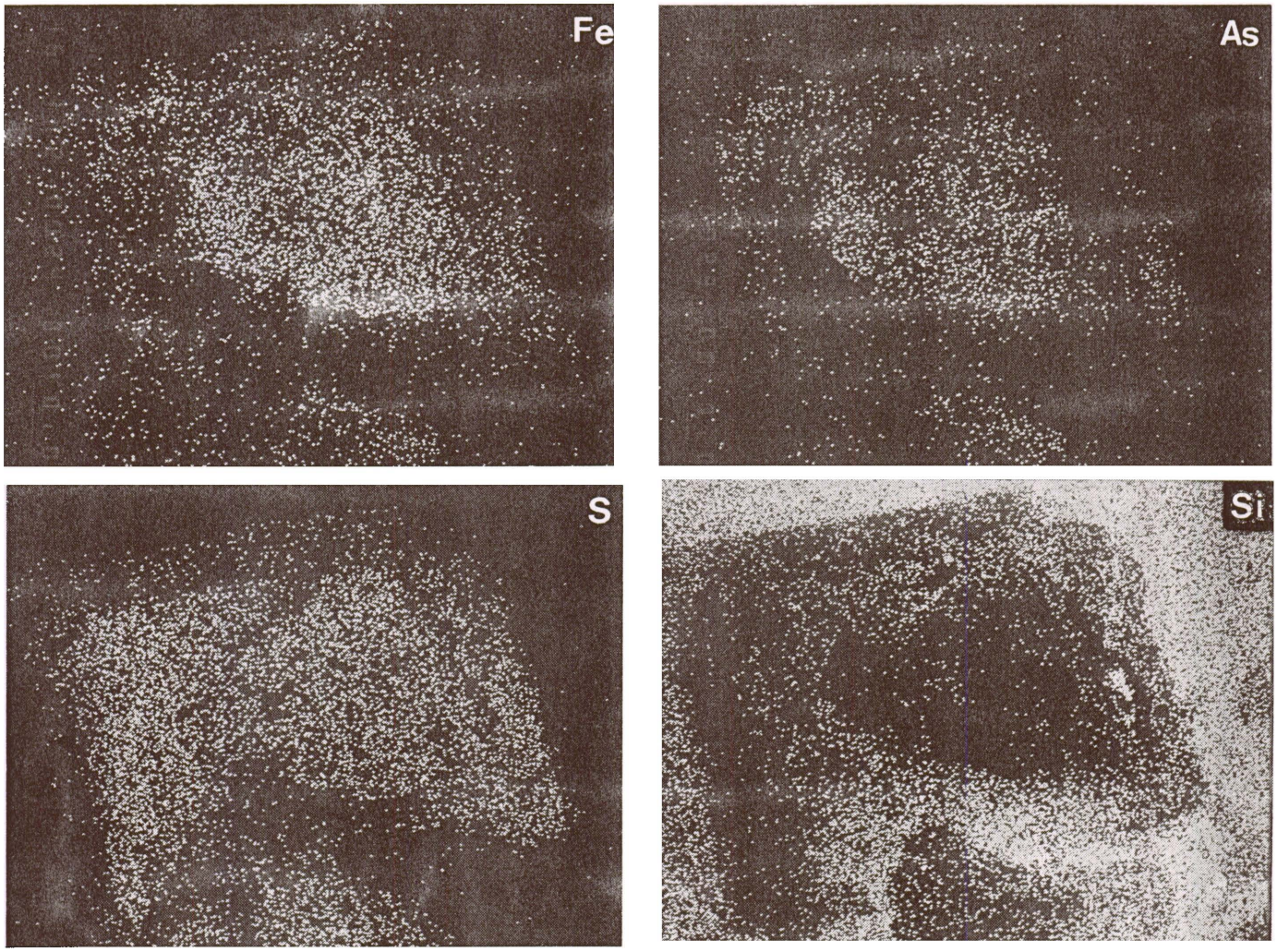

Figure 144. X-ray map of elemental distribution in the partially-leached arsenopyrite above. Fe and As have been removed leaving a sulphur residue and a S-rich core. Si in the surrounding rock is also shown.

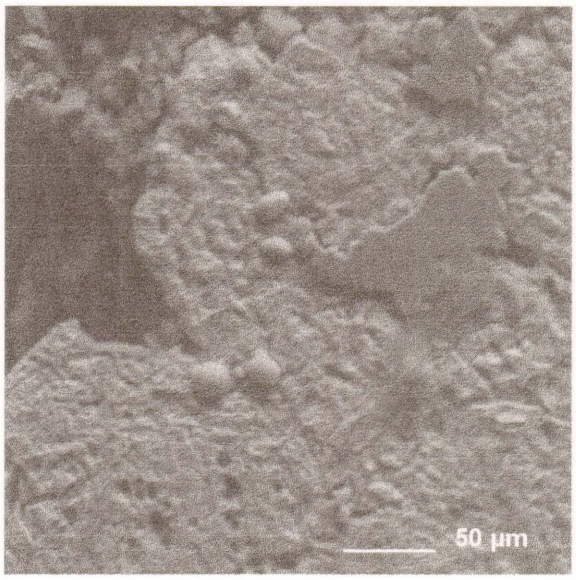

Figure 145. Balls of elemental sulphur which formed over Zandrivier arsenopyrite after two weeks in bacterial leach 3.

12.1.1 Silver contamination

Another unexpected phenomenon was the presence of small amounts of silver – up to 5 mass % on the surface of well-leached arsenopyrite in the ferric sulphate leach, and in lesser amounts (up to 2 mass %) on the surface of bacterially-leached arsenopyrite crystals. Silver was also detected on the surface of leached pyrrhotite and sphalerite, but was confined exclusively to the surface of the sulphide minerals. Little to no silver had been found in the sulphide minerals by ICP-MS or electron microprobe analysis, so the ferric sulphate powder, the gangue minerals in the rock samples, and the overhead stirrer blade were analysed for silver, but none was detected. Silver contamination may be an important factor affecting the leach rate, because silver has been found to act as a catalyst in the leaching of chalcopyrite, enargite and sphalerite (MILLER & PORTILLO, 1979, BALLESTER *et al.,* 1990, 1992, GÓMEZ *et al.,* 1997, ESCOBAR *et al.,* 1997).

The only other source of the silver could have been the introduction through the frequent use of the pH and ORP electrodes during measurement (GROOT, *pers. com.,* 1997). Such electrodes are also used in the bacterial leach pachucas, and release small amounts of silver into solution which would then be attracted to sulphide surfaces. A calculation involving the solubility of AgCl in 3M KCl solution inside the electrode, and the natural electrode leakage rate, suggests that the electrodes may indeed have been the source of the silver contamination.

12.2 Reflectance of leached arsenopyrite

The reflectance of arsenopyrite can be used to gauge the depth of oxidation, even when an elemental sulphur layer is present (RICHARDSON & VAUGHAN, 1989). The reflectance of arsenopyrite exposed to a number of inorganic oxidising agents was measured by the authors, and related to the depth of oxidation as determined by AES. Reflectance lower than 23 % was not measured – at this level a depth of oxidation of over 60 µm was estimated. This technique was used in this study to characterise the colours, as perceived by the eye, of the leached arsenopyrite particles.

12.2.1 Ferric sulphate leach 8

A composite crystal section was leached simultaneously with the rock sections in leach 7 for the purpose of taking reflectance readings on crystals of sufficiently large size. The leach liquor contained 10 g/l of ferric iron, and the pH was held as close to 0.5 as possible. The leach conditions were shown in Table 39 above.

12.2.2 Reflectance measurement results

The reflectance of arsenopyrite crystals displaying even leach colouration from the Klipwal, Zandrivier and West African sections were measured in five locations per particle, and the results, which have already been described in Section 6 under arsenopyrite reflectance, are shown in Table A5 (Appendix pages 181–185). As leaching progresses, the reflectance falls steadily to the dark multi-coloured stage, and then rises during the second order blue and cream stages. Bireflectance also increases with time in leach, depending on crystal orientation. The changes in reflectivity as leaching proceeds are shown in Figures 146 and 147.

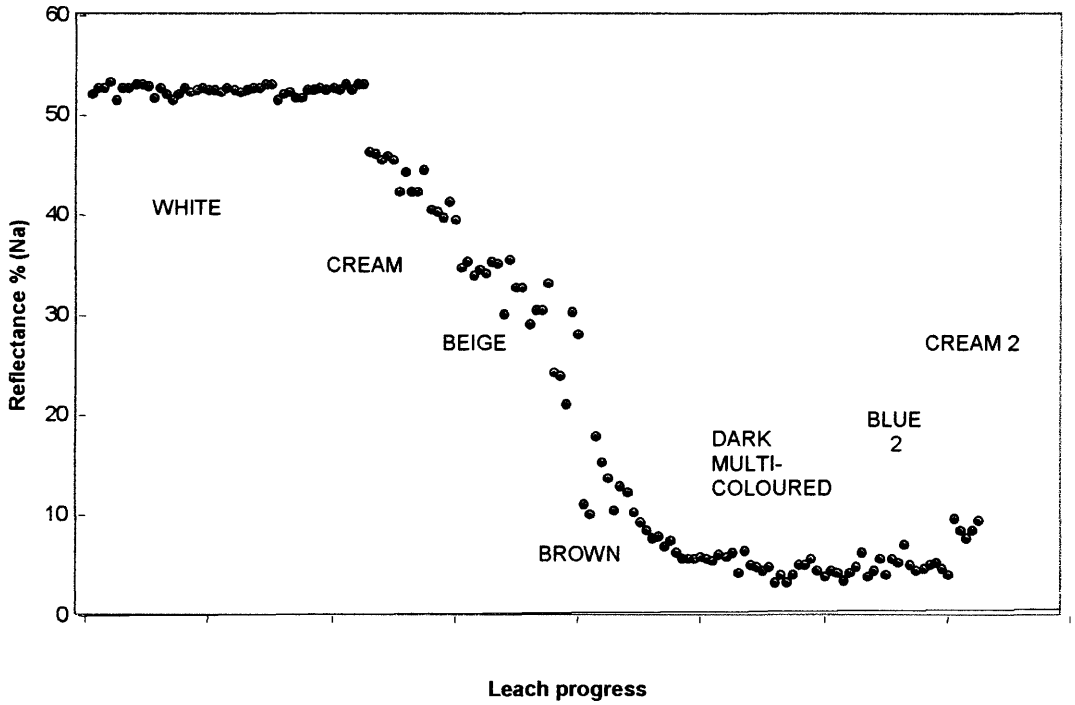

Figure 146. Change in arsenopyrite reflectance at 589 mm (Na) as leach colours advance.

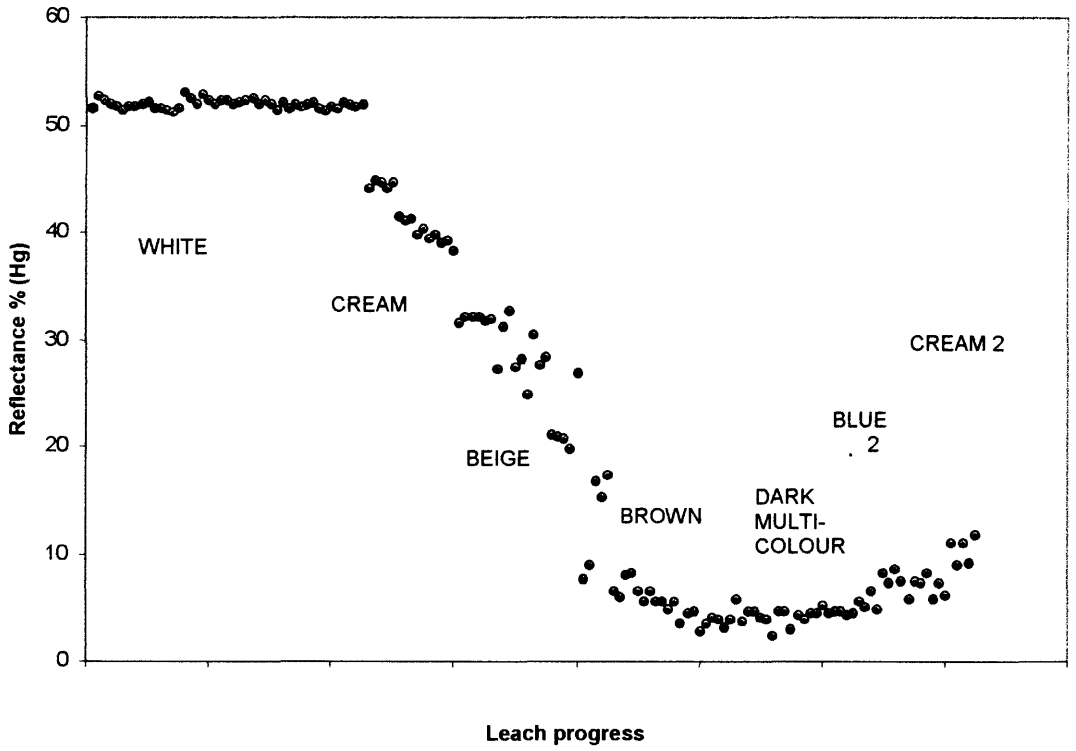

Figure 147. Change in arsenopyrite reflectance at 546 mm (Hg) as leach colours advance.

12.3 Auger Electron Spectroscopy (AES)

Klipwal arsenopyrite crystals were chosen for the AES study because they were relatively large, and the visual resolution of the spectroscope was limited to specimens over 1mm in diameter.

12.3.1 Ferric sulphate leach tests 9 and 10

Two crystals were leached in 10 g/l ferric iron solution at pH 0.5 for three days and one week respectively (ferric sulphate leach 9). The same experiment was repeated with 4 % dissolved arsenic (leach 10). The fifth crystal was an unleached control. The pH and ORP readings taken during leaching are shown in Table 41 below. The 3-day crystals were added to the leach on day 4.

TABLE 41

pH AND OXYGEN REDUCTION POTENTIAL (ORP) VARIATION DURING FERRIC SULPHATE LOOSE CRYSTAL LEACHES 9 AND 10
(10 g/l ferric iron concentration, temperature 35±1 °C)

Time (days)	9	Ferric sulphate solution	10	Ferric sulphate solution + 4 mass% As
	pH	ORP (mV)	pH	ORP (mV)
0	0.52	610	0.51	n.d.
1	0.56*	620	0.56*	550
4	0.48	620	0.49	510
7	0.51	615	0.50	500

*Acid added
n.d. = not determined

12.3.2 AES analysis

Two types of investigation were performed by AES - qualitative analyses of the surface of the crystals, and depth analysis by sputtering down into the crystals to depths of approximately 1 µm. AES is extremely sensitive to very small amounts of organic contamination, so no attempt was made to examine bacterially-leached crystals.

Elements detected on the surface of the unleached arsenopyrite crystal were Fe, As, S, O, C (from the isopropanol cleaner) N, F (from HF), Cu, Cl, Se, Au, and Si. Detection limits are in the order of ppb, so the method is very sensitive, if not quantitative. Elements detected on the surface of leached arsenopyrite were S, O, Fe, As, Ag, C, N, and Si. Elements detected at depth inside the arsenopyrite were only As, S and Fe, with occasional Si. Depth profiles

produced during sputtering are shown in Figures 148 to 151. It is interesting to note that sulphur-enrichment of the leached arsenopyrite extends into the crystals to depths of over 1 µm, even after only three days in the leach. When examining the figures it should be emphasized that these are qualitative, and that the technique is more sensitive to light than heavy elements.

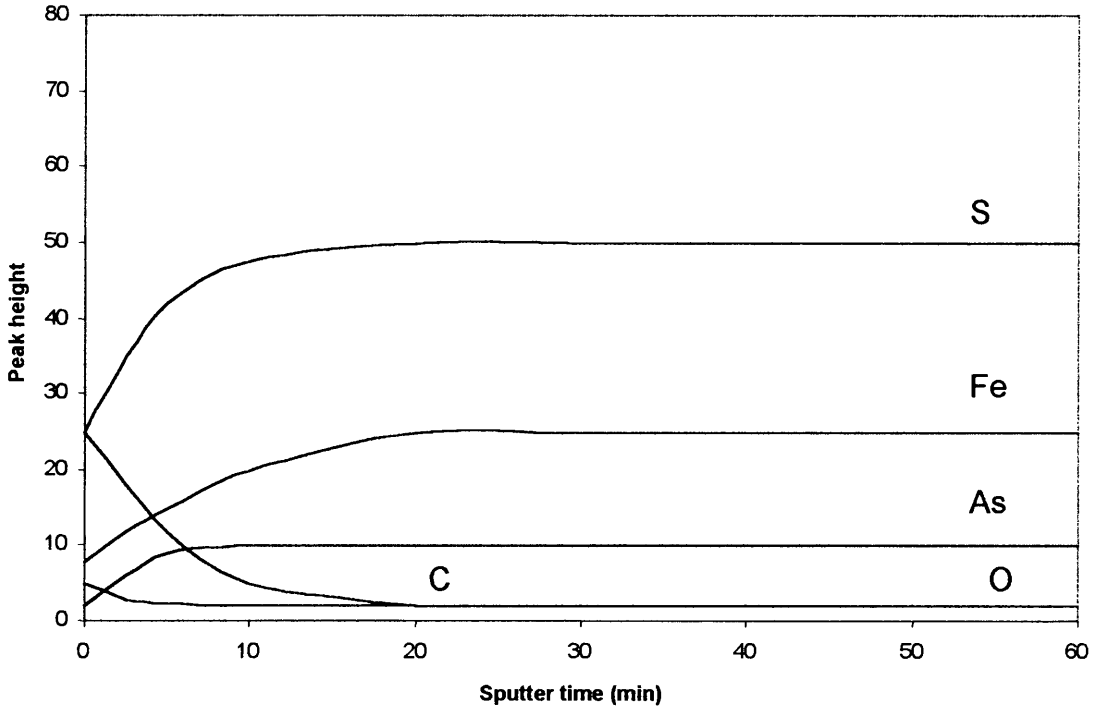

Figure 148. Depth profile produced by sputtering into unleached arsenopyrite. The depth corresponding to 60 minutes sputtering is around 1 µm.

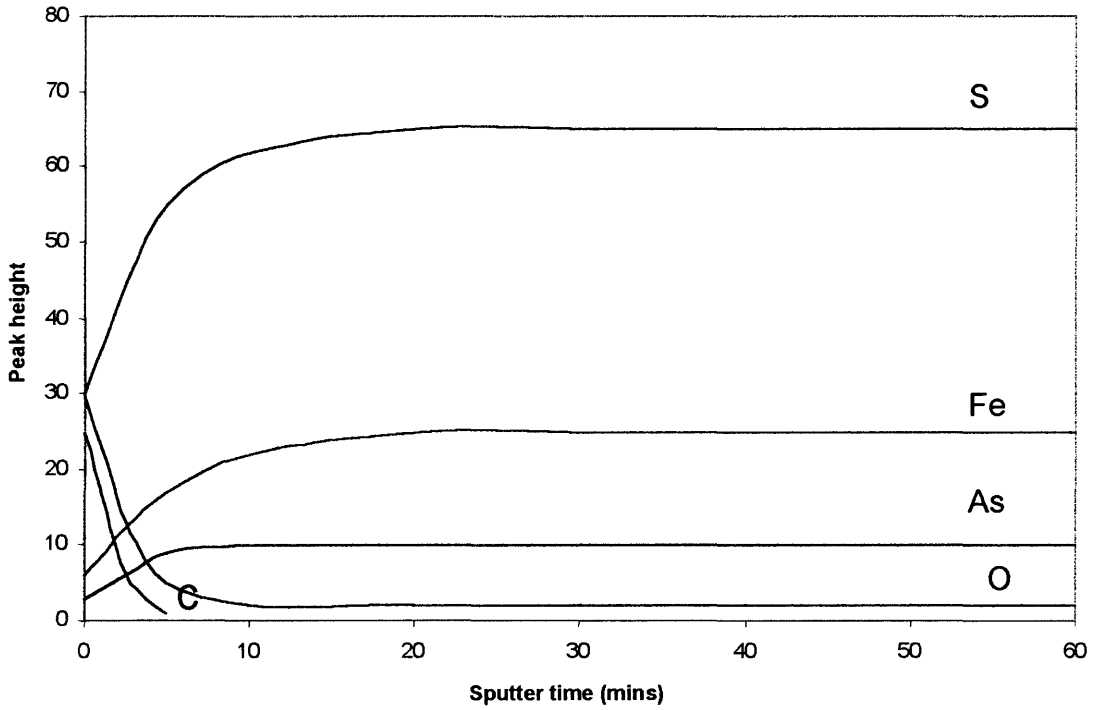

Figure 149. Depth profile produced by sputtering into arsenopyrite leached for three days in As-saturated ferric sulphate solution.

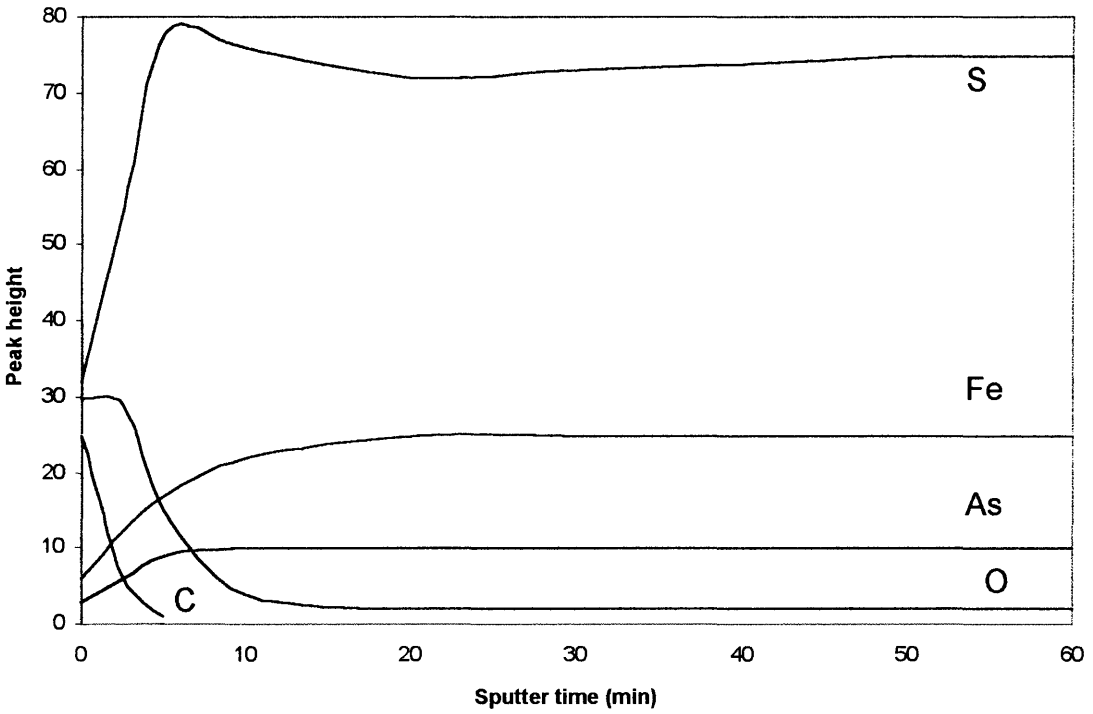

Figure 150. Depth profile produced by sputtering in to arsenopyrite leached in ferric sulphate solution for three days.

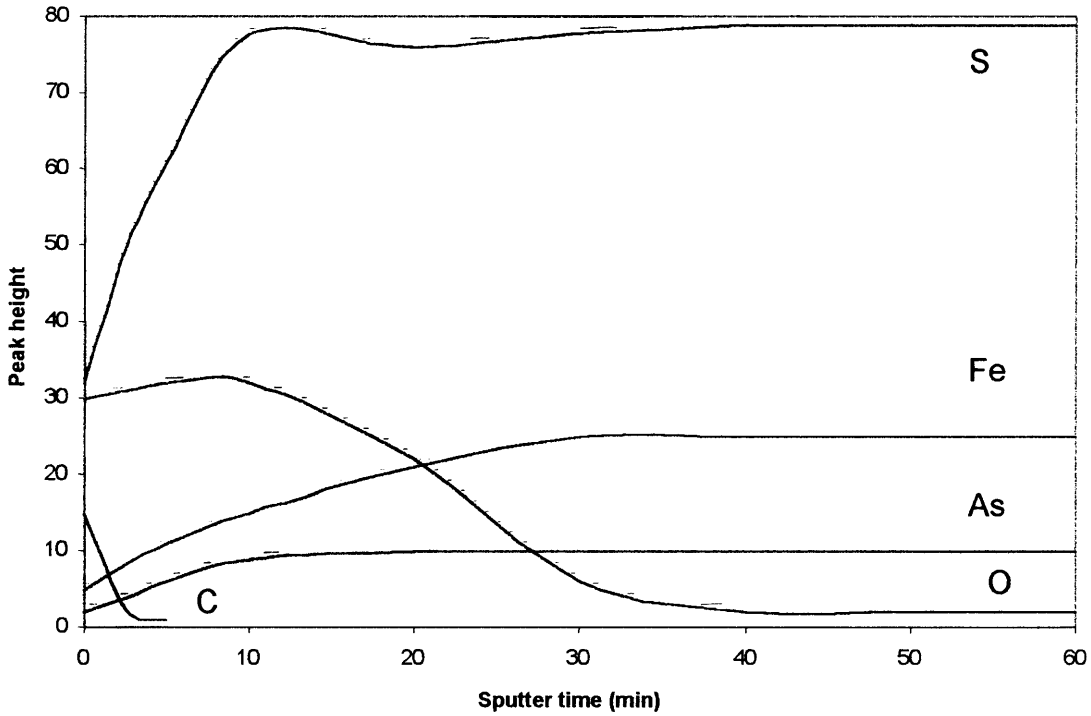

Figure 151. Depth profile produced by sputtering into arsenopyrite leached in ferric sulphate solution for one week.

Interesting information can be obtained from the AES results. The sulphur on the surface of the leached crystal, for instance, is not present as sulphate, but elemental sulphur. As leaching progresses, the layer of elemental sulphur increases in thickness, and the layer of oxygen extends further into the crystal. The sulphur layer does not appear to passivate the surface with regard to oxidation. It is also noteworthy that the unleached arsenopyrite crystal was not totally unoxidised – a thin oxide layer had formed on the surface from exposure to the atmosphere over time.

The extent of oxidation of the arsenopyrite crystals leached with 4 mass % dissolved As in the leach solution was found to be much lower. This was obvious by the golden colour of both crystals, as distinct from the plain ferric sulphate-leached crystals, which were blue (3 days) and grey (1week). The depth profiles also show a much shallower oxygen layer. This could be due to the presence of arsenic in solution, and also to the lower ORP. The cause of the low ORP is also likely to be the arsenic – this was added as As_2O_3 which puts As^{3+} into solution.

12.4 Discussion of leached arsenopyrite mineralogy

The following important factors have been established:

- As leaching progresses, iron and arsenic dissolve preferentially, a layer of elemental sulphur forms on the surface of the leaching arsenopyrite particle, and the depth of oxidation increases.
- The sulphur layer does not appear to passivate the leaching surface.
- The depth of oxidation and the sulphur layer affect arsenopyrite reflectance and colour in reflected light. The reflectance of arsenopyrite can be directly related to the colours perceived during leaching.
- The presence of arsenic in the ferric sulphate leach solution retards the arsenopyrite oxidation rate, either by inhibiting arsenic dissolution or by reducing the ORP, or both.
- Silver contamination of sulphide surfaces occurs during both bacterial and ferric sulphate leaching, possibly due to the use of Ag/AgCl electrodes. The presence of silver may catalyse the arsenopyrite oxidation rate.
- Although some jarosite was detected on bacterially-leached arsenopyrite surfaces, no scorodite or iron sulpharsenate precipitates were detected.

13. POWDER LEACHING AND ARSENIC SPECIES IN SOLUTION

In order to investigate the truth of the claim that Zandrivier arsenopyrite, apart from leaching more slowly than Sheba arsenopyrite, also gives rise to a higher As^{3+}/As^{5+} in solution, two leach tests were carried out on loose powders.

13.1 Ferric sulphate powder leach tests 11 and 12

Six grams each of Sheba and Zandrivier HF residue milled to 38 – 150 µm were leached in the reactor for one week, during which liquor samples were taken regularly and sent for chemical analysis (see Section 5.2, Table 10 – Analysis Schedule). The variation of pH and ORP during the leaches is shown in Tables 42 and 43 below.

TABLE 42

pH AND OXYGEN REDUCTION POTENTIAL (ORP) VARIATION DURING FERRIC SULPHATE LEACH 11 (ZANDRIVIER POWDER LEACH)
(10 g/l ferric iron concentration, temperature 35±1 °C)

Time	pH	ORP (mV)	Liquor sample removed (ml)*
0	0.53	720	–
1 hour	0.5	630	30
3 hours	0.49	620	30
8 hours	0.53	610	60
20 hours	0.52	605	30
1 day	0.51	600	60
2 days	0.47	590	30
3 days	0.55	580	60
4 days	n.d.	n.d.	–
5 days	0.45	570	30
1 week	0.48	555	60

*Liquor samples taken for chemical analysis, and the replacement liquor added.
n.d. = not determined.

TABLE 43

pH AND OXYGEN REDUCTION POTENTIAL (ORP) VARIATION DURING FERRIC SULPHATE LEACH 12 (SHEBA POWDER LEACH)
(10 g/l ferric iron concentration, temperature 35±1 °C)

TIME	pH	ORP (mV)	Liquor removed then added (ml)*
0	0.51	700	–
1 hour	0.50	640	30
3 hours	0.49	630	30
8 hours	0.43	615	30
1 day	0.49	600	60
2 days	0.52	590	30
3 days	0.48	580	60
5 days	0.57	565	30
1 week	0.48	550	60

*Liquor samples taken for chemical analysis, and the replacement liquor added.

After leaching, the leach solids were filtered out, dried and weighed. The loss of solids (dissolved material) of the Zandrivier sample was 0.9 g (15%), and that of the Sheba sample was 1.2 g (20%). Microscopic and electron microprobe examination of polished sections of the leach residues showed that these were almost exclusively arsenopyrite, with trace amounts of pyrite, silicate and rutile inclusions. No jarosite or arsenate precipitate was present.

The results of chemical and semi-quantitative XRF analysis of the two powders before and after the leach are shown in Tables 44 and 45. Unfortunately the small amount of sample

available dictated the analysis of arsenic by AA. This method is not as accurate as titration, the error being in the order of ± 2 mass % *absolute.*

As far as the trace elements go, the slight increase in silica content is to be expected after preferential dissolution of 15–20 mass % of arsenopyrite. In the case of the Sheba sulphide concentrate, lower nickel and antimony content is probably due to the preferential dissolution of gersdorffite.

TABLE 44

CHEMICAL ANALYSIS OF ZANDRIVIER AND SHEBA POWDER SAMPLES BEFORE AND AFTER FERRIC SULPHATE LEACHING (in mass %)

	Zandrivier arsenopyrite	Zandrivier arsenopyrite after leaching	Sheba arsenopyrite	Sheba arsenopyrite after leaching
As	36.5	31.2	36.4	38.5
Fe	35.1	34.0	35.4	35.3
S	21.0	21.8	22.5	22.5

TABLE 45

SEMI-QUANTITATIVE XRF ANALYSIS OF TRACE ELEMENTS IN ZANDRIVIER AND SHEBA POWDER SAMPLES BEFORE AND AFTER FERRIC SULPHATE LEACHING (in mass %)

	Zandrivier arsenopyrite	Zandrivier arsenopyrite after leaching	Sheba arsenopyrite	Sheba arsenopyrite after leaching
NiO	0.02	0.02	0.20	0.07
TiO_2	0.04	0.02	0.20	0.20
SiO_2	0.10	0.50	0.10	0.30
CaO	0.06	0.02	0.05	0.02
Al_2O_3	0.00	0.20	0.00	0.20

13.2 Results of liquor analysis

The results of leach liquor chemical analysis are presented in Tables 46 and 47 below, and the amount of total arsenic (As_T) in solution, corrected for liquor removal, is shown in Table 48 and plotted in Figure 152. The error in arsenic analysis in solution at these levels is quoted as being 10 % (relative).

TABLE 46

RESULTS OF LEACH LIQUOR CHEMICAL ANALYSIS DURING FERRIC SULPHATE LEACH 11 (ZANDRIVIER POWDER LEACH)

Time	As_T (ppm)	As^{3+} (ppm)	Fe_T (g/l)	Fe^{2+} (g/l)	SO_4^{2-} (g/l)
0	<5*	n.d.#	10.5	<0.1*	67.1
1 hour	6.8	n.d.	11.8	n.d.	67.5
3 hours	8.2	n.d.	10.0	n.d.	67.5
8 hours	8.4	<10*	10.9	<0.1	69.2
20 hours	12.1	n.d.	11.5	n.d.	67.2
1 day	12.6	<10	12.8	<0.1	66.9
2 days	16.4	n.d.	11.9	n.d.	76.3
3 days	22.6	24	11.1	0.2	59.2
5 days	35.0	n.d.	12.3	n.d.	74.5
1 week	43.7	35	11.4	0.4	61.6

*Below detection limit.
n.d. = not determined

TABLE 47

RESULTS OF LEACH LIQUOR ANALYSIS DURING FERRIC SULPHATE LEACH 12 (SHEBA POWDER LEACH)

Time	As_T (ppm)	As^{3+} (ppm)	Fe_T (g/l)	Fe^{2+} (g/l)	SO_4^{2-} (g/l)
0	<5*	n.d.#	10.7	<0.1*	72.2
1 hour	<5	n.d.	8.1	n.d.	50.0
3 hours	<5	n.d.	8.3	n.d.	50.0
8 hours	6.7	n.d.	8.1	n.d.	50.0
1 day	10.1	<10*	11.5	<0.1	49.4
2 days	14.6	n.d.	7.2	n.d.	49.4
3 days	21.7	<10	10.6	0.2	49.7
5 days	40.0	n.d.	6.7	n.d.	50.0
1 week	50.5	34	7.0	0.4	48.6

*Below detection limit.
#n.d. = not determined.

TABLE 48

TOTAL ARSENIC IN SOLUTION CORRECTED FOR LIQUOR REMOVAL DURING FERRIC SULPHATE LEACHES 11 AND 12

Time	Zandrivier leach Corrected As_T (ppm)	Sheba leach Corrected As_T (ppm)
0	<5	<5
1 hour	6.8	<5
3 hours	8.2	<5
8 hours	8.5	6.7
20 hours	12.3	n.d.*
1 day	12.9	10.1
2 days	16.9	14.7
3 days	23.2	21.9
5 days	35.9	40.7
1 week	44.9	51.5

*n.d. = not determined

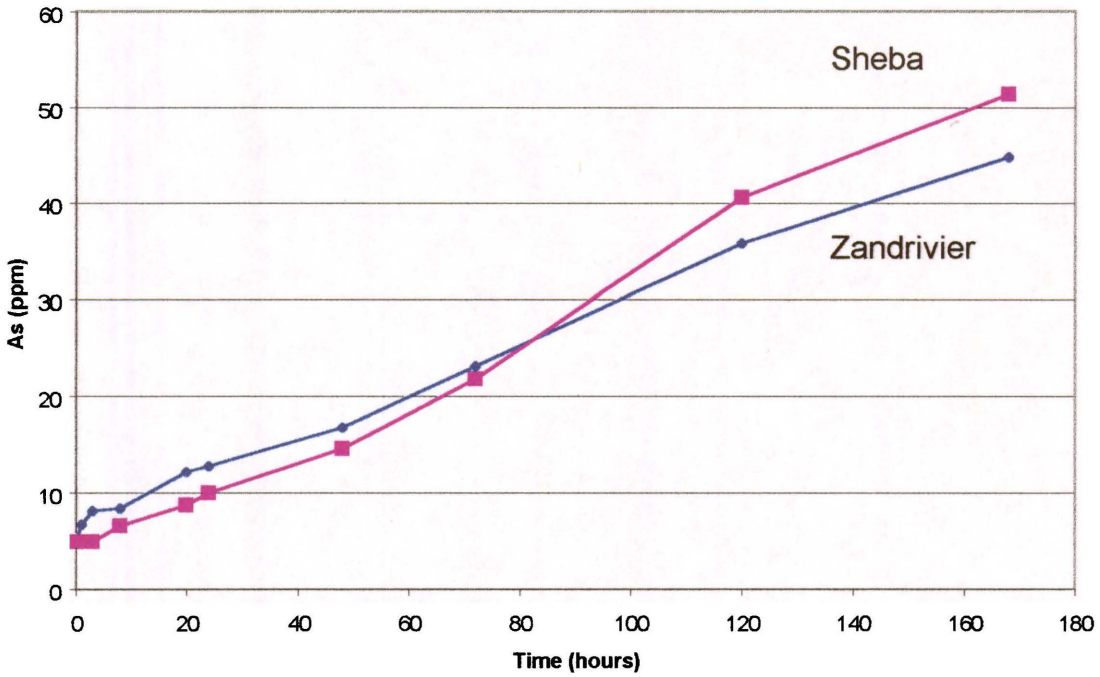

Figure 152. Corrected total arsenic in solution for the ferric sulphate leach tests on powdered Sheba and Zandrivier arsenopyrite.

13.3 Discussion of liquor analysis results

Although the higher As_T in solution value for the Sheba arsenopyrite ties in with the greater solids loss, there is a problem with the mass balance. If the dissolved arsenic is calculated from the chemical arsenic analysis of the feed and residue samples, the amount of As_T in solution should average 66 ppm (but with a range of 24–110 ppm due to the error) for Sheba, and 120 ppm (with a range of 76–164 ppm) for Zandrivier. It would seem that the amount of As_T measured in solution is probably low.

According to the literature similar problems have been encountered by other workers (BREED *et al.*, 1997) who claimed that arsenic was being removed from solution by the precipitation of ferric arsenate. However, these workers did not have pH control, and no ferric arsenate precipitate was found in the solid residue of this study. Another possibility is that some precipitate formed while the liquor samples were waiting for chemical analysis and was not redissolved before readings were taken. Examination of the total iron (Fe_T) results, especially for the Sheba samples, shows a direct relationship between the low iron values and the time which elapsed before liquor analysis. Some of the liquor samples were not analysed for over

three weeks after being taken from the reactor – a factor which was, unfortunately, beyond the control of the author.

The sulphate analysis results are relatively consistent. This, and the low pH, argues against a jarosite precipitate having formed. The most likely species to have precipitated is $Fe(OH)_3$, which probably changed to goethite over time. In the presence of sulphate, goethite can precipitate out at pH as low as 0.7–8 during ageing at 25° C (McANDREW *et al.*, 1975). The effect that such precipitation would have upon the arsenic in solution is not known, but it seems reasonable to assume that some arsenic may have been removed and incorporated into goethite *via* ferric hydroxide. Ferric hydroxide is used to capture arsenate ions by coprecipitation for environmental control (ROBINS & HUANG, 1987).

The relative proportions of As^{3+} to As^{5+} as measured in solution are also problematical, and it may be that the total arsenic concentrations in solution are too small to measure accurately, although the claimed detection limit is 10 ppm. The problem could also be related to that of ageing and ferric hydroxide precipitation as discussed above, as the adsorption of As^{5+} compared to As^{3+} is much higher at low pH (PIERCE & MOORE, 1982, SULLIVAN & ALLER, 1996).

Although the analytical results of the final samples taken in the powder leach tests suggest that there is little difference between the As^{3+}/As^{5+} ratio in solution between Zandrivier and Sheba samples, therefore, more work should be focused on arsenic speciation in solution.

In retrospect, it may have been preferable to leach the two powder samples for longer. Reruns were not feasible due to time constraints and lack of sample material. It is interesting to note that the results plotted in Figure 151 mirror the point counting results from leach 6, in that the Sheba leach rate is similar to, or lags behind, the Zandrivier leach rate initially, then overtakes it between two and four days in the leach.

14. DISCUSSION

The variables which can affect the rate and mechanism of sulphide leaching are shown in Table 49. These are adapted from a table on the uncertainty in the collection and interpretation of leaching data, and do not include the presence of bacteria in the leach, as this would introduce far more uncertainty than that already present under sterile leach conditions (PROSSER, 1995).

In this study, attempts were made to hold some of the variables as constant as possible, so that the effect of only one variable at a time could be studied. Alteration of the leach conditions can affect sulphide oxidation considerably. Conditions increasing the leach rate were found to be high temperature, high ORP, small particle size, the presence of bacteria, and, to a lesser degree, low pH and high ferric iron concentration (to a maximum of 40 g/l). As mentioned previously, the action of light is also reported to increase the oxidation rate, as is the presence of catalytic ions in solution, which will be discussed in more detail later.

There are still many variables over which no control is possible: compositional zonation, foreign mineral inclusions, crystal defects and impurity ions are impossible to avoid in naturally-occurring arsenopyrite and pyrite, and these all have an affect on the leach rate. They are the major factors in determining the leach rate variation between different arsenopyrite types under both sterile and bacterial leach conditions.

The order in which the sulphide minerals were oxidised in this study did not differ between bacterial and sterile oxidation conditions. The leach rate of free sulphides in order of decreasing susceptibility was recorded as – pyrrhotite, galena, sphalerite, gersdorffite, arsenopyrite, pyrite, chalcopyrite, and tennantite-tetrahedrite. Considering that there was only a small difference in rate between the first four members of the series and that the rate will also depend on particle size, this data is in reasonable agreement with the literature. The only exception is the behaviour of chalcopyrite. In fact authors differ as to the oxidation rates of the sulphide minerals, some taking this according to the electrode potential (NESTEROVICH, 1988) and others to the rest potential (MEHTA & MURR, 1983, HOLMES & CRUNDWELL, 1995), which, as quoted, produce different values for the sulphide minerals. The reason for this is that measured rest potentials vary depending on the type and pH of the solution, and

TABLE 49

VARIABLES AFFECTING LEACH RATE
(adapted from PROSSER, 1995)

Variables in italics were held as constant as possible during the leach tests.

System variables	Solution variables	Solid state variables	Variable phenomena
Temperature *Stirring speed* *Solids content (pulp density)*	*Reagent concentration* *pH* *ORP* Catalytic ion concentration	Crystal species and morphology Phase composition *Grain size* Internal cracks and pores Lattice defects	*Photo-irradiation* Galvanic effects *Surface tarnish before leach* Presence of inclusions Solid species catalysis (impurity ions) Competing reagent reactions Product reactions Surface passivation

mineral impurities (ATTIA & EL-ZEKY, 1990). The slower relative oxidation rate of chalcopyrite is due to the fact that it passivates at lower temperatures, such as those used in this study.

Examples of galvanic couples which form between sulphide minerals in contact were also observed during this investigation. This effect was less obvious during ferric sulphate leaching than during bacterial leaching, an effect that has been observed by other workers as well (ATTIA & EL-ZEKY, 1990). The most common galvanic couple was pyrite/arsenopyrite in all arsenopyrite types.

Compositional analysis of the four arsenopyrite types used in this investigation showed that they are all sulphur-rich, in common with most naturally-occurring arsenopyrite. The arsenopyrite types differ from each other in the extent of compositional zonation and the trace element content. The composition of pyrite, which is present in the four type samples, but in much smaller amounts than arsenopyrite, reflects the arsenopyrite composition in the extent of compositional zonation and trace element content.

The major factors influencing oxidative attack of the sulphide minerals were found to be the extent and strength of compositional zonation, trace element content, the presence of crystal defects and cracks, and crystal orientation of the arsenopyrite particles.

The higher leach rates of strongly-zoned arsenopyrite crystals, such as those from Sheba Mine, are caused by an interaction between the zones within crystals, involving electron transfer. Areas of differing As/S within arsenopyrite particles act as galvanic couples in the presence of an electrolyte (MÖLLER *et al.*, 1997). The galvanic couple between zones in contact as expressed by Δ(As/S), as well as the size of such zones, was found to be very important in both bacterial and sterile ferric sulphate leaching in this study. This effect was, however, subordinate to crystal orientation effects under sterile leach conditions.

The presence of excess arsenic in sulphur atom sites produces strain, providing high-energy sites for oxidative attack. Arsenic is claimed 'to diffuse towards the crystal surface during oxidation' (NESBITT *et al.*, 1995, NESBITT & MUIR, 1997) and to oxidise preferentially, promoting electron transfer to the less reactive S-rich zone of the crystal. No evidence for the diffusion of arsenic, however, was seen on the AES depth profiles.

Unzoned or weakly-zoned arsenopyrite leaches slowly, regardless of whether it is As-rich (p-type) or S-rich (n-type). As-rich New Consort arsenopyrite oxidised relatively slowly when compared to Sheba arsenopyrite during bacterial oxidation (CLAASSEN, 1991), and weakly-zoned areas of S-rich Klipwal and Zandrivier arsenopyrite particles also leached more slowly than Sheba arsenopyrite in the test work described here. Klipwal arsenopyrite crystals are weakly zoned. Where present, usually towards the edge of the crystal, zones alternate on a fine scale. Zandrivier arsenopyrite is weakly zoned – commonly unzoned. Where zonation is marked, it is on a relatively coarse scale. Both these arsenopyrite types display a relatively slow oxidation rate during sterile ferric sulphate and bacterial leaching.

Sheba arsenopyrite, by contrast, displays a faster oxidation rate, after an initial lag phase. The arsenopyrite is strongly zoned on a fine scale, many zones being only 1 to 5 µm apart, and this promotes oxidation, which is further accelerated by trace element impurities (see below). The West African crystals usually consist of two generations of arsenopyrite, both weakly zoned, the later generation being more arsenic-rich than the main phase arsenopyrite. Differences in Δ(As/S), however, are not always adequate to explain the differing leach rates between the zones which are strongly influenced by cobalt substitution.

As far as the trace element content of the four arsenopyrite types is concerned, submicroscopic gold was not detected in Klipwal arsenopyrite, but nickel, cobalt and antimony are found in some of the crystals. Trace elements are rare in Zandrivier arsenopyrite – gold was not detected in submicroscopic form, but cobalt and nickel were found in some particles. Sheba arsenopyrite has a relatively high trace element content of gold, antimony, cobalt and nickel. The main phase West African arsenopyrite has a moderate trace element content, whereas the later-formed rims have a high trace element content, especially of cobalt, which is often present in amounts of over 1 mass %.

The relatively high trace element content of Sheba arsenopyrite contributes to its faster leach rate, both by the formation of galvanic ion couples and by the production of strain in the crystal lattice, especially in the case of gold for iron atomic substitution. An obvious example of a trace element accelerating the oxidation process was seen in West African arsenopyrite, where cobalt substitution for iron produced higher leach rates during both ferric sulphate and bacterial oxidation. Initially this effect is hard to understand, since Co^{2+} is so similar to Fe^{2+} in

charge and ionic radius. The ionic radius of Fe^{2+} is 0.74 Å, and that of Co^{2+} is 0.72 Å (ionic radii in octahedral co-ordination from KRAUSKOPF, 1967). Most iron in arsenopyrite, however, is now thought to be present as Fe^{3+} (SHUEY, 1975, FERNANDEZ *et al.*, 1996) and this has a smaller ionic radius (0.64 Å). Although cobalt is known to be present as Co^{3+} in garnets and in skutterudite (COTTON & WILKINSON, 1972, VAUGHAN & CRAIG, 1979) it is almost certainly present in arsenopyrite as Co^{2+}, as it is in cobaltite.

The catalytic effect of cobalt in the arsenopyrite lattice is most likely to be due to its $3d^7$ electron configuration, as distinct from the iron it replaces which has a $3d^5$ configuration. This means that cobalt is an electron donor in the arsenopyrite structure, increasing conductivity and electron transfer during leaching (SHUEY, 1975, VAUGHAN & CRAIG, 1979). Cobalt ions have been shown to catalyse the oxidation of chalcopyrite and sphalerite. This has an immediate effect under sterile leach conditions, but shows a lag phase during bacterial oxidation (BALLESTER *et al.*, 1990, 1992).

The structure of the arsenopyrite crystal also has an influence on the leach rate in sterile ferric sulphate and bacterial oxidation. During sterile leaching, the orientation of the crystal in the section supercedes galvanic effects in determining the rate of dissolution. Attack is always retarded along [001] – in other words basal sections leach slowly*. This is obvious in all four arsenopyrite types, but especially marked in Sheba crystals. Occasionally a section with basal geometry is seen to be well leached, but this has probably been sectioned along [101] which would produce identical internal angles, but which would leach more quickly. Observation of mimetic twin leach behaviour suggests that there are also differing leach rates along the [100] and [010] axial direction as compared to along [111] and other non-axial directions. The reason for differential oxidative attack upon certain crystal orientations is probably due to the situation of the atomic bonding within the arsenopyrite crystal. During this study no direct evidence of any crystal orientation effect was noticed under bacterial leaching conditions, except in the location of leach channels (see below). Since inorganic ferric sulphate oxidation is known to play a major part in bacterial oxidation of arsenopyrite, it would seem that the effect must be present. Perhaps it is masked by the stronger galvanic effects, or by the non-selective attachment of the bacteria to the crystal faces of arsenopyrite.

* The symmetry of the arsenopyrite is assumed to be monoclinic, but pseudo-orthorhombic through twinning, as found in the space groups $B12_1/d1$ and $C112_1/d$ (FUESS *et al.*, 1987).

The primary sites for oxidative attack of all arsenopyrite types was found to be along pre-existing cracks, and also along scratches produced during the polishing process. Channels formed along these features during sterile and bacterial leach tests. Other sites for pit, pore and channel formation were grain boundaries, and at compositional zone boundaries. This was also observed in pyrite crystals.

The channels which formed were between 1 and 5 μm in diameter, and up to 100 μm in length. Apart from channels along cracks, scratches and zone boundaries, channels also developed parallel to, and sometimes perpendicular to, crystal faces in Sheba, Klipwal and West African arsenopyrite particles. In some West African crystals, and most of the Zandrivier massive arsenopyrite, curious branching and bending of channels occurred, usually superimposed upon 'swarms' of channels displaying a general lineation. This was most obvious under ferric sulphate leach conditions. When arsenopyrite cools during crystal formation, space group symmetry reduction is experienced from a body-centred to a primitive cell. These reductions give rise to microscopic twin domains, and with further reduction to antiphase domains. These types of crystal defect may be seen on the Transmission Electron Microscope (FUESS *et al.*, 1987). Leach etching revealed the presence of micro-twinning in Zandrivier arsenopyrite, and the leach channel deflections have been described as being reminiscent of antiphase domain boundary control (DE VILLIERS, *pers. com.*, 1998). The channel formation patterns, however, are rather large to correspond to antiphase domains, and may merely be a reflection of the symmetry of underlying crystal planes (NELL, *pers. com.*, 1998).

The pitting and channeling seen in arsenopyrite during this investigation provides no evidence that these structures were caused by bacterial action. They could be entirely due to inorganic oxidation. The widening of the channels in bacterially-leached arsenopyrite, however, could indicate that channels which form inorganically are later exploited by bacteria. Pits and pores in pyrite commonly do not coalesce to form channels – this may merely be a sign that oxidation is not as advanced as it is in arsenopyrite.

The most common leach products that form during bacterial leaching of arsenopyrite are hydronium jarosite, elemental sulphur, ferric arsenates and sulpharsenates, and ferric hydroxides or goethite. These substances can cause a problem if they form a passivating layer over the reacting sulphide surface. As mentioned in Section 2, previous bacterial leaching of

Zandrivier arsenopyrite concentrates produced a thick, passivating layer of zykaite (iron sulpharsenate). This was almost certainly due to high arsenic in solution, high solids content, and poor pH control. No evidence of zykaite formation was seen in the Zandrivier samples examined in this study, although the arsenopyrite certainly leaches more slowly than that in most refractory arsenopyrite concentrates during bacterial oxidation.

Electron microprobe and Auger Electron Spectroscopy examination of leached arsenopyrite surfaces from sterile ferric sulphate and bacterial leach tests in this investigation showed that a small amount of jarosite forms when the pH of the leach liquor is over 0.8. Jarosite should not form at such a low pH, but possibly pH is locally higher, especially when influenced on a micro-scale by bacteria. The most common leach product in all leach tests was found to be elemental sulphur. In theory, an elemental sulphur layer should not build up during bacterial leaching, because the bacteria present should oxidise it to sulphate in solution. Similarly, the sulphur layer formed during sterile leaching should not be removed, as no sulphur oxidising agents are present. In practice, similar sulphur layer behaviour was observed under both leach conditions. The sulphur-oxidising bacteria removed the sulphur layer only after it attained a certain thickness, and elemental sulphur was removed from sterile sulphide surfaces, possibly by mechanical action, after the sulphur layer became too thick.

The reflectance, and colour, of leached arsenopyrite is proportional to the depth of oxidation (RICHARDSON & VAUGHAN, 1989). The set of first order interference colours produced on the surface of arsenopyrite by permanganate in sulphuric acid, however, is thought to be due to interference from a thin sulphur layer on the surface (FLEET *et al.*, 1993). The leach colours observed in arsenopyrite, pyrite and pyrrhotite in this study are also very reminiscent of the first and second order optical interference colours produced by a thin film effect. This is not to say that reflectance, or colour, is not proportional to oxidation depth, since oxidation depth is itself proportional to elemental sulphur layer thickness, at least during the initial stages of oxidation (as proved in this study by use of electron microprobe and AES techniques). Interference colours for white light at normal incidence are given by:

$$m\lambda = 2ndcos\phi$$

where m is order, λ is wavelength of light (colour), d is film thickness, and ϕ is the angle of incidence. The colour developed is related to the thickness of surface film, and first order colours would require a film thickness of only around 0.2 μm (FLEET *et al.*, 1993).

Although some authors have described the formation of an As_2S_2 product which appears over leaching arsenopyrite after preferential iron removal (LAZARO *et al.*, 1997), most favour the non-stoichiometric model of arsenopyrite dissolution where both arsenic and iron are preferentially removed, leaving a layer of sulphur enrichment (SASAKI *et al.*, 1995, NESBITT *et al.*, 1995). The latter situation was observed in this study, both on ferric sulphate and bacterially-leached arsenopyrite surfaces. AES studies have recently suggested that the layer of highest observed sulphur content lies about 5Å *beneath* a sulphur-depleted oxidation layer (NESBITT *et al.*, 1995).

The nature of elemental sulphur layers which form over leaching sulphide minerals is variable, and the layer may be porous and crystalline or non-porous and amorphous. The latter type of layer would passivate the surface of the leaching arsenopyrite, and could bring oxidation to a halt. The exact form of the sulphur layers produced in this study is not known, but passivation does not seem to have occurred to any extent, so it seems reasonable to assume that the layers were relatively porous. Whether this was due to the small amount of silver contamination found to be present over some sulphide surfaces is also not known. The action of silver on the leaching surface of chalcopyrite not only catalyses leach rate through Ag_2S electron transfer, but by producing a more porous, crystalline, sulphur layer (MILLER & PORTILLO, 1979).

The surface speciation of As, Fe and S during arsenopyrite oxidation is a complex subject. Different species are known to exist in near-surface, surface and solution, and to change in type within nanometres. Arsenic migrates to the arsenopyrite surface and, through various intermediates, achieves both +3 and +5 oxidation states on the surface, which are released into solution as arsenites (AsO_3^{3-}) and arsenates (AsO_4^{3-}) (NESBITT *et al.*, 1995). The relative amount of As^{3+} to As^{5+} released to solution is important, because As^{3+} is reported to be in the order of sixty times as toxic to life as As^{5+} (FERGUSON & GARVIS, 1972). In practice, this ratio will depend on the amount of arsenic in the solids and solution, and on the ORP of the solution. Previous claims that the As^{3+}/As^{5+} ratio produced by the bacterial leaching of Zandrivier arsenopyrite was unusually high cannot be substantiated by this study. The results

of sterile ferric sulphate leach tests on Zandrivier and Sheba arsenopyrite powders suggest that there is no significant difference in the As^{3+}/As^{5+} ratio produced in solution between the two arsenopyrite types, although the effect of the bacterial presence is not known. More research is required in this area, as will be outlined in Section 16 below. Since the ratio of As^{3+}/As^{5+} is raised by excess of arsenic in the leach solution, it is possible that the problem of high As^{3+} in Zandrivier leach liquors was brought about by high arsenic content in the feed and improper pH control.

It is clear from the results of this investigation that a thorough examination of the mineralogy of an arsenopyrite concentrate can provide information on its potential behaviour during bacterial leaching. There is also no reason that initial amenability test work on a laboratory scale should not commence with cheaper and more easily controlled sterile ferric sulphate leach test work as is currently the practice with copper concentrates.

15. CONCLUSIONS

The aim of this study was

- to compare the sterile ferric sulphate leach behaviour of four compositionally distinct arsenopyrite types,
- to establish the effect of sulphide composition on leach rate, and
- to evaluate whether the method gives a true reflection of oxidation behaviour in the presence of bacteria.

The results show that the oxidation rate of arsenopyrite does depend upon its composition, both of major and trace elements. It is not so much the overall major element composition of the arsenopyrite that is important, as the strength and size of local compositional zonation which sets up microscopic galvanic cells thereby increasing electron transfer and accelerating leach rates. Arsenopyrite with strong compositional zonation oxidises rapidly under both sterile ferric sulphate and bacterial leach conditions. The size of the zones is also important, with finely-spaced zones showing a higher leach rate.

The presence of trace elements in the arsenopyrite structure often increases the oxidation rate. In this study, Sheba arsenopyrite with high gold and antimony content, and the cobalt-rich zones of the West African arsenopyrite are the most rapidly-leaching phases of those which were examined. Since the most refractory arsenic-rich gold-bearing ores are those with gold chemically-bound within the arsenopyrite structure, the very presence of gold should accelerate gold recovery by bacterial leach methods. If a complete mineralogical examination, coupled, perhaps, with diagnostic leach tests, of Klipwal, Zandrivier and West African arsenopyrite types had been carried out, they would not normally have been considered refractory, and therefore would not have been bacterially-leached for gold.

The speciation of arsenic in solution has only been touched on in this work. More accurate sampling and analysis techniques are required to establish whether trivalent arsenic is more readily produced from Zandrivier arsenopyrite than Sheba arsenopyrite. Initial tests do suggest, however, that there should be little difference between the two types, provided that arsenic levels and solution pH are controlled.

Similarly, no evidence for the production of passivating and environmentally unstable iron sulpharsenate leach products from arsenopyrite was found in this investigation. Again, this seems to be a problem related to process control.

Finally, sterile ferric sulphate leach tests in the laboratory appear to be a viable alternative for initial bacterial amenability tests, and should also prove to be more cost-effective.

16. RECOMMENDATIONS

There are many areas requiring further research in the field of arsenopyrite bacterial leaching. Among those specific to this study, the most obvious research subject would be that of arsenic speciation, both on the surface of leaching arsenopyrite, and in leach solutions, under both sterile ferric sulphate and bacterial leach conditions.

More information of the variation of leach rate with crystal orientation would be valuable, even if only for academic interest. Oriented samples of Sheba arsenopyrite from this study

were sent overseas for Electron Backscatter Scanning Diffraction (EBSD) analysis eighteen months ago, but unfortunately no results have been received to date.

The quantification of the actual oxidation conditions, such as arsenic content of feed and leach liquor, which lead to the formation of problematic leach products, should also be a key area of research. This information would be extremely useful, as such leach products not only reduce gold recovery, but also pose a potential threat to the environment.

17. ACKNOWLEDGEMENTS

The following persons and institutions contributed to this project and are gratefully acknowledged:

Mintek, where the project was initiated and where most of the experimental research was carried out. Special mention should be made of my supervisor, Dr J.P.R. de Villiers, my chemical adviser, Dr D. Groot, and my bioleaching adviser, Mr J. Neale. A great deal of advice on microbeam techniques was received from Mr Viljoen and Dr Oosthuyzen, and on leaching pore patterns from Dr J. Nel. I am in debt to many staff members of the Mineralogy, Process Chemistry, Minerals Engineering and Analytical Services Divisions for assistance in one form or another.

I would also like to acknowledge the Anglo American Corporation of S.A. (now Anglogold) for their permission to work on Zandrivier arsenopyrite, and to describe this in my thesis. Similarly I acknowledge Sheba Mine, of the ETC Division of AVGOLD Ltd., and Klipwal Gold Mine in Kwa-Zulu Natal.

Professors D.J. Vaughan of Manchester University, and Professor F. Crundwell of the University of the Witwatersrand, supplied valuable advice and information on leaching sulphide behaviour.

Mr Paul den Hoed, a friend and colleague, provided a great deal of assistance with endless patience, particularly in the field of literature study and thesis construction.

Another friend and colleague, Dr R.P. Schouwstra, deserves thanks as he was the one who encouraged me to study, and to finish what I'd started!

I am grateful to the staff at the University of Pretoria Geology Department, particularly to my supervisor Professor RKW Merkle who was always available for advice and encouragement, and also to Professor J. Malherbe of the Physics Department where the AES work was carried out.

Thanks must also go to my parents, my late mother-in-law, my sister-in-law and brother-in law, all of whom put up with one month of thesis-typing in Natal.

And of course last, but *definitely* not least, I acknowledge my long-suffering husband and sons who have supported me throughout.

REFERENCES

AFENYA, P.M. (1991). Treatment of carbonaceous refractory gold ores. *Minerals Engineering* **4**:1043–1055.

AL, T.A., BLOWES, D.W., MARTIN, C.J., CABRI, L.J. & JAMBOR, J.L. (1997). Aqueous geochemistry and analysis of pyrite surfaces in sulfide-rich mine tailings. *Geochimica et Cosmochimica Acta* **61**:2353–2366.

ANDREWS, L. & NEALE, J.W. (1995). A mineralogical evaluation of arsenate products formed during the bacterial oxidation of gold ores. *In* Barton, J.M. and Copperthwaite, Y.E. (eds) *Extended abstracts of the Centennial Geocongress 1995*:907–910. Johannesburg:Geological Society of South Africa,

ANHAEUSSER, C.R. (1976). The nature and distribution of Archaean gold mineralization in Southern Africa. *Minerals Science Engineering* **8**:46–84.

ATTIA, Y.A. & EL-ZEKY, M. (1990). Effects of galvanic interactions of sulphides on extraction of precious metals from refractory complex sulfides by bioleaching. *International Journal of Mineral Processing*, **30**:99–111.

BALLESTER, A., GONZÁLEZ, F., BLÁZQUEZ, M.L., GÓMEZ, C. & MIER, J.L. (1992). The use of catalytic ions in bioleaching. *Hydrometallurgy* **29**:145–160.

BALLESTER, A., GONZÁLEZ, F., BLÁZQUEZ, M.L. & MIER, J.L. (1990). The influence of various ions in the bioleaching of metal sulphides. *Hydrometallurgy* **23**:221–235.

BANFIELD, J.F. & HAMERS, R.J. (1997). Processes at minerals and surfaces with relevance to microorganisms and prebiotic synthesis. *In* Banfield, J.F. and Nielson, K.H. (eds) *Reviews in Mineralogy, Vol.35: Geomicrobiology: interactions between microbes and minerals:* 81–122. Washington: Mineral. Soc. Am.

BARRETT, J., HUGHES, M.N. & RUSSELL, A. (1990). Oxidation of arsenopyrite by iron (III). In *Randol Gold Forum '90:*135–136. Golden, Colorado: Randol International.

BJÖRLING, G & KOLTA, G.A. (1965). Oxidizing leach of sulfide concentrates and other materials catalyzed by nitric acid. *In* Arbiter, N. (ed.) *VII International Mineral Processing Congress:*127–138. New York:Gordon & Breach.

BOON, M. & HEIJNEN, J.J. (1993). Mechanisms and rate limiting steps in bioleaching of sphalerite, chalcopyrite and pyrite with *T. ferrooxidans. In* Torma, A.E., Wey, J.E. & Lakshmanan, V.I. (eds) *Biohydrometallurgical technologies Vol.1:*217–235. Pennsylvania: Minerals, Metals and Materials Society.

BREED, A.W., GLATZ, A., HANSFORD, G.S. & HARRISON, S.T.L. (1996). The effect of As(III) and As(V) on the batch bioleaching of a pyrite-arsenopyrite concentrate. *Minerals Engineering* **9**: 1235–1252.

BREED, A.W., HARRISON, S.T.L. & HANSFORD, G.S. (1997). The bioleaching of a pyrite-arsenopyrite flotation concentrate in a continuous bioleaching mini-plant. Steady-state operation and behaviour during periods without aeration and agitation. In *Proceedings of the International Biohydrometallurgy Symposium, Sydney:* M8.3.1–M8.3.10. Glenside, Australia: Australian Mineral Foundation.

BREED, A.W., HARRISON, S.T.L. & HANSFORD, G.S. (1997). Technical note – a preliminary investigation of the ferric leaching of a pyrite/arsenopyrite flotation concentrate. *Minerals Engineering* **10**:1023–1030.

BRIERLEY, C.L. (1982). Microbiological mining. *Scientific American* **247**:42–52.

CABRI, L.J., CHRYSSOULIS, S.L., DE VILLIERS, J.P.R., LAFLAMME, J.H.G. & BUSECK, P.R. (1989). The nature of 'invisible' gold in arsenopyrite. *Canadian Mineralogist* **27**:353–362.

CABRI, L.J. (1994). Current status of determination of mineralogical balances for platinum-group element-bearing ores. *Transactions of the Institute pf Mining and Metallurgy B:* B3–9.

CAMERON, E.N. (1961). *Ore microscopy.* New York: John Wiley & Sons.

CATHELINEAU, M., BOIRON, M.C., HOLLIGER, P., MARION, P. & DENNIS, M. (1989). Gold in arsenopyrites: Crystal chemistry, location and state, physical and chemical conditions of deposition. *In* Keays, R.R., Ramsay, W.H.R. & Groves, D.I. (eds) *The geology of gold deposits: The perspective in 1988:* 328–341. Littleton, Colorado: The Economic Geology Publishing Company.

CLAASSEN, R. (1991). Microbiological oxidation of sulphide minerals from Agnes, New Consort and Sheba Gold Mines. M.Sc. Thesis. University of Pretoria, Pretoria.

CLAASSEN, R. , LOGAN, C.T. & SNYMAN, C.P. (1993). Bio-oxidation of refractory gold-bearing arsenopyritic ores. *In* Torma, A.E., Wey, J.E. & Lakshmanan, V.I. (eds) *Biohydrometallurgical technologies Vol.1:*479–488. Pennsylvania: Minerals, Metals and Materials Society.

CLARK, L.A. (1960). The Fe-As-S system: Phase relations and applications. *Economic Geology* **55**(I):1345–1381, (II):1631–1632.

COOK, N.J. & CHRYSSOULIS, S.L. (1990). Concentrations of 'invisible gold' in the common sulphides. *Canadian Mineralogist* **28**:1–16.

COTTON, F.A. & WILKINSON, G. (1968). *Advanced inorganic chemistry.* New York: Interscience.

CRUNDWELL, F.K. (1988). The influence of the electronic structure of solids on the anodic dissolution and leaching of semiconducting sulphide minerals. *Hydrometallurgy* **21**:155–190.

DANA, J.D. & DANA, E.S. (1944). *The system of mineralogy, Vol 1: Elements, sulfides, sulfosalts and oxides*. 7th edition. London: John Wiley.

DE, G.C., OLIVER, D.J. & PESIC, B.M. (1997). Effect of heavy metals on the ferrous iron oxidizing ability of *Thiobacillus ferrooxidans*. *Hydrometallurgy* **44**:53–63.

DUNN, J.G. & CHAMBERLAIN, A.C. (1997). The recovery of gold from refractory arsenopyrite concentrates by pyrolysis-oxidation. *Minerals Engineering* **10**:919–928.

ERLICH, H.L. (1964). Bacterial oxidation of arsenopyrite and enargite. *Economic Geology* **59**:1306–1312.

ESCOBAR, B., WIERTZ, J. & DE LOS ANGELES RUIZ, M. (1997). The effect of silver in the leaching and bioleaching of enargite. In *Proceedings of the International Biohydrometallurgy Symposium, Sydney:* PM18.1–PM18.2. Glenside, Australia: Australian Mineral Foundation.

ESCUDERO, M.E., GONZÁLEZ, F., BLÁZQUEZ, M.L., BALLESTER, A. & GÓMEZ, C. (1993). The catalytic effect of some cations on the biological leaching of a Spanish complex sulphide. *Hydrometallurgy* **34**:151–169.

FERGUSON, J.F. & GAVIS, J. (1972). A review of the arsenic cycle in natural waters. *Water Research* **6**:1259–1274.

FERNANDEZ, P.G., LINGE, H.G. & WADSLEY, M.W. (1996). Oxidation of arsenopyrite (FeAsS) in acid. Part 1: Reactivity of arsenopyrite. *Journal of Applied Electrochemistry* **26**:575–583.

FERNANDEZ, P.G., LINGE, H.G. & WILLING, M.J. (1996). Oxidation of arsenopyrite (FeAsS) in acid. Part 2: Stoichiometry and reaction scheme. *Journal of Applied Electrochemistry* **26**:585–591.

FLEET, M.E., CHRYSSOULIS, S.L., MACLEAN, P.J., DAVIDSON, R. & WEISENER, C.G. (1993). Arsenian pyrite from gold deposits : Au and As distribution investigated by SIMS and EMP, and color staining and surface oxidation by XPS and LIMS. *Canadian Mineralogist* **31**:1–17.

FLEET, M.E. & MUMIN, A.H. (1997). Gold-bearing arsenian pyrite and marcasite and arsenopyrite from Carlin Trend gold deposits and laboratory synthesis. *American Mineralogist* **82**:182–193.

FREE, M.L., OOLMAN, T., NAGPAL, S. & DAHLSTROM, D.A. (1993). A comparison of leaching by attached and non-attached bacteria of a pyrite/arsenopyrite gold-ore concentrate. *In* Torma, A.E., Wey, J.E. & Lakshmanan, V.I. (eds) *Biohydrometallurgical technologies Vol.1:*459–468. Pennsylvania: Minerals, Metals and Materials Society.

FRIEDL, J., WAGNER, F.E., ADAMS, M.D., SCHOUWSTRA, R.P., MARAIS, H.J. & DEW, D. (1994). The bio-oxidation of refractory arsenopyritic gold ore from Fairview Gold Mine - a Mössbauer study. *XVth CMMI Congress notes Vol.2*: 403–410. Johannesburg: S.A.I.M.M.

FROESE, E. (1976). Applications of thermodynamics in metamorphic petrology. *Paper of the Geological Survey of Canada 75–54,* 37pp.

FUESS, H., KRATZ, T., TOPEL-SCHADT, J., & MIEHE, G. (1987). Crystal structure refinement and electron microscopy of arsenopyrite. *Zeitschrift für Kristallographie* **179**:335–346.

GAMMON, J.B. (1966). Some observations on minerals in the system CoAsS - FeAsS. *Norsk Geologisk Tidsskrift* **46**:405–426.

GEESEY, G. (1997). Microscale heterogeneities at mineral surfaces that influence bioleaching. In *Proceedings of the International Biohydrometallurgy Symposium, Sydney:* PSB1.1–PSB1.6. Glenside, Australia: Australian Mineral Foundation.

GENKIN, A.D., BORTNIKOV, N.S., CABRI, L.J., WAGNER, F.E., STANLEY, C.J., SAFONOV, Y.G., McMAHON, G., FRIEDL, J., KERZIN, A.L. & GAMYANIN, G.N. (1998). A multidisciplinary study of invisible gold in arsenopyrite from four mesothermal gold deposits in Siberia, Russian Federation. *Economic Geology* **93**:463–487.

GODDARD, E.N., TRASK, P.D., DeFORD, R.K., ROVE, O.N., SINGEWALD, J.T. & OVERBECK, R.M. (1963). Rock color chart. New York: the Geological Society of America.

GOLDSTEIN, J.I., NEWBURY, D.E., ECHLIN, P., JOY, D.C., FIORI, C. & LIFSHIN, E. (1981). *Scanning electron microscopy and X-ray microanalysis.* New York and London: Plenum Press.

GÓMEZ, C., ROMAN, E., BLÁZQUEZ, M.L. & BALLESTER, A. (1997). SEM and AES studies of chalcopyrite bioleaching in the presence of catalytic ions. *Minerals Engineering* **10**:825–835.

GÓMEZ, E., BLÁZQUEZ, M.L., BALLESTER, A & GONZÁLEZ, F. (1996). Study by SEM and EDS of chalcopyrite bioleaching using a new thermophilic bacteria. *Minerals Engineering* **9**:985–999.

HACKL, R.P. & JONES, L. (1997). Bacterial sulfur oxidation pathways and their effect on the cyanidation characteristics of biooxidized refractory gold concentrates. In *Proceedings of the International Biohydrometallurgy Symposium, Sydney:* M14.2.1–M14.2.10. Glenside, Australia: Australian Mineral Foundation.

HAMER, R.D. (1991). The structural controls and setting of gold mineralization in the Mount Mare area of the Pietersburg greenstone belt, South Africa. *In* Ladeira, E.A. (ed.) *Brazil Gold '91*: 661–664. Rotterdam: Balkema.

HAMMERBECK, E.C.I. (1976). Gold outside the Witwatersrand Triad. *In* Coetzee, C.B. (ed.) *Mineral Resources of the Republic of South Africa:* 75–92. Pretoria: S. Afr. Geol. Survey.

HENLEY, K.J. (1993). The mineralogy of refractory gold ores. The biological oxidation of arsenopyrite ore. In *Proceedings of the International Conference and Workshop Applications of Biotechnology to the Minerals Industry, Adelaide:* 5.1–5.13. Glenside, Australia: Australian Mineral Foundation.

HILTUNEN, P., VUORINEN, A. REHTIJARVI, P. & TUOVINEN, O.H. (1981). Bacterial pyrite oxidation: Release of iron and scanning electron microscopic observations. *Hydrometallurgy* **7**:147–157.

HOLMES, P.R. & CRUNDWELL, F.K. (1995). Kinetic aspects of galvanic interactions between minerals during dissolution. *Hydrometallurgy* **39**:353–375.

IGLESIAS, N. & CARRANZA, F. (1994). Refractory gold-bearing ores: A review of treatment methods and recent advances in biotechnological techniques. *Hydrometallurgy* **34**:383–395.

IXER, R.A., STANLEY,C.J. & VAUGHAN, D.J. (1979). Cobalt-, nickel- and iron-bearing sulpharsenides from the North of England. *Mineralogical Magazine* **43**:389–395.

JONES, M.P. (1987). *Applied mineralogy: A quantitative approach.* London: Graham & Trotman.

JOSHI, A. (1986). Auger Electron Spectroscopy. In *The Metals Handbook Vol.10: Materials characterisation:* 549–567. 9th edition. Ohio: Am. Soc. Metal.

KAISER, H. & SPECKER, H. (1956). Bewertung und vergleich von analysenverfahren. *Zeitschrift für Analytische Chemie* **149**:46–66.

KARAVAIKO, G.I., CHUCHALIN, L.K., PIVOVAROVA, T.A., YEMEL'YANOV, B.A., & DOROFEYEV, A.G. (1986). Microbiological leaching of metals from arsenopyrite containing concentrates. *In* Lawrence, R.W., Branion, R.M.R., & Ebner, H.G. (eds) *Fundamental and Applied Biohydrometallurgy Vol.4: Process Metallurgy*: 115–126. Amsterdam: Elsevier Science Publishing.

KELLER, L. & MURR, L.E. (1982). Acid-bacterial and ferric sulphate leaching of pyrite single crystals. *Biotechnology and Bioengineering* **24**:83–96.

KLEMM, D.D. (1965). Synthesen und Analsen in den Dreiecksdiagrammen FeAsS–CoAsS–NiAsS und FeS_2–CoS_2–NiS_2. *N. Jb. Miner. Abh.* **103**: 205–255.

KOH, Y.K., CHOI, S.G., SO, C.S., CHOI, S.H. AND UCHIDA, E. (1992). Application of arsenopyrite geothermometry and sphalerite geobarometry to the Taebaek Pb-Zn(-Ag) deposit at Yeonhwa I Mine, Republic of Korea. *Mineralium Deposita* **27**:58–65.

KOSLIDES, T. & CIMINELLI, V.S.T. (1992). Pressure oxidation of arsenopyrite and pyrite in alkaline solutions. *Hydrometallurgy* **30**:87–106.

KRAUSKOPF, K.B. (1967). *Introduction to geochemistry.* New York: McGraw-Hill.

KRETSCHMAR,U. & SCOTT, S.D. (1976). Phase relations involving arsenopyrite in the system Fe-As-S and their application. *Canadian Mineralogist* **14**:364–386.

KWONG, Y.T.J., LAWRENCE, J.R. & SWERHONE, G.D.W. (1995). Interplay of geochemical, electrochemical, and microbial controls in the oxidation of common sulfide minerals. *Proc. Int. Land Reclam. Mine Drainage Conf. and 3rd Int. Conf. Abatement Acidic Drainage* 2:419.

LAWSON, E.N. (1997). The composition of mixed populations of leaching bacteria active in gold and nickel recovery from sulphide ores. In *Proceedings of the International Biohydrometallurgy Symposium, Sydney:* QP4.1–QP4.10. Glenside, Australia: Australian Mineral Foundation.

LAZARO, I., CRUZ, R., RODRIGUEZ, J.M., GONZÁLEZ, I. & MONROY, M. (1997). An approach of electrochemistry and electrokinetics to study the mechanisms involved in the oxidation of arsenopyrite by *T. ferrooxidans.* In *Proceedings of the International Biohydrometallurgy Symposium, Sydney:* M2.2.1–M2.2.10. Glenside, Australia: Australian Mineral Foundation.

LAZARO, I., CRUZ, R., RODRIGUEZ, J.M., GONZÁLEZ, I. & MONROY, M. (1997). Electrochemical oxidation of arsenopyrite in acidic media. *International Journal of Minerals Processing* **50**:63–75.

LAZER, M.J., SOUTHWOOD, M.J. & SOUTHWOOD, A.J. (1986). The release of refractory gold from sulphide minerals during bacterial leaching. *GOLD 100: Proceedings of the International Conference on Gold Vol.2: Extractive metallurgy of gold.* Johannesburg: S.A.I.M.M.

LINGE, H.G. & WELHAM, N.J. (1997). Gold recovery from a refractory arsenopyrite (FeAsS) concentrate by in-situ slurry oxidation. *Minerals Engineering* **10**:557–566.

LITTLE, B.J., WAGNER, P.A., & LEWANDOWSKI, Z. (1997). Spatial relationships between bacteria and mineral surfaces. *In* Banfield, J.F. and Nielson, K.H. (eds) *Reviews in mineralogy, Vol.35: Geomicrobiology: Interactions between microbes and minerals:* 123–159. Washington: Mineral. Soc. Am.

LOWELL, G.R. & GASPARRINI, C. (1982). Composition of arsenopyrite from Topaz Greaisen Veins in Southeastern Missouri. *Mineralium Deposita* **17**:229–238.

MARION, P., MONROY, M., MUSTIN,C. & BERTHELIN, J. (1991). Effects of auriferous sulphide minerals structure and composition on their bacterial weathering. *In* Pagel and Leroy (eds) *Source, Transport and Deposition of Metals*: Rotterdam, 561–564.

McANDREW, R.T., WANG, S.S. & BROWN, W.R. (1975). Precipitation of iron compounds from sulphuric acid leach solutions. *Cim Bulletin* January 1975.

McKIBBEN, M.A. & BARNES, H.L. (1986). Oxidation of pyrite in low temperature acidic solutions : rate laws and surface textures. *Geochimica et Cosmochimica Acta* **50**:1509–1520.

MEHTA, A.P. & MURR, L.E. (1983). Fundamental studies of the contribution of galvanic interaction to acid-bacterial leaching of mixed metal sulfides. *Hydrometallurgy* **9**:235–256.

MILLER, J.D. & PORTLLO, H.Q. (1979). Silver catalysis in ferric sulphate leaching of chalcopyrite. *In* Laskowski, J. (ed.) *Developments in mineral processing, Vol.2A*: 851–897.

MONROY, M., MARION, P., BERTHELIN, J. & VIDEAU, G. (1993). Heap-bioleaching of simulated refractory sulfide gold ores by *T. ferrooxidans* : a laboratory approach on the influence of mineralogy. *In* Torma, A.E., Wey, J.E. & Lakshmanan, V.I. (eds) *Biohydrometallurgical technologies Vol.1:*489–498. Pennsylvania: Minerals, Metals and Materials Society.

MONROY FERNANDEZ, M.G., MUSTIN, C., DE DONATO, P, BARRES, O, MARION, P. & BERTHELIN, J. (1995). Occurrences at mineral-bacteria interface during oxidation of arsenopyrite by *Thiobacillus ferrooxidans. Biotechnology & Bioengineering* **46**:13–21.

MORIMOTO, N. & CLARK, L.A. (1961). Arsenopyrite crystal–chemical relations. *American Mineralogist* **46**:1448–1469.

MÖLLER, P., SASTRI, C.S., KLUCKNER, M., RHEDE, D. & ORTNER, H.M. (1997). Evidence for electrochemical deposition of gold onto arsenopyrite. *European Journal of Mineralogy* **9**:1217–1226.

NEALE, J.W., PINCHES, A., KRUGER, P.P. & VAN STADEN, P.J. (1996). Copper bioleaching. Paper presented at ALTA 1996 Copper Hydrometallurgy Forum, Brisbane, Australia. ALTA Metallurgical Services, Melbourne.

NESBIT, H.W. & MUIR, I.J. (1998). Oxidation states and speciation of secondary products on pyrite and arsenopyrite reacted with mine waste waters and air. *Mineralogy and Petrology* **62**:123–144.

NESBIT, H.W., MUIR, I.J. & PRATT, A.R. (1995). Oxidation of arsenopyrite by air and air-saturated distilled water, and implications for mechanism of oxidation. *Geochimica et Cosmochimica Acta* **59**:1773–1786

NESTEROVICH, L.G. (1988). *In* Karavaiko, G.I., Rossi, G., Agate, A.D., Groudev, S.N. & Avakyan, Z.A. (eds) *Biogeotechnology of metals:* 101–112. Moscow: United Nations Environment Programme, USSR Commission.

NEUERBURG, G.J. (1975). A procedure, using hydrofluoric acid, for quantitative mineral separations from silicate rocks. *Journal of Research U.S. Geological Survey* **3**:377–378.

NORDSTROM, D.K. & SOUTHAM, G. (1997). Geomicrobiology of sulfide mineral oxidation. *In* Banfield, J.F. and Nielson, K.H. (eds) *Reviews in mineralogy, Vol.35: Geomicrobiology: Interactions between microbes and minerals:* 361–390. Washington: Mineral. Soc. Am.

OHMURA, N. & BLAKE II, R. (1997). Aporusticyanin mediates the adhesion of *Thiobacillus Ferrooxidans* to pyrite. In *Proceedings of the International Biohydrometallurgy Symposium, Sydney:* PB1.1–PB1.10. Glenside, Australia: Australian Mineral Foundation.

OOSTHUYZEN, E.J. (1983). The application of automatic image analysis to mineralogy and extractive metallurgy. *In* De Villiers, J.P.R. & Cawthorn, P.A. (eds) *ICAM 81: Proceedings of the First International Congress on Applied Mineralogy*: 449–464. Johannesburg: Geol. Soc. S. Afr.

OOSTHUYZEN, E.J. (1987). Ore microscopy, image analysis, and the extractive metallurgy of sulphide minerals – an overview. Report M338. MINTEK, Randburg, S. Afr.

PETERSEN, E.U., PETERSEN, U. & HACKBARTH, C.J. (1990). Ore zoning and tetrahedrite compositional variation at Orcopampa, Peru. *Economic Geology* **85**:1491–1503.

PETRUK,W., HARRIS, D.C. & STEWART, J.M. (1971). Characteristics of the arsenides, sulpharsenides and antimonides. *Canadian Mineralogist* **11**:150–186.

PIERCE, M.L. & MOORE, C.B. (1982). Adsorption of arsenite and arsenate on amorphous iron hydroxide. *Water Research* **16**:1247–1253.

PILLER, H. (1977). *Microscope Photometry.* Berlin: Springer-Verlag.

PINCHES, A. (1975). Bacterial leaching of an arsenic-bearing sulphide concentrate. *In* Burkin A.R. (ed.) *Leaching and reduction in hydrometallurgy*: 28–35. London: Inst. Min. Metall.

PROSSER, A.P. (1996). Review of uncertainty in the collection and interpretation of leaching data. *Hydrometallurgy* **41**:119–153.

RALPH, D & WENSHENG, Z. (1993). The biological oxidation of arsenopyrite ore. In *Proceedings of the International Conference and Workshop Applications of Biotechnology to the Minerals Industry, Adelaide:* 7.1–7.9. Glenside, Australia: Australian Mineral Foundation.

RAMDOHR, P. (1980). *The ore minerals and their intergrowths, Vol.2.* 2nd edition. Oxford: Pergamon Press.

REED, S.J.B. (1996). *Electron microprobe analysis and scanning electron microscopy in geology.* Cambridge: Cambridge University Press.

RICHARDSON, S. & VAUGHAN, D.J. (1989). Arsenopyrite: A spectroscopic investigation of altered surfaces. *Mineralogical Magazine* **53**:223–229.

ROBINS, R.G., HUANG, J.C.Y., NISHIMURA, T. & KHOE, G.H. (1987). The adsorption of arsenate ion by ferric hydroxide. *In* Reddy, G., Hendrix, L. & Queneau, P.B. (eds). *Arsenic metallurgy Fundamentals and Applications.* The Metallurgical Society Inc., New York.

RUCKLIDGE, J.C. (1976). Electron microprobe instrumentation. *In* Smith, D.G.W. (ed.) *Microbeam techniques*: 1–44. Edmonton, Alberta: Can. Mineral. Assoc.

RUSSELL, J.A. (1985). A mineralogical investigation of the gold ore of the Klipwal Mine near Piet Retief. M.Sc.Thesis. Rand Afrikaans University, Johannesburg.

SASAKI, K., TSUNEKAWA, M., OHTSUKA, T. & KONNO, H. (1995). Confirmation of a sulfur-rich layer on pyrite after oxidative dissolution by Fe(III) ions around pH 2. *Geochimica et Cosmochimica Acta* **59**:3155–3158.

SCHOUWSTRA, R.P. (1990). Mineralogical and geochemical investigation of the Zwartkoppie type ore, Sheba Gold Mine. D.Sc Thesis. Potchefstroom University for Higher Christian Education, Potchefstroom, South Africa.

SCHOUWSTRA, R.P. & DE VILLIERS, J.P.R. (1988).Gold mineralization and associated wallrock alteration in Main Reef Complex at Sheba Mine, South Africa. *Transactions of the Institute of Mining and Metallurgy* **97**:B158–B170.

SHUEY, R.T. (1975). *Semiconducting ore minerals*. Amsterdam: Elsevier Scientific Publishing Company.

SINDEEVA, N.D. (1964). *Mineralogy and types of deposits of selenium and tellurium.* New York: Interscience Publishers, John Wiley and Sons.

STANTON, R.L. (1972). *Ore petrology.* New York: McGraw Hill.

SUKLA, L.B., CHAUDHURY, G.R. & DAS, R.P. (1990). Effect of silver ion on kinetics of biochemical leaching of chalcopyrite concentrate. *Transactions of the Institiue of Mining and Metallurgy* **99**:C43–C46.

SULLIVAN, K.A.& ALLER, R.C. (1996). Diagenetic cycling of arsenic in Amazon shelf sediments. *Geochimica et Cosmochimica Acta* **60**:1465–1477.

SUNDBLAD, K., ZACHRISSON, E., SMEDS, S.A., BERGLUND, S. AND ÅLINDER, C. (1984). Sphalerite geobarometry and arsenopyrite geothermometry applied to metamorphosed sulfide ores in the Swedish Caledonides. *Economic Geology* **79**:1660–1668.

SWASH, P.M. (1986). A mineralogical investigation of refractory gold ores and their beneficiation. Report M295. MINTEK, Randburg, S. Afr.

SWASH, P.M. (1988). A mineralogical investigation of refractory gold ores and their beneficiation, with special reference to arsenical ores. *Journal of the South African Institute of Mining and Metallurgy* **88**:173–180.

TAXIARCHOU, M., ADAM, K. & KONTOPOULOS, A. (1994). Bacterial oxidation conditions for gold extraction from Olympias refractory arsenical pyrite concentrate. *Hydrometallurgy* **36**:169–185.

VAUGHAN, D.J. (1984). Electronic structures of sulfides and leaching behaviour. *In* R.G. Bautista (ed.) *Hydrometallurgical Process Fundamentals:*23–40. New York: Plenum.

VAUGHAN, D.J. & CRAIG, J.R. (1979). *Mineral chemistry of metal sulphides.* Cambridge: Cambridge University Press.

VESSELINOV, I. & KERESTEDJIAN, T. (1995). Kinetic aspects of sector zoning in arsenopyrite: A case study. *Mineralogy and Petrology* **52**:85–106.

VILJOEN, E.A. & JOHNSON, J.A. (1983). Microbeam techniques in applied mineralogy. *Special Publications of the Geological Society of South Africa* **7**:499–506.

VOKES, F.M. & STRAND, G.S. (1982). Atoll texture in minerals of the cobaltite-gersdorffite series from the Raipas Mine, Finnmark, Norway. *In* Amstutz, G.C., El Goresy, A., Frenzel, G., Kluth, C., Moh, G., Wauschkuhn, R.A. and Zimmerman, R.A. (eds) *Ore Genesis: the State of the Art:* 118–130. Berlin: Springer-Verlag.

WAGENER, J.H.F. & WIEGAND, J. (1986). The Sheba Gold Mine, Barberton greenstone belt. *In* Annhaeusser, C.R. & Maske, S. (eds) *Mineral Deposits of Southern Africa Volume 1:*155–161.

WEIR, D.R. & BEREZOWSKY, R.M.G.S. (1986). Refractory gold: the role of pressure oxidation. *GOLD 100 – Proceedings of the International Conference on Gold* **2**:275–285.

WILLEMSE, J. (1938). The gold occurrences south-west of Pietersburg. Geological Series Bulletin No.12, Geological Survey Division, Department of Mines, Union of South Africa.

WU, X., DELBOVE, F. & TOURAY, J.C. (1990). Conditions of formation of gold-bearing arsenopyrite: A comparison of synthetic crystals with sample from Le Chatelet gold deposit, Creuse, France. *Mineralium Deposita* **25**:S8–S12.

ZHANG, Y.Z., LU, Y.Y. & ZHAO, T.C. (1996). Oxidation mechanism of arsenopyrite in acidic ferric sulphate media in the absence and presence of bacteria *T. Ferrooxidans. In* Warren, G.W. (ed.) *EPD Congress 1996*: 429–442. Pennsylvania: Minerals, Metals and Materials Society.

APPENDIX

TABLE A1

ABBREVIATIONS USED IN THE TEXT

ABBREVIATION	NAME IN FULL
AA	Atomic absorption spectroscopy
AES	Auger electron spectroscopy
As_T	Total arsenic
atm. %	Atomic per cent
BSE	Back-scattered electron
EBSD	Electron backscatter scanning diffraction
EDS	Energy-dispersive X-ray spectroscopy
EMP	Electron microprobe
Fe_T	Total iron
ICP-MS	Inductively-coupled plasma mass spectrometry
M	Molar
MRC	Main Reef Complex (Sheba Mine)
ORP	Overvoltage reduction potential
PGE	Platinum group element(s)
PHA	Pulse height analyser
ROM	Run of mine
SEM	Scanning electron microscope
UV	Ultra-violet
WDS	Wavelength-dispersive X-ray spectroscopy
XPS	X-ray photoelectron spectroscopy
XRD	X-ray diffraction
XRF	X-ray fluorescence

TABLE A2

FORMULAE OF SULPHIDE MINERALS

Mineral Name	Formula
Arsenopyrite	FeAsS
Pyrite	FeS_2
Pyrrhotite	$Fe_{1-x}S$
Chalcopyrite	$CuFeS_2$
Gersdorffite	NiAsS
Sphalerite	ZnS
Galena	PbS
Tennantite-tetrahedrite	$(Cu,Fe)_{12}As_4S_{13} - (Cu,Fe)_{12}Sb_4S_{13}$
Stibnite	Sb_2S_3
Pentlandite	$(Fe,Ni)_9S_8$

TABLE A3

FORMULAE OF NON-SULPHIDE MINERALS

Mineral Name	Formula
Quartz	SiO_2
Albite	$NaAlSi_3O_8$
Orthoclase	$KAlSi_3O_8$
Sericite	$KAl_2(AlSi_3)O_{10}(OH,F)_2$
Biotite	$K(Mg,Fe)_2(AlSi_3)O_{10}(OH,F)_2$
Chlorite	$(Mg,Fe)_5Al(AlSi_3)O_{10}(OH)_9$
Tourmaline	$(Na,Ca)(Mg,Fe,Al,Li)B_3(Al,Fe)_6O_{27}(OH,F)_4$
Zircon	$ZrSiO_4$
Ankerite	$Ca(Mg,Fe)(CO_3)_2$
Siderite	$FeCO_3$
Dolomite	$CaMg(CO_3)_2$
Rutile	TiO_2
Ilmenite	$FeTiO_3$
Chromite	$FeCr_2O_4$ (ideal)
Goethite	α-FeO·OH
Barite	$BaSO_4$
Apatite	$Ca_5(OH,Cl,F)(PO_4)_3$
Fluorapatite	$Ca_5F(PO_4)_3$
Monazite	$(Ce,La,Y)PO_4$
Xenotime	YPO_4
Gold	(Au,Ag)

TABLE A4

FORMULAE OF THE MORE COMMON LEACH PRODUCTS PRODUCED DURING THE BACTERIAL OXIDATION OF ARSENOPYRITIC GOLD CONCENTRATES

Mineral Name	Formula
Sulphur	S_8
Gypsum	$CaSO_4·2H_2O$
Jarosite	$MFe_3(SO_4)_2(OH)_6$ M = K^+, Na^+, H_3O^+, NH_4^+
Ferric hydroxide	$Fe(OH)_3$
Goethite	FeO·OH
Scorodite	$FeAsO_4·2H_2O$
Hydrated ferric arsenate	$FeAsO_4·xH_2O$
Zykaite	$Fe_4(AsO_4)_3(SO_4)(OH)·15H_2O$
Sarmienite	$Fe_2(AsO_4)(SO_4)(OH)·5H_2O$
Bukovskyite	$Fe_2(AsO_4)(SO_4)(OH)·7H_2O$

TABLE A5

ARSENOPYRITE REFLECTANCE READINGS

All readings are in reflectance %. R_{min} is the minimum reflectance at a point, and R_{max} is the maximum reflectance. R_{ave} is the average of R_{min} and R_{max}. The bireflectance (biref.) is the difference between R_{min} and R_{max}. The two measuring filters used were Na 589 (orange) and Hg 546 (green).

COLOUR	TYPE	Na 589 (orange)				Hg 546 (green)			
		R_{min}	R_{max}	R_{av}	Biref.	R_{min}	R_{max}	R_{av}	Biref.
WHITE (unleached)	West African	52.0	52.5	52.3	0.5	51.4	51.6	51.5	0.2
		52.5	53.0	52.8	0.5	52.6	52.7	52.7	0.1
		52.6	52.9	52.8	0.3	52.3	52.5	52.4	0.2
		53.2	53.5	53.4	0.3	51.8	52.0	51.9	0.2
		51.4	52.0	51.7	0.6	51.5	52.0	51.8	0.5
WHITE (unleached)	West African	52.7	53.1	52.9	0.4	51.0	51.7	51.4	0.7
		52.6	53.0	52.8	0.4	51.5	52.1	51.8	0.6
		53.1	53.3	53.2	0.2	51.5	52.2	51.9	0.7
		52.9	53.4	53.2	0.5	51.8	52.2	52.0	0.4
		52.8	53.3	53.1	0.5	51.8	52.5	52.2	0.7
WHITE (unleached)	Zandrivier	51.7	51.9	51.8	0.2	51.5	51.8	51.7	0.3
		52.6	52.9	52.8	0.3	51.4	51.8	51.6	0.4
		52.0	52.4	52.2	0.4	51.3	51.5	51.4	0.2
		51.5	51.8	51.7	0.3	51.0	51.4	51.2	0.4
		51.9	52.5	52.2	0.6	51.5	51.6	51.6	0.1
WHITE (unleached)	Zandrivier	52.2	53.4	52.8	1.2	52.9	53.3	53.1	0.4
		51.8	53.0	52.4	1.2	52.3	52.8	52.6	0.5
		52.3	53.1	52.7	0.8	51.7	52.2	52.0	0.5
		52.4	53.1	52.8	0.7	52.6	53.1	52.9	0.5
		52.3	53.1	52.7	0.8	52.0	52.5	52.3	0.5
WHITE (unleached)	Zandrivier	52.4	52.7	52.6	0.3	51.7	52.1	51.9	0.4
		52.3	52.6	52.5	0.3	52.0	52.5	52.3	0.5
		52.7	53.0	52.9	0.3	52.1	52.5	52.3	0.4
		52.4	52.7	52.6	0.3	51.7	52.2	52.0	0.5

TABLE A5 (cont.)

COLOUR	TYPE	Na 589 (orange)				Hg 546 (green)			
		R_{min}	R_{max}	R_{av}	Biref.	R_{min}	R_{max}	R_{av}	Biref.
	Zandrivier (cont.)	52.3	52.5	52.4	0.2	51.9	52.4	52.2	0.5
WHITE (unleached)	Zandrivier	52.4	52.9	52.7	0.5	52	52.5	52.3	0.5
		52.5	53	52.8	0.5	52.2	52.9	52.6	0.7
		52.6	53.1	52.9	0.5	51.8	52.2	52	0.4
		52.9	53.4	53.2	0.5	52.0	52.6	52.3	0.6
		53.0	53.3	53.2	0.3	51.7	52.1	51.9	0.4
WHITE (unleached)	Klipwal	50.8	52.4	51.6	1.6	51.0	51.8	51.4	0.8
		51.5	52.9	52.2	1.4	51.9	52.5	52.2	0.6
		51.7	53.2	52.5	1.5	51.2	52.1	51.7	0.9
		51.1	52.6	51.9	1.5	51.7	52.1	51.9	0.4
		51.2	52.6	51.9	1.4	51.6	52.1	51.9	0.5
WHITE (unleached)	Klipwal	52.5	52.8	52.7	0.3	51.8	52.3	52.1	0.5
		52.5	52.7	52.6	0.2	52.0	52.4	52.2	0.4
		52.6	53.0	52.8	0.4	51.3	51.8	51.6	0.5
		52.4	52.7	52.6	0.3	51.2	51.6	51.4	0.4
		52.7	53.0	52.9	0.3	51.4	52.0	51.7	0.6
WHITE (unleached)	Klipwal	52.5	52.9	52.7	0.4	51.4	51.7	51.6	0.3
		53.0	53.3	53.2	0.3	52.0	52.2	52.1	0.2
		52.5	52.8	52.7	0.3	51.9	52.1	52.0	0.2
		53.1	53.5	53.3	0.4	51.7	52.0	51.9	0.3
		53.0	53.4	53.2	0.4	51.7	52.2	52.0	0.5
CREAM	Klipwal	45.8	46.9	46.4	1.1	43.9	44.3	44.1	0.4
		45.7	46.7	46.2	1.0	44.7	44.9	44.8	0.2
		45.1	46.1	45.6	1.0	44.3	44.9	44.6	0.6
		45.4	46.6	46.0	1.2	44.0	44.4	44.2	0.4
		45.2	46.1	45.7	0.9	44.6	44.8	44.7	0.2
CREAM	Klipwal	42.1	42.8	42.5	0.7	41.1	42.0	41.6	0.9
		43.8	44.9	44.4	1.1	41.0	41.3	41.2	0.3
		42.0	43.0	42.5	1.0	41.2	41.3	41.3	0.1
		42.0	42.8	42.4	0.8	39.8	40.0	39.9	0.2
		44.1	45.0	44.6	0.9	40.0	40.6	40.3	0.6

TABLE A5 (cont.)

COLOUR	TYPE	Na 589 (orange)				Hg 546 (green)			
		R_{min}	R_{max}	R_{av}	Biref.	R_{min}	R_{max}	R_{av}	Biref.
CREAM	Klipwal	40.2	40.9	40.6	0.7	38.8	40.0	39.4	1.2
		40.0	40.8	40.4	0.8	39.6	40.2	39.9	0.6
		39.2	40.3	39.8	1.1	38.4	39.6	39.0	1.2
		41.0	42.0	41.5	1.0	39.1	39.3	39.2	0.2
		39.4	40.0	39.7	0.6	38.1	38.7	38.4	0.6
BEIGE	Klipwal	33.7	35.9	34.8	2.2	30.8	32.4	31.6	1.6
		34.4	36.3	35.4	1.9	31.7	32.7	32.2	1.0
		33.1	34.7	33.9	1.6	31.6	32.7	32.2	1.1
		33.5	35.8	34.7	2.3	31.2	33.0	32.1	1.8
		33.0	35.3	34.2	2.3	31.1	32.6	31.9	1.5
BEIGE	Klipwal	34.9	36.1	35.5	1.2	31.4	32.7	32.1	1.3
		34.8	35.8	35.3	1.0	26.6	27.8	27.2	1.2
		29.7	30.8	30.3	1.1	30.5	32.0	31.3	1.5
		35.1	36.0	35.6	0.9	31.6	33.8	32.7	2.2
		31.7	33.8	32.8	2.1	26.8	28.3	27.6	1.5
BEIGE	Klipwal	32.4	33.2	32.8	0.8	27.0	29.3	28.2	2.3
		28.6	29.8	29.2	1.2	24.0	25.9	25.0	1.9
		30.1	31.2	30.7	1.1	29.6	31.2	30.4	1.6
		30.2	31.0	30.6	0.8	26.6	28.9	27.8	2.3
		32.7	33.8	33.3	1.1	27.5	29.4	28.5	1.9
BEIGE	Klipwal	24.0	24.8	24.4	0.8	20.4	21.9	21.2	1.5
		23.6	24.5	24.1	0.9	20.0	21.7	20.9	1.7
		20.8	21.5	21.2	0.7	19.9	21.5	20.7	1.6
		29.0	31.7	30.4	2.7	18.8	20.7	19.8	1.9
		27.3	29.2	28.3	1.9	25.5	28.2	26.9	2.7
BROWN	Zandrivier	10.5	12.1	11.3	1.6	6.6	8.8	7.7	2.2
		9.6	11.0	10.3	1.4	7.9	9.9	8.9	2.0
		17.3	18.8	18.1	1.5	15.6	18.2	16.9	2.6
		14.0	16.7	15.4	2.7	14.9	15.7	15.3	0.8
		13.1	14.4	13.8	1.3	16.8	17.9	17.4	1.1

TABLE A5 (cont.)

COLOUR	TYPE	Na 589 (orange)				Hg 546 (green)			
		R_{min}	R_{max}	R_{av}	Biref.	R_{min}	R_{max}	R_{av}	Biref.
BROWN	Klipwal	9.5	11.7	10.6	2.2	6.2	6.9	6.6	0.7
		12.2	13.7	13.0	1.5	5.6	6.3	6.0	0.7
		11.8	13.2	12.5	1.4	7.6	8.3	8.0	0.7
		9.6	11.3	10.5	1.7	8.0	8.6	8.3	0.6
		9.0	9.7	9.4	0.7	6.2	6.7	6.5	0.5
BROWN	Klipwal	8.2	8.9	8.6	0.7	5.3	6.1	5.7	0.8
		7.4	8.3	7.9	0.9	6.1	6.8	6.5	0.7
		7.3	8.7	8.0	1.4	5.4	5.8	5.6	0.4
		6.4	7.5	7.0	1.1	5.4	6.0	5.7	0.6
		7.0	8.2	7.6	1.2	4.5	5.4	5.0	0.9
M/COL	Klipwal	6.1	6.8	6.5	0.7	5.1	6.2	5.7	1.1
		5.6	6.0	5.8	0.4	3.2	3.8	3.5	0.6
		5.6	5.9	5.8	0.3	3.8	5.0	4.4	1.2
		5.7	6.1	5.9	0.4	4.4	5.1	4.8	0.7
		5.9	6.3	6.1	0.4	2.4	3.2	2.8	0.8
M/COL	Zandrivier	5.3	6.3	5.8	1.0	3.3	3.8	3.6	0.5
		5.1	6.0	5.6	0.9	3.9	4.4	4.2	0.5
		5.6	7.0	6.3	1.4	3.6	4.2	3.9	0.6
		5.5	6.4	6.0	0.9	3.0	3.5	3.3	0.5
		5.5	7.4	6.5	1.9	3.7	4.3	4.0	0.6
M/COL	Klipwal	4.1	4.7	4.4	0.6	5.6	6.0	5.8	0.4
		6.4	6.9	6.7	0.5	3.5	4.1	3.8	0.6
		4.9	5.4	5.2	0.5	4.2	5.2	4.7	1.0
		4.8	5.2	5.0	0.4	4.4	5.0	4.7	0.6
		4.5	4.9	4.7	0.4	3.7	4.4	4.1	0.7
M/COL	Klipwal	4.7	5.4	5.1	0.7	3.4	4.5	4.0	1.1
		3.1	3.9	3.5	0.8	2.2	2.6	2.4	0.4
		3.6	4.7	4.2	1.1	4.2	5.0	4.6	0.8
		2.7	4.0	3.4	1.3	4.3	5.0	4.7	0.7
		3.8	4.6	4.2	0.8	2.8	3.1	3.0	0.3
M/COL	West African	4.9	5.4	5.2	0.5	3.9	4.6	4.3	0.7
		4.7	5.6	5.2	0.9	3.6	4.4	4.0	0.8

TABLE A5 (cont.)

COLOUR	TYPE	Na 589 (orange)				Hg 546 (green)			
		R_{min}	R_{max}	R_{av}	Biref.	R_{min}	R_{max}	R_{av}	Biref.
	West African (cont.)	5.4	6.1	5.8	0.7	4.1	4.7	4.4	0.6
		4.3	5.0	4.7	0.7	4.0	4.8	4.4	0.8
		3.5	4.5	4.0	1.0	4.7	5.6	5.2	0.9
M/COL	Klipwal	3.7	5.5	4.6	1.8	3.4	5.4	4.4	2.0
		3.5	5.4	4.5	1.9	3.6	5.8	4.7	2.2
		3.0	4.1	3.6	1.1	3.9	5.6	4.8	1.7
		3.8	5.1	4.5	1.3	3.3	5.4	4.4	2.1
		4.0	6.2	5.1	2.2	3.6	5.5	4.6	1.9
BLUE	Klipwal	5.2	7.7	6.5	2.5	5.0	6.2	5.6	1.2
		3.3	4.9	4.1	1.6	4.5	5.7	5.1	1.2
		4.0	5.1	4.6	1.1	5.8	7.3	6.6	1.5
		5.0	6.8	5.9	1.8	4.2	5.6	4.9	1.4
		3.6	4.7	4.2	1.1	7.7	8.7	8.2	1.0
BLUE	Zandrivier	5.4	6.3	5.9	0.9	7.2	7.3	7.3	0.1
		5.2	5.5	5.4	0.3	8.1	9.0	8.6	0.9
		6.8	7.7	7.3	0.9	7.4	7.6	7.5	0.2
		5.1	5.3	5.2	0.2	5.7	5.9	5.8	0.2
		4.4	4.7	4.6	0.3	6.5	8.5	7.5	2.0
BLUE	West African	4.5	5.1	4.8	0.6	7.0	7.6	7.3	0.6
		4.9	5.5	5.2	0.6	7.9	8.7	8.3	0.8
		5.0	5.7	5.4	0.7	5.5	6.0	5.8	0.5
		4.4	5.2	4.8	0.8	6.7	7.7	7.2	1.0
		4.0	4.5	4.3	0.5	5.8	6.5	6.2	0.7
CREAM 2	Klipwal	8.5	11.3	9.9	2.8	10.1	12.0	11.1	1.9
		7.4	9.8	8.6	2.4	8.1	9.8	9.0	1.7
		6.9	8.8	7.9	1.9	10.3	11.7	11.0	1.4
		7.7	9.5	8.6	1.8	8.8	9.7	9.3	0.9
		8.6	10.5	9.6	1.9	11.1	12.6	11.9	1.5

TABLE A6

HOMOGENEITY TEST ON AS-2

Position	S mass %	Fe mass %	As mass %	Total mass %
1	21.29	35.32	44.69	101.30
2	21.01	35.19	45.18	101.39
3	20.79	35.25	45.03	101.07
4	20.81	35.05	44.78	100.64
5	20.81	35.05	44.99	100.84
6	20.93	35.01	44.80	100.75
7	20.48	34.90	45.40	100.77
8	20.77	35.10	45.12	100.99
9	20.43	35.08	45.75	101.25
10	20.77	34.90	45.05	100.72
11	20.80	34.88	44.90	100.59
12	21.11	35.03	44.30	100.44
13	21.03	34.94	44.26	100.23
14	21.23	34.98	44.02	100.24
15	21.10	35.18	44.43	100.71
16	21.23	35.12	44.17	100.52
17	21.02	34.89	44.34	100.25
18	20.99	34.76	44.18	99.93
19	21.33	35.08	44.16	100.57
20	20.88	34.86	44.54	100.28
21	20.90	34.82	44.30	100.02
22	21.03	34.89	44.61	100.52
23	21.06	34.91	44.74	100.71
24	21.01	34.77	44.45	100.23
25	20.80	34.53	44.47	99.80
26	20.96	34.82	44.43	100.21
27	21.01	34.96	44.51	100.48
28	20.82	34.60	44.70	100.11
29	20.85	35.05	44.72	100.61
30	21.17	35.01	44.21	100.38
31	20.89	34.93	44.65	100.48
32	20.73	34.56	44.48	99.76
33	20.75	34.92	44.86	100.53
34	20.70	34.85	45.15	100.69
35	20.63	34.85	44.97	100.44
36	20.70	35.23	44.90	100.83
37	20.65	34.72	44.92	100.29
38	20.85	34.75	44.77	100.36
39	20.82	35.13	45.03	100.98
40	20.66	34.76	44.94	100.35
41	20.60	34.69	45.08	100.37
42	20.68	34.91	44.88	100.48
43	20.76	34.84	44.79	100.39
44	20.74	35.14	45.03	100.91
45	20.83	35.04	44.98	100.86
46	20.76	35.17	44.90	100.83

TABLE A6 (cont.)

Position	S mass %	Fe mass %	As mass %	Total mass %
47	20.75	34.77	44.87	100.39
48	20.88	35.00	45.04	100.91
49	20.80	34.67	44.67	100.14
50	20.82	34.68	44.34	99.84
mean	20.87	34.93	44.73	100.53
std.dev.	0.19	0.18	0.35	0.37
norm. mean	20.76	34.75	44.49	100.00
std.dev.	0.19	0.18	0.28	

TABLE A7

HOMOGENEITY TEST ON ASP-1

Position	S mass %	Fe mass %	As mass %	Total mass %
1	19.02	34.72	45.10	98.84
2	19.36	34.82	45.72	99.90
3	19.19	34.66	45.41	99.26
4	19.30	34.70	46.12	100.12
5	18.79	34.65	45.41	98.85
6	19.18	34.74	44.76	98.68
7	19.83	34.84	45.06	99.73
8	19.74	34.93	44.67	99.34
9	19.83	34.77	45.86	100.45
10	19.21	34.59	46.87	100.67
11	19.97	34.88	45.62	100.47
12	19.73	35.18	44.36	99.26
13	19.02	34.80	45.67	99.50
14	18.86	34.41	46.37	99.64
15	18.86	34.58	46.51	99.95
16	19.45	35.04	45.65	100.14
17	18.77	34.60	46.58	99.95
18	18.93	34.53	46.94	100.40
19	18.78	34.52	46.22	99.53
20	18.90	34.72	46.03	99.65
21	19.47	34.80	45.32	99.59
22	19.05	34.97	45.84	99.86
23	19.12	35.01	45.82	99.94
24	18.72	34.42	45.05	98.18
25	19.28	34.94	44.80	99.02
26	18.91	34.71	46.00	99.62
27	18.84	34.74	46.13	99.72
28	18.95	34.59	46.51	100.05
29	19.54	34.79	45.64	99.96
30	19.98	35.17	45.06	100.20
31	19.28	34.54	46.82	100.63
32	19.23	34.68	46.29	100.21
33	19.25	34.40	46.68	100.33
34	19.17	34.79	45.74	99.70
35	19.38	34.93	46.18	100.50
36	19.34	34.75	46.45	100.53
37	19.43	34.73	45.92	100.08
38	19.61	34.89	46.13	100.63
39	19.25	34.60	47.00	100.85
40	19.51	34.74	46.21	100.47
41	19.23	34.65	46.21	100.09
42	19.27	34.89	46.28	100.44
43	19.30	34.74	46.70	100.75
44	19.36	34.89	46.28	100.53
45	19.40	34.68	46.27	100.35
46	19.63	34.85	45.29	99.77

TABLE A7 (cont.)

Position	S mass %	Fe mass %	As mass %	Total mass %
47	19.05	34.55	46.31	99.91
48	19.07	34.68	46.15	99.91
49	19.12	34.56	46.62	100.31
50	19.42	34.96	45.86	100.23
mean	19.26	34.75	45.93	99.93
std.dev.	0.32	0.18	0.63	0.58
norm. mean	19.27	34.77	45.96	100.00
std.dev.	0.30	0.26	0.48	

TABLE A8

RANDOM MICROPROBE ANALYSIS OF KLIPWAL ARSENOPYRITE

Trace element detection limits (dl) are as follows: Cu 290ppm, Ni 240ppm, Co 210ppm, Au 350ppm, Sb 210ppm.

Point	As mass %	Fe mass %	S mass %	Cu ppm	Ni ppm	Co ppm	Au ppm	Sb ppm	TOTAL mass %
1	42.40	35.15	22.28	<dl	<dl	<dl	<dl	<dl	99.83
2	42.63	35.31	22.28	<dl	<dl	<dl	<dl	365	100.26
3	42.89	35.09	22.16	<dl	975	430	<dl	<dl	100.29
4	41.85	35.23	22.53	<dl	<dl	<dl	<dl	<dl	99.62
5	44.17	34.93	21.55	<dl	510	320	<dl	280	100.76
6	42.55	34.98	22.45	<dl	285	<dl	<dl	<dl	100.01
7	41.50	35.20	22.33	<dl	<dl	<dl	<dl	420	99.07
8	42.70	35.24	22.34	<dl	<dl	<dl	<dl	220	100.31
9	41.70	35.54	22.82	<dl	<dl	<dl	<dl	<dl	100.06
10	42.00	35.21	22.10	<dl	<dl	<dl	<dl	<dl	99.31
11	41.43	35.29	22.60	<dl	810	800	<dl	<dl	99.48
12	42.27	35.04	22.69	<dl	320	585	<dl	270	100.12
13	42.07	35.08	22.74	<dl	490	385	<dl	<dl	99.98
14	41.71	35.31	22.40	<dl	1095	800	<dl	<dl	99.61
15	42.09	35.15	22.17	405	1695	1335	<dl	<dl	99.76
16	43.73	35.20	21.36	<dl	540	<dl	<dl	<dl	100.34
17	43.89	34.71	21.58	<dl	1135	500	<dl	<dl	100.35
18	43.26	34.81	21.89	<dl	780	1010	<dl	<dl	100.13
19	41.12	35.40	22.58	<dl	<dl	<dl	<dl	620	99.16
20	41.55	35.53	22.49	<dl	340	<dl	<dl	720	99.69
21	41.75	35.43	22.66	<dl	440	<dl	<dl	490	99.94
22	42.24	35.48	22.98	<dl	<dl	<dl	<dl	605	100.76
23	41.98	35.06	22.45	<dl	<dl	<dl	<dl	<dl	99.49
24	43.06	35.17	21.89	<dl	<dl	<dl	<dl	<dl	100.13
25	41.97	35.18	21.90	<dl	<dl	300	<dl	<dl	99.07
26	42.80	34.89	21.82	<dl	710	285	<dl	<dl	99.61
27	41.87	35.48	22.38	360	<dl	<dl	<dl	<dl	99.76
28	42.87	35.09	22.25	<dl	710	<dl	<dl	<dl	100.29

TABLE A8 (cont.)

Point	As mass %	Fe mass %	S mass %	Cu ppm	Ni ppm	Co ppm	Au ppm	Sb ppm	TOTAL mass %
29	42.92	35.17	22.09	<dl	<dl	220	<dl	<dl	100.20
30	42.51	34.91	21.74	<dl	<dl	415	<dl	<dl	99.20
31	41.72	35.52	22.31	<dl	<dl	<dl	<dl	730	99.63
32	41.67	35.56	22.93	<dl	<dl	<dl	<dl	600	100.23
33	41.84	35.02	21.65	<dl	530	630	<dl	<dl	98.63
34	41.99	34.81	21.56	<dl	2630	675	<dl	<dl	98.69
35	42.31	35.23	22.11	<dl	435	<dl	<dl	<dl	99.69
36	42.67	35.30	22.33	<dl	1085	235	<dl	<dl	100.44
37	43.12	34.77	21.93	<dl	340	<dl	<dl	<dl	99.86
38	43.63	34.88	21.71	<dl	<dl	300	<dl	<dl	100.25
39	42.12	35.13	22.32	<dl	<dl	<dl	<dl	<dl	99.57
40	42.83	34.67	21.77	<dl	2965	660	<dl	<dl	99.63
41	42.22	35.20	22.57	<dl	<dl	365	<dl	<dl	100.03
42	42.41	35.38	22.46	<dl	<dl	<dl	<dl	<dl	100.25
43	42.04	35.04	22.73	<dl	580	395	<dl	<dl	99.91
44	42.19	35.47	22.71	<dl	<dl	<dl	435	<dl	100.42
45	41.50	35.40	22.78	<dl	<dl	<dl	<dl	625	99.74
46	41.45	35.58	23.18	<dl	<dl	<dl	<dl	855	100.31
47	43.57	35.15	21.82	<dl	<dl	<dl	<dl	<dl	100.54
48	42.86	35.40	22.24	<dl	515	<dl	<dl	<dl	100.55
49	43.28	35.06	21.93	<dl	<dl	<dl	<dl	<dl	100.27
50	42.47	35.32	22.34	<dl	<dl	<dl	<dl	<dl	100.13
51	42.51	35.65	22.44	<dl	545	370	<dl	<dl	100.70
52	43.12	35.26	22.18	<dl	670	430	<dl	<dl	100.67
53	40.91	35.73	23.71	<dl	<dl	260	<dl	1225	100.50
54	41.24	35.76	23.27	<dl	<dl	<dl	<dl	830	100.36
55	43.03	35.13	21.47	<dl	<dl	<dl	<dl	<dl	99.63
56	42.96	35.40	21.97	<dl	<dl	<dl	430	<dl	100.37
57	42.55	35.18	21.98	<dl	300	<dl	<dl	<dl	99.74
58	42.73	35.05	21.87	<dl	<dl	<dl	<dl	<dl	99.65
59	42.13	35.02	22.16	<dl	265	<dl	<dl	<dl	99.33
60	42.05	35.38	21.99	<dl	<dl	<dl	<dl	<dl	99.42

TABLE A8 (cont.)

Point	As mass %	Fe mass %	S mass %	Cu ppm	Ni ppm	Co ppm	Au ppm	Sb ppm	TOTAL mass %
61	41.49	35.08	22.25	<dl	2965	935	<dl	<dl	99.20
62	41.91	35.25	22.66	<dl	1010	0	<dl	<dl	99.92
63	43.10	34.90	21.87	<dl	<dl	0	<dl	<dl	99.87
64	42.73	35.28	21.78	<dl	350	0	<dl	<dl	99.82
65	41.57	35.34	22.60	<dl	<dl	0	<dl	<dl	99.50
66	41.89	35.26	22.98	<dl	945	760	<dl	<dl	100.30
67	42.14	34.41	22.19	<dl	4850	1510	<dl	<dl	99.38
68	42.20	35.18	22.88	<dl	245	0	<dl	220	100.30
69	42.51	35.31	22.52	<dl	<dl	0	<dl	<dl	100.34
70	42.77	35.16	21.90	<dl	<dl	0	<dl	<dl	99.83
71	43.17	34.99	21.69	<dl	<dl	0	<dl	<dl	99.85
72	43.12	35.17	21.46	<dl	<dl	0	<dl	<dl	99.75
73	43.09	34.76	21.85	<dl	1650	0	<dl	<dl	99.87
74	43.01	34.86	21.80	<dl	2165	290	<dl	<dl	99.92
75	41.95	35.20	22.16	<dl	<dl	0	<dl	<dl	99.31
76	41.78	35.11	22.20	<dl	335	370	<dl	<dl	99.15
77	41.64	34.83	22.40	<dl	<dl	0	<dl	335	98.90
78	41.68	35.12	22.04	<dl	715	670	<dl	270	99.01
79	41.71	35.44	22.63	<dl	<dl	0	<dl	270	99.81
80	42.77	34.48	22.14	375	6780	585	<dl	<dl	100.17
81	43.51	35.07	21.98	<dl	<dl	415	<dl	<dl	100.60
82	42.85	35.32	21.65	<dl	<dl	0	<dl	390	99.85
83	42.01	35.37	22.15	<dl	<dl	0	<dl	<dl	99.54
84	42.90	35.14	22.18	<dl	<dl	0	<dl	<dl	100.22
85	42.51	35.21	22.06	<dl	530	0	<dl	<dl	99.82
86	42.77	34.87	21.85	<dl	730	0	<dl	<dl	99.56
87	42.94	35.22	21.98	<dl	<dl	0	<dl	<dl	100.15
88	42.43	35.18	21.87	<dl	<dl	0	<dl	<dl	99.48
89	41.71	35.22	22.28	<dl	<dl	215	<dl	<dl	99.23
90	42.42	35.60	22.33	<dl	<dl	0	<dl	350	100.39
91	40.75	35.60	22.79	<dl	295	0	<dl	430	99.22
92	42.58	34.99	21.51	<dl	1955	570	<dl	<dl	99.34

TABLE A8 (cont.)

Point	As mass %	Fe mass %	S mass %	Cu ppm	Ni ppm	Co ppm	Au ppm	Sb ppm	TOTAL mass %
93	42.38	35.21	22.01	<dl	<dl	265	<dl	<dl	99.63
94	43.17	35.18	21.98	<dl	1550	255	<dl	<dl	100.52
95	43.35	34.74	21.61	<dl	1950	1505	<dl	<dl	100.04
96	42.78	34.29	21.40	340	3315	2550	<dl	<dl	99.09
97	41.76	35.32	22.40	<dl	<dl	230	<dl	<dl	99.50
98	41.91	35.23	22.23	<dl	<dl	315	<dl	<dl	99.40
99	43.73	34.71	21.06	<dl	<dl	<dl	<dl	<dl	99.50
100	44.58	33.94	20.74	<dl	8070	1035	<dl	<dl	100.17
mean	42.42	35.15	22.81						99.85
std.dev	0.72	0.30	0.47						0.48

TABLE A9

RANDOM MICROPROBE ANALYSIS OF ZANDRIVIER ARSENOPYRITE

Trace element detection limits (dl) are as follows: Cu 290ppm, Ni 240ppm, Co 210ppm, Au 350ppm, Sb 210ppm.

POINT	As mass %	Fe mass %	S mass %	Cu ppm	Ni ppm	Co ppm	Au ppm	Sb ppm	TOTAL mass %
1	43.17	34.90	21.56	295	<dl	385	<dl	<dl	99.70
2	42.46	35.10	21.75	<dl	<dl	<dl	<dl	<dl	99.31
3	44.73	34.75	20.75	<dl	<dl	<dl	<dl	<dl	100.23
4	46.16	34.47	20.09	300	<dl	<dl	<dl	<dl	100.75
5	43.82	35.33	21.56	<dl	240	<dl	<dl	250	100.76
6	43.04	34.86	21.35	265	560	<dl	<dl	<dl	99.33
7	43.82	35.11	21.75	<dl	240	300	<dl	<dl	100.73
8	45.17	34.57	20.64	<dl	<dl	<dl	<dl	<dl	100.38
9	45.24	34.33	20.08	410	<dl	<dl	<dl	<dl	99.69
10	44.64	34.56	20.61	<dl	<dl	<dl	<dl	440	99.85
11	44.04	34.94	21.50	<dl	325	320	<dl	<dl	100.54
12	43.86	35.09	21.41	<dl	<dl	235	<dl	<dl	100.39
13	44.62	34.69	20.86	<dl	435	320	<dl	<dl	100.25
14	44.79	34.89	21.08	<dl	<dl	<dl	<dl	<dl	100.76
15	43.25	34.98	21.31	<dl	425	<dl	<dl	<dl	99.58
16	41.22	35.53	23.08	<dl	<dl	<dl	<dl	<dl	99.82
17	45.99	34.55	19.53	<dl	<dl	<dl	<dl	<dl	100.07
18	45.85	34.74	19.80	<dl	<dl	<dl	<dl	<dl	100.40
19	46.06	34.60	19.50	<dl	<dl	620	<dl	230	100.24
20	44.09	35.29	20.60	<dl	<dl	<dl	<dl	<dl	99.98
21	43.37	35.44	21.21	<dl	270	360	<dl	<dl	100.09
22	43.64	35.10	20.94	<dl	<dl	<dl	<dl	240	99.72
23	42.96	35.40	21.54	320	<dl	<dl	<dl	<dl	99.94
24	43.34	35.46	21.03	<dl	<dl	<dl	<dl	<dl	99.82
25	44.33	35.39	20.79	395	<dl	225	<dl	<dl	100.58
26	43.98	35.52	20.80	<dl	<dl	<dl	<dl	<dl	100.31
27	44.81	34.94	20.04	<dl	<dl	<dl	<dl	<dl	99.79
28	42.94	35.50	21.19	<dl	485	<dl	<dl	<dl	99.68

TABLE A9 (cont.)

POINT	As mass %	Fe mass %	S mass %	Cu ppm	Ni ppm	Co ppm	Au ppm	Sb ppm	TOTAL mass %
29	43.72	35.16	20.96	<dl	<dl	<dl	<dl	<dl	99.83
30	44.79	35.04	20.25	<dl	<dl	<dl	<dl	<dl	100.08
31	43.98	34.44	19.68	<dl	840	3600	<dl	295	98.57
32	44.62	35.05	20.01	<dl	<dl	<dl	<dl	<dl	99.69
33	43.56	35.21	20.58	<dl	<dl	<dl	<dl	<dl	99.35
34	42.91	35.54	21.24	<dl	<dl	<dl	<dl	<dl	99.69
35	43.61	35.06	20.44	<dl	315	305	<dl	<dl	99.17
36	43.74	35.37	20.59	305	<dl	<dl	<dl	<dl	99.73
37	42.84	35.32	21.02	<dl	<dl	260	<dl	370	99.24
38	43.14	35.27	20.92	<dl	<dl	<dl	<dl	385	99.37
39	44.82	35.02	19.62	<dl	<dl	275	<dl	<dl	99.49
40	44.66	35.12	19.60	<dl	370	<dl	<dl	<dl	99.41
41	42.31	35.48	21.46	<dl	300	<dl	<dl	<dl	99.28
42	43.00	35.50	21.74	<dl	<dl	<dl	<dl	345	100.27
43	44.45	34.95	20.48	<dl	<dl	<dl	<dl	550	99.94
44	44.62	34.75	19.95	<dl	<dl	210	<dl	<dl	99.34
45	43.14	35.09	20.74	<dl	<dl	<dl	<dl	<dl	98.96
46	41.58	35.52	22.18	455	<dl	<dl	405	<dl	99.37
47	44.82	34.92	19.47	455	<dl	<dl	<dl	<dl	99.26
48	45.47	34.64	19.55	<dl	<dl	<dl	<dl	<dl	99.66
49	44.38	34.93	20.19	<dl	<dl	250	<dl	<dl	99.53
50	44.28	35.10	20.21	<dl	<dl	<dl	<dl	<dl	99.59
51	42.58	35.52	20.95	<dl	<dl	335	<dl	<dl	99.09
52	41.57	35.65	21.88	<dl	240	<dl	<dl	<dl	99.12
53	43.04	35.32	21.49	<dl	<dl	<dl	<dl	<dl	99.85
54	45.15	34.74	20.19	<dl	<dl	265	<dl	<dl	100.11
55	45.05	34.61	19.97	<dl	235	<dl	<dl	<dl	99.65
56	45.44	34.77	19.71	<dl	465	<dl	<dl	<dl	99.98
57	44.55	35.05	19.94	<dl	<dl	<dl	<dl	245	99.56
58	44.52	35.16	20.15	390	<dl	<dl	<dl	<dl	99.86
59	44.68	34.69	19.92	<dl	<dl	<dl	<dl	<dl	99.30
60	45.39	34.74	19.79	<dl	<dl	235	<dl	<dl	99.94

TABLE A9 (cont.)

POINT	As mass %	Fe mass %	S mass %	Cu ppm	Ni ppm	Co ppm	Au ppm	Sb ppm	TOTAL mass %
61	45.18	34.91	20.19	<dl	<dl	<dl	<dl	<dl	100.27
62	45.27	34.91	20.01	<dl	<dl	240	<dl	<dl	100.20
63	44.64	34.95	20.27	<dl	370	1735	<dl	<dl	100.07
64	45.55	34.94	19.86	<dl	<dl	<dl	<dl	<dl	100.35
65	45.78	34.85	20.03	<dl	<dl	<dl	<dl	<dl	100.66
66	44.14	35.10	20.94	<dl	<dl	<dl	<dl	<dl	100.18
67	44.96	34.96	20.03	<dl	<dl	<dl	<dl	<dl	99.95
68	44.31	34.70	20.08	<dl	<dl	<dl	<dl	<dl	99.08
69	45.85	34.86	19.77	<dl	<dl	<dl	<dl	<dl	100.49
70	44.85	35.32	20.40	305	<dl	<dl	<dl	<dl	100.60
71	44.87	34.99	20.15	<dl	<dl	400	<dl	215	100.08
72	44.09	35.03	21.18	<dl	<dl	<dl	<dl	205	100.32
73	45.70	34.78	19.87	<dl	<dl	<dl	<dl	<dl	100.35
74	42.34	35.21	22.10	290	<dl	<dl	<dl	<dl	99.68
75	44.01	34.70	20.80	<dl	<dl	<dl	465	225	99.58
76	44.56	34.90	21.05	<dl	<dl	<dl	<dl	<dl	100.52
77	44.46	34.87	20.77	<dl	<dl	<dl	<dl	<dl	100.10
78	43.78	35.00	21.52	<dl	280	<dl	430	250	100.40
79	42.06	35.37	22.29	<dl	<dl	<dl	<dl	<dl	99.72
80	44.43	35.09	21.12	<dl	<dl	<dl	<dl	<dl	100.64
81	41.84	35.69	22.28	<dl	<dl	<dl	<dl	<dl	99.82
82	43.92	34.72	20.97	<dl	2280	<dl	<dl	<dl	99.84
83	43.24	34.80	21.35	<dl	<dl	285	<dl	<dl	99.43
84	45.92	34.30	19.81	<dl	<dl	<dl	<dl	<dl	100.04
85	45.86	34.32	19.96	<dl	<dl	<dl	<dl	<dl	100.14
86	42.61	34.55	21.31	<dl	<dl	1695	<dl	<dl	98.64
87	43.55	34.49	20.90	<dl	<dl	<dl	<dl	<dl	98.94
88	44.33	34.41	20.74	<dl	<dl	<dl	<dl	<dl	99.47
89	42.88	35.10	22.26	<dl	<dl	<dl	<dl	245	100.26
90	43.51	34.94	21.84	<dl	<dl	<dl	<dl	420	100.32
91	43.95	34.95	21.45	<dl	<dl	290	<dl	<dl	100.38
92	42.83	34.74	21.53	<dl	605	375	<dl	300	99.24

TABLE A9 (cont.)

POINT	As mass %	Fe mass %	S mass %	Cu ppm	Ni ppm	Co ppm	Au ppm	Sb ppm	TOTAL mass %
93	42.82	35.30	21.84	<dl	<dl	<dl	<dl	<dl	99.96
94	42.66	35.42	22.19	<dl	<dl	<dl	<dl	<dl	100.26
95	44.05	35.14	21.31	<dl	<dl	245	<dl	<dl	100.52
96	44.09	34.62	21.26	<dl	350	<dl	<dl	<dl	100.00
97	43.66	34.73	20.60	<dl	270	<dl	<dl	250	99.05
98	44.79	34.41	20.44	<dl	<dl	340	<dl	520	99.72
99	42.44	35.42	22.18	<dl	<dl	<dl	<dl	<dl	100.04
100	42.59	35.23	22.69	<dl	<dl	<dl	<dl	<dl	100.51
mean	44.04	34.99	20.81						99.88
std.dev	1.12	0.33	0.82						0.50

TABLE A10

RANDOM ANALYSIS OF SHEBA ARSENOPYRITE

Trace element detection limits (dl) are as follows: Cu 290ppm, Ni 240ppm, Co 210ppm, Au 350ppm, Sb 210ppm.

POINT	As mass %	Fe mass %	S mass %	Cu ppm	Ni ppm	Co ppm	Au ppm	Sb ppm	TOTAL mass %
1	43.59	34.79	21.10	<dl	555	<dl	490	<dl	99.58
2	43.70	34.85	21.30	265	530	<dl	850	<dl	100.02
3	43.09	35.08	21.50	<dl	1005	<dl	<dl	1160	99.88
4	43.64	34.86	21.26	<dl	1590	<dl	<dl	360	99.95
5	43.81	35.04	20.88	<dl	390	235	<dl	<dl	99.79
6	44.75	34.96	20.83	<dl	<dl	<dl	<dl	<dl	100.54
7	43.61	34.86	21.04	<dl	570	<dl	1065	<dl	99.67
8	44.42	35.00	20.44	<dl	400	<dl	<dl	<dl	99.90
9	42.19	34.87	20.90	<dl	605	215	<dl	<dl	98.04
10	42.44	35.05	21.59	<dl	890	<dl	1050	<dl	99.26
11	41.69	35.41	22.39	<dl	1270	215	<dl	1360	99.77
12	43.68	34.79	20.84	<dl	570	<dl	<dl	460	99.42
13	41.61	35.66	22.28	<dl	420	<dl	<dl	2060	99.80
14	43.22	34.83	21.31	<dl	3533	820	<dl	530	99.85
15	43.51	35.23	21.18	<dl	<dl	<dl	<dl	540	99.98
16	43.62	34.83	20.45	<dl	<dl	<dl	<dl	<dl	98.90
17	43.72	35.12	20.65	<dl	840	<dl	<dl	<dl	99.57
18	42.76	35.36	21.52	<dl	450	<dl	<dl	1200	99.81
19	43.59	35.04	21.42	<dl	1745	<dl	<dl	635	100.29
20	44.65	34.45	20.08	<dl	<dl	<dl	<dl	<dl	99.18
21	43.66	35.15	21.23	<dl	1625	<dl	455	300	100.27
22	43.45	35.11	21.14	<dl	275	<dl	<dl	<dl	99.74
23	40.71	35.71	22.67	<dl	<dl	<dl	<dl	3160	99.41
24	43.50	35.19	21.02	<dl	<dl	<dl	<dl	<dl	99.71
25	42.56	35.60	22.00	<dl	<dl	<dl	<dl	1815	100.34
26	43.40	34.93	21.33	<dl	<dl	<dl	<dl	<dl	99.65
27	42.15	35.39	21.87	<dl	560	<dl	<dl	505	99.52
28	43.52	35.00	20.79	<dl	255	<dl	<dl	<dl	99.34

TABLE A10 (cont.)

POINT	As mass %	Fe mass %	S mass %	Cu ppm	Ni ppm	Co ppm	Au ppm	Sb ppm	TOTAL mass %
29	41.09	35.76	22.33	<dl	<dl	<dl	<dl	1970	99.39
30	44.17	34.97	20.40	<dl	<dl	<dl	<dl	<dl	99.54
31	43.32	35.43	21.23	<dl	<dl	<dl	<dl	530	100.02
32	43.52	34.94	20.85	<dl	270	<dl	<dl	<dl	99.34
33	44.08	34.84	20.50	<dl	1375	<dl	515	240	99.64
34	43.68	34.79	20.26	<dl	435	<dl	635	260	98.86
35	44.04	35.07	20.61	<dl	480	<dl	<dl	<dl	99.77
36	44.38	34.92	21.03	<dl	470	<dl	<dl	<dl	100.38
37	42.94	35.12	21.34	<dl	660	<dl	<dl	925	99.56
38	43.45	35.11	21.05	<dl	<dl	<dl	<dl	<dl	99.61
39	41.91	35.42	22.08	<dl	<dl	<dl	<dl	600	99.47
40	43.53	35.07	21.06	<dl	970	<dl	710	<dl	99.83
41	43.29	35.44	21.52	<dl	<dl	<dl	<dl	1035	100.35
42	43.70	35.03	20.97	<dl	935	<dl	775	<dl	99.87
43	43.12	35.64	21.96	<dl	535	<dl	<dl	1125	100.89
44	42.87	35.26	21.66	<dl	680	<dl	840	<dl	99.94
45	42.04	35.12	21.46	<dl	540	<dl	400	<dl	98.71
46	43.74	35.03	20.66	<dl	<dl	<dl	<dl	<dl	99.43
47	42.07	35.54	22.15	<dl	285	<dl	<dl	2795	100.07
48	40.62	36.02	23.26	<dl	255	<dl	<dl	3620	100.28
49	41.35	36.10	23.05	<dl	290	<dl	<dl	3265	100.86
50	43.37	35.48	21.38	<dl	610	<dl	410	525	100.38
51	43.70	35.17	20.94	<dl	465	<dl	<dl	205	99.88
52	42.61	35.30	21.54	<dl	1560	<dl	<dl	220	99.63
53	44.45	34.80	20.33	<dl	<dl	<dl	<dl	<dl	99.58
54	43.74	35.11	21.27	<dl	<dl	<dl	680	<dl	100.19
55	43.43	34.97	21.18	<dl	2215	875	<dl	450	99.93
56	44.11	34.86	20.66	<dl	320	<dl	615	580	99.79
57	43.04	35.20	21.40	<dl	1540	<dl	395	240	99.86
58	43.86	35.05	20.93	<dl	<dl	210	525	245	99.94
59	44.21	34.86	20.94	<dl	865	<dl	<dl	1315	100.23
60	43.33	35.06	21.32	<dl	835	<dl	450	440	99.89

TABLE A10 (cont.)

POINT	As mass %	Fe mass %	S mass %	Cu ppm	Ni ppm	Co ppm	Au ppm	Sb ppm	TOTAL mass %
61	44.51	35.25	21.02	<dl	460	305	460	<dl	100.91
62	43.59	35.05	21.48	<dl	420	<dl	<dl	1125	100.27
63	44.18	34.93	20.65	<dl	1350	345	<dl	510	99.98
64	42.88	35.36	21.77	<dl	470	<dl	<dl	1760	100.23
65	43.86	34.87	21.36	<dl	1195	<dl	<dl	770	100.28
66	43.91	34.96	21.15	<dl	1245	<dl	850	<dl	100.23
67	45.11	34.81	20.28	<dl	570	<dl	1065	<dl	100.36
68	42.95	35.09	21.32	<dl	590	270	<dl	1095	99.56
69	42.92	35.00	20.99	<dl	1230	<dl	<dl	545	99.08
70	43.89	34.88	20.81	<dl	560	<dl	<dl	260	99.65
71	42.31	35.10	22.18	<dl	1435	240	450	1180	99.92
72	44.10	35.03	21.17	<dl	2165	260	865	<dl	100.62
73	43.87	35.22	21.25	<dl	<dl	<dl	<dl	725	100.40
74	42.89	35.20	21.23	<dl	<dl	<dl	<dl	930	99.41
75	43.82	35.00	20.91	<dl	595	235	<dl	1475	99.96
76	44.99	35.24	20.61	<dl	325	<dl	<dl	<dl	100.87
77	44.64	35.33	20.68	<dl	<dl	275	<dl	<dl	100.68
78	44.45	35.13	20.86	<dl	280	<dl	<dl	<dl	100.46
79	45.29	34.85	20.15	<dl	<dl	<dl	<dl	2015	100.49
80	43.33	34.78	20.87	<dl	765	<dl	<dl	300	99.09
81	43.61	34.87	20.83	<dl	1220	<dl	<dl	<dl	99.43
82	43.92	34.86	21.00	<dl	2230	250	430	365	100.11
83	42.62	35.51	22.24	<dl	<dl	<dl	<dl	<dl	100.37
84	44.17	35.27	20.99	<dl	275	<dl	<dl	330	100.48
85	44.80	35.16	20.55	<dl	255	<dl	480	<dl	100.57
86	43.36	35.26	21.10	<dl	645	<dl	<dl	490	99.83
87	43.96	34.83	21.07	<dl	325	235	<dl	345	99.94
88	44.33	34.94	20.90	<dl	585	<dl	470	<dl	100.27
89	44.21	34.51	20.12	<dl	800	<dl	<dl	325	98.95
90	44.08	35.12	21.20	<dl	305	<dl	<dl	1255	100.55
91	44.56	35.19	20.57	<dl	900	<dl	<dl	<dl	100.41
92	44.39	35.08	20.59	<dl	780	<dl	<dl	<dl	100.14

TABLE A10 (cont.)

POINT	As mass %	Fe mass %	S mass %	Cu ppm	Ni ppm	Co ppm	Au ppm	Sb ppm	TOTAL mass %
93	43.92	35.38	21.10	<dl	<dl	<dl	<dl	995	100.50
94	44.07	35.16	21.10	650	<dl	<dl	875	345	100.52
95	43.97	35.16	20.75	<dl	<dl	<dl	430	240	99.95
96	43.61	34.63	20.71	<dl	325	<dl	<dl	240	99.00
97	43.10	34.96	21.41	290	740	<dl	<dl	215	99.58
98	44.57	35.16	20.72	<dl	530	330	<dl	765	100.61
99	43.43	35.20	21.62	<dl	560	<dl	<dl	1075	100.42
100	42.94	35.05	21.86	<dl	<dl	<dl	<dl	1815	100.04
mean	43.48	35.11	21.17						99.90
std.dev	0.91	0.28	0.60						0.52

TABLE A11

RANDOM MICROPROBE ANALYSIS OF WEST AFRICAN ARSENOPYRITE

Trace element detection limits (dl) are as follows: Cu 290ppm, Ni 240ppm, Co 210ppm, Au 350ppm, Sb 210ppm

Point	As mass %	Fe mass %	S mass %	Cu ppm	Ni ppm	Co ppm	Au ppm	Sb ppm	TOTAL mass %
1	42.69	35.44	22.00	<dl	<dl	290	<dl	<dl	100.16
2	41.69	35.60	22.94	<dl	300	<dl	<dl	<dl	100.25
3	42.51	35.49	22.07	<dl	330	360	<dl	<dl	100.14
4	42.80	35.41	22.00	<dl	<dl	230	760	<dl	100.31
5	43.46	35.40	21.34	<dl	<dl	<dl	<dl	<dl	100.20
6	43.09	35.47	21.92	<dl	<dl	<dl	<dl	<dl	100.49
7	42.40	35.43	22.07	<dl	<dl	360	810	<dl	100.01
8	42.57	35.67	22.42	<dl	255	<dl	1320	<dl	100.81
9	42.45	35.84	22.31	<dl	<dl	<dl	<dl	<dl	100.60
10	45.42	34.93	20.41	<dl	<dl	870	<dl	865	100.93
11	41.85	35.55	22.61	<dl	850	885	<dl	1410	100.31
12	43.36	35.34	21.78	<dl	<dl	<dl	<dl	<dl	100.47
13	43.06	35.48	22.09	<dl	<dl	220	1525	<dl	100.81
14	43.12	35.30	21.63	<dl	400	<dl	1175	<dl	100.21
15	43.06	35.34	21.65	<dl	<dl	<dl	700	<dl	100.12
16	43.07	35.25	21.74	<dl	920	740	<dl	<dl	100.23
17	42.90	35.49	21.96	<dl	<dl	<dl	<dl	<dl	100.35
18	42.04	35.41	21.91	<dl	490	305	<dl	<dl	99.44
19	41.69	35.18	22.43	<dl	<dl	220	<dl	375	99.36
20	42.51	35.66	22.01	<dl	<dl	345	<dl	<dl	100.22
21	42.61	34.81	21.38	<dl	<dl	225	600	<dl	98.89
22	41.49	35.88	23.06	<dl	260	385	<dl	350	100.53
23	41.05	35.81	22.64	<dl	<dl	320	<dl	270	99.56
24	42.75	35.31	21.75	340	<dl	650	<dl	250	99.93
25	42.16	35.27	22.08	<dl	<dl	515	<dl	<dl	99.57
26	45.35	34.56	19.77	<dl	290	<dl	400	<dl	99.75
27	44.17	34.90	20.63	<dl	<dl	<dl	<dl	<dl	99.70
28	43.38	35.22	21.34	<dl	<dl	<dl	<dl	<dl	99.94

TABLE A11 (cont.)

Point	As mass %	Fe mass %	S mass %	Cu ppm	Ni ppm	Co ppm	Au ppm	Sb ppm	TOTAL mass %
29	42.50	35.59	22.54	265	<dl	<dl	840	<dl	100.74
30	42.63	35.48	22.15	<dl	<dl	320	770	<dl	100.38
31	43.01	35.53	21.71	<dl	<dl	310	810	<dl	100.35
32	43.33	35.42	21.67	<dl	<dl	300	<dl	<dl	100.45
33	42.52	35.54	22.20	<dl	245	445	<dl	<dl	100.33
34	42.60	35.81	22.23	<dl	<dl	380	415	<dl	100.71
35	42.60	35.58	22.01	<dl	<dl	<dl	<dl	320	100.22
36	41.99	35.67	23.01	<dl	<dl	295	<dl	<dl	100.69
37	43.02	35.41	22.26	<dl	<dl	<dl	<dl	<dl	100.69
38	41.99	35.46	22.29	<dl	320	<dl	405	<dl	99.81
39	44.37	35.05	20.96	<dl	270	490	<dl	215	100.49
40	44.59	34.98	20.89	<dl	290	3410	<dl	285	100.85
41	45.66	34.49	20.05	<dl	<dl	4095	<dl	735	100.69
42	41.01	35.99	23.43	<dl	<dl	495	<dl	<dl	100.48
43	42.10	35.54	22.25	<dl	<dl	355	<dl	<dl	99.92
44	43.79	35.05	21.64	<dl	<dl	500	<dl	<dl	100.53
45	43.44	35.20	21.78	<dl	<dl	670	<dl	<dl	100.52
46	41.43	35.74	23.02	375	<dl	<dl	<dl	1085	100.35
47	40.77	35.68	23.20	<dl	<dl	<dl	<dl	1610	99.81
48	42.16	35.72	22.55	<dl	<dl	<dl	<dl	<dl	100.44
49	43.05	35.47	22.06	<dl	<dl	<dl	<dl	<dl	100.57
50	42.74	35.49	22.35	<dl	<dl	<dl	<dl	<dl	100.58
51	42.46	35.34	22.10	<dl	<dl	<dl	<dl	<dl	99.91
52	41.74	35.16	22.43	<dl	<dl	235	<dl	<dl	99.36
53	42.05	35.58	22.27	<dl	<dl	830	<dl	<dl	99.99
54	40.80	35.56	22.78	<dl	270	380	520	<dl	99.26
55	42.29	35.33	22.84	<dl	<dl	575	<dl	<dl	100.51
56	42.15	35.17	22.49	<dl	300	405	410	<dl	99.93
57	45.66	34.28	20.01	<dl	390	990	<dl	395	100.11
58	45.58	34.56	20.19	<dl	<dl	1005	<dl	485	100.47
59	42.81	35.54	22.11	<dl	<dl	<dl	<dl	<dl	100.45
60	42.21	35.54	22.75	<dl	285	770	775	<dl	100.69

TABLE A11 (cont.)

Point	As mass %	Fe mass %	S mass %	Cu ppm	Ni ppm	Co ppm	Au ppm	Sb ppm	TOTAL mass %
61	41.68	35.90	23.04	<dl	<dl	350	<dl	<dl	100.66
62	39.48	36.36	24.26	<dl	690	495	685	<dl	100.28
63	42.28	34.89	22.06	<dl	340	<dl	720	<dl	99.34
64	43.56	35.26	22.03	<dl	<dl	305	410	<dl	100.92
65	41.09	35.87	23.52	<dl	<dl	<dl	<dl	<dl	100.48
66	40.49	36.01	23.60	<dl	295	480	<dl	<dl	100.18
67	40.85	35.87	23.41	<dl	510	<dl	<dl	335	100.21
68	41.99	35.60	22.51	<dl	<dl	225	<dl	<dl	100.13
69	43.38	35.23	21.76	<dl	<dl	<dl	620	<dl	100.43
70	43.32	35.27	21.85	295	<dl	<dl	<dl	<dl	100.47
71	41.95	35.46	22.69	<dl	335	<dl	615	<dl	100.19
72	42.36	35.36	22.21	<dl	<dl	<dl	1140	<dl	100.04
73	42.20	35.36	22.10	<dl	545	<dl	<dl	<dl	99.71
74	42.99	35.44	22.33	<dl	<dl	885	<dl	<dl	100.85
75	44.24	34.80	21.00	<dl	805	460	<dl	<dl	100.17
76	42.29	35.24	22.12	<dl	<dl	955	<dl	<dl	99.75
77	42.40	35.13	22.68	<dl	<dl	<dl	1045	<dl	100.32
78	41.60	35.39	23.10	<dl	<dl	<dl	1400	<dl	100.23
79	42.69	35.04	22.37	<dl	<dl	450	<dl	<dl	100.15
80	42.65	35.13	21.87	<dl	<dl	225	400	<dl	99.71
81	41.63	35.65	22.75	<dl	<dl	<dl	<dl	<dl	100.03
82	42.03	35.33	22.20	<dl	315	430	420	<dl	99.68
83	42.28	35.44	22.90	<dl	<dl	<dl	<dl	<dl	100.61
84	42.26	35.04	22.51	<dl	<dl	220	<dl	<dl	99.83
85	42.67	35.31	22.09	<dl	<dl	325	<dl	<dl	100.12
86	42.95	35.04	22.14	<dl	<dl	645	<dl	<dl	100.19
87	41.19	35.67	23.19	335	1335	450	1025	<dl	100.36
88	40.52	35.49	23.14	<dl	595	<dl	<dl	<dl	99.22
89	41.24	35.57	23.40	<dl	<dl	310	<dl	<dl	100.23
90	41.21	35.61	23.16	<dl	460	<dl	<dl	<dl	100.03
91	42.68	35.69	22.47	<dl	<dl	315	<dl	<dl	100.87
92	42.36	35.38	22.43	<dl	<dl	<dl	1255	<dl	100.30

TABLE A11 (cont.)

Point	As mass %	Fe mass %	S mass %	Cu ppm	Ni ppm	Co ppm	Au ppm	Sb ppm	TOTAL mass %
93	41.83	35.40	22.14	<dl	<dl	<dl	<dl	<dl	99.36
94	43.09	35.17	21.73	<dl	<dl	<dl	<dl	<dl	99.99
95	41.67	35.43	22.85	540	<dl	275	<dl	<dl	100.04
96	41.70	35.27	22.77	<dl	325	325	560	<dl	99.87
97	42.59	35.30	22.27	<dl	275	<dl	<dl	<dl	100.19
98	42.29	35.35	22.30	<dl	<dl	<dl	<dl	<dl	99.93
99	41.63	35.47	22.67	<dl	<dl	255	920	<dl	99.90
100	41.74	35.54	22.63	<dl	<dl	<dl	595	265	99.99
mean	42.51	35.39	22.20						100.19
std.dev	1.11	0.33	0.78						0.42

TABLE A12

ZONE ANALYSIS OF KLIPWAL ARSENOPYRITE

Trace element detection limits (dl) are as follows: Cu 290ppm, Ni 240ppm, Co 210ppm, Au 350ppm.

Zone*	As mass %	Fe mass %	S mass %	Cu ppm	Ni ppm	Co ppm	Au ppm	Sb ppm	TOTAL mass %
Bright	43.54	36.06	20.72	<dl	<dl	<dl	<dl	<dl	100.33
Bright	44.96	35.67	20.39	<dl	585	<dl	<dl	235	101.11
mean	44.25	35.87	20.56						100.72
Dark	42.99	34.64	21.18	<dl	3070	810	<dl	<dl	99.19
Dark	40.95	35.90	22.26	<dl	<dl	<dl	<dl	<dl	99.11
mean	41.97	35.27	21.72						99.15

*Zones are distinguished by the intensity of the backscattered electron image.

TABLE A13

ZONE ANALYSIS OF ZANDRIVIER ARSENOPYRITE

Trace element detection limits (dl) are as follows: Cu 290ppm, Ni 240ppm, Co 210ppm, Au 350ppm, Sb 210ppm.
*Zones are distinguished by the intensity of the backscattered electron image.

*Bright zone	As mass %	Fe mass %	S mass %	Cu ppm	Ni ppm	Co ppm	Au ppm	Sb ppm	TOTAL mass %
A26	43.71	35.24	19.68	<dl	<dl	<dl	<dl	<dl	98.63
	43.51	35.12	19.65	<dl	<dl	<dl	<dl	<dl	98.28
A27	43.80	35.15	20.49	<dl	<dl	<dl	<dl	<dl	99.44
	43.15	35.42	20.75	450	<dl	260	<dl	<dl	99.39
A 28	44.13	34.90	20.12	<dl	<dl	220	<dl	<dl	99.17
	45.02	34.69	20.06	<dl	255	<dl	<dl	<dl	99.79
A 29	45.09	34.27	19.32	370	<dl	<dl	<dl	<dl	98.72
	44.72	34.20	19.54	330	<dl	270	<dl	215	98.55
A30	44.79	34.20	19.99	<dl	<dl	250	<dl	<dl	99.01
	43.86	34.59	19.92	<dl	<dl	<dl	<dl	515	98.42
A31	43.16	35.03	20.02	<dl	<dl	<dl	<dl	310	98.24
	45.22	34.54	19.79	<dl	<dl	<dl	<dl	<dl	99.54
A 35	44.50	34.60	19.42	<dl	<dl	<dl	<dl	<dl	98.51
	44.67	33.91	19.50	<dl	<dl	235	<dl	<dl	98.11
A36	45.28	34.16	19.65	<dl	<dl	<dl	<dl	<dl	99.14
	45.87	34.37	19.57	<dl	<dl	<dl	<dl	<dl	99.81
A 37	45.81	34.05	19.81	<dl	<dl	<dl	<dl	<dl	99.67
	45.42	34.09	19.74	345	<dl	210	<dl	<dl	99.30
A 38	44.99	34.17	19.49	<dl	<dl	<dl	<dl	<dl	98.65
	44.84	34.37	19.56	<dl	<dl	<dl	<dl	<dl	98.78
A 46	44.61	34.33	19.72	<dl	<dl	<dl	<dl	<dl	98.65
	44.59	34.54	19.80	<dl	<dl	<dl	<dl	<dl	98.93
A 47	44.32	34.96	19.95	<dl	<dl	<dl	<dl	<dl	99.23
	44.08	34.94	19.94	<dl	<dl	<dl	<dl	<dl	98.96
A 48	45.25	34.51	20.00	<dl	<dl	510	<dl	<dl	99.81
	44.97	34.61	20.13	<dl	<dl	<dl	<dl	<dl	99.72

TABLE A13 (cont.)

Bright zone	As mass %	Fe mass %	S mass %	Cu ppm	Ni ppm	Co ppm	Au ppm	Sb ppm	TOTAL mass %
A 49	44.86	34.37	19.51	<dl	<dl	<dl	<dl	<dl	98.74
	45.28	34.56	19.45	<dl	<dl	230	<dl	<dl	99.32
A 50	44.84	34.44	19.63	<dl	1640	<dl	<dl	<dl	99.08
	44.68	35.35	20.21	<dl	<dl	<dl	<dl	<dl	100.23
mean	44.63	34.59	19.81						99.06
std.dev	0.70	0.41	0.32						0.54

Medium zone	As mass %	Fe mass %	S mass %	Cu ppm	Ni ppm	Co ppm	Au ppm	Sb ppm	TOTAL mass %
A27	42.33	35.36	21.03	<dl	<dl	<dl	<dl	<dl	98.72
	42.09	35.49	21.17	<dl	<dl	<dl	<dl	265	98.77
A28	44.06	33.79	20.33	<dl	<dl	<dl	<dl	<dl	98.19
	43.80	34.12	20.56	<dl	<dl	<dl	<dl	<dl	98.48
A29	41.84	35.43	21.42	<dl	<dl	220	<dl	365	98.74
	41.91	35.32	21.36	555	<dl	<dl	<dl	<dl	98.65
A31	43.36	35.20	21.14	<dl	<dl	<dl	<dl	595	99.76
	42.52	35.00	21.09	<dl	250	295	<dl	<dl	98.66
A35	42.05	34.97	21.20	<dl	<dl	240	<dl	305	98.28
	42.65	34.67	21.14	<dl	260	230	<dl	<dl	98.51
A46	43.82	34.48	20.49	<dl	<dl	524	<dl	<dl	98.85
	44.21	34.25	20.71	450	<dl	<dl	<dl	<dl	99.21
A47	44.73	34.61	20.26	<dl	<dl	<dl	<dl	245	99.63
	44.37	34.42	20.43	<dl	<dl	<dl	<dl	<dl	99.22
A48	44.45	34.97	20.63	<dl	515	385	<dl	<dl	100.14
	44.54	34.33	20.57	<dl	<dl	<dl	<dl	<dl	99.43
A49	45.18	34.74	20.41	<dl	555	<dl	<dl	235	100.40
	45.38	34.60	20.12	<dl	<dl	500	<dl	<dl	100.15
A50	43.96	34.55	20.28	<dl	<dl	<dl	<dl	<dl	98.80
	43.78	35.02	20.50	<dl	<dl	<dl	<dl	<dl	99.29
mean	43.55	34.77	20.74						99.09
std.dev	1.13	0.47	0.41						0.65

TABLE A13 (cont.)

Dark zone	As mass %	Fe mass %	S mass %	Cu ppm	Ni ppm	Co ppm	Au ppm	Sb ppm	TOTAL mass %
A 26	43.91	35.62	20.64	<dl	<dl	<dl	<dl	<dl	100.17
	43.46	35.09	20.27	<dl	<dl	<dl	<dl	<dl	98.82
A 27	41.14	35.87	21.54	<dl	1105	225	<dl	<dl	98.68
	41.34	35.93	21.62	<dl	240	445	<dl	470	99.01
A28	42.55	34.92	21.44	<dl	<dl	240	<dl	<dl	98.93
	42.51	34.42	21.43	<dl	<dl	265	<dl	<dl	98.38
A29	42.60	34.16	21.67	<dl	<dl	<dl	<dl	270	98.45
	42.08	34.78	21.72	<dl	<dl	<dl	<dl	<dl	98.58
A30	42.66	34.78	21.35	<dl	<dl	<dl	<dl	<dl	98.79
	43.61	34.90	21.35	<dl	<dl	<dl	<dl	<dl	99.86
A31	42.30	34.86	21.22	<dl	<dl	<dl	<dl	270	98.41
	41.32	35.62	21.76	<dl	440	<dl	<dl	<dl	98.75
A 36	42.88	34.41	20.84	<dl	<dl	<dl	<dl	<dl	98.13
	43.61	34.27	20.34	<dl	<dl	<dl	<dl	265	98.25
A37	43.57	34.51	20.17	<dl	<dl	<dl	<dl	<dl	98.25
	44.11	34.24	20.13	<dl	<dl	<dl	<dl	565	98.53
A38	44.48	34.89	20.14	<dl	<dl	305	<dl	<dl	99.54
	44.22	34.69	20.12	<dl	<dl	<dl	<dl	<dl	99.03
A46	43.28	34.40	21.41	<dl	<dl	<dl	<dl	240	99.11
	42.77	35.06	21.34	<dl	<dl	<dl	<dl	<dl	99.17
A47	42.79	34.45	21.44	<dl	<dl	<dl	<dl	<dl	98.67
	43.49	35.09	21.47	<dl	255	<dl	<dl	<dl	100.08
A48	42.99	35.25	21.18	<dl	<dl	345	<dl	<dl	99.45
	42.62	35.39	20.48	<dl	400	<dl	<dl	<dl	98.53
A49	44.10	34.85	20.50	<dl	<dl	<dl	<dl	<dl	99.45
	44.60	35.01	20.14	<dl	485	460	<dl	<dl	99.85
A50	42.14	35.20	21.64	<dl	275	700	<dl	<dl	99.07
	43.10	35.26	21.39	<dl	285	1480	<dl	<dl	99.92
mean	43.01	34.93	21.03						99.00
std.dev	0.93	0.48	0.59						0.59

TABLE A13 (cont.)

Unzoned	As mass %	Fe mass %	S mass %	Cu ppm	Ni ppm	Co ppm	Au ppm	Sb ppm	TOTAL mass %
A 24	45.13	34.62	19.89	<dl	<dl	<dl	<dl	<dl	99.65
	45.11	34.68	20.05	340	<dl	<dl	<dl	<dl	99.88
A 25	44.19	34.74	19.98	<dl	<dl	<dl	<dl	<dl	98.91
	44.53	34.37	19.90	<dl	<dl	<dl	<dl	270	98.83
A 45	44.82	34.58	20.17	<dl	<dl	<dl	<dl	<dl	99.58
	44.85	34.31	19.81	460	<dl	<dl	<dl	<dl	99.00
	44.81	34.13	20.39	<dl	<dl	<dl	<dl	<dl	99.33
	44.97	33.94	20.21	<dl	<dl	220	<dl	<dl	99.15
mean	44.80	34.42	20.05						99.29
std.dev	0.31	0.29	0.20						0.38

TABLE A14

ZONE ANALYSIS OF SHEBA ARSENOPYRITE

Trace element detection limits (dl) are as follows: Cu 290ppm, Ni 240ppm, Co 210ppm, Au 350ppm, Sb 210ppm.
*Zones are distinguished by the intensity of the backscattered electron image.

Bright zone	As mass %	Fe mass %	S mass %	Cu ppm	Ni ppm	Co ppm	Au ppm	Sb ppm	TOTAL mass %
A1	43.66	34.00	20.46	<dl	3990	2130	<dl	800	98.81
	44.29	33.31	20.39	<dl	6220	4470	<dl	870	99.15
A2	44.05	34.62	20.96	<dl	290	<dl	880	<dl	99.74
	44.14	34.53	20.98	<dl	950	<dl	480	<dl	99.79
A3	45.20	34.47	20.99	<dl	560	<dl	1340	240	100.88
	43.22	35.05	21.86	<dl	870	<dl	<dl	670	100.28
A4	44.13	34.50	21.04	<dl	<dl	<dl	<dl	<dl	99.67
	43.37	34.36	21.17	320	<dl	<dl	<dl	<dl	98.93
A5	43.44	35.05	21.32	<dl	830	<dl	390	<dl	99.93
	45.03	34.92	21.54	<dl	640	<dl	370	340	101.62
A7	44.28	34.42	21.29	<dl	<dl	650	<dl	<dl	100.05
	45.39	34.86	21.62	<dl	<dl	<dl	<dl	<dl	101.87
A8	44.33	34.76	20.55	<dl	410	<dl	430	<dl	99.73
	45.46	34.52	21.02	<dl	<dl	<dl	<dl	<dl	101.00
A9	45.79	34.79	20.13	<dl	470	590	<dl	<dl	100.81
	45.06	34.47	20.22	<dl	<dl	640	<dl	210	99.84
A10	44.08	34.95	20.21	<dl	420	<dl	<dl	<dl	99.29
	44.39	34.58	20.18	<dl	320	<dl	880	<dl	99.27
A11	44.78	34.75	19.57	<dl	<dl	<dl	850	<dl	99.19
	46.11	33.65	19.60	<dl	<dl	590	420	<dl	99.47
A12	43.06	35.75	21.21	<dl	<dl	280	900	<dl	100.14
	45.52	34.88	20.63	<dl	<dl	<dl	<dl	<dl	101.02
A13	43.54	34.66	21.31	<dl	930	<dl	<dl	<dl	99.60
	44.93	34.55	20.61	<dl	680	<dl	<dl	300	100.19
A15	43.64	34.28	20.84	<dl	<dl	<dl	515	<dl	98.82
	45.87	34.06	20.36	<dl	825	<dl	720	<dl	100.44

TABLE A14 (cont.)

Bright zone	As mass %	Fe mass %	S mass %	Cu ppm	Ni ppm	Co ppm	Au ppm	Sb ppm	TOTAL mass %
A16	45.08	34.98	20.57	<dl	<dl	<dl	<dl	260	100.65
	43.30	35.26	20.70	<dl	<dl	<dl	955	<dl	99.35
A17	44.11	34.94	21.44	575	265	<dl	745	<dl	100.65
	44.63	34.40	21.08	<dl	455	<dl	510	470	100.24
A18	44.35	34.68	20.94	<dl	<dl	<dl	<dl	<dl	99.98
	44.11	35.09	20.70	<dl	<dl	<dl	<dl	<dl	99.89
A19	44.87	34.82	21.39	340	<dl	<dl	355	295	101.18
	45.50	35.35	20.64	<dl	<dl	<dl	<dl	260	101.51
A21	45.28	34.15	20.38	680	<dl	245	530	<dl	99.96
	45.12	34.75	20.92	<dl	695	<dl	<dl	<dl	100.86
A22	43.46	36.09	20.90	<dl	<dl	<dl	<dl	410	100.49
	43.67	36.17	20.53	<dl	<dl	<dl	<dl	400	100.41
A23	44.42	34.80	20.82	<dl	615	<dl	940	<dl	100.20
	44.03	35.75	21.63	<dl	450	<dl	525	<dl	101.50
G7	44.24	35.06	20.69	<dl	325	<dl	1145	<dl	100.14
	42.73	35.63	20.90	<dl	465	<dl	740	<dl	99.38
G8	46.26	34.81	19.87	<dl	4220	1770	<dl	855	101.63
	45.71	35.06	19.63	<dl	5305	1180	<dl	1330	101.19
G15	43.73	35.91	20.37	<dl	420	<dl	<dl	210	100.07
	42.80	36.08	20.21	<dl	<dl	<dl	<dl	445	99.13
mean	44.44	34.84	20.75						100.17
std.dev	0.90	0.60	0.54						0.81

TABLE A14 (cont.)

Dark zone	As mass %	Fe mass %	S mass %	Cu ppm	Ni ppm	Co ppm	Au ppm	Sb ppm	TOTAL mass %
A1	38.97	35.80	23.60	<dl	<dl	610	<dl	3180	98.74
	40.14	35.81	23.09	<dl	<dl	<dl	<dl	3220	99.36
A2	41.86	35.28	22.93	<dl	<dl	<dl	1080	1200	100.30
	41.93	35.22	22.95	<dl	430	680	<dl	2020	100.41
A3	40.31	35.79	23.91	<dl	<dl	<dl	<dl	3500	100.36
	40.59	35.68	24.20	<dl	<dl	<dl	<dl	4210	100.89
A4	39.88	35.44	23.97	<dl	<dl	<dl	<dl	3520	99.65
	40.18	35.36	23.95	<dl	<dl	<dl	<dl	3430	99.84
A5	40.22	35.88	23.97	<dl	<dl	<dl	<dl	4750	100.54
	42.88	35.14	22.60	<dl	1360	<dl	<dl	1060	100.86
A7	39.98	35.44	23.45	<dl	<dl	<dl	<dl	2220	99.10
	39.85	35.60	23.37	<dl	<dl	640	<dl	3090	99.20
A8	40.31	35.58	23.24	<dl	<dl	<dl	<dl	4610	99.59
	39.62	35.82	23.17	<dl	<dl	<dl	<dl	4530	99.06
A9	42.06	35.04	22.08	<dl	<dl	<dl	<dl	1880	99.36
	41.35	35.39	21.96	<dl	<dl	<dl	<dl	1760	98.88
A10	41.29	35.52	21.74	<dl	<dl	<dl	8640	2630	99.68
	41.21	35.54	21.98	<dl	<dl	<dl	<dl	2340	98.95
A11	40.81	35.69	21.84	<dl	<dl	<dl	<dl	3010	98.64
	40.82	35.47	21.75	<dl	<dl	<dl	<dl	3750	98.41
A12	42.14	35.75	22.01	<dl	<dl	<dl	<dl	1775	100.08
	41.99	36.20	22.21	<dl	<dl	<dl	<dl	1595	100.56
A13	40.86	35.13	23.11	<dl	610	235	<dl	3530	99.53
	40.29	35.46	23.26	<dl	250	<dl	<dl	3805	99.41
A15	40.56	35.32	23.38	<dl	<dl	<dl	<dl	4075	99.67
	40.20	34.99	23.04	<dl	<dl	<dl	<dl	4145	98.64
A16	41.92	35.55	23.03	<dl	<dl	230	<dl	4080	100.92
	41.53	35.35	22.85	<dl	<dl	<dl	<dl	3510	100.09
A17	41.14	35.25	22.69	<dl	<dl	<dl	<dl	3440	99.43
	40.95	35.06	22.74	<dl	<dl	<dl	<dl	4215	99.16
A18	41.28	36.05	22.82	<dl	<dl	<dl	<dl	4180	100.57
	41.03	35.73	22.20	<dl	<dl	<dl	<dl	2290	99.18

TABLE A14 (cont.)

Dark zone	As mass %	Fe mass %	S mass %	Cu ppm	Ni ppm	Co ppm	Au ppm	Sb ppm	TOTAL mass %
A19	41.53	35.69	22.92	<dl	<dl	250	<dl	1865	100.35
	42.16	35.43	22.55	<dl	<dl	<dl	<dl	1585	100.30
A21	41.34	35.77	23.25	<dl	<dl	<dl	<dl	3345	100.70
	42.17	35.33	22.98	<dl	<dl	<dl	<dl	2915	100.76
A22	42.64	35.00	21.95	<dl	<dl	<dl	<dl	950	99.69
	42.46	35.50	22.25	<dl	<dl	<dl	<dl	1635	100.37
A23	41.69	36.33	22.59	<dl	<dl	<dl	<dl	2370	100.85
	41.92	34.98	22.15	<dl	<dl	230	<dl	2050	99.27
G7	41.75	36.28	21.84	<dl	<dl	<dl	<dl	1775	100.05
	41.52	36.32	22.23	<dl	<dl	<dl	<dl	1845	100.25
G8	40.16	36.53	22.67	<dl	<dl	<dl	<dl	3550	99.72
	39.81	36.91	22.95	<dl	<dl	<dl	<dl	4035	100.07
G15	42.42	35.55	21.56	<dl	<dl	<dl	<dl	1545	99.68
	42.37	35.68	21.75	<dl	<dl	<dl	<dl	1325	99.93
mean	41.13	35.60	22.75					2855	99.81
std.dev	0.94	0.42	0.70					1090	0.68

Medium zone	As mass %	Fe mass %	S mass %	Cu ppm	Ni ppm	Co ppm	Au ppm	Sb ppm	TOTAL mass %
A4	43.01	34.64	22.29	<dl	1040	<dl	<dl	330	100.08
	43.46	34.44	21.88	<dl	930	<dl	<dl	220	99.90
A11	43.76	34.91	20.42	<dl	<dl	<dl	<dl	<dl	99.09
	44.54	34.36	20.70	<dl	<dl	<dl	<dl	<dl	99.59
A12	43.22	35.79	20.41	<dl	330	<dl	880	<dl	99.54
	44.21	34.80	21.07	360	405	<dl	605	<dl	100.21
A18	42.10	35.37	21.88	355	<dl	<dl	<dl	1355	99.52
	43.06	35.06	20.91	<dl	425	<dl	365	265	99.13
A22	42.96	35.57	21.48	390	<dl	215	845	<dl	100.16
	43.26	36.09	20.95	530	<dl	<dl	780	290	100.46
mean	43.36	35.10	21.20						99.77
std.dev	0.69	0.58	0.65						0.47

TABLE A14 (cont.)

Unzoned	As mass %	Fe mass %	S mass %	Cu ppm	Ni ppm	Co ppm	Au ppm	Sb ppm	TOTAL mass %
G1	44.03	35.12	21.14	<dl	<dl	<dl	<dl	<dl	100.30
	43.95	35.40	21.38	<dl	<dl	<dl	<dl	<dl	100.73
	41.53	36.02	22.58	<dl	<dl	<dl	<dl	3220	100.46
	41.32	35.82	22.80	<dl	<dl	<dl	<dl	2540	100.20
mean	42.71	35.59	21.98						100.42
std.dev	1.48	0.40	0.84						0.23

TABLE A15

ZONE ANALYSIS OF W.AFRICAN ARSENOPYRITE

Trace element detection limits (dl) are as follows: Cu 290ppm, Ni 240ppm, Co 210ppm, Au 350ppm, Sb 210ppm.
*Zones are distinguished by the intensity of the backscattered electron image.

V.bright zone	As mass %	Fe mass %	S mass %	Cu ppm	Ni ppm	Co ppm	Au ppm	Sb ppm	TOTAL mass %
A51	43.80	33.61	19.39	<dl	445	7800	<dl	680	97.69
	43.63	33.77	19.96	<dl	<dl	6845	<dl	585	98.10
G47A	45.90	33.74	19.80	<dl	<dl	5215	<dl	495	100.00
	45.95	33.37	19.85	<dl	<dl	5745	<dl	650	99.81
G47B	45.70	35.24	19.43	<dl	385	2685	<dl	710	100.74
	45.09	34.79	19.43	<dl	405	2730	365	800	99.75
G48	46.34	33.88	19.14	<dl	555	4240	<dl	830	99.92
	47.53	33.96	19.09	<dl	650	4135	<dl	320	101.09
G49	45.60	35.07	19.85	340	<dl	1045	<dl	450	100.71
	45.79	34.88	19.49	<dl	<dl	1005	<dl	560	100.32
G50	44.22	34.67	20.08	<dl	3435	3650	<dl	340	99.71
	44.05	34.99	20.07	<dl	5805	1270	<dl	275	99.85
G51	46.70	34.62	19.41	<dl	<dl	4710	<dl	320	101.24
	46.02	34.31	19.60	<dl	345	5435	<dl	805	100.59
G53	45.68	35.27	19.57	<dl	375	1530	<dl	685	100.78
	46.56	35.28	19.64	<dl	<dl	1040	<dl	380	101.62
G56	42.00	35.91	19.93	<dl	2925	505	<dl	215	98.21
	43.61	34.28	20.07	<dl	3515	565	<dl	<dl	98.37
G58	44.10	34.62	19.96	<dl	<dl	6775	<dl	540	99.40
	44.64	34.62	19.02	<dl	350	2590	<dl	835	98.65
G66	44.90	34.22	19.43	<dl	540	5400	<dl	585	99.20
	44.89	33.95	19.33	<dl	<dl	5825	<dl	380	98.78
mean	45.12	34.50	19.61			3670			99.75
std.dev	1.28	0.65	0.33			2285			1.10

TABLE A15 (cont.)

Bright zone	As mass %	Fe mass %	S mass %	Cu ppm	Ni ppm	Co ppm	Au ppm	Sb ppm	TOTAL mass %
A51	43.20	35.63	21.06	<dl	<dl	<dl	<dl	<dl	99.89
	42.69	35.47	21.30	<dl	300	<dl	<dl	<dl	99.49
G47A	43.87	34.30	20.36	<dl	<dl	2685	<dl	310	98.83
	44.31	34.04	20.50	<dl	280	6815	<dl	635	99.63
G47B	44.76	35.22	20.34	<dl	450	5230	<dl	485	100.94
	44.28	33.38	20.05	<dl	<dl	3890	<dl	870	98.19
G48	44.43	33.90	21.18	<dl	1160	12490	<dl	300	100.90
	44.98	34.09	20.90	<dl	340	7185	<dl	565	100.78
G49	44.20	34.14	20.43	<dl	<dl	4890	<dl	315	99.29
	43.47	34.19	20.62	<dl	<dl	6715	<dl	615	99.01
G50	41.30	37.66	21.23	<dl	<dl	<dl	<dl	<dl	100.19
	41.32	36.84	21.25	<dl	<dl	<dl	<dl	<dl	99.41
G51	44.04	33.97	20.78	<dl	640	12915	<dl	685	100.21
	44.57	34.17	20.44	<dl	<dl	12645	<dl	665	100.51
G53	44.93	35.16	20.78	<dl	265	2615	<dl	595	101.21
	43.85	35.22	21.00	<dl	335	1100	<dl	355	100.26
G56	40.66	36.54	21.85	<dl	<dl	<dl	<dl	<dl	99.05
	41.22	35.79	21.79	<dl	<dl	<dl	<dl	<dl	98.79
G57	40.99	35.65	21.29	305	<dl	<dl	<dl	<dl	97.97
	41.29	35.91	21.27	<dl	270	215	1015	<dl	98.61
G58	43.24	33.80	20.40	<dl	635	17925	<dl	905	99.39
	43.91	33.81	20.44	<dl	960	15480	<dl	460	99.85
G60	42.04	35.28	21.70	<dl	<dl	<dl	<dl	<dl	99.06
	42.31	35.42	21.00	<dl	305	265	495	<dl	98.84
G61	42.27	35.30	22.03	<dl	275	230	560	<dl	99.72
	41.56	35.38	21.67	<dl	<dl	<dl	<dl	<dl	98.61
G65	44.60	34.34	20.40	<dl	<dl	11225	<dl	435	100.51
	44.49	34.80	20.34	<dl	<dl	9605	<dl	1150	100.70
G66	43.74	33.34	20.26	<dl	300	23575	<dl	670	99.79
	42.77	33.88	20.70	<dl	<dl	14995	<dl	735	98.93
mean	43.18	34.89	20.91						99.62
std.dev	1.36	1.05	0.54						0.87

TABLE A15 (cont.)

Medium zone	As mass %	Fe mass %	S mass %	Cu ppm	Ni ppm	Co ppm	Au ppm	Sb ppm	TOTAL mass %
G47A	43.79	35.03	21.10	<dl	<dl	210	<dl	395	99.99
	44.44	35.08	21.49	<dl	<dl	<dl	<dl	<dl	101.02
G47B	42.68	36.17	21.65	<dl	<dl	230	675	<dl	100.59
	42.79	36.24	21.66	665	1530	<dl	655	515	101.03
G48	43.19	35.15	21.15	<dl	1400	905	<dl	<dl	99.72
	43.54	35.16	21.18	<dl	815	<dl	<dl	<dl	99.95
G49	43.32	35.93	21.16	<dl	<dl	<dl	<dl	<dl	100.40
	42.78	36.02	21.60	<dl	<dl	485	<dl	<dl	100.45
G51	42.07	35.75	21.56	<dl	<dl	<dl	<dl	235	99.41
	41.40	35.91	21.53	<dl	295	<dl	<dl	<dl	98.87
G53	42.33	36.83	21.57	<dl	<dl	305	<dl	285	100.79
	42.23	35.91	21.84	<dl	<dl	<dl	<dl	<dl	99.98
G58	41.59	36.39	21.40	<dl	<dl	250	385	<dl	99.44
	41.84	36.25	21.18	<dl	<dl	<dl	485	<dl	99.32
G65	43.45	35.85	21.58	<dl	<dl	<dl	<dl	<dl	100.89
	43.48	35.67	21.62	<dl	<dl	<dl	<dl	<dl	100.78
G66	41.63	35.98	21.54	<dl	<dl	480	<dl	<dl	99.19
	41.93	35.92	21.50	<dl	<dl	270	<dl	<dl	99.37
mean	42.69	35.85	21.46						100.07
std.dev	0.87	0.49	0.22						0.70

Dark zone	As mass %	Fe mass %	S mass %	Cu ppm	Ni ppm	Co ppm	Au ppm	Sb ppm	TOTAL mass %
A51	40.33	35.69	22.89	<dl	285	830	<dl	230	99.05
	39.71	35.83	23.17	<dl	350	<dl	<dl	390	98.78
G47A	41.17	35.12	23.32	<dl	<dl	500	<dl	405	99.70
	40.39	36.14	23.78	<dl	375	<dl	<dl	360	100.38
G47B	42.95	35.48	22.10	<dl	<dl	<dl	<dl	<dl	100.52
	40.96	35.84	22.49	330	<dl	755	<dl	<dl	99.40
G48	42.94	35.24	21.73	<dl	260	<dl	<dl	<dl	99.94
	42.54	35.01	21.85	<dl	<dl	<dl	<dl	<dl	99.40

TABLE A15 (cont.)

Dark zone	As mass %	Fe mass %	S mass %	Cu ppm	Ni ppm	Co ppm	Au ppm	Sb ppm	TOTAL mass %
G49	39.45	36.75	23.62	<dl	320	<dl	<dl	<dl	99.86
	39.79	36.70	23.12	<dl	<dl	265	<dl	<dl	99.64
G50	39.75	37.05	22.48	<dl	<dl	<dl	<dl	2620	99.54
	39.40	37.11	22.34	<dl	<dl	<dl	<dl	2915	99.15
G51	39.66	36.47	23.08	<dl	<dl	640	<dl	<dl	99.27
	40.06	36.24	22.82	<dl	<dl	695	<dl	480	99.24
G53	41.61	36.69	22.60	<dl	360	<dl	<dl	<dl	100.93
	42.22	36.25	22.21	<dl	<dl	<dl	365	<dl	100.72
G56	39.81	36.68	22.42	<dl	<dl	<dl	<dl	<dl	98.91
	39.89	36.55	22.30	<dl	<dl	<dl	<dl	<dl	98.73
G57	40.40	36.45	22.16	<dl	375	305	495	<dl	99.12
	40.71	36.10	22.36	290	720	275	<dl	<dl	99.30
G58	41.75	36.31	21.23	<dl	<dl	<dl	<dl	<dl	99.28
	39.55	37.92	20.70	<dl	315	295	<dl	<dl	98.22
G60	38.10	36.93	23.26	<dl	<dl	<dl	<dl	395	98.33
	38.48	36.39	23.49	<dl	1000	520	<dl	<dl	98.51
G61	40.73	35.77	22.79	<dl	<dl	315	<dl	365	99.35
	39.71	35.79	23.37	<dl	<dl	310	<dl	400	98.94
G65	43.92	35.14	21.28	<dl	<dl	305	395	<dl	100.41
	43.13	34.63	21.56	<dl	<dl	390	<dl	290	99.39
G66	40.58	35.41	22.65	<dl	<dl	1260	<dl	<dl	98.77
	40.29	35.86	22.55	<dl	<dl	435	<dl	<dl	98.75
mean	40.67	36.12	22.52						99.38
std.dev	1.41	0.73	0.75						0.69

TABLE A15 (cont.)

Unzoned	As mass %	Fe mass %	S mass %	Cu ppm	Ni ppm	Co ppm	Au ppm	Sb ppm	TOTAL mass %
G55	40.65	35.98	22.31	<dl	<dl	225	<dl	<dl	98.96
	41.04	35.39	21.56	<dl	280	<dl	<dl	<dl	98.02
	42.36	35.00	21.77	<dl	<dl	340	<dl	<dl	99.16
	42.20	35.62	21.71	<dl	<dl	585	<dl	<dl	99.59
G59	40.68	35.37	22.14	<dl	265	605	<dl	<dl	98.28
	40.59	36.00	21.64	<dl	<dl	945	440	<dl	98.37
	41.56	35.93	22.04	<dl	270	580	<dl	<dl	99.61
G64	40.31	36.14	21.85	<dl	630	<dl	<dl	<dl	98.36
	40.78	36.02	21.92	<dl	315	225	<dl	<dl	98.77
	40.95	35.89	22.04	935	<dl	490	655	<dl	99.08
	40.56	35.58	22.53	<dl	<dl	<dl	560	<dl	98.73
mean	41.06	35.72	21.96						98.81
std.dev	0.68	0.36	0.30						0.53

TABLE A16

QUANTITATIVE ANALYSIS OF KLIPWAL PYRITE

Trace element detection limits (dl) are as follows: As 200ppm, Cu 570ppm, Sb 300ppm, Co 415ppm, Ni 405ppm, Au 505ppm, Ag 240ppm.

Pyrite	Fe mass %	S mass %	As mass %	Cu ppm	Sb ppm	Co ppm	Ni ppm	Au ppm	Ag ppm	TOTAL mass %
1	47.45	52.77	1.05	<dl	405	<dl	<dl	<dl	<dl	101.30
	47.30	53.06	0.93	<dl	415	<dl	<dl	<dl	<dl	101.33
2	46.39	52.66	1.53	<dl	<dl	<dl	845	<dl	<dl	100.66
	47.18	53.15	1.04	<dl	<dl	<dl	<dl	<dl	<dl	101.37
3	46.72	53.08	0.66	<dl	<dl	<dl	<dl	<dl	<dl	100.46
	47.48	53.51	0.45	<dl	<dl	<dl	<dl	<dl	<dl	101.44
4	46.78	52.60	1.46	<dl	<dl	<dl	<dl	<dl	<dl	100.84
	47.03	52.63	1.36	<dl	<dl	<dl	<dl	<dl	<dl	101.02
5	46.42	52.26	1.35	<dl	<dl	<dl	3255	<dl	<dl	100.35
	46.86	51.97	1.90	<dl	<dl	<dl	695	<dl	<dl	100.80
6	47.48	53.29	0.18	<dl	<dl	<dl	620	<dl	<dl	101.01
	47.86	53.30	0.19	<dl	<dl	<dl	1045	<dl	<dl	101.44
7	47.19	52.73	0.98	<dl	<dl	<dl	1920	<dl	<dl	101.08
	47.65	52.30	0.96	<dl	<dl	<dl	1245	<dl	<dl	101.03
8	47.56	52.80	0.65	<dl	<dl	<dl	<dl	<dl	<dl	101.01
	47.57	52.28	1.34	<dl	<dl	<dl	<dl	<dl	<dl	101.19
9	48.01	51.62	1.40	<dl	<dl	<dl	<dl	<dl	<dl	101.03
	47.87	52.44	1.18	<dl	<dl	<dl	<dl	<dl	<dl	101.49
10	47.90	52.10	0.92	<dl	<dl	<dl	<dl	<dl	<dl	100.91
	48.07	52.25	0.76	<dl	<dl	<dl	445	<dl	<dl	101.13
mean	47.34	52.64	1.01							101.05
std.dev	0.51	0.50	0.45							0.32

TABLE A17

QUANTITATIVE ANALYSIS OF ZANDRIVIER PYRITE

Trace element detection limits (dl) are as follows: As 200ppm, Cu 570ppm, Sb 300ppm, Co 415ppm, Ni 405ppm, Au 505ppm, Ag 240ppm.

Pyrite	Fe mass %	S mass %	As mass %	Cu ppm	Sb ppm	Co ppm	Ni ppm	Au ppm	Ag ppm	TOTAL mass %
G20	47.66	52.28	0.15	<dl	<dl	<dl	<dl	<dl	<dl	100.08
	48.29	51.91	0.35	<dl	<dl	<dl	<dl	<dl	<dl	100.55
G21	48.33	51.75	0.00	<dl	<dl	<dl	<dl	<dl	<dl	100.08
	47.53	52.67	0.08	1135	<dl	<dl	<dl	<dl	270	100.43
G24	47.41	52.58	0.38	<dl	<dl	<dl	<dl	<dl	<dl	100.37
	47.54	52.06	0.31	<dl	<dl	<dl	<dl	<dl	<dl	99.91
G26	47.45	52.41	0.10	<dl	2055	<dl	<dl	<dl	<dl	100.16
	47.42	52.49	0.09	<dl	1015	<dl	<dl	<dl	<dl	100.10
G27	47.47	52.04	0.24	<dl	<dl	<dl	<dl	<dl	<dl	99.75
	46.97	52.53	0.19	<dl	<dl	<dl	<dl	<dl	<dl	99.70
G28	47.68	52.61	0.32	<dl	<dl	<dl	<dl	<dl	<dl	100.62
	47.27	52.72	0.34	<dl	<dl	<dl	<dl	<dl	<dl	100.33
G31	47.79	52.59	0.02	<dl	<dl	<dl	<dl	<dl	<dl	100.39
	47.74	51.92	0.33	<dl	<dl	<dl	590	<dl	<dl	100.05
G32	48.01	52.43	0.25	<dl	<dl	<dl	<dl	<dl	<dl	100.70
	47.82	52.45	0.30	<dl	<dl	<dl	<dl	<dl	<dl	100.57
G33	47.33	50.95	1.25	<dl	<dl	430	3435	<dl	<dl	99.92
	47.59	51.41	1.21	<dl	<dl	920	2875	<dl	305	100.62
G35	47.51	51.71	0.43	<dl	<dl	<dl	<dl	<dl	<dl	99.65
	47.45	51.54	0.50	680	<dl	<dl	<dl	<dl	<dl	99.56
G36	46.37	52.47	1.16	<dl	<dl	<dl	<dl	<dl	<dl	100.00
	46.43	52.62	0.44	<dl	<dl	<dl	<dl	<dl	<dl	99.49
G37	46.56	52.65	1.00	<dl	<dl	<dl	<dl	<dl	<dl	100.21
	46.42	53.14	0.27	<dl	<dl	<dl	<dl	<dl	<dl	99.83

TABLE A17 (cont.)

Pyrite	Fe mass %	S mass %	As mass %	Cu ppm	Sb ppm	Co ppm	Ni ppm	Au ppm	Ag ppm	TOTAL mass %
G38	46.82	53.51	0.18	<dl	<dl	<dl	<dl	<dl	<dl	100.51
	46.60	53.22	0.25	<dl	<dl	<dl	<dl	<dl	<dl	100.06
G39	45.79	52.36	0.78	<dl	<dl	<dl	<dl	<dl	<dl	98.93
	46.41	53.02	0.42	<dl	<dl	<dl	<dl	<dl	<dl	99.85
G40	46.11	53.43	0.05	<dl	<dl	<dl	<dl	<dl	<dl	99.58
	46.74	53.07	0.16	<dl	<dl	<dl	<dl	<dl	<dl	99.96
mean	47.22	52.42	0.39							100.07
std.dev	0.65	0.59	0.35							0.41

TABLE A18

QUANTITATIVE ANALYSIS OF WEST AFRICAN PYRITE

Trace element detection limits (dl) are as follows: As 200ppm, Cu 570ppm, Sb 300ppm, Co 415ppm, Ni 405ppm, Au 505ppm, Ag 240ppm.

Pyrite	Fe mass %	S mass %	As mass %	Cu ppm	Sb ppm	Co ppm	Ni ppm	Au ppm	Ag ppm	TOTAL mass %
G44	46.35	52.25	0.13	<dl	450	<dl	<dl	<dl	<dl	98.78
	45.97	52.66	0.18	665	<dl	6390	<dl	<dl	<dl	99.51
G46/1	45.51	53.30	0.70	<dl	<dl	5915	950	<dl	<dl	100.20
	44.94	52.68	1.37	<dl	<dl	8395	2095	<dl	<dl	100.04
G46/2	44.84	52.63	1.17	<dl	<dl	11295	740	<dl	<dl	99.85
	45.57	52.48	0.79	<dl	<dl	9755	<dl	<dl	<dl	99.81
G46/3	45.10	53.17	0.51	<dl	<dl	6225	570	<dl	<dl	99.46
	44.76	52.96	1.10	<dl	<dl	7215	1330	<dl	<dl	99.67
G47A	46.01	52.88	0.27	<dl	535	4465	2595	<dl	<dl	99.91
	44.54	51.64	2.01	<dl	<dl	18110	3540	<dl	<dl	100.35
G47B/1	45.13	51.92	1.34	<dl	<dl	5835	2050	<dl	<dl	99.17
	45.31	51.93	1.42	<dl	<dl	11700	2575	<dl	<dl	100.09
G47B/2	44.76	51.71	1.81	<dl	<dl	9120	2755	<dl	<dl	99.47
	44.56	51.20	2.33	<dl	<dl	21275	2660	<dl	<dl	100.49
G48/1	45.27	51.71	1.39	<dl	<dl	7020	1900	<dl	<dl	99.26
	45.36	52.03	1.49	<dl	<dl	13450	2320	<dl	<dl	100.45
G48/2	45.46	52.26	1.23	<dl	710	7480	1110	<dl	<dl	99.87
	45.47	52.19	1.16	<dl	<dl	13610	1260	<dl	<dl	100.31
G49	45.95	52.33	1.25	<dl	<dl	990	4235	<dl	<dl	100.05
	44.81	52.62	0.55	<dl	<dl	1230	980	<dl	<dl	98.20
G49/1	46.12	53.07	0.14	<dl	<dl	<dl	4225	<dl	<dl	99.76
	45.82	52.82	0.55	<dl	<dl	11155	<dl	<dl	<dl	100.30
G49/2	45.42	52.10	0.87	660	<dl	6300	415	<dl	<dl	99.13
	44.61	51.48	2.25	<dl	<dl	15715	4060	<dl	<dl	100.32
G49/3	46.22	53.16	0.33	<dl	<dl	665	1675	<dl	<dl	99.94
	46.94	53.41	0.08	<dl	<dl	6005	<dl	<dl	<dl	101.02

TABLE A18 (cont.)

Pyrite	Fe mass %	S mass %	As mass %	Cu ppm	Sb ppm	Co ppm	Ni ppm	Au ppm	Ag ppm	TOTAL mass %
G49/4	45.53	52.37	1.43	<dl	<dl	4100	3165	<dl	<dl	100.06
	46.79	53.43	0.46	<dl	<dl	6780	1725	<dl	355	101.56
G55/1	45.28	51.52	1.81	<dl	<dl	<dl	7690	<dl	<dl	99.38
	44.97	51.58	1.81	<dl	<dl	<dl	7605	<dl	<dl	99.12
G55/2	46.06	52.26	0.93	<dl	<dl	615	3285	<dl	<dl	99.64
	45.52	51.31	1.98	<dl	<dl	<dl	7975	<dl	<dl	99.61
G57	45.80	52.66	0.36	<dl	<dl	<dl	1062	<dl	<dl	98.93
	46.48	52.53	0.32	<dl	<dl	2080	510	<dl	<dl	99.59
mean	45.51	52.36	1.04							99.80
std.dev	0.63	0.62	0.66							0.64

TABLE A19

QUANTITATIVE ANALYSIS OF SHEBA PYRITE

Trace element detection limits (dl) are as follows: As 200ppm, Cu 570ppm, Sb 300ppm, Co 415ppm, Ni 405ppm, Au 505ppm, Ag 240ppm.

*Zones are distinguished by the intensity of the backscattered electron image.

Pyrite zone*	Fe mass %	S mass %	As mass %	Cu ppm	Sb ppm	Co ppm	Ni ppm	Au ppm	Ag ppm	TOTAL mass %
G3 bright	39.92	45.83	9.54	600	<dl	<dl	44470	<dl	<dl	99.79
	42.09	48.54	6.19	<dl	<dl	<dl	30180	<dl	<dl	99.84
G3 dark	45.99	52.54	0.20	<dl	<dl	<dl	3860	<dl	<dl	99.11
	45.74	52.29	0.19	<dl	<dl	<dl	3560	<dl	<dl	98.58
G6	46.55	52.55	0.18	<dl	<dl	<dl	720	<dl	<dl	99.36
	46.09	52.40	0.22	<dl	<dl	<dl	1060	<dl	<dl	98.82
G10	46.35	52.28	0.53	<dl	<dl	<dl	<dl	<dl	<dl	99.16
	46.36	52.41	0.32	<dl	<dl	<dl	<dl	<dl	<dl	99.10
G13	47.38	53.18	0.09	<dl	<dl	<dl	<dl	<dl	<dl	100.64
	46.60	53.20	0.00	<dl	<dl	<dl	<dl	<dl	<dl	99.79
G16	47.08	52.30	0.38	<dl	<dl	<dl	3405	<dl	<dl	100.10
	47.72	52.26	0.29	<dl	<dl	<dl	<dl	<dl	<dl	100.26
G18	47.99	53.05	0.05	<dl	<dl	3240	1090	<dl	<dl	101.52
	46.95	52.73	0.00	<dl	360	<dl	3110	<dl	<dl	100.03
G19 bright	46.35	49.79	3.77	<dl	<dl	<dl	<dl	665	<dl	99.98
	46.34	50.42	3.36	975	<dl	<dl	<dl	585	<dl	100.28
G19 dark	46.75	51.77	0.97	<dl	<dl	<dl	<dl	<dl	<dl	99.49
	46.42	52.14	1.05	<dl	<dl	<dl	<dl	<dl	<dl	99.61
S4 bright	44.72	47.44	7.89	<dl	<dl	<dl	405	<dl	<dl	100.09
	44.66	47.91	7.35	1370	<dl	<dl	535	<dl	<dl	100.11
S4 dark	46.28	53.00	0.25	755	395	<dl	730	<dl	<dl	99.72
	46.05	52.16	0.41	1090	320	<dl	535	<dl	<dl	98.81
S5	46.82	52.39	0.63	<dl	<dl	<dl	<dl	<dl	<dl	99.85
	46.87	52.91	0.54	<dl	<dl	<dl	<dl	<dl	<dl	100.32

TABLE A19 (cont.)

Pyrite zone	Fe mass %	S mass %	As mass %	Cu ppm	Sb ppm	Co ppm	Ni ppm	Au ppm	Ag ppm	TOTAL mass %
S7	46.30	52.81	0.11	875	<dl	<dl	1125	<dl	<dl	99.41
	46.07	52.99	0.17	<dl	<dl	<dl	930	<dl	<dl	99.33
S8 bright	46.02	51.08	2.80	2695	<dl	<dl	<dl	635	<dl	100.23
	45.60	51.17	2.60	<dl	<dl	<dl	<dl	<dl	<dl	99.37
S8 dark	47.32	52.97	0.05	<dl	<dl	<dl	415	<dl	<dl	100.38
	47.24	53.40	0.04	<dl	<dl	<dl	<dl	<dl	<dl	100.68
S9	45.79	50.44	3.63	<dl	<dl	3105	<dl	<dl	<dl	100.17
	46.33	50.86	3.31	<dl	<dl	<dl	<dl	<dl	<dl	100.50
S10 bright	46.08	51.65	2.19	<dl	<dl	<dl	<dl	<dl	<dl	99.93
	46.13	50.70	2.67	<dl	<dl	<dl	<dl	<dl	<dl	99.50
S10 dark	47.02	53.29	0.05	<dl	<dl	<dl	<dl	<dl	<dl	100.36
	46.97	53.16	0.02	<dl	<dl	<dl	<dl	<dl	<dl	100.15
S11	45.67	50.41	3.83	725	<dl	<dl	<dl	<dl	<dl	99.98
	45.23	49.84	4.79	<dl	<dl	<dl	<dl	1580	<dl	100.02
S12	47.21	53.44	0.03	<dl	<dl	<dl	<dl	<dl	<dl	100.68
	47.33	52.92	0.11	<dl	320	4595	<dl	<dl	<dl	100.85
S18	47.34	52.83	0.00	<dl	<dl	<dl	475	<dl	<dl	100.22
	46.94	52.86	0.02	<dl	<dl	<dl	2245	<dl	<dl	100.05
S19	47.41	52.43	0.23	<dl	<dl	<dl	720	<dl	<dl	100.15
	47.23	52.44	0.31	<dl	<dl	<dl	995	<dl	<dl	100.08
S23	45.66	51.78	0.61	<dl	<dl	<dl	<dl	<dl	<dl	98.05
	45.97	51.84	0.50	<dl	<dl	<dl	<dl	<dl	<dl	98.31
S24 bright	44.20	49.34	4.74	645	710	<dl	825	<dl	<dl	98.50
S24 dark	45.57	52.17	0.29	<dl	<dl	<dl	<dl	<dl	<dl	98.03
S25	45.99	51.87	0.30	<dl	<dl	<dl	<dl	<dl	<dl	98.16
	45.64	52.40	0.30	<dl	<dl	<dl	<dl	<dl	<dl	98.35
S26	45.62	51.93	0.54	<dl	<dl	2985	<dl	<dl	<dl	98.39
	45.89	52.38	0.46	<dl	<dl	<dl	<dl	<dl	<dl	98.74
mean	46.15	51.75	1.52							99.67
std.dev	1.32	1.62	2.29							0.80

TABLE A20

QUANTITATIVE ANALYSIS OF PYRRHOTITTE

Trace element detection limits (dl) are as follows: As 230ppm, Cu 705ppm, Sb 305ppm, Co 410ppm, Ni 425ppm, Au 505ppm.

West African pyrrhotite	Fe mass %	S mass %	As ppm	Cu ppm	Sb ppm	Co ppm	Ni ppm	Au ppm	TOTAL mass %
G 50	59.00	39.05	<dl	<dl	<dl	1055	1175	<dl	98.27
	59.77	38.90	295	<dl	<dl	855	670	<dl	98.86
G51	60.53	38.52	<dl	<dl	<dl	<dl	1145	<dl	99.17
	59.77	38.71	<dl	<dl	<dl	<dl	925	<dl	98.57
G 53	59.77	39.15	<dl	<dl	<dl	590	900	<dl	99.08
	59.41	38.93	<dl	<dl	<dl	465	770	<dl	98.46
G 55	60.50	38.75	<dl	<dl	<dl	770	1110	<dl	99.44
	60.48	38.57	<dl	<dl	310	860	925	<dl	99.27
G 56	60.85	38.25	<dl	<dl	<dl	515	760	<dl	99.22
	60.40	38.46	370	<dl	<dl	375	790	<dl	98.98
G 57	59.64	39.00	<dl	<dl	<dl	1070	800	<dl	98.83
	59.80	38.43	235	<dl	<dl	1275	565	<dl	98.44
G 58	61.04	39.01	300	<dl	<dl	1180	705	<dl	100.27
	59.84	38.68	<dl	<dl	<dl	1005	940	<dl	98.71
G 59	60.90	38.83	<dl	<dl	<dl	<dl	525	<dl	99.78
	60.63	38.76	<dl	<dl	<dl	<dl	1215	<dl	99.51
G 60	61.27	38.97	<dl	<dl	<dl	455	705	520	100.40
	59.86	38.80	<dl	<dl	<dl	570	1265	<dl	98.85
G 61	60.38	38.83	435	<dl	<dl	<dl	495	<dl	99.29
	60.59	38.81	320	<dl	<dl	<dl	1175	<dl	99.54
G 64	60.57	38.70	525	<dl	<dl	<dl	1135	<dl	99.43
	59.56	39.11	305	<dl	<dl	<dl	640	<dl	98.76
G65	60.43	39.16	<dl	<dl	<dl	550	750	<dl	99.72
	60.56	38.87	<dl	<dl	<dl	510	660	<dl	99.52
G 66	60.57	39.03	<dl	<dl	<dl	570	825	<dl	99.74
	59.77	38.29	<dl	<dl	<dl	480	920	<dl	98.20

TABLE A20 (cont.)

West African pyrrhotite	Fe mass %	S mass %	As ppm	Cu ppm	Sb ppm	Co ppm	Ni ppm	Au ppm	TOTAL mass %
G 44	60.30	38.98	<dl	<dl	<dl	710	<dl	<dl	99.35
	59.96	38.78	<dl	<dl	<dl	700	<dl	<dl	98.81
G 45	59.69	38.96	<dl	<dl	<dl	605	520	<dl	98.76
	59.68	39.50	<dl	<dl	<dl	550	1015	<dl	99.34
G 46	60.70	38.81	<dl	<dl	<dl	495	1035	<dl	99.67
	59.84	39.26	<dl	<dl	<dl	405	1410	<dl	99.28
G 47 A	59.53	38.80	<dl	<dl	<dl	920	550	<dl	98.47
	59.53	39.14	<dl	<dl	<dl	840	900	<dl	98.84
G 47 B	58.83	38.96	<dl	<dl	<dl	635	835	<dl	97.94
	59.52	39.03	<dl	<dl	<dl	580	<dl	<dl	98.62
G 48	59.44	39.23	<dl	1450	<dl	600	1085	<dl	98.99
	59.38	39.29	<dl	<dl	<dl	485	1075	<dl	98.82
G 49	60.00	38.91	<dl	<dl	<dl	830	915	<dl	99.09
	59.66	39.12	<dl	<dl	<dl	750	1195	<dl	98.98
S 33	59.74	38.77	<dl	<dl	<dl	<dl	820	<dl	98.59
	58.90	39.11	<dl	<dl	<dl	<dl	595	<dl	98.07
mean	60.01	38.89							99.05
std.dev	0.59	0.26							0.55

Zandrivier pyrrhotite	Fe mass %	S mass %	As ppm	Cu ppm	Sb ppm	Co ppm	Ni ppm	Au ppm	TOTAL mass %
G 22	59.82	38.31	1010	<dl	<dl	<dl	<dl	<dl	98.23
	60.31	38.22	665	<dl	<dl	<dl	<dl	<dl	98.60
G 29	58.98	38.93	925	<dl	<dl	<dl	<dl	<dl	97.99
	59.23	39.21	1115	<dl	<dl	<dl	<dl	<dl	98.55
G33	60.83	38.22	1000	<dl	<dl	<dl	<dl	<dl	99.15
	59.78	38.41	705	<dl	<dl	<dl	<dl	<dl	98.26
G35	61.12	38.23	940	<dl	<dl	<dl	<dl	<dl	99.45
	61.36	38.35	1000	<dl	<dl	<dl	<dl	<dl	99.81
mean	60.18	38.49	920						98.76
std.dev	0.87	0.37	156						0.65

TABLE A21

QUANTITATIVE ANALYSIS OF SHEBA GERSDORFFITE

Trace element detection limits (dl) are as follows: Cu 290ppm, Co 210ppm, Au 350ppm.

Gersdorffite	As mass %	Fe mass %	S mass %	Ni mass %	Co ppm	Cu ppm	Au ppm	Sb ppm	TOTAL mass %
G7	45.66	12.18	19.01	22.71	2935	<dl	<dl	2720	100.12
	45.70	11.07	18.79	24.09	2420	<dl	<dl	3860	100.28
G15	44.48	13.23	18.81	21.76	4240	<dl	<dl	2060	98.91
	44.88	13.00	18.72	21.81	3720	655	595	2225	99.13
G3 large	45.95	13.38	19.13	21.54	3740	<dl	<dl	2030	100.58
	45.57	11.01	18.85	24.84	1640	<dl	<dl	6840	101.12
G3 small	45.66	12.27	19.14	22.58	3470	340	<dl	2685	100.30
	46.14	10.85	19.15	23.90	2500	<dl	<dl	6965	101.00
G5/1	45.43	12.16	19.37	22.77	2740	1265	<dl	3055	100.43
	44.85	9.84	18.87	24.99	3745	<dl	<dl	5140	99.43
G5/2	45.54	10.75	19.28	23.25	3270	<dl	<dl	3270	99.48
	45.26	7.33	18.68	27.06	1345	430	<dl	10445	99.55
S1 large	45.21	8.82	18.94	25.04	2225	2700	<dl	12310	99.74
	44.72	7.82	18.53	26.66	1835	490	<dl	7935	98.75
S1 small	45.90	7.23	18.99	27.87	1305	475	<dl	9855	101.15
	45.83	7.77	18.81	26.65	1655	475	<dl	9225	100.21
G6	45.00	12.77	19.65	21.42	5160	<dl	<dl	2225	99.58
	44.28	11.08	18.99	22.59	4245	385	<dl	3290	97.73
G12	46.28	13.76	19.35	21.67	<dl	<dl	<dl	1840	101.24
	45.47	12.56	19.26	22.68	335	<dl	<dl	2415	100.25
G18	45.94	8.07	19.04	27.63	1435	<dl	<dl	8475	101.68
	45.95	12.40	19.41	22.42	4415	320	<dl	1835	100.83
S27/1	44.13	5.64	18.94	30.14	<dl	695	<dl	18620	100.77
	45.32	8.85	18.87	26.65	720	430	<dl	10445	100.85
S27/2	46.30	8.76	18.95	26.41	860	445	<dl	7555	101.31
	45.61	7.96	18.91	26.77	1405	<dl	<dl	9240	100.32
mean	45.43	10.41	19.02	24.46				6022	100.18
std.dev	0.59	2.33	0.26	2.43				4224	0.92

TABLE A22

KLIPWAL ARSENOPYRITE COLOUR VARIATION WITH TIME IN LEACH

(*FS = ferric sulphate leach test, and B = bacterial leach test)

			Time in leach						
Leach*	Section	Colour	6 hours	1 day	2 days	3 days	4 days	5 days	1 week
FS 1	Crystal	Most common Range	W W – C	W – C W – B	C W – B	C W – B	C W – B	n.d.	C – B W – BR
FS 2	Crystal	Most common Range	W W – C	C – B W – BR	B C – BR	B C – BR	n.d.	B C – BR	B – BR B – BL
FS 2	Milled	Most common Range	C W – BR	B – BR W – MC	B – BR C – BL	B – BR C – BL	n.d.	B – BR C – BL	n.d.
FS 3	Milled	Most common Range	W W – C	C – B W –BR	B C – MC	n.d.	n.d.	BR C – BL	BR – MC C – BL
FS 4	Milled	Most common Range	W – C W – B	W – C W – BR	C W – MC	C – B C – BL	n.d.	n.d.	B – BR C – C2
FS 5	Crystal	Most common Range	C W – B	B C – MC	BR B – MC	n.d.	MC – BL B – BL	n.d.	MC – BL BR – C2
FS 5	Milled	Most common Range	W W – C	C – B W – MC	n.d.	n.d.	n.d.	BR – MC B – G	n.d.
B 1	Crystal	Average Range	C W – B	BR B – BL	MC C – G	n.d.	MC C – G	n.d.	MC – BL B – G

W = white, C = cream, B = beige, BR = brown, MC = multicoloured, BL = blue, C2 = 2nd order cream, MC2 = bright multicoloured, G = grey.
n.d. = not determined.

TABLE A23

ZANDRIVIER ARSENOPYRITE COLOUR VARIATION WITH TIME IN LEACH

(*FS = ferric sulphate leach test, and B = bacterial leach test)

			Time in leach						
Leach*	Section	Colour	6 hours	1 day	2 days	3 days	4 days	5 days	1 week
FS 1	Crystal	Most common Range	W W – C	W – C W – B	C W – B	C W – B	C W – B	n.d.	C – B W – B
FS 2	Crystal	Most common Range	W W – C	C – B W – BR	B C – BR	B C – MC	n.d.	B C – MC	B – BR C – MC
FS 2	Milled	Most common Range	C W – BR	B – BR W – MC	B – BR C – MC	BR C – BL	n.d.	BR – MC C – BL	n.d.
FS 3	Milled	Most common Range	W – C W – B	C – B W – BR	B C – MC	n.d.	n.d.	BR B – BL	B – MC C – BL
FS 4	Milled	Most common Range	W – C W – B	C – B C – BL	B C – BL	n.d.	B – BR C – BL	n.d.	MC C – C2
FS 5	Crystal	Most common Range	C W – B	C – B C – MC	B C – MC	n.d.	BR – MC C – BL	n.d.	MC – BL BR – C2
Sterile 5	Milled	Most common Range	W – C W – B	C – B C – MC	n.d.	n.d.	n.d.	BR – MC B – G	n.d.
B 1	Crystal	Most common Range	C W – B	BR B – BL	MC B – G	n.d.	MC B – G	n.d.	MC – BL B – G

W = white, C = cream, B = beige, BR = brown, MC = multicoloured, BL = blue, C2 = 2nd order cream, MC2 = bright multicoloured, G = grey.
n.d. = not determined.

TABLE A24

WEST AFRICAN ARSENOPYRITE COLOUR VARIATION WITH TIME IN LEACH

(*FS = ferric sulphate leach test, and B = bacterial leach test)

			Time in leach						
Leach*	Section	Colour	6 hours	1 day	2 days	3 days	4 days	5 days	1 week
FS 1	Crystal	Most common Range	W W – C	W – C W – B	C – B W – B	C – B W – B	C – B W – B	n.d.	B W – MC
FS 2	Crystal	Most common Range	W W – C	B C – BR	B – B C – MC	BR B – MC	n.d.	BR B – MC	n.d.
FS 2	Milled	Most common Range	C W – BR	B – BR W – MC	BR C – MC	BR – MC C – BL	n.d.	BR – MC C – C2	BR B – BL
FS 3	Milled	Most common Range	W – C W – B	C – B W– BR	B C – MC	n.d.	n.d.	BR B – BL	BR – MC C – C2
FS 4	Milled	Most common Range	W – C W – B	B C – BL	B C – BL	n.d.	B – BR C – BL	n.d.	MC – BL C – C2
FS 5	Crystal	Most common Range	C C – B	BR BR – MC	MC B – BL	n.d.	BL B – C2	n.d.	BL – C2 MC – MC2
FS 5	Milled	Most common Range	W – C W – BR	BR – MC C – BL	n.d.	n.d.	n.d.	BL B – G	n.d.
B 1	Crystal	Average Range	C W – B	BR B – BLS	MC – G B – G	n.d.	G B – G	n.d.	G MC – G

W = white, C = cream, B = beige, BR = brown, MC = multicoloured, BL = blue, C2 = 2nd order cream, MC2 = bright multicoloured, G = grey.
n.d. = not determined.

TABLE A25

SHEBA ARSENOPYRITE COLOUR VARIATION WITH TIME IN LEACH

(*FS = ferric sulphate leach test, and B = bacterial leach test)

			Time in leach						
Leach*	Section	Colour	6 hours	1 day	2 days	3 days	4 days	5 days	1 week
FS 1	Crystal	Most common Range	W W – C	W – C W – B	C – B W – BR	C – B W – BR	C – B W – BR	n.d.	B W – MC
FS 2	Crystal	Most common Range	W – C W – B	B – BR W – MC	BR C – BL	BR – MC C – C2	n.d.	n.d.	MC – BL C – MC 2
FS 2	Milled	Most common Range	C W – BR	B – BR W – BL	BR – MC C – BL	MC C – C2	n.d.	MC – BL C – C2	n.d.
Sterile 3	Milled	Most common Range	W – C W – B	C – B W – BR	B – BR C – MC	n.d.	n.d.	BR – MC C – BL	BR – MC C – C2
FS 4	Milled	Most common Range	W – C W – B	B – BR W – MC	BR C – C2	n.d.	BR C – C2	n.d.	MC – BL C – C2
FS 5	Crystal	Most common Range	B C – BR	B – BR C – MC	MC C – BL	n.d.	BL B – C2	n.d.	BL – C2 BR – MC2
FS 5	Milled	Most common Range	W – C W –BR	MC W – C2	n.d.	n.d.	n.d.	BL – C2 B – G	n.d.
B 1	Crystal	Average Range	C W – B	BR – MC B – BL	G C – G	n.d.	G B – G	n.d.	G BR – G

W = white, C = cream, B = beige, BR = brown, MC = multicoloured, BL = blue, C2 = 2nd order cream, MC2 = bright multicoloured, G = grey.
n.d. = not determined.

TABLE A26

PROGRESS OF PRE-ANALYSED SULPHIDE MINERALS DURING FERRIC SULPHATE LEACH 7 AND BACTERIAL LEACH 3

W = white, C = cream, B = beige, BR = brown, MC = multicoloured, BL = blue, C2 = 2nd order cream, MC2 = bright multicoloured, G = grey, Y = yellow, Y2 = 2nd order yellow, P = pink, PU = purple, L = lime green.

No.	SULPHIDE	SOURCE	LEACH	TIME IN LEACH	PROGRESS	ZONE-RELATED?
A1	Arsenopyrite	Sheba	FS7	End of leach	BR/BL–C2	Yes
A2	Arsenopyrite	Sheba	FS7	End of leach	Faintly etched (Basal section)	Yes
A3	Arsenopyrite	Sheba	FS7	12 hours End of leach	B MC/C2	 Yes
A4	Arsenopyrite	Sheba	FS7	End of leach	B/BR	Yes
A5	Arsenopyrite	Sheba	FS7	End of leach	MC/C2	Yes
A6	Arsenopyrite	Sheba	FS7	End of leach	MC/C2	Yes
A7	Arsenopyrite	Sheba	FS7	End of leach	BL/C2	Yes
A8	Arsenopyrite	Sheba	FS7		CASE HISTORY IN TEXT	
A9	Arsenopyrite	Sheba	FS7		CASE HISTORY IN TEXT	
A10	Arsenopyrite	Sheba	FS7	12 hours 10 days End of leach	B BL/C2 BL–C2/MC2	 Yes Yes
A11	Arsenopyrite	Sheba	FS7		CASE HISTORY IN TEXT	
A12	Arsenopyrite	Sheba	FS7	1 day 6 days End of leach	CR–B BR/B G with internal reflections	 Yes
A13	Arsenopyrite	Sheba	B3	6 days End of leach	B B/G with internal reflections	 Yes
A14	Arsenopyrite	Sheba	B3		FELL OUT	
A15	Arsenopyrite	Sheba	B3		FELL OUT	
A16	Arsenopyrite	Sheba	B3		FELL OUT	
A17	Arsenopyrite	Sheba	B3	2 days 6 days	C–B Gone (leached or fallen out)	
A18	Arsenopyrite	Sheba	B3	1 day 2 days 6 days	C B Gone (leached or fallen out)	
A19	Arsenopyrite	Sheba	B3	7 days 10 days	C/B B/MC	Yes Yes

TABLE A26 (cont.)

No.	SULPHIDE	S0URCE	LEACH	TIME IN LEACH	PROGRESS	ZONE-RELATED?
A19	Galena	Sheba	B3	7 days	Leached out	
A20	Arsenopyrite	Sheba	B3	7 days End of leach	C/BR G with internal reflections	Yes
A21	Arsenopyrite	Sheba	B3	7 days	B–BR/G with internal reflections	Yes
A22	Arsenopyrite	Sheba	B3	2 days 7 days End of leach	C B B with etch	 Yes
A23	Arsenopyrite	Sheba	B3	2 days 7 days End of leach	B B/BR Br/G with internal reflections	 Yes Yes
A24	Arsenopyrite	Zandrivier	FS7	End of leach	Unleached (crystal)	
A25	Arsenopyrite	Zandrivier	FS7	End of leach	Unleached (crystal)	
A26	Arsenopyrite	Zandrivier	FS7	End of leach	Unleached (crystal)	
A28	Arsenopyrite	Zandrivier	FS7		CASE HISTORY IN TEXT	
A29	Arsenopyrite	Zandrivier	FS7	End of leach	BR/C2	Yes
A30	Arsenopyrite	Zandrivier	FS7		CASE HISTORY IN TEXT	
A31	Arsenopyrite	Zandrivier	FS7	7 days End of leach	B/MC G with internal reflections	Yes (veins leach first)
A35	Arsenopyrite	Zandrivier	FS7	End of leach	B/BR	Yes
A36	Arsenopyrite	Zandrivier	B3	2 days 6 days 10 days	B G with internal reflections Leached out	No
A37	Arsenopyrite	Zandrivier	B3	2 days 10 days	B G with internal reflections	
A38	Arsenopyrite	Zandrivier	B3	2 days 6 days 10 days	B/MC BR/MC BR/MC with precipitate	Yes Yes Yes
A40	Arsenopyrite	Zandrivier	B3	1 day 6 days End of leach	B B/BR BL/G with internal reflections	 Yes Yes
A42	Arsenopyrite	Zandrivier	B3	10 days	B/MC	Yes
A45	Arsenopyrite	Zandrivier	B3	2 days 10 days	B/BR G with internal reflections	Yes

TABLE A26 (cont.)

No.	SULPHIDE	SOURCE	LEACH	TIME IN LEACH	PROGRESS	ZONE-RELATED?
A46	Arsenopyrite	Zandrivier	B3	1 day 2 days 10 days	B B/BR B/G with internal reflections	 Yes Yes
A47	Arsenopyrite	Zandrivier	B3		CASE HISTORY IN TEXT	
A48	Arsenopyrite	Zandrivier	B3	1 day 6 days 10 days End of leach	C/B B/BR B/BL G with internal reflections	Yes Yes Yes
A50	Arsenopyrite	Zandrivier	B3	1 day 10 days	B B/MC–BL	 Yes
A51	Arsenopyrite	West African	B3	1 day	MC	No
A52	Arsenopyrite	West African	B3	10 days End of leach	B/MC G with internal reflections	Yes
A53	Arsenopyrite	Klipwal	FS7		CASE HISTORY IN TEXT	
A54	Arsenopyrite	Klipwal	FS7	4 days 10 days	B–BR patches MC	Unzoned
A55	Arsenopyrite	Klipwal	FS7	4 days 10 days	B–BR MC	Unzoned
A56	Arsenopyrite	Klipwal	FS7	4 days 10 days	B–BR MC	Unzoned
A57	Arsenopyrite	Klipwal	FS7	4 days 10 days	B–BR BR–MC	Unzoned
G1	Arsenopyrite	Sheba	FS7		CASE HISTORY IN TEXT	
G1	Tetrahedrite	Sheba	FS7		CASE HISTORY IN TEXT	
G2	Arsenopyrite	Sheba	FS7	12 hours 8 days	B MC/BL	 Yes
G2	Tetrahedrite	Sheba	FS7	12 hours 8 days End of leach	Unleached Unleached Unleached	
G3	Gersdorffite	Sheba	FS7		CASE HISTORY IN TEXT	
G3	Pyrite	Sheba	FS7		CASE HISTORY IN TEXT	
G4	Arsenopyrite	Sheba	FS7	End of leach	Leached out	
G4	Pyrite	Sheba	FS7	End of leach	Purple/BL/C2	Yes

TABLE A26 (cont.)

No.	SULPHIDE	SOURCE	LEACH	TIME IN LEACH	PROGRESS	ZONE-RELATED?
G5	Gersdorffite	Sheba	FS7	3 hours 12 hours	BR BL	
G6	Gersdorffite	Sheba	FS7	12 hours End of leach	BL Leached out	
G6	Pyrite	Sheba	FS7	12 hours End of leach	Unleached Gone (leached out or fell out)	
G6	Chalcopyrite	Sheba	FS7	12 hours End of leach	Unleached Gone (fallen out)	
G7	Arsenopyrite	Sheba	FS7	8 days 10 days End of leach	B/BR MC/BL MC/C2	Yes Yes Yes
G7	Gersdorffite	Sheba	FS7	4 days 8 days 10 days End of leach	Etched BL C2 G with internal reflections	
G8	Arsenopyrite	Sheba	FS7	4 days 10 days End of leach	B etched B/BR B/MC	 Yes Yes
G8	Gold	Sheba	FS7	End of leach	Unleached	
G9	Arsenopyrite	Sheba	FS7	12 hours	Leached out	
G9	Pyrite	Sheba	FS7	12 hours	B/BR	Yes
G10	Arsenopyrite	Sheba	FS7		CASE HISTORY IN TEXT	
G10	Pyrite	Sheba	FS7		CASE HISTORY IN TEXT	
G11	Arsenopyrite	Sheba	FS7	End of leach	B	
G11	Pyrite	Sheba	FS7	End of leach	W	
G12	Gersdorffite	Sheba	FS7	End of leach	Leached out	
G12	Pyrite	Sheba	FS7	End of leach	BR	
G13	Arsenopyrite	Sheba	FS7	1 day	Leached out	
G13	Pyrite	Sheba	FS7	1 day 6 days 10 days End of leach	Y Y P PU – BL	 No No
G14	Arsenopyrite	Sheba	FS7	End of leach	B/BR	Yes
G14	Pyrite	Sheba	FS7	End of leach	Unleached	

TABLE A26 (cont.)

No.	SULPHIDE	SOURCE	LEACH	TIME IN LEACH	PROGRESS	ZONE-RELATED?
G14	Galena	Sheba	FS7	End of leach	Leached out	
G15	Arsenopyrite	Sheba	FS7	End of leach	G with internal reflections	
G15	Gersdorffite	Sheba	FS7	End of leach	Leached out	
G15	Gold	Sheba	FS7	End of leach	Unleached	
G17	Arsenopyrite	Sheba	B3	2 days 10 days	C/BR C2/G with internal reflections	Yes Yes
G17	Pyrite	Sheba	B3	End of leach	Unleached	
G18	Gersdorffite	Sheba	B3	3 hours End of leach	G with internal reflections Leached out	
G18	Pyrite	Sheba	B3	3 hours End of leach	Unleached Gone (fallen out)	
G19	Pyrite	Sheba	B3		FELL OUT	
G19	Chalcopyrite	Sheba	B3		FELL OUT	
G19	Tetrahedrite	Sheba	B3		FELL OUT	
G20	Pyrite	Zandrivier	FS7	End of leach	Unleached	
G24	Pyrite	Zandrivier	FS7	End of leach	Unleached	
G25	Arsenopyrite	Zandrivier	FS7		CASE HISTORY IN TEXT	
G25	Chalcopyrite	Zandrivier	FS7		CASE HISTORY IN TEXT	
G25	Gold	Zandrivier	FS7		CASE HISTORY IN TEXT	
G26	Pyrite	Zandrivier	FS7	End of leach	Unleached	
G27	Pyrite	Zandrivier	FS7	End of leach	Unleached	
G28	Pyrite	Zandrivier	FS7	End of leach	Unleached	
G29	Pyrrhotite	Zandrivier	FS7	3 hours End of leach	BR Thick sulphur coating	
G30	Arsenopyrite	Zandrivier	FS7		CASE HISTORY IN TEXT	
G30	Gold	Zandrivier	FS7		CASE HISTORY IN TEXT	
G31	Pyrite	Zandrivier	FS7	End of leach	Unleached	
G32	Arsenopyrite	Zandrivier	FS7	End of leach	BR/BL	Yes
G32	Pyrite	Zandrivier	FS7	End of leach	C	
G37	Pyrite	Zandrivier	B3	End of leach	Unleached	
G40	Pyrite	Zandrivier	B3	End of leach	Unleached	
G44	Pyrite	West Africa	FS7		FELL OUT	
G44	Pyrrhotite	West Africa	FS7		FELL OUT	

TABLE A26 (cont.)

No.	SULPHIDE	S0URCE	LEACH	TIME IN LEACH	PROGRESS	ZONE-RELATED?
G45	Pyrrhotite	West Africa	FS7		CASE HISTORY IN TEXT	
G45	Chalcopyrite	West Africa	FS7		CASE HISTORY IN TEXT	
G45	Sphalerite	West Africa	FS7		CASE HISTORY IN TEXT	
G46	Arsenopyrite	West Africa	FS7		CASE HISTORY IN TEXT	
G46	Pyrite	West Africa	FS7		CASE HISTORY IN TEXT	
G46	Pyrrhotite	West Africa	FS7		CASE HISTORY IN TEXT	
G46	Sphalerite	West Africa	FS7		CASE HISTORY IN TEXT	
G47	Arsenopyrite	West Africa	FS7		CASE HISTORY IN TEXT	
G47	Pyrite	West Africa	FS7		CASE HISTORY IN TEXT	
G47	Pyrrhotite	West Africa	FS7		CASE HISTORY IN TEXT	
G48	Arsenopyrite	West Africa	FS7	3 days	BR–MC/BL–C2	Yes
G48	Pyrite	West Africa	FS7		CASE HISTORY IN TEXT	
G48	Pyrrhotite	West Africa	FS7		CASE HISTORY IN TEXT	
G50	Arsenopyrite	West Africa	B3	6days 10 days	C–B, Co-rich BR B, Co-rich MC	Yes Yes
G50	Pyrrhotite	West Africa	B3	3 hours 10 hours	BR MC–BL	
G51	Arsenopyrite	West Africa	B3		CASE HISTORY IN TEXT	
G51	Pyrrhotite	West Africa	B3		CASE HISTORY IN TEXT	
G52	Arsenopyrite	West Africa	B3	10 days	B, coated	
G52	Pyrrhotite	West Africa	B3	10 days	Y–BR with internal reflections	
G53	Arsenopyrite	West Africa	B3	10 days	B etched	Yes
G53	Pyrrhotite	West Africa	B3	10 days	BR with internal reflections	
G54	Arsenopyrite	West Africa	B3	10 days	B, Co-rich BR	Yes
G54	Pyrrhotite	West Africa	B3	10 days	Black with internal reflections	
G55	Arsenopyrite	West Africa	B3		FELL OUT	
G55	Pyrite	West Africa	B3		FELL OUT	
G55	Pyrrhotite	West Africa	B3		FELL OUT	
G56	Arsenopyrite	West Africa	B3	6 days 10 days	Unleached C	
G56	Pyrrhotite	West Africa	B3	3 hours	BR	
G57	Arsenopyrite	West Africa	B3		FELL OUT	
G57	Pyrilte	West Africa	B3		FELL OUT	

TABLE A26 (cont.)

No.	SULPHIDE	S0URCE	LEACH	TIME IN LEACH	PROGRESS	ZONE-RELATED?
G57	Pyrrhotite	West Africa	B3		FELL OUT	
G58	Arsenopyrite	West Africa	B3	2 days 10 days	C–B B, Co-rich BR	 Yes
G58	Pyrrhotite	West Africa	B3	2 days	BR	
G59	Arsenopyrite	West Africa	B3		FELL OUT	
G59	Pyrrhotite	West Africa	B3		FELL OUT	
G60	Arsenopyrite	West Africa	B3	10 days	C–B	
G60	Pyrrhotite	West Africa	B3	10 days	BR	
G61	Arsenopyrite	West Africa	B3		FELL OUT	
G61	Pyrrhotite	West Africa	B3		FELL OUT	
G62	Arsenopyrite	West Africa	B3		FELL OUT	
G62	Pyrrhotite	West Africa	B3		FELL OUT	
G63	Arsenopyrite	West Africa	B3		FELL OUT	
G63	Pyrrhotite	West Africa	B3		FELL OUT	
G65	Arsenopyrite	West Africa	B3	10 days End of leach	Co-rich etched B, Co-rich BR	Yes Yes
G66	Arsenopyrite	West Africa	B3	End of leach	Unleached	
G66	Pyrrhotite	West Africa	B3	End of leach	BR	
G67	Arsenopyrite	West Africa	B3		FELL OUT	
G67	Pyrrhotite	West Africa	B3		FELL OUT	
G68	Arsenopyrite	West Africa	B3	10 days	B/BR	Yes
G68	Pyrrhotite	West Africa	B3	10 days	BR–Black	
G69	Arsenopyrite	West Africa	B3	10 days	C etched	
G69	Pyrrhotite	West Africa	B3	10 days	BR–Black with internal reflections	
G70	Arsenopyrite	West Africa	B3	10 days	C etched	
G70	Pyrrhotite	West Africa	B3	10 days	BR–Black with internal reflections	
S1	Gersdorffite	Sheba	FS7	3 hours	Leached out	
S1	Gersdorffite 2	Sheba	FS7	1 day 2 days	BR G with internal reflections	
S2	Chalcopyrite	Sheba	FS7		FELL OUT	
S3	Tetrahedrite	Sheba	FS7		FELL OUT	
S4	Pyrite	Sheba	FS7	End of leach	Leached out	

TABLE A26 (cont.)

No.	SULPHIDE	S0URCE	LEACH	TIME IN LEACH	PROGRESS	ZONE-RELATED?
S8	Pyrite	Sheba	FS7	12 hours 4 days 8 days End of leach	W/B PU/Y BL/dark BL Y2/C2	Yes Yes Yes Yes
S9	Pyrite	Sheba	FS7	End of leach	B	
S9	Galena			End of leach	Leached out	
S10	Pyrite	Sheba	FS7	4 days 6 days 10 days End of leach	B B P BL/C2	 Yes
S11	Pyrite	Sheba	FS7	12 hours 4 days 10 days	Y B Y2	
S12	Pyrite	Sheba	FS7	End of leach	BL–PU	
S13	Pyrite	Sheba	FS7	End of leach	C2–L	
S14	Pyrite	Sheba	FS7	End of leach	C2–L	
S15	Pyrite	Sheba	FS7	End of leach	C2–L	
S16	Pyrite	Sheba	FS7	End of leach	C2–L	
S17	Pyrite	Sheba	FS7	End of leach	C2–L	
S18	Pyrite	Sheba	FS7	End of leach	Unleached	
S19	Pyrite	Sheba	FS7	End of leach	BL–PU/Y2	Yes?
S20	Pyrite	Sheba	FS7	End of leach	Gone (leached out?)	
S21	Pyrite	Sheba	FS7	End of leach	Gone (leached out?)	
S22	Pyrite	Sheba	FS7	End of leach	Gone (leached out?)	
S23	Pyrite	Sheba	B3	End of leach	BL–C2	
S24	Pyrite	Sheba	B3	End of leach	Y2/BL	Yes
S25	Pyrite	Sheba	B3	End of leach	BL–C2	
S26	Pyrite	Sheba	B3	End of leach	C	
S27	Gersdorffite	Sheba	B3	3 hours 1 day	MC Leached out	
S27	Gersdorffite 2	Sheba	B3	1 day	MC2	
S29	Pyrite	Sheba	B3		OFF MICROSCOPE SCALE	
S30	Chalcopyrite	Zandrivier	B3	End of leach	Unleached	

TABLE A26 (cont.)

No.	SULPHIDE	S0URCE	LEACH	TIME IN LEACH	PROGRESS	ZONE-RELATED?
S31	Chalcopyrite	Zandrivier	B3	End of leach	Unleached	
S33	Pyrrhotite	West Africa	FS7	12 hours 2–3 days End of leach	BR BL, cross-hatched Black with internal reflections	